January 2015

High-throughput Screening of Age-related Changes in Caenorhabditis elegans

Neil Copes
University of South Florida, ncopes@mail.usf.edu

High-throughput Screening of Age-related Changes in *Caenorhabditis elegans*

by

Neil Copes

A dissertation submitted in partial fulfillment
of the requirements for the degree of
Doctor of Philosophy
Department of Cell Biology, Microbiology and Molecular Biology
College of Arts and Sciences
University of South Florida

Major Professor: Patrick Bradshaw, Ph.D.
Meera Nanjundan, Ph.D.
Stanley Stevens, Ph.D.
Sandy Westerheide, Ph.D.

Date of Approval:
June 17, 2015

Keywords: aging, genetics, respiration, ATP, redox

ACKNOWLEDGMENTS

I would like to thank my mentor, Dr. Patrick Bradshaw, for all of the help and guidance he has given me over these past few years. I would also like to thank the members of my Ph.D. committee – Dr. Nanjundan, Dr. Stevens, and Dr. Westerheide – for their helpful advice and their investment of time. I would like to thank my parents and my sister for their love and support. Finally, I would like to thank Clare Canfield for being my friend all these years.

TABLE OF CONTENTS

LIST OF TABLES

LIST OF FIGURES

ABBREVIATIONS

AA: Ascorbic acid
ACDH-13: Acyl CoA dehydrogenase 13
AD: Alzheimer's disease
AGEs: Advanced-glycation end-products
AGXT-2: Alanine-glyoxylate aminotransferase-2
AIPL-1: Actin interacting protein 1-like protein 1
AMPK: AMP-activated protein kinase
AR: Aldose reductase
ATP: Adenosine triphosphate
AUC: Area under curve
βHB: beta-hydroxybutyrate
CI: Confidence interval
CSRP: Cysteine and glycine-rich protein
DAF-2: Dauer formation-2
DHA: Dehydroascorbic acid
DNMT: DNA methyltransferase
DPH-2: Diphthamide biosynthesis protein 2
EA: Erythronic acid
ER: Endoplasmic reticulum
ETC: Electron transport chain
$FADH_2$: Flavin adenine dinucleotide
FEP: Fluorinated ethylene–propylene
FSH: Follicle stimulating hormone
FUdR: 5-fluoro-2′-deoxyuridine
GABA: Gamma-aminobutyric acid
GAPDH: Glyceraldehyde 3-phosphate dehydrogenase
GC-MS: Gas chromatography-mass spectroscopy
GFP: Green fluorescent protein
GH: Growth hormone
GLOD-4: Glyoxalase-1 enzyme
GnRH: Gonadotropin-releasing hormone
GO: Gene ontology
HDAC: Histone deacetylases
HPG: Hypothalamus-pituitary-gonadal axis
HPLC: High performance liquid chromatography
IDH2: Isocitrate dehydrogenase 2
IGF-1: Insulin and insulin-like growth factor 1
IIS: Insulin and insulin-like growth factor 1 signaling
iTRAQ: Isobaric Tags for Relative and Absolute Quantitation

KEGG: Kyoto Encyclopedia of Genes and Genomes
LD: Lipid droplet
LH: Luteinizing hormone
MG: α-dicarbonyl methylglyoxal
MLC-2: Myosin regulatory light chain 2
MLP-1: Muscle LIM protein 1
MSR-A: Methionine sulfoxide reductase-A
NAD: Nicotinamide adenine dinucleotide
NADPH: Nicotinamide adenine dinucleotide phosphate-oxidase
NAG: N-acetylglucosamine
NGM: Nematode growth medium
NRA-2: Nicotinic receptor associated protein 2
NRF2: Nuclear factor erythroid 2–related factor 2
PAB-2: Poly(A) binding protein 2
PC: Phosphatidylcholine
PCA: Principal component analysis
PE: Phosphatidylethanolamine
PEAMT: Phosphomethylethanolamine N-methyltransferase
PD: Parkinson's disease
PGC-1α: Peroxisome proliferator-activated receptor gamma coactivator 1α
PINK1: PTEN induced putative kinase 1
PME-1: Poly(ADP-ribose) polymerase-1
PP1: Protein phosphatase 1
PRMT-3: Protein arginine methyltransferase-3
RAGE: Receptor for advanced glycation end-products
RNAi: RNA interference
RNS: Reactive nitrogen species
ROC: Receiver operating characteristic
ROS: Reactive oxygen species
RPE: Retinal pigment epithelium
RSP-6: Arginine/serine-rich protein 6
SAMS-1: S-adenosyl methionine synthetase
SASP: Senescence-associated secretory phenotype
SCA-1: Sarco-endoplasmic reticulum calcium ATPase 1
SEM: Standard error of the mean
Sir2: Sirtuin 2
SSMD: Strictly standardized mean difference
TCA: Tricarboxylic acid cycle
TCWF: Total corrected worm fluorescence
TOR: Target of rapamycin
XRN-2: 5'-3' exoribonuclease 2 homolog
8OHdG: 8-hydroxy-2' -deoxyguanosine

ABSTRACT

This project was developed to identify novel methods for high-throughput culturing and screening of *C. elegans* to investigate age-related metabolic changes and to survey the proteomic and metabolomic factors associated with age-related changes. To accomplish these goals we developed a novel way to grow *C. elegans* in liquid culture in 96-well microplates for several weeks without suffering significant fluid loss due to evaporation and without needing to shake or unseal the plates for aeration. We also developed methods for assaying the total volume of live *C. elegans* in microplate cultures using a fluorescence microplate reader and for performing RNAi experiments with dead instead of live bacteria, which allows for the measurement of nematode metabolic parameters without bacterial interference. Using these methods, along with established methods for the global identification of metabolites and proteins by mass spectroscopy, we observed an integrated pattern of changes that occurred at the molecular level in aged *C. elegans*. Specifically, we found protein changes suggesting muscle dysfunction and sarcopenia, an increase in free fatty acids, a decrease in the S-adenosylmethionine cycle, altered or impaired protein synthesis, changes in free amino acid levels consistent with an increase in cell size, indications of epigenetic changes and alteration of DNA repair, and a shift toward a more oxidizing cellular environment, as well as a decrease in NAD^+ relative to NADH. Through the use of an automated RNAi screen targeting potential EF-hand Ca^{2+} binding proteins, we identified genes that are associated with high culture medium Ca^{2+} toxicity. In addition, from a screen of X chromosome RNAi clones, we identified clones that partially prevented the age-dependent decline in nematode ATP levels, oxygen consumption, and reductive capacity. The

set of genes targeted by these RNAi clones is enriched in both anti-longevity genes and negative regulators of cellular processes and are potential targets for anti-aging interventions.

CHAPTER 1:

INTRODUCTION AND BACKGROUND

1.1 Maximal Lifespans

There is enormous variability among animal lifespans. The maximum lifespan of the east African fish, *Nothobranchius furzeri*, is only three months, whereas radiocarbon dating suggests members of the newly-discovered species of deep sea oyster, *Neopycnodonte zibrowii*, can live in excess of 500 years [1, 2]. In addition, specific mutations have been shown to dramatically extend the lifespans of model organisms. There are now more than 200 single gene mutations known to extend the lifespans of nematodes and fruit flies and more than 20 single gene mutations capable of extending the lifespans of laboratory mice [3]. Taken together, these facts show that lifespans are subject to genetic control, and amenable to manipulation. However, even though the genetic composition of a species determines its maximal lifespan, there is still a lack of consensus regarding the extent to which the process of aging is part of a species' evolved developmental program versus a stochastic process more governed by a failure to adequately repair all molecular and cellular damage.

1.2 Aging

In the broadest sense, aging can be defined as the physical decline in fitness and stress tolerance of an organism. All multicellular eukaryotic organisms age in a manner specific to

their species, however several recurring traits are common (for a review of mammalian aging see López-Otín *et al*., [4]). These traits can be summarized as changes in tissue composition and function, genomic changes, mitochondrial dysfunction, the accumulation of macromolecular damage, hormonal dyscrasia, and immune system dysfunction. Notably, these traits appear to be interdependent, providing for a large degree of overlap among the categories. Nutrient sensing also plays a major role in the aging process and has been studied extensively in model organisms.

1.2.1 Changes in Tissue Composition and Function

Animals experience an age-related shift in the population of cell types within tissues. Stem cell pools within tissues are exhausted with age, by both a loss in stem cell number and function, leading to a decrease in regenerative capacity [5]. This cell loss correlates with the accumulation of DNA damage [6], with the up-regulation of cell-cycle inhibitory proteins such as $p16^{INK4a}$, which is a marker for cellular senescence [7], and with an exhaustion of function due to excess signaling for proliferation [8, 9]. Stem cell attrition has been identified in aging mouse and human tissues including the brain and muscle [10-17], as well as with hematopoietic and mesenchymal stem cells [6, 18-20]. Furthermore, the loss of stem cells function in myosatellite cells has been identified as a contributing factor for sarcopenia, the age-related loss of muscle strength and mass [21, 22]. The benefits of stem cells may also extend beyond their intrinsic regenerative capacity. Muscle-derived stems cells from young wild-type mice have been shown to promote neovascularization and tissue regeneration when injected into progeroid mice, even in tissues where the transplanted stem cells are not detected [23]. The benefits also extended to a

restoration of endogenous stem cells function and an extension of lifespan, suggesting that secreted factors from the younger stem cells contributed to the therapeutic effect.

The loss of stem cell function with age is possibly a combination of cell signaling changes [22], and the loss of a portion of the stem cell pool to cellular senescence or apoptosis. Cellular senescence can be defined as a permanent exit from the cell-cycle accompanied by the acquirement of a characteristic cellular and secretory phenotype. This cellular state was initially observed by Hayflick in 1961 as the exit from the cell-cycle of serially-passaged human fibroblasts in culture [24], and was later identified to be attributed to the gradual shortening of telomeres (repetitive regions of DNA at the ends of chromosomes) upon somatic cell division [25]. This shortening can be counteracted by the expression of the enzyme telomerase, however since most somatic cells lack telomerase, telomere length tends to decrease over time in populations of dividing somatic cells. It has since been shown that cellular senescence also can be induced by DNA damage and sustained activation of the DNA damage response [26]. Telomeres are shortened by oxidative damage from such sources as reactive oxygen species (ROS), and the cellular response to excessively short telomeres is similar to the response to double-strand breaks. Notably, telomeric DNA is especially prone to oxidative damage due to its high guanine content, which has the lowest oxidation potential among the nucleobases and forms 8-oxoguanine upon oxidation. In addition to exiting from the cell-cycle, senescent cells acquire a specific phenotype that includes an enlarged and flattened morphology, increased ROS production, an increased lysosomal accumulation of lipofuscin (oxidatively cross-linked proteins and lipids), decreased mitochondrial membrane potential, increased mitochondrial mass, decreased PGC1-α driven mitochondrial biogenesis, the formation of heterochromatin foci, and increased expression of the cell cycle inhibitor $p16^{INK4a}$ and the lysosomal hydrolase β-

galactosidase [26-31]. Additionally, senescent cells secrete proinflammatory cytokines and matrix metalloproteinases, collectively referred to as the senescence-associated secretory phenotype (SASP) [32, 33]. Evidence suggests that the presence of senescent cells contributes to the aging process, as the chemical removal of senescent from progeroid mice extends lifespan [34].

One likely result of the SASP is signaling to the immune system to remove senescent cells, and evidence indicates that senescent tumor cells are selectively removed by the immune system by phagocytosis [35-37]. Estimates of senescent cell accumulation in mouse livers, skin, lung, and spleen based on markers such as β-galactosidase expression and DNA damage suggest an approximate doubling of senescent cell content with age in these tissues, with ~8% of livers cells appearing senescent in young mice versus ~17% in very old mice [38]. Interestingly, the heart, skeletal muscle, and kidneys showed no obvious accumulation of senescent cells, suggesting that senescent cell accumulation may be tissue specific.

1.2.2 Genomic Changes

As mentioned above, telomeres shorten within somatic cells due to repeated cell division or the presence of genotoxic stress such as that caused by ROS. As a consequence, telomere length has been demonstrated to shorten over time within mouse and human tissues [39], and shortened telomeres progressively predispose cells to apoptosis and senescence. Additional changes include a specific age-dependent change in the pattern of DNA methylation, which progresses at different rates in individual human tissues [40]. This change seems to consist of global hypomethylation with local islands of hypermethylation occurring at least partially at sites of tumor suppressor genes and Polycomb target genes in mice [41]. Chromatin remodeling has

also been observed as a typical age-related change, characterized by heterochromatin loss and redistribution [42]. Widespread chromatin restructuring should be expected to affect cellular gene expression patterns, and notably these age-dependent changes have been linked to changes in the functionality of stem cells [43]. More specifically histones, the protein complexes that bind and package DNA within chromatin, have been found to play a role in the aging of various species. Deletion of components of histone methylation enzymes have been shown to extend the lifespan of both flies and nematodes [44, 45], and inhibition of histone demethylases specific for H3K27 have been also shown to extend the lifespan of nematodes [46]. Histone deacetylase (HDAC) enzyme family members appear also to affect the aging process in at least nematodes, flies, and mice. Specifically the sirtuin enzyme SIR2, which is a member of the class III HDAC family, was identified to extend the lifespan of yeast when overexpressed [47]. There is still some debate about the applicability of this finding to other model organisms [48], but the nematode ortholog SIR-2.1 appears to at least produce a small extension of lifespan when overexpressed in this organism [49]. Furthermore, the transgenic overexpression of the mammalian homolog *Sirt1* failed to extend the lifespan of mice, but did lower the age-dependent incidence of DNA damage, $p16^{INK4a}$ expression, and spontaneous carcinoma and sarcoma formation [50]. The activity of the mammalian sirtuin SIRT6 appears to be more pertinent to aging, and overexpression of SIRT6 extends the lifespan of male transgenic mice [51], while mice deficient in SIRT6 exhibit a high degree of DNA damage and die by approximately 4 weeks of age [10]. Finally, transposable elements (transposons) become active during normal brain again in *Drosophila* and likely contribute to the age-dependent loss of neuronal cells in that organism [52]. Transposons have been also shown to become active in the tissues of older mice

as a consequence of chromatin remodeling, and a similar remodeling pattern accompanied by transposon activation has been observed in human senescent cells maintained in culture [53].

1.2.3 Mitochondrial Dysfunction

The number of dysfunctional mitochondria in postmitotic tissue increases with age. These mitochondria generally exhibit a large number of distinct changes, including decreased membrane potential, decreased respiration, increased mitochondrial DNA damage such as point mutations, deletions, and 8OHdG, structural changes such as the loss of cristae and mitochondrial enlargement or swelling, and the oxidation and subsequent loss of cardiolipin, which is an inner membrane phospholipid that interacts with the complexes of the electron transport chain [54-57]. General reductions in membrane potential and respiratory capacity imply that ATP production through oxidative phosphorylation likely decreases with age in postmitotic tissue, and this reduction may be accompanied by a cellular shift to anaerobic metabolism in an attempt to meet energy needs [58].

Under normal conditions, the biogenesis of mitochondria is balanced by their elimination through autophagy (termed mitophagy), resulting in a mostly constant number of mitochondria within cells [59]. Few studies have sought to determine mitochondrial turnover rates, however depending on the tissue and technique used, turnover estimates for rodents have ranged from roughly one week to two months [60, 61], and a study in mice indicates that mitochondrial half-lives in some tissues of that organism may be as short as 1 – 2 days [62]. Mitophagy is up-regulated in cells under conditions of low nutrient availability, and starvation-induced mitophagy in isolated hepatocytes has been shown to be entirely nonselective [63-67]. However, under normal conditions damaged mitochondria can be selectively eliminated based on their lowered

membrane potential [68, 69]. The protein PINK1 accumulates specifically on the membranes of mitochondria with lowered, or nonexistent membrane potential, where it recruits the action of Parkin [70, 71]. This protein then serves to ubiquitinate the mitochondrial fusion-promoting protein mitofusin, rendering the mitochondrion incapable of fusing with other mitochondria, and signaling the cell to degrade the mitochondrion through autophagy. This PINK1/Parkin system of selective mitochondrial degradation has been demonstrated in multiple tissues and cell types, in humans, mice, *C. elegans*, and *Drosophila* [72-75].

Mitochondria are morphologically active organelles that regularly fuse together to create tubular networks, or fission into separate discrete structures [59]. Through fusion, oxidatively-damaged mitochondrial components can be diluted throughout a cell, whereas fission allows the spreading of components to daughter cells during cellular division. Fusion events between mitochondria are often followed by fission events that create separate mitochondria that are structurally and metabolically unequal. In these cases mitochondrial fission produces one larger mitochondrion with higher membrane potential, and one smaller mitochondrion with lower membrane potential [59, 76]. The smaller of the two new mitochondria generally differs in membrane structure [77]. Furthermore, the smaller mitochondrion generally has a greatly reduced ability to fuse with other mitochondria, and is much more likely to be eliminated through autophagy, suggesting that it is prone to PINK1/Parkin membrane potential-dependent mitophagic degradation [78]. The facts that mitochondrial fission can be induced through oxidative stress, and that, under normal conditions, the inhibition of mitochondrial fission results in an intracellular accumulation of oxidatively-damaged mitochondrial proteins, additionally suggest that mitochondrial fission can function to segregate oxidatively damaged components for disposal through mitophagy [77, 78]. In addition stem cells exclude dysfunctional mitochondria

by asymmetric apportioning of dysfunctional mitochondria between daughter cells and this is required to maintain stemness. This process may be altered with age leading to stem cell exhaustion and senescence [79].

One of the characteristics of mitochondria in long-lived postmitotic tissues, such as the myocardium, skeletal muscle and the brain, is the accumulation of enlarged mitochondria, often referred to as giant mitochondria [80, 81]. The factors that affect the accumulation of giant mitochondria are still not fully understood, but they appear to form partly by a failure of fission/fusion and the mitophagy system of mitochondrial turnover [80, 82]. In support of this connection, the appearance of giant mitochondria are one consequence of inhibition of autophagy following in vitro treatment with 3-methyladenine [82, 83]. It is interesting that the increased mass and decreased membrane potential associated with giant mitochondria mirror the same mitochondrial changes that occur within senescent cells, and that conditions that up-regulate autophagy, such as endurance training and intermittent fasting, also protect against mitochondrial dysfunction [84-86].

1.2.4 Macromolecular Damage

Damaging agents are generated endogenously within cells. Ionizing radiation is capable of splitting water molecules within cells, generating, in the process reactive hydrogen peroxide, and two types of unstable molecules with unpaired electrons – superoxide anion radicals and hydroxyl radicals [87]. These compounds are capable of reacting with biological macromolecules, such as lipids, through peroxidation reactions, and DNA, primarily through the oxidation of guanosine into 8-hydroxyguanosine. Reactions with proteins occur through either the oxidation of amino acid residues to form reactive carbonyls, or through the oxidative

cleavage of peptide backbones [88, 89]. It was found in 1954 that living cells naturally contain these reactive compounds, categorized as ROS, and in 1956 Denham Harman proposed that these compounds contribute to the macromolecular damage that occurs in aging (known as the free radical theory of aging) [90, 91]. After details of the ROS-generating nature of the mitochondrial electron transport chain (ETC) became clear, Harman updated his theory in 1972 to implicate mitochondria as the major contributor to the aging process (known as the mitochondrial theory of aging) [92]. In support of Harman's theories, the rates of mitochondrial hydrogen peroxide production and superoxide anion production have been found to be inversely proportional to the maximum lifespans of a variety of species [93, 94].

Mitochondria are the major consumers of molecular oxygen within eukaryotic cells. Electrons are supplied by the carrier molecules NADH and $FADH_2$ to ETC complexes I and II, respectively, on the inner membrane of mitochondria. The electrons are then passed across the complexes and deposited onto molecular oxygen, converting it to water and supplying energy to move protons across the inner membrane. As electrons are passed among the complexes, the potential exists for single electrons to exit the ETC early and to be deposited on molecular oxygen forming superoxide anion radicals. Thermodynamically, each of the ETC complexes have the potential to generate superoxide, however studies with isolated mitochondria have indicated complexes I and III as the major physiological suppliers of cellular superoxide. It is generally accepted that Complex I releases superoxide on the matrix side of the inner membrane, whereas Complex III releases superoxide on both sides of the membrane. The exact contribution of Complex III is still in debate [95-98].

Between 0.1% and 2% of the total oxygen consumed by animal cells is converted into superoxide, and estimates suggest that this total may raise to 10% during vigorous exercise [87,

99]. Once it is generated superoxide is capable of damaging mitochondrial DNA, lipids, and proteins, and if it reacts with the signaling molecule nitric oxide it can generate peroxynitrite anions (a reactive nitrogen species or RNS) [100-103]. Most superoxide though is converted both enzymatically and nonenzymatically into hydrogen peroxide. Left on its own, superoxide will undergo dismutation into hydrogen peroxide, with a half-life of 10^{-6} seconds [59]. However, in a cellular environment most superoxide is enzymatically converted into hydrogen peroxide by superoxide dismutases (SODs), and the presence of SODs, which are found in almost every known living organism, increase the rate of dismutation by approximately 1,000-fold. The fact that enzymes evolved that dramatically increase the rate of an already rapid and spontaneous process can be interpreted as an indication of how dangerous superoxide may be to cells, and this interpretation is supported by the observation that the mitochondrial superoxide production rate, when measured as a proportion of respiration rate, is inversely correlated with lifespan in both closely and distantly-related species [59, 87, 104-107].

Once formed, hydrogen peroxide is transformed by eukaryotic cells into water. This transformation is mediated by the peroxiredoxin/thioredoxin system and glutathione peroxidase in mitochondria, and by glutathione peroxidase and catalase in the cytosol and peroxisomes [59, 108]. Hydrogen peroxide is more stable than superoxide, and unlike superoxide, it can readily cross cellular membranes, allowing hydrogen peroxide to diffuse throughout cells [109]. This combination of relative stability and mobility enable hydrogen peroxide to function as an important signaling molecule that affects most cytosolic redox activity [110]. If not eliminated however, hydrogen peroxide can react with cellular Fe(II), in what is known as a Fenton reaction to generate Fe(III) and the highly-reactive hydroxyl radical [59, 87]. Furthermore, superoxide can regenerate Fe(II) from Fe(III), additionally fueling hydroxyl radical production.

The incidence of oxidatively damaged DNA, proteins, and lipids increases in an age-dependent manner [111]. One consequence of this increase is that oxidized methionine residues causes an increase in the surface hydrophobicity of proteins [112, 113], which has been observed in the liver proteins of older rats [114], and in human skin collagen over the range of 10 – 80 years [115]. Methionine oxidation is reversible through the action of methionine sulfoxide reductase-A (MSR-A), which also declines in an age-related manner in rats [114, 116]. Furthermore, deficiency in MSR-A activity in mice leads to a ~40% reduction in lifespan [117], and overexpression of MSR-A in flies produces an approximate doubling of lifespan [118]. Oxidative modifications have been observed to accrue in key metabolic enzymes, such as GAPDH [119], aconitase, and α-ketoglutarate [120], and both oxidative and nitrosative modification to key signaling proteins may contribute directly to aging [121, 122]. Furthermore, several of the cellular mechanisms that are capable of removing oxidatively damaged proteins, such as chaperone-mediated autophagy and the proteasome, decrease in function with age and within senescent cells [86, 123-126].

Aldose sugars, such as glucose, are another source of macromolecular damage. When in their acyclic open-chain form, aldose sugars have a reactive aldehyde chemical group at the end of their carbon backbone. This aldehyde group can act as a reducing agent in redox reactions, and can form covalent bonds with nitrogen atoms on protein residues, forming a Schiff base. Ketose sugars such as fructose, which are sugars with a ketone group in place of an aldehyde group, are also capable of participating in these reactions, but they do so by first undergoing a series of tautomeric shifts that result in the generation of an aldehyde group. Once formed, Schiff bases are unstable and easily reversible, however they can also re-arrange through an enaminol intermediate into a more-stable ketoamine, termed an Amadori product. Multiple

reaction pathways are then possible for the Amadori product, depending on the structure of the initial reacting sugar and the presence or absence of an oxidizing agent. The diverse array of sugar-derived protein adducts are collectively referred to as advanced-glycation end-products (AGEs), and the entire progression from sugar to AGE is called the Maillard reaction [127].

AGE formation is largely irreparable and has been found to accumulate over time within long-lived proteins such as collagen [111] and lens crystallins [128], and in tissues such as the dura mater, skin, and cartilage [111]. Furthermore, the protein cross-linking structures of some AGEs have been found to decrease collagen elasticity and contribute to arterial stiffening [129, 130]. The AGE carboxymethyl lysine also has been found to act as a chelating agent that is capable of promoting the metal-catalyzed oxidation of surrounding residues in proteins [131]. The α-dicarbonyl methylglyoxal (MG) is an especially reactive glycating agent that forms from the nonoxidative degradation of the glycolytic intermediates glyceraldehyde and dihydroxyacetone phosphate, and as a by-product of the metabolism of ketone bodies acetone and aminoacetone, and the metabolism of threonine [132]. MG has been linked to age-related damage to proteins, lipids, and DNA, and it has been implicated in mitochondrial dysfunction [111]. Notably, the chronic hyperglycemia of diabetes leads to an increased rate of AGE formation that contributes to the etiology of the disease [133]. Physiological changes commonly seen in aging, such as atherosclerosis, the stiffening of joints, arteries, and the lung, loss of bone mass and lens accommodation, cataract formation, systemic inflammation, and cardiovascular disease, progress faster or more severely for diabetics [134, 135].

Besides directly modifying macromolecules, AGEs bind to the receptor for advanced glycation end-products (RAGE), which is a 35 kDa transmembrane, cell-surface receptor of the immunoglobulin superfamily present at low levels in a wide range of tissues [136-138]. RAGE-

ligand binding has been shown to activate numerous intracellular signaling cascades through the short cytoplasmic tail of the receptor. Activation of ERK1/2 (p44/p42) and SAPK/JNK MAP kinases has been observed to follow RAGE-ligand binding in various cells types, and the PI3K and JAK/STAT pathways have been implicated in RAGE signaling [139-141]. RAGE-ligand binding may also directly stimulate the production of reactive oxygen species (ROS) through the activation of NADPH oxidases [142]. Activation of these pathways through ligand-RAGE binding has been further linked to the activation of the pro-inflammatory transcription factor NF-κB [139-141]. Since the initial discovery of RAGE, the link between RAGE activation, NF-κB, and inflammation has been firmly established, and it now appears that the activation of RAGE serves both to initiate and prolong inflammatory responses [137, 138, 143-147]. It is easy to speculate then that AGE accumulation and its signaling through RAGE may contribute to the general increase in tissue inflammation observed in mammalian aging.

One consequence of the production of cellular macromolecular damage is that the lysosomes progressively accumulate lipofuscin, a brownish-yellow, polymorphous, electron-dense, autofluorescent mix of oxidatively cross-linked proteins and lipids [148]. The accumulation of lipofuscin begins at birth and continues nearly linearly in postmitotic cells [149]. Additionally, the rate of lipofuscin accumulation in postmitotic cells appears to be inversely correlated with lifespan, indicating that this accumulation may be harmful to an organism [150-152]. Lipofuscin collects within postmitotic cells because it cannot be degraded or removed by exocytosis; it is essentially a non-degradable, non-excretable polymer [153-155]. Furthermore, actively dividing cells avoid this unimpeded accumulation only because they are able to dilute their stored lipofuscin among daughter cells [156].

The accumulation of lipofuscin is capable of reaching astounding levels, with one study showing lipofuscin occupying up to 75% of the cellular volume of aged neurons in some human centenarians [157]. Such a dramatic morphological change should be expected to affect cellular function, especially with functions pertaining to lysosomal activity. Indeed, lipofuscin accumulation in RPE cells was found to interfere with heterophagocytosis [158]. Lipofuscin-loaded cultured human fibroblasts show diminished autophagocytosis and decreased survival during amino acid starvation, and lipofuscin-containing aged mouse hepatocytes display reduced autophagic vacuole formation and elimination [159, 160].

1.2.5 Hormonal Dyscrasia

In mammals, the hypothalamus-pituitary-gonadal axis (HPG) changes with age as sex hormone levels decline in the post-reproductive portion of the lifespan. The hypothalamus, which is located in the middle of the brain between the thalamus and the pituitary gland, secretes gonadotropin-releasing hormone (GnRH). The presence of GnRH causes the anterior pituitary gland to release follicle stimulating hormone (FSH) and luteinizing hormone (LH) into the blood stream. In both males and females, FSH and LH affect growth, development, germ cell maturation, and the release of the protein complex inhibin from the gonads. In ovaries, FSH triggers follicular growth while LH supports the production of both estradiol and progesterone in a manner dependent of the phase of the reproductive cycle. In testis, FSH promotes spermatogenesis, and LH signals for the release of testosterone from the Leydig cells. Progesterone and testosterone inhibit the release of GnRH from the hypothalamus, thus completing a negative feed-back loop that regulates the release of FSH and LH from the pituitary gland. Furthermore, inhibin directly inhibits the pituitary gland from releasing FSH and LH, and

estradiol either inhibits or stimulates the release of LH depending on the phase of the reproductive cycle. However, receptors for the hormones of the HPG axis are found in various tissues throughout the body, implying that the true effects of the HPG axis are widespread [161, 162].

During the post-reproductive life-stage in female mammals (following menopause in humans), the release of progesterone and estradiol becomes erratic and begins to steeply decline. This change is mirrored by a gradual decrease in testosterone in human males beginning at about middle age [163], and a loss of inhibin production in both sexes [164]. This decline in gonadal hormone production disrupts the negative feed-back of the HPG, potentially affecting the entire organism. The pattern of effect seems to be a short-term increase in GnRH, FSH, and LH in women as gonadal hormone levels drop, followed by a more long-term decrease in FSH and LH in women and in GnRH in both sexes [165, 166]. In mice, the re-establishment of the HPG feed-back loop by the transplantation of viable ovaries from young mice into older post-reproductive mice has been demonstrated to lead to a ~40% increase in lifespan [167, 168]. A negative correlation also has been identified both between serum estradiol levels in women and the incidence of Alzheimer's disease (AD) [169] and between serum testosterone levels in men with AD [170]. Additionally, a decline in GnRH in mice contributes to reduced neurogenesis, skin thickness, and muscle and bone mass, as well as an increase in collagen cross-linking [166], and supplementation with GnRH was shown to prevent these changes in neurons, skin, and muscle.

1.2.6 Immune System Dysfunction

Aging of the immune system (termed immunosenescence) is characterized by a loss of functional hematopoietic stem cells, involution of the thymus and an associated decrease in the

number of circulating naive T cells, increased levels of pro-inflammatory cytokines, such as interleukin (IL)-6 and TNF-α, an increased number of differentiated memory $CD28^-$ T cells with a diminished capacity for proliferation, a decreased CD4/CD8 cell ratio, and an increase in systemic inflammation [171-174]. The immediate effect of immunosenescence is a reduction in the body's capacity to fight parasites and infectious agents and to remove infected cells. However, since the immune system also functions to remove both senescent and hyperploid cells, immunosenescence may also contribute to the increased incidence of cancer and the accumulation of senescent cells observed in the aging process [35-37, 175, 176]. Additionally, the increase in pro-inflammatory cytokines and inflammation seen with age may result from a decreased ability to fight infection, as well as the SASP produced by senescent cells and the continual activation of RAGE by the accumulation of AGEs within tissues. Interestingly, the inflammation associated with aging has also been shown to have the downstream effect of inhibiting stem cell function in the epidermis [177], and conditional over-expression of an inhibitor of the pro-inflammatory transcription factor NF-κB in the skin of transgenic mice resulted in a restoration of a more youthful skin phenotype [178]. Also, age-related inflammation has been shown to activate NF-κB in the hypothalamus, leading to a reduction in the release of GnRH, and prevention of this inflammatory effect extends the lifespan of mice [166]. Finally, SIRT1 and SIRT6 have been shown to have an anti-inflammatory function, which may partially explain their observed effects on health and lifespan [179-184].

1.2.7 Nutrient Sensing

The insulin and insulin-like growth factor 1 (IGF-1) signaling (IIS) pathway is the most conserved aging-associated pathway identified among species [4, 185-187]. In mammals,

growth hormone (GH) is secreted by the anterior pituitary gland in response to a complex array of stimulatory signals, including sleep, hunger, nutrition, stress, exercise, and developmental state [188-192]. The release of GH induces the production of IGF-1, primarily from hepatocytes. Receptors for IGF-1 are present in many tissues and cell types, and affect the same intracellular signally pathway as insulin, which informs cells of the presence of glucose, and which activate downstream targets such as AKT and the mTOR complex, and inhibit nuclear translocation of the FOXO family of transcription factors. Multiple polymorphisms, mutations, and genetic alterations linked to longevity have been identified that decrease GH and IGF-1 function, or that attenuate intracellular signaling of the IIS pathway in humans and model organisms [185, 187, 193-195]. Furthermore, dietary restriction (DR) is the most consistent treatment found to extend the lifespan of model organisms, and the genetic analysis of worms and flies has shown the IIS pathway to contribute to at least part of this effect [193]. Interestingly, GH and IGF-1 levels have been shown to decline with age in both wild-type mice and progeroid mice, suggesting that pro-longevity signaling changes may gradually occur with normal mammalian aging [196].

1.3 *Caenorhabditis elegans* as an Accelerated Aging Model

C. elegans are free-living 1 mm-long nematodes found in the soil of temperate climates. Interest in the laboratory use of *C. elegans* as a model organism began in the 1970s with the work of Sidney Brenner [197], and the popularity of the organism continues to grow. Among the laboratory benefits of the organism are its ease of cultivation and its tractability for genetic analysis. Additionally, homologs of many human genes are present within the nematode genome. *C. elegans* can be maintained on solid agar plates or in liquid cultures, and they readily eat common non-pathogenic strains of laboratory bacteria [198]. Large volumes of the

nematodes also can be grown without much additional labor or expense. *C. elegans* are mostly hermaphroditic, with only 0.1 – 0.2% of normal populations consisting of males, and individual hermaphrodites can lay up to ~300 self-fertilized genetically-identical eggs during their reproductive period, which begins after ~3 – 4 days in culture [199, 200]. Experiments involving analyses of lifespan can be performed quickly with *C. elegans* given their short lifespan. Developmental rate and lifespan of the nematode are highly temperature sensitive across the 16 – 25 °C optimal temperature range for cultivation, with individuals grown at 16 °C attaining a mean lifespan of 23 days and individuals grown at 25 °C living for a mean of only 9 days [201].

Much of the interest in *C. elegans* aging research began in the late 1980s with the identification in the nematode of the first genetic mutation found to directly extend the lifespan of an organism [202]. Thomas Johnson identified a mutant recessive allele in the catalytic subunit of the *C. elegans* phosphoinositide 3-kinase gene *age-1* (a downstream target of intracellular IGF-1 signaling) that produces a decrease in fertility and a ~40% increase in mean lifespan. Interest in *C. elegans* aging research grew even further after the 1993 publication by Cynthia Kenyon of a mutation in the *C. elegans* IGF-1 receptor gene *daf-2* that resulted in a doubling of lifespan dependent on the activity of the FOXO transcription factor ortholog *daf-16* [203]. Since this time, much of the research into dissecting the lifespan-affecting aspects of the IIS pathway has been performed in this organism [204-211]. Many of the age-related changes discussed above are present in *C. elegans* and appear in a relatively accelerated fashion matching the organism's shorter lifespan, and appear mostly after then end of the reproductive period (starting at about the end of the first week of adulthood when grown at the standard temperature of 20 °C).

All 959 *C. elegans* adult somatic cells are post-mitotic. Only the germ cells actively divide, and only the distal tip cells at either end of the two U-shaped uterine projections function as stem cells, generating a supply of germ cells during the reproductive period [212]. The fate of these cells during post-reproductive aging has not been adequately addressed, however senescent cells have been shown to develop within older *C. elegans* [213]. These cells have been identified by β-galactosidase staining, which indicates that senescent cells accumulate with age, starting primarily at the head and tail of nematodes. Given the post-mitotic nature of adult *C. elegans* somatic cells, it is likely that the onset of cellular senescence is driven by sustained DNA damage, and indeed extensive changes to *C. elegans* DNA have been observed with age. At the beginning of the post-reproductive period, muscle cells begin to develop small dark nuclear patches, and the nucleus and nucleolus become misshapen [214]. Nematodes also begin to lose nuclei from their tail and experience a dysregulation and heterogeneity of cellular genome copy number [215]. The capacity for DNA repair also begins to decline with age, starting as early as the first day of adulthood [216]. Additionally, normal aging *C. elegans* is associated with a number of histone modification changes, including an increase in demethylase activity and a decline in H3K27me3 methylation [46, 217], and treatment with a histone deacetylase inhibitor has been shown to increase *C. elegans* lifespan [218].

Sarcopenia is another prominent feature of the *C. elegans* aging process. The nematodes begin experiencing defects in locomotion by about day 9 – 10 of adulthood (at 20 °C) [214]. This change is then followed by muscle shrinkage due to cytoplasmic loss, myocyte plasma membrane invagination and fragmentation, sarcomere disorganization, and a reduction in the number of myosin thick filaments. This muscular dysfunction extends beyond just the body wall of the nematode. In *C. elegans*, food is ground and forced into the intestine by the rhythmic

contraction of a set of 20 muscle cells and 20 neuronal cells, termed the pharyngeal pump. As *C. elegans* age, the pumping rate gradually slows, and the loss of pump structure and function can be nearly total by late in the *C. elegans* lifespan [219].

Obstruction of the pharyngeal pump by bacteria can also occur in older nematodes, which can form a plug blocking passage of substances into the intestine. Bacterial colonization of the intestine is also a common feature observed in older *C. elegans* and appears to slightly limit the lifespan of colonized nematodes [220]. Given that younger *C. elegans* are more resistant to bacterial infection that older nematodes [221, 222], and that longer-lived *C. elegans* strains are more resistant than shorter-lived strains [220], suggests that immunosenescence of the innate immune system is a factor in *C. elegans* aging.

During the first week of adulthood, *C. elegans* experience a dramatic decrease in mitochondrial function. Over this time period, oxygen consumption, ATP content, and metabolic heat production drop by between approximately 50 to 75% [223]. Total enzymatic reductive capacity also has been shown to decline to a similar extent during this interval, possibly indicating the cellular transition to a more oxidized state. Giant mitochondria have been reported to accumulate with age in the body wall muscle of *C. elegans* as determined by electron microscopy [224], although a second group using a fluorescence based approach failed to replicate the observation, instead finding an age-dependent accumulation of smaller, fragmented, circular mitochondria [225]. By the end of the first week of adulthood, nematode ETC Complex I activity declines by ~60%, and Complex II activity declines by ~30% [224], and mitochondrial carbonylated protein content (indicative of ROS-mediated protein oxidation) increases 4-fold compared to carbonylated cytoplasmic proteins.

Global levels of AGE-modified proteins have been shown to increase over time in *C. elegans* [226]. Specifically, carboxymethyllysine, which is derived from the α-dicarbonyl glyoxal, was shown to increase ~11-fold over the first 12 days of adulthood. Additionally, MG-derived carboxymethyllysine increases ~1.2-fold over the same period, during which MG itself appears to increase ~5-fold fold. Interestingly, the *C. elegans* glyoxalase-1 enzyme GLOD-4, which can remove MG by enzymatically converting it to D-lactate, is susceptible to modification and deactivation by both ROS and MG. During this same 12-day time period, GLOD-4 activity has been observed to decrease 10-fold, likely contributing to the age-dependent increase in MG and MG-derived modifications. Additionally, over-expression of GLOD-4 decreases MG content and increases *C. elegans* lifespan, indicating that under normal conditions MG production limits nematode lifespan.

Until recently it was assumed that lipofuscin accumulated with age in *C. elegans* in lysosome-like intestinal organelles called gut granules. Lipofuscin is autofluorescent *in vivo* with a peak fluorescence in the yellow range (540–640 nm) [227], however *in vitro* extracted lipofuscin often emits a blue peak fluorescence (340 nm) [227, 228]. Gut granules possess a blue autofluorescence, which has been attributed to lipofuscin [229, 230], and studies of entire *C. elegans* populations have indicated that blue-range autofluorescence increases in an age-dependent manner [148, 201, 229, 231, 232]. A recent report examining individual nematodes, however, observed that this blue autofluorescence stays relatively constant over the *C. elegans* lifespan, but increases by ~400% for an ~8-hour period surrounding a nematode's death [233]. The blue autofluorescence now has been identified as anthranilic acid, which is released by the gut granules upon activation of the cellular necrosis pathway, and the resulting spike in blue fluorescence is a product of concentration and pH changes to anthranilic acid upon reaching the

cytosol. The question of whether lipofuscin accumulation actually occurs within aging *C. elegans*, however, has not been fully resolved.

1.4 *C. elegans* and High-throughput Screening

Due largely to their small size, ease of growth, and susceptibility to RNA interference when fed bacteria containing dsRNA, *C. elegans* have proven to be a valuable organism for high-throughput genetic screens. Furthermore, *C. elegans* are largely transparent, which allows for the development of assays based on the incorporation of fluorescent transgenes or luminescent or fluorescent compounds. Through the extensive work invested in *C. elegans*, especially over the last 20 years, methods of high-throughput screening with this organism have become fairly standardized, but usually require labor-intensive manual observation of phenotypes [234]. However, difficulties still exist in the logistics of performing many types of screen, use of agar in microplates usually negates the ability for many types of optical measurements, and maintenance of nematodes in long-term liquid cultures suffers from systematic biases in measurements due evaporation along the outside edges of microplates (termed "edge effects") [235]. Furthermore, assays involving the investigation of metabolites or metabolic parameters are complicated by the presence of bacteria as a food source. Axenic liquid media (growth media that does not require the addition of bacteria as a food source) has been developed to overcome this difficulty [236], however the preparation of axenic *C. elegans* cultures is elaborate. Also, the elimination of bacteria from liquid cultures serves as an obstacle to nematode RNAi gene knockdown, which traditionally has been performed through feeding *C. elegans* bacteria expressing gene-targeted dsRNA, and it is incompatible with currently-available RNAi libraries. Methods have been established for killing dsRNA-expressing *Escherichia coli*

prior to experimentation, using either ultraviolet light or γ-irradiation [237], but these methods damage dsRNA needed for RNAi, require dedicated equipment, and are difficult to scale to the quantities necessary for high-throughput screening. Given the interest in *C. elegans* use for aging research, whole-genome large-scale RNAi knockdown screens have been performed to identify genetic factors regulating lifespan [238-241]. Due to the difficulties in assaying metabolic parameters though, similar screens have not been performed to identify genes associated with many age-related changes. Therefore, we set out to investigate the broader physiological context of *C. elegans* aging (through metabolomic and proteomic analysis of young and old nematodes) and to develop novel high-throughput RNAi knockdown assays for measuring relevant age-dependent metabolic parameters.

1.5 Hypothesis and Objectives

Broad-scale biological screening itself generally serves as a hypothesis-generating procedure, however for the work reported here we hypothesize that the protein and metabolite changes observed between young and old *C. elegans* will reflect the overall age-related changes discussed above, and that through the use of optimized experimental techniques semi-automated 96-well plate RNAi screens can be used to identify genes responsible for the aging-related loss of mitochondrial function and those responsible for limiting viability in the presence of toxic calcium levels in the culture media.

Specific aim 1 (Chapter 2): Determine age-related changes in metabolite composition and protein levels in *C. elegans*.

Aim 1.1 Perform a metabolomic analysis of young and old *C. elegans* and determine aging-induced changes. Age-synchronization of the culture will be maintained using the conditionally-sterile SS104 strain of *C. elegans*, which expresses a temperature-sensitive mutant allele of *glp-4* (abnormal germ line proliferation 4) that restricts germ cell development when cultured at 25 °C. Days 4 and 10 of culture will be sampled as the young and aged groups, respectively.

Aim 1.2 Perform a proteomic analysis of young and old *C. elegans* and determine aging-induced changes. To allow adequate comparison to the proteomic results, days 4 and 10 of culture will be sampled as representative of young and aged nematodes. A stable-isotope incorporation strategy will be employed to improve proteomic quantitation, utilizing $^{15}N_4$-$^{13}C_6$-arginine and $^{15}N_2$-$^{13}C_6$-lysine. Furthermore, to prevent the complicating enzymatic conversion of isotopically-labeled arginine into isotopically-labeled proline, expression of the ornithine transaminase 1 gene ORN-1 will be knocked-down using RNAi.

Specific aim 2 (Chapter 3): Investigate long-term microplate *C. elegans* liquid culturing methods that reduce or prevent evaporation, and determine an appropriate normalizing parameter for the number of live *C. elegans* in culture that is required due to the high variation in numbers per well when pipetting nematodes into microplates.

Aim 2.1 Determine the effectiveness of several microplate sealing methods, and examine both the correspondence of green fluorescence of several GFP-expressing strains of *C. elegans* to the total volume of live nematodes in culture and the anthranilate autofluorescence to the rate of nematode death in culture.

Aim 2.2 As a proof of principle for assay culture conditions and normalization methods, perform a small-scale RNAi screen of Ca^{2+}-binding EF-hand genes in the presence of toxic high Ca^{2+} levels to identify genes mediatingCa^{2+}-induced nematode death.

Specific aim 3 (Chapter 4): Determine ideal bacterial treatment methods and conditions for performing RNAi gene knockdown using dead *E. coli*, and perform a small-scale RNAi screen for genes affecting the age-related decline in *C. elegans* oxygen consumption, ATP content, and reductive capacity.

Aim 2.3 Perform a screen of *E. coli* treatment methods and conditions that preserves dsRNA for adequate RNAi gene knockdown.

Aim 2.4 Perform a small-scale screen using dead *E. coli* and RNAi knockdown of genes on the *C. elegans* X chromosome, assaying for RNAi clones that delay the age-related decline in oxygen consumption, ATP content, and reductive capacity in *C. elegans*.

1.6 Impact and Significance

The overall goal of this project is to develop a better understanding of factors affecting specific age-related changes. Due to the many similarities between *C. elegans* and mammalian aging, insights obtained through these experiments will shed light on the factors behind similar age-related changes in humans.

1.7 References

1. Terzibasi E, Valenzano DR, Cellerino A. The short-lived fish nothobranchius furzeri as a new model system for aging studies. Exp Gerontol. 2007;42(1-2):81-9. doi: 10.1016/j.exger.2006.06.039. PubMed PMID: WOS:000243648500013.

2. Wisshak M, López Correa M, Gofas S, Salas C, Taviani M, Jakobsen J, et al. Shell architecture, element composition, and stable isotope signature of the giant deep-sea oyster neopycnodonte zibrowii sp. N. From the ne atlantic. Deep Sea Research Part I: Oceanographic Research Papers. 2009;56(3):374-407.

3. Ladiges W, Van Remmen H, Strong R, Ikeno Y, Treuting P, Rabinovitch P, et al. Lifespan extension in genetically modified mice. Aging Cell. 2009;8(4):346-52. doi: 10.1111/j.1474-9726.2009.00491.x. PubMed PMID: WOS:000268213300001.

4. Lopez-Otin C, Blasco MA, Partridge L, Serrano M, Kroemer G. The hallmarks of aging. Cell. 2013;153(6):1194-217. doi: 10.1016/j.cell.2013.05.039. PubMed PMID: 23746838; PubMed Central PMCID: PMC3836174.

5. Conboy IM, Rando TA. Aging, stem cells and tissue regeneration: Lessons from muscle. Cell Cycle. 2005;4(3):407-10. Epub 2005/02/24. PubMed PMID: 15725724.

6. Rossi DJ, Bryder D, Seita J, Nussenzweig A, Hoeijmakers J, Weissman IL. Deficiencies in DNA damage repair limit the function of haematopoietic stem cells with age. Nature. 2007;447(7145):725-9.

7. Janzen V, Forkert R, Fleming HE, Saito Y, Waring MT, Dombkowski DM, et al. Stem-cell ageing modified by the cyclin-dependent kinase inhibitor p16ink4a. Nature. 2006;443(7110):421-6.

8. Rera M, Bahadorani S, Cho J, Koehler CL, Ulgherait M, Hur JH, et al. Modulation of longevity and tissue homeostasis by the drosophila pgc-1 homolog. Cell metabolism. 2011;14(5):623-34.

9. Chakkalakal JV, Jones KM, Basson MA, Brack AS. The aged niche disrupts muscle stem cell quiescence. Nature. 2012;490(7420):355-60.

10. Mostoslavsky R, Chua KF, Lombard DB, Pang WW, Fischer MR, Gellon L, et al. Genomic instability and aging-like phenotype in the absence of mammalian sirt6. Cell. 2006;124(2):315-29.

11. Conboy IM, Rando TA. Heterochronic parabiosis for the study of the effects of aging on stem cells and their niches. Cell Cycle. 2012;11(12):2260-7.

12. Gruber R, Koch H, Doll BA, Tegtmeier F, Einhorn TA, Hollinger JO. Fracture healing in the elderly patient. Exp Gerontol. 2006;41(11):1080-93.

13. Conboy IM, Conboy MJ, Wagers AJ, Girma ER, Weissman IL, Rando TA. Rejuvenation of aged progenitor cells by exposure to a young systemic environment. Nature. 2005;433(7027):760-4.

14. Villeda SA, Luo J, Mosher KI, Zou B, Britschgi M, Bieri G, et al. The ageing systemic milieu negatively regulates neurogenesis and cognitive function. Nature. 2011;477(7362):90-4.

15. Conboy IM, Yousef H, Conboy MJ. Embryonic anti-aging niche. Aging (Albany NY). 2011;3(5):555.

16. Conboy IM, Conboy MJ, Smythe GM, Rando TA. Notch-mediated restoration of regenerative potential to aged muscle. Science. 2003;302(5650):1575-7.

17. Carlson ME, Conboy MJ, Hsu M, Barchas L, Jeong J, Agrawal A, et al. Relative roles of tgf-β1 and wnt in the systemic regulation and aging of satellite cell responses. Aging Cell. 2009;8(6):676-89.

18. Ergen AV, Goodell MA. Mechanisms of hematopoietic stem cell aging. Exp Gerontol. 2010;45(4):286-90.

19. Stenderup K, Justesen J, Clausen C, Kassem M. Aging is associated with decreased maximal life span and accelerated senescence of bone marrow stromal cells. Bone. 2003;33(6):919-26.

20. Lu C, Miclau T, Hu D, Hansen E, Tsui K, Puttlitz C, et al. Cellular basis for age-related changes in fracture repair. Journal of orthopaedic research. 2005;23(6):1300-7.

21. Miljkovic N, Lim JY, Miljkovic I, Frontera WR. Aging of skeletal muscle fibers. Ann Rehabil Med. 2015;39(2):155-62. Epub 2015/05/02. doi: 10.5535/arm.2015.39.2.155. PubMed PMID: 25932410; PubMed Central PMCID: PMCPMC4414960.

22. Price FD, von Maltzahn J, Bentzinger CF, Dumont NA, Yin H, Chang NC, et al. Inhibition of jak-stat signaling stimulates adult satellite cell function. Nat Med. 2014;20(10):1174-81. Epub 2014/09/10. doi: 10.1038/nm.3655. PubMed PMID: 25194569; PubMed Central PMCID: PMCPMC4191983.

23. Lavasani M, Robinson AR, Lu A, Song M, Feduska JM, Ahani B, et al. Muscle-derived stem/progenitor cell dysfunction limits healthspan and lifespan in a murine progeria model. Nature communications. 2012;3:608.

24. Hayflick L, Moorhead PS. The serial cultivation of human diploid cell strains. Experimental cell research. 1961;25(3):585-621.

25. Bodnar AG, Ouellette M, Frolkis M, Holt SE, Chiu C-P, Morin GB, et al. Extension of life-span by introduction of telomerase into normal human cells. Science. 1998;279(5349):349-52.

26. Adams PD, Sedivy JM. Cellular senescence and tumor suppression: Springer; 2010.

27. Cho S, Park J, Hwang ES. Kinetics of the cell biological changes occurring in the progression of DNA damage-induced senescence. Molecules and cells. 2011;31(6):539-46.

28. Hwang ES, Yoon G, Kang HT. A comparative analysis of the cell biology of senescence and aging. Cellular and molecular life sciences. 2009;66(15):2503-24.

29. Dimri GP, Lee X, Basile G, Acosta M, Scott G, Roskelley C, et al. A biomarker that identifies senescent human cells in culture and in aging skin in vivo. Proceedings of the National Academy of Sciences. 1995;92(20):9363-7.

30. Campisi J, di Fagagna FdA. Cellular senescence: When bad things happen to good cells. Nature reviews Molecular cell biology. 2007;8(9):729-40.

31. Krizhanovsky V, Xue W, Zender L, Yon M, Hernando E, Lowe S, editors. Implications of cellular senescence in tissue damage response, tumor suppression, and stem cell biology. Cold Spring Harbor symposia on quantitative biology; 2008: Cold Spring Harbor Laboratory Press.

32. Kuilman T, Michaloglou C, Mooi WJ, Peeper DS. The essence of senescence. Genes & development. 2010;24(22):2463-79.

33. Rodier F, Campisi J. Four faces of cellular senescence. The Journal of cell biology. 2011;192(4):547-56.

34. Baker DJ, Wijshake T, Tchkonia T, LeBrasseur NK, Childs BG, van de Sluis B, et al. Clearance of p16ink4a-positive senescent cells delays ageing-associated disorders. Nature. 2011;479(7372):232-6.

35. Hoenicke L, Zender L. Immune surveillance of senescent cells—biological significance in cancer-and non-cancer pathologies. Carcinogenesis. 2012:bgs124.

36. Kang T-W, Yevsa T, Woller N, Hoenicke L, Wuestefeld T, Dauch D, et al. Senescence surveillance of pre-malignant hepatocytes limits liver cancer development. Nature. 2011;479(7374):547-51.

37. Xue W, Zender L, Miething C, Dickins RA, Hernando E, Krizhanovsky V, et al. Senescence and tumour clearance is triggered by p53 restoration in murine liver carcinomas. Nature. 2007;445(7128):656-60.

38. Wang C, Jurk D, Maddick M, Nelson G, Martin-Ruiz C, Von Zglinicki T. DNA damage response and cellular senescence in tissues of aging mice. Aging Cell. 2009;8(3):311-23.

39. Blasco MA. Telomere length, stem cells and aging. Nature chemical biology. 2007;3(10):640-9.

40. Horvath S. DNA methylation age of human tissues and cell types. Genome biology. 2013;14(10):R115.

41. Maegawa S, Hinkal G, Kim HS, Shen L, Zhang L, Zhang J, et al. Widespread and tissue specific age-related DNA methylation changes in mice. Genome research. 2010;20(3):332-40.

42. Oberdoerffer P, Sinclair DA. The role of nuclear architecture in genomic instability and ageing. Nature Reviews Molecular Cell Biology. 2007;8(9):692-702.

43. Pollina E, Brunet A. Epigenetic regulation of aging stem cells. Oncogene. 2011;30(28):3105-26.

44. Greer EL, Maures TJ, Hauswirth AG, Green EM, Leeman DS, Maro GS, et al. Members of the h3k4 trimethylation complex regulate lifespan in a germline-dependent manner in c. Elegans. Nature. 2010;466(7304):383-7.

45. Siebold AP, Banerjee R, Tie F, Kiss DL, Moskowitz J, Harte PJ. Polycomb repressive complex 2 and trithorax modulate drosophila longevity and stress resistance. Proceedings of the National Academy of Sciences. 2010;107(1):169-74.

46. Jin C, Li J, Green CD, Yu X, Tang X, Han D, et al. Histone demethylase utx-1 regulates c. Elegans life span by targeting the insulin/igf-1 signaling pathway. Cell metabolism. 2011;14(2):161-72.

47. Kaeberlein M, McVey M, Guarente L. The sir2/3/4 complex and sir2 alone promote longevity in saccharomyces cerevisiae by two different mechanisms. Genes & development. 1999;13(19):2570-80.

48. Burnett C, Valentini S, Cabreiro F, Goss M, Somogyvári M, Piper MD, et al. Absence of effects of sir2 overexpression on lifespan in c. Elegans and drosophila. nature. 2011;477(7365):482-5.

49. Viswanathan M, Guarente L. Regulation of caenorhabditis elegans lifespan by sir-2.1 transgenes. Nature. 2011;477(7365):E1-E2.

50. Herranz D, Muñoz-Martin M, Cañamero M, Mulero F, Martinez-Pastor B, Fernandez-Capetillo O, et al. Sirt1 improves healthy ageing and protects from metabolic syndrome-associated cancer. Nature communications. 2010;1:3.

51. Kanfi Y, Naiman S, Amir G, Peshti V, Zinman G, Nahum L, et al. The sirtuin sirt6 regulates lifespan in male mice. Nature. 2012;483(7388):218-21.

52. Li W, Prazak L, Chatterjee N, Gruninger S, Krug L, Theodorou D, et al. Activation of transposable elements during aging and neuronal decline in drosophila. Nat Neurosci. 2013;16(5):529-31. Epub 2013/04/09. doi: 10.1038/nn.3368. PubMed PMID: 23563579; PubMed Central PMCID: PMCPMC3821974.

53. De Cecco M, Criscione SW, Peterson AL, Neretti N, Sedivy JM, Kreiling JA. Transposable elements become active and mobile in the genomes of aging mammalian somatic tissues. Aging (Albany NY). 2013;5(12):867.

54. Paradies G, Petrosillo G, Paradies V, Ruggiero FM. Mitochondrial dysfunction in brain aging: Role of oxidative stress and cardiolipin. Neurochemistry international. 2011;58(4):447-57.

55. Navratil M, Terman A, Arriaga EA. Giant mitochondria do not fuse and exchange their contents with normal mitochondria. Experimental cell research. 2008;314(1):164-72.

56. Terman A, Gustafsson B, Brunk UT. Mitochondrial damage and intralysosomal degradation in cellular aging. Molecular aspects of medicine. 2006;27(5):471-82.

57. Wei Y-H, Wu S-B, Ma Y-S, Lee H-C. Respiratory function decline and DNA mutation in mitochondria, oxidative stress and altered gene expression during aging. Chang Gung Med J. 2009;32(2):113-32.

58. Brewer GJ. Epigenetic oxidative redox shift (eors) theory of aging unifies the free radical and insulin signaling theories. Exp Gerontol. 2010;45(3):173-9.

59. Terman A, Kurz T, Navratil M, Arriaga EA, Brunk UT. Mitochondrial turnover and aging of long-lived postmitotic cells: The mitochondrial-lysosomal axis theory of aging. Antioxid Redox Signal. 2010;12(4):503-35. doi: 10.1089/ars.2009.2598. PubMed PMID: WOS:000273845700006.

60. Menzies RA, Gold PH. The turnover of mitochondria in a variety of tissues of young adult and aged rats. Journal of Biological Chemistry. 1971;246(8):2425.

61. Aschenbrenner V, Druyan R, Albin R, Rabinowitz M. Haem a, cytochrome c and total protein turnover in mitochondria from rat heart and liver. Biochemical Journal. 1970;119(2):157.

62. Miwa S, Lawless C, Von Zglinicki T. Mitochondrial turnover in liver is fast in vivo and is accelerated by dietary restriction: Application of a simple dynamic model. Aging Cell. 2008;7(6):920-3.

63. Seglen P, Gordon P, Holen I, editors. Non-selective autophagy1990.

64. Takano-Ohmuro H, Mukaida M, Kominami E, Morioka K. Autophagy in embryonic erythroid cells: Its role in maturation. European Journal of Cell Biology. 2000;79(10):759-64.

65. Davis WL, Jacoby B, Goodman DBP. Immunolocalization of ubiquitin in degenerating insect flight muscle. The Histochemical Journal. 1994;26(4):298-305.

66. Shitara H, Kaneda H, Sato A, Inoue K, Ogura A, Yonekawa H, et al. Selective and continuous elimination of mitochondria microinjected into mouse eggs from spermatids, but not from liver cells, occurs throughout embryogenesis. Genetics. 2000;156(3):1277.

67. Sutovsky P, Moreno RD, Ramalho-Santos J, Dominko T, Simerly C, Schatten G. Ubiquitinated sperm mitochondria, selective proteolysis, and the regulation of mitochondrial inheritance in mammalian embryos. Biology of Reproduction. 2000;63(2):582.

68. Kim I, Mizushima N, Lemasters J. Selective removal of damaged mitochondria by autophagy (mitophagy). Hepatology. 2006;44.

69. Kim I, Rodriguez-Enriquez S, Lemasters JJ. Selective degradation of mitochondria by mitophagy. Archives of Biochemistry and Biophysics. 2007;462(2):245-53.

70. Pallanck LJ. Culling sick mitochondria from the herd. The Journal of Cell Biology. 2010;191(7):1225.

71. Matsuda N, Sato S, Shiba K, Okatsu K, Saisho K, Gautier CA, et al. Pink1 stabilized by mitochondrial depolarization recruits parkin to damaged mitochondria and activates latent parkin for mitophagy. The Journal of Cell Biology. 2010;189(2):211.

72. Rakovic A, Grünewald A, Kottwitz J, Brüggemann N, Pramstaller PP, Lohmann K, et al. Mutations in pink1 and parkin impair ubiquitination of mitofusins in human fibroblasts. Plos One. 2011;6(3):e16746.

73. Mitsuhashi S, Hatakeyama H, Karahashi M, Koumura T, Nonaka I, Hayashi YK, et al. Muscle choline kinase beta defect causes mitochondrial dysfunction and increased mitophagy. Human Molecular Genetics. 2011.

74. Clark IE, Dodson MW, Jiang C, Cao JH, Huh JR, Seol JH, et al. Drosophila pink1 is required for mitochondrial function and interacts genetically with parkin. Nature. 2006;441(7097):1162-6.

75. Yang Y, Gehrke S, Imai Y, Huang Z, Ouyang Y, Wang JW, et al. Mitochondrial pathology and muscle and dopaminergic neuron degeneration caused by inactivation of drosophila pink1 is rescued by parkin. Proceedings of the National Academy of Sciences. 2006;103(28):10793.

76. Twig G, Hyde B, Shirihai OS. Mitochondrial fusion, fission and autophagy as a quality control axis: The bioenergetic view. Biochimica et Biophysica Acta (BBA)-Bioenergetics. 2008;1777(9):1092-7.

77. Barsoum MJ, Yuan H, Gerencser AA, Liot G, Kushnareva Y, Gräber S, et al. Nitric oxide-induced mitochondrial fission is regulated by dynamin-related gtpases in neurons. The EMBO journal. 2006;25(16):3900-11.

78. Twig G, Elorza A, Molina AJA, Mohamed H, Wikstrom JD, Walzer G, et al. Fission and selective fusion govern mitochondrial segregation and elimination by autophagy. The EMBO journal. 2008;27(2):433-46.

79. Katajisto P, Dohla J, Chaffer CL, Pentinmikko N, Marjanovic N, Iqbal S, et al. Stem cells. Asymmetric apportioning of aged mitochondria between daughter cells is required for stemness. Science. 2015;348(6232):340-3. Epub 2015/04/04. doi: 10.1126/science.1260384 [doi]. PubMed PMID: 25837514; PubMed Central PMCID: PMC4405120.

80. Brunk UT, Terman A. The mitochondrial-lysosomal axis theory of aging. European Journal of Biochemistry. 2002;269(8):1996-2002.

81. de Grey AD. The reductive hotspot hypothesis of mammalian aging. European Journal of Biochemistry. 2002;269(8):2003-9.

82. Stroikin Y, Dalen H, Lööf S, Terman A. Inhibition of autophagy with 3-methyladenine results in impaired turnover of lysosomes and accumulation of lipofuscin-like material. European journal of cell biology. 2004;83(10):583-90.

83. Terman A, Dalen H, Eaton JW, Neuzil J, Brunk UT. Mitochondrial recycling and aging of cardiac myocytes: The role of autophagocytosis. Exp Gerontol. 2003;38(8):863-76.

84. Castello L, Maina M, Testa G, Cavallini G, Biasi F, Donati A, et al. Alternate-day fasting reverses the age-associated hypertrophy phenotype in rat heart by influencing the erk and pi3k signaling pathways. Mechanisms of ageing and development. 2011;132(6):305-14.

85. Safdar A, Bourgeois JM, Ogborn DI, Little JP, Hettinga BP, Akhtar M, et al. Endurance exercise rescues progeroid aging and induces systemic mitochondrial rejuvenation in mtdna mutator mice. Proceedings of the National Academy of Sciences. 2011;108(10):4135-40.

86. Rubinsztein DC, Mariño G, Kroemer G. Autophagy and aging. Cell. 2011;146(5):682-95.

87. Lane N. Oxygen: The molecule that made the world. Oxford: Oxford University Press; 2002. 374 p.

88. Davies MJ, Dean RT. Radical-mediated protein oxidation: From chemistry to medicine: Oxford University Press; 1997.

89. Dalle-Donne I, Scaloni A, Butterfield DA. Redox proteomics: From protein modifications to cellular dysfunction and diseases: Wiley-Interscience; 2006.

90. Commoner B, Townsend J, Pake GE. Free radicals in biological materials. Nature. 1954;174(4432):689.

91. Harman D. Aging: A theory based on free radical and radiation chemistry. J Gerontol. 1956;11(3):298-300. PubMed PMID: WOS:A1956CHD5000009.

92. Harman D. The biologic clock: The mitochondria? Journal of the American Geriatrics Society. 1972;20(4):145.

93. Sohal R, Svensson I, Sohal B, Brunk U. Superoxide anion radical production in different animal species. Mechanisms of Ageing and Development. 1989;49(2):129-35.

94. Sohal R, Svensson I, Brunk U. Hydrogen peroxide production by liver mitochondria in different species. Mechanisms of Ageing and Development. 1990;53(3):209-15.

95. Muller FL, Liu Y, Van Remmen H. Complex iii releases superoxide to both sides of the inner mitochondrial membrane. Journal of Biological Chemistry. 2004;279(47):49064.

96. Boveris A, Cadenas E, Stoppani A. Role of ubiquinone in the mitochondrial generation of hydrogen peroxide. Biochemical Journal. 1976;156(2):435.

97. Votyakova TV, Reynolds IJ. M dependent and independent production of reactive oxygen species by rat brain mitochondria. Journal of Neurochemistry. 2001;79(2):266-77.

98. Liu Y, Fiskum G, Schubert D. Generation of reactive oxygen species by the mitochondrial electron transport chain. Journal of Neurochemistry. 2002;80(5):780-7.

99. Fridovich I. Mitochondria: Are they the seat of senescence? Aging Cell. 2004;3(1):13-6.

100. Nauser T, Koppenol W. The rate constant of the reaction of superoxide with nitrogen monoxide: Approaching the diffusion limit. The Journal of Physical Chemistry A. 2002;106(16):4084-6.

101. de La Asunción JG, Millan A, Pla R, Bruseghini L, Esteras A, Pallardo F, et al. Mitochondrial glutathione oxidation correlates with age-associated oxidative damage to mitochondrial DNA. The FASEB journal. 1996;10(2):333.

102. Hansford RG. Lipid oxidation by heart mitochondria from young adult and senescent rats. Biochemical Journal. 1978;170(2):285.

103. Meany DL, Xie H, Thompson LDV, Arriaga EA, Griffin TJ. Identification of carbonylated proteins from enriched rat skeletal muscle mitochondria using affinity chromatography stable isotope labeling and tandem mass spectrometry. Proteomics. 2007;7(7):1150-63.

104. Sohal R, Ku HH, Agarwal S. Biochemical correlates of longevity in two closely related rodent species. Biochemical and Biophysical Research Communications. 1993;196(1):7-11.

105. Ku HH, Sohal R. Comparison of mitochondrial pro-oxidant generation and anti-oxidant defenses between rat and pigeon: Possible basis of variation in longevity and metabolic potential. Mechanisms of Ageing and Development. 1993;72(1):67-76.

106. Barja G, Cadenas S, Rojas C, Perez-Campo R, Lopez-Torres M. Low mitochondrial free radical production per unit o2 consumption can explain the simultaneous presence of high longevity and high aerobic metabolic rate in birds. Free radical research. 1994;21(5):317-27.

107. Sohal RS, Arnold LA, Sohal BH. Age-related changes in antioxidant enzymes and prooxidant generation in tissues of the rat with special reference to parameters in two insect species* 1. Free Radic Biol Med. 1990;9(6):495-500.

108. Zhang H, Go YM, Jones DP. Mitochondrial thioredoxin-2/peroxiredoxin-3 system functions in parallel with mitochondrial gsh system in protection against oxidative stress. Archives of Biochemistry and Biophysics. 2007;465(1):119-26.

109. Gus' kova RA, Ivanov II, Kol'tover VK, Akhobadze VV, Rubin AB. Permeability of bilayer lipid membranes for superoxide (o2-) radicals. Biochimica et Biophysica Acta (BBA)-Biomembranes. 1984;778(3):579-85.

110. Stone JR, Yang S. Hydrogen peroxide: A signaling messenger. Antioxid Redox Signal. 2006;8(3-4):243-70.

111. Grune T, Catalgol B, Jung T, Uversky V. Protein oxidation and aging: Wiley; 2012.

112. Chao C-C, Ma Y-S, Stadtman ER. Modification of protein surface hydrophobicity and methionine oxidation by oxidative systems. Proceedings of the National Academy of Sciences. 1997;94(7):2969-74.

113. Zull J, Smith S, Wiltshire R. Effect of methionine oxidation and deletion of amino-terminal residues on the conformation of parathyroid hormone. Circular dichroism studies. Journal of Biological Chemistry. 1990;265(10):5671-6.

114. PETROPOULOS I, Mary J, PERICHON M, FRIGUET B. Rat peptide methionine sulphoxide reductase: Cloning of the cdna, and down-regulation of gene expression and enzyme activity during aging. Biochem J. 2001;355:819-25.

115. Wells-Knecht MC, Lyons TJ, McCance DR, Thorpe SR, Baynes JW. Age-dependent increase in ortho-tyrosine and methionine sulfoxide in human skin collagen is not accelerated in diabetes. Evidence against a generalized increase in oxidative stress in diabetes. Journal of Clinical Investigation. 1997;100(4):839.

116. Stadtman ER, Moskovitz J, Berlett BS, Levine RL. Cyclic oxidation and reduction of protein methionine residues is an important antioxidant mechanism. Molecular and cellular biochemistry. 2002;234(1):3-9.

117. Moskovitz J, Bar-Noy S, Williams WM, Requena J, Berlett BS, Stadtman ER. Methionine sulfoxide reductase (msra) is a regulator of antioxidant defense and lifespan in mammals. Proceedings of the National Academy of Sciences. 2001;98(23):12920-5.

118. Ruan H, Tang XD, Chen M-L, Joiner M, Sun G, Brot N, et al. High-quality life extension by the enzyme peptide methionine sulfoxide reductase. Proceedings of the National Academy of Sciences. 2002;99(5):2748-53.

119. Gafni A, Noy N. Age-related effects in enzyme catalysis. Molecular and cellular biochemistry. 1984;59(1-2):113-29.

120. Yarian CS, Toroser D, Sohal RS. Aconitase is the main functional target of aging in the citric acid cycle of kidney mitochondria from mice. Mechanisms of ageing and development. 2006;127(1):79-84.

121. Smith MA, Harris PLR, Sayre LM, Beckman JS, Perry G. Widespread peroxynitrite-mediated damage in alzheimer's disease. The Journal of neuroscience. 1997;17(8):2653-7.

122. Leeuwenburgh C, Hardy MM, Hazen SL, Wagner P, Oh-ishi S, Steinbrecher UP, et al. Reactive nitrogen intermediates promote low density lipoprotein oxidation in human atherosclerotic intima. Journal of Biological Chemistry. 1997;272(3):1433-6.

123. Tomaru U, Takahashi S, Ishizu A, Miyatake Y, Gohda A, Suzuki S, et al. Decreased proteasomal activity causes age-related phenotypes and promotes the development of metabolic abnormalities. The American journal of pathology. 2012;180(3):963-72.

124. Kiffin R, Christian C, Knecht E, Cuervo AM. Activation of chaperone-mediated autophagy during oxidative stress. Molecular biology of the cell. 2004;15(11):4829-40.

125. Merker K, Sitte N, Grune T. Hydrogen peroxide-mediated protein oxidation in young and old human mrc-5 fibroblasts. Archives of biochemistry and biophysics. 2000;375(1):50-4.

126. Passi A, Albertini R, Bardoni A, Rindi S, Salvini R, Pallavicini G, et al. Modifications of proteoglycans produced by human skin fibroblast cultures during replicative senescence. Cell biochemistry and function. 1993;11(4):263-9.

127. Hodge JE. Dehydrated foods, chemistry of browning reactions in model systems. Journal of Agricultural and Food Chemistry. 1953;1(15):928-43.

128. Nagaraj RH, Shipanova IN, Faust FM. Protein cross-linking by the maillard reaction isolation, characterization, and in vivo detection of a lysine-lysine cross-link derived from methylglyoxal. Journal of Biological Chemistry. 1996;271(32):19338-45.

129. Fleenor BS. Large elastic artery stiffness with aging: Novel translational mechanisms and interventions. Aging Dis. 2013;4(2):76-83. Epub 2013/05/23. PubMed PMID: 23696949; PubMed Central PMCID: PMCPMC3659253.

130. Sell DR, Monnier VM. Molecular basis of arterial stiffening: Role of glycation - a mini-review. Gerontology. 2012;58(3):227-37. Epub 2012/01/10. doi: 10.1159/000334668. PubMed PMID: 22222677.

131. Requena JR, Stadtman ER. Conversion of lysine to n ϵ-(carboxymethyl) lysine increases susceptibility of proteins to metal-catalyzed oxidation. Biochemical and biophysical research communications. 1999;264(1):207-11.

132. Thornalley PJ. Advanced glycation and the development of diabetic complications. Unifying the involvement of glucose, methylglyoxal and oxidative stress. Endocrinology And Metabolism-London-. 1996;3:149-66.

133. Nowotny K, Jung T, Hohn A, Weber D, Grune T. Advanced glycation end products and oxidative stress in type 2 diabetes mellitus. Biomolecules. 2015;5(1):194-222. Epub 2015/03/19. doi: 10.3390/biom5010194. PubMed PMID: 25786107; PubMed Central PMCID: PMCPMC4384119.

134. Cerami A. Hypothesis. Glucose as a mediator of aging. Journal of the American Geriatrics Society. 1985;33(9):626-34.

135. Monnier V, Sell D, Nagaraj R, Miyata S. Mechanisms of protection against damage mediated by the maillard reaction in aging. Gerontology. 1991;37(1-3):152-65.

136. Neeper M, Schmidt AM, Brett J, Yan SD, Wang F, Pan YCE, et al. Cloning and expression of a cell-surface receptor for advanced glycosylation end-products of proteins. Journal of Biological Chemistry. 1992;267(21):14998-5004. PubMed PMID: ISI:A1992JF08800074.

137. Sparvero LJ, Asafu-Adjei D, Kang R, Tang DL, Amin N, Im J, et al. Rage (receptor for advanced glycation endproducts), rage ligands, and their role in cancer and inflammation. J Transl Med. 2009;7:21. doi: 10.1186/1479-5876-7-17. PubMed PMID: ISI:000265143700001.

138. Bierhaus A, Humpert PM, Morcos M, Wendt T, Chavakis T, Arnold B, et al. Understanding rage, the receptor for advanced glycation end products. J Mol Med. 2005;83(11):876-86. doi: 10.1007/s00109-005-0688-7. PubMed PMID: ISI:000233938500006.

139. Li JH, Wang WS, Huang XR, Oldfield M, Schmidt AM, Cooper ME, et al. Advanced glycation end products induce tubular epithelial-myofibroblast transition through the rage-erk1/2 map kinase signaling pathway. Am J Pathol. 2004;164(4):1389-97. PubMed PMID: ISI:000220410900027.

140. Yeh CH, Sturgis L, Haidacher J, Zhang XN, Sherwood SJ, Bjercke RJ, et al. Requirement for p38 and p44/p42 mitogen-activated protein kinases in rage-mediated nuclear factor-kappa b transcriptional activation and cytokine secretion. Diabetes. 2001;50(6):1495-504. PubMed PMID: ISI:000168961900033.

141. Huang JS, Guh JY, Chen HC, Hung WC, Lai YH, Chuang LY. Role of receptor for advanced glycation end-product (rage) and the jak/stat-signaling pathway in age-induced collagen production in nrk-49f cells. J Cell Biochem. 2001;81(1):102-13. PubMed PMID: ISI:000167248700009.

142. Wautier MP, Chappey O, Corda S, Stern DM, Schimidt AM, Wautier JL. Activation of nadph oxidase by age links oxidant stress to altered gene expression via rage. Am J Physiol-Endocrinol Metab. 2001;280(5):E685-E94. PubMed PMID: ISI:000168125800002.

143. Ramasamy R, Vannucci SJ, Yan SSD, Herold K, Yan SF, Schmidt AM. Advanced glycation end products and rage: A common thread in aging, diabetes, neurodegeneration, and inflammation. Glycobiology. 2005;15(7):16R-28R. doi: 10.1093/glycob/cwi053. PubMed PMID: ISI:000230002800002.

144. Chavakis T, Bierhaus A, Nawroth PP. Rage (receptor for advanced glycation end products): A central player in the inflammatory response. Microbes Infect. 2004;6(13):1219-25. doi: 10.1016/j.micinf.2004.08.004. PubMed PMID: ISI:000224728700012.

145. Bierhaus A, Stern DM, Nawroth PP. Rage in inflammation: A new therapeutic target? Curr Opin Investig Drugs. 2006;7(11):985-91. PubMed PMID: ISI:000241571200005.

146. Hofmann MA, Drury S, Fu CF, Qu W, Taguchi A, Lu Y, et al. Rage mediates a novel proinflammatory axis: A central cell surface receptor for s100/calgranulin polypeptides. Cell. 1999;97(7):889-901. PubMed PMID: ISI:000081162800010.

147. Riehl A, Nemeth J, Angel P, Hess J. The receptor rage: Bridging inflammation and cancer. Cell Commun Signal. 2009;7:7. doi: 10.1186/1478-811x-7-12. PubMed PMID: ISI:000271931100001.

148. Brunk UT, Terman A. Lipofuscin: Mechanisms of age-related accumulation and influence on cell function. Free Radical Biology and Medicine. 2002;33(5):611-9.

149. Strehler BL, Mark DD, Mildvan AS, Gee MV. Rate and magnitude of age pigment accumulation in the human myocardium. Journal of Gerontology. 1959;14(4):430.

150. Sheehy MRJ, Greenwood JG, Fielder DR. Lipofuscin as a record of "rate of living" in an aquatic poikilotherm. The Journals of Gerontology Series A: Biological Sciences and Medical Sciences. 1995;50(6):B327.

151. Nakano M, Gotoh S. Accumulation of cardiac lipofuscin depends on metabolic rate of mammals. Journal of Gerontology. 1992;47(4):B126.

152. Munnell JF, Getty R. Rate of accumulation of cardiac lipofuscin in the aging canine. Journal of Gerontology. 1968;23(2):154.

153. Terman A, Brunk UT. On the degradability and exocytosis of ceroid/lipofuscin in cultured rat cardiac myocytes. Mechanisms of Ageing and Development. 1998;100(2):145-56.

154. Terman A, Brunk UT. Ceroid/lipofuscin formation in cultured human fibroblasts: The role of oxidative stress and lysosomal proteolysis. Mechanisms of Ageing and Development. 1998;104(3):277-91.

155. Elleder M, Drahota Z, Lisa V, Mare V, Mandys V, Müller J, et al. Tissue culture loading test with storage granules from animal models of neuronal ceroid lipofuscinosis (batten disease): Testing their lysosomal degradability by normal and batten cells. American journal of medical genetics. 1995;57(2):213-21.

156. Terman A. Garbage catastrophe theory of aging: Imperfect removal of oxidative damage? Redox report. 2001;6(1):15-26.

157. Treff W. Das involutionsmuster des nucleus dentatus cerebelli: Eine morphometrische analyse. Altern Zentralnervensystem-Pharmaka-Stoffwechsel Schattauer, Stuttgart-New York. 1974.

158. Sundelin S, Wihlmark U, Nilsson SEG, Brunk UT. Lipofuscin accumulation in cultured retinal pigment epithelial cells reduces their phagocytic capacity. Current eye research. 1998;17(8):851-7.

159. Terman A, Dalen H, Brunk UT. Ceroid/lipofuscin-loaded human fibroblasts show decreased survival time and diminished autophagocytosis during amino acid starvation. Exp Gerontol. 1999;34(8):943-57.

160. Terman A. The effect of age on formation and elimination of autophagic vacuoles in mouse hepatocytes. Gerontology. 1995;41(2):319-26.

161. Bowen RL, Atwood CS. Living and dying for sex. A theory of aging based on the modulation of cell cycle signaling by reproductive hormones. Gerontology. 2004;50(5):265-90. Epub 2004/08/28. doi: 10.1159/000079125. PubMed PMID: 15331856.

162. Vadakkadath Meethal S, Atwood CS. The role of hypothalamic-pituitary-gonadal hormones in the normal structure and functioning of the brain. Cell Mol Life Sci. 2005;62(3):257-70. Epub 2005/02/22. doi: 10.1007/s00018-004-4381-3. PubMed PMID: 15723162.

163. Singh P. Andropause: Current concepts. Indian J Endocrinol Metab. 2013;17(Suppl 3):S621-9. Epub 2014/06/10. doi: 10.4103/2230-8210.123552. PubMed PMID: 24910824; PubMed Central PMCID: PMCPMC4046605.

164. Atwood CS, Bowen RL. The reproductive-cell cycle theory of aging: An update. Exp Gerontol. 2011;46(2-3):100-7. Epub 2010/09/21. doi: 10.1016/j.exger.2010.09.007. PubMed PMID: 20851172.

165. Yin W, Gore AC. Neuroendocrine control of reproductive aging: Roles of gnrh neurons. Reproduction. 2006;131(3):403-14. Epub 2006/03/04. doi: 10.1530/rep.1.00617. PubMed PMID: 16514184.

166. Zhang G, Li J, Purkayastha S, Tang Y, Zhang H, Yin Y, et al. Hypothalamic programming of systemic ageing involving ikk-[bgr], nf-[kgr] b and gnrh. Nature. 2013;497(7448):211-6.

167. Mason JB, Cargill SL, Anderson GB, Carey JR. Transplantation of young ovaries to old mice increased life span in transplant recipients. J Gerontol A Biol Sci Med Sci. 2009;64(12):1207-11. Epub 2009/09/25. doi: 10.1093/gerona/glp134. PubMed PMID: 19776215; PubMed Central PMCID: PMCPMC2773817.

168. Cargill SL, Carey JR, Muller HG, Anderson G. Age of ovary determines remaining life expectancy in old ovariectomized mice. Aging Cell. 2003;2(3):185-90. Epub 2003/07/29. PubMed PMID: 12882411; PubMed Central PMCID: PMCPMC2386250.

169. Manly JJ, Merchant CA, Jacobs DM, Small SA, Bell K, Ferin M, et al. Endogenous estrogen levels and alzheimer's disease among postmenopausal women. Neurology. 2000;54(4):833-7. Epub 2000/02/26. PubMed PMID: 10690972.

170. Burkhardt MS, Foster JK, Clarnette RM, Chubb SP, Bruce DG, Drummond PD, et al. Interaction between testosterone and apolipoprotein e ε4 status on cognition in healthy older men. The Journal of Clinical Endocrinology & Metabolism. 2006;91(3):1168-72.

171. Deeks SG. Hiv infection, inflammation, immunosenescence, and aging. Annu Rev Med. 2011;62:141-55. Epub 2010/11/26. doi: 10.1146/annurev-med-042909-093756. PubMed PMID: 21090961; PubMed Central PMCID: PMCPMC3759035.

172. Czesnikiewicz-Guzik M, Lee WW, Cui D, Hiruma Y, Lamar DL, Yang ZZ, et al. T cell subset-specific susceptibility to aging. Clin Immunol. 2008;127(1):107-18. Epub 2008/01/29. doi: 10.1016/j.clim.2007.12.002. PubMed PMID: 18222733; PubMed Central PMCID: PMCPMC2435295.

173. Deng Y, Jing Y, Campbell AE, Gravenstein S. Age-related impaired type 1 t cell responses to influenza: Reduced activation ex vivo, decreased expansion in ctl culture in vitro, and blunted response to influenza vaccination in vivo in the elderly. J Immunol. 2004;172(6):3437-46. Epub 2004/03/09. PubMed PMID: 15004143.

174. Salminen A, Kaarniranta K, Kauppinen A. Inflammaging: Disturbed interplay between autophagy and inflammasomes. Aging (Albany NY). 2012;4(3):166.

175. Davoli T, de Lange T. The causes and consequences of polyploidy in normal development and cancer. Annual review of cell and developmental biology. 2011;27:585-610.

176. Senovilla L, Vitale I, Martins I, Tailler M, Pailleret C, Michaud M, et al. An immunosurveillance mechanism controls cancer cell ploidy. Science. 2012;337(6102):1678-84.

177. Doles J, Storer M, Cozzuto L, Roma G, Keyes WM. Age-associated inflammation inhibits epidermal stem cell function. Genes & development. 2012;26(19):2144-53.

178. Adler AS, Sinha S, Kawahara TL, Zhang JY, Segal E, Chang HY. Motif module map reveals enforcement of aging by continual nf-κb activity. Genes & development. 2007;21(24):3244-57.

179. Xie J, Zhang X, Zhang L. Negative regulation of inflammation by sirt1. Pharmacological Research. 2013;67(1):60-7.

180. Gillum MP, Kotas ME, Erion DM, Kursawe R, Chatterjee P, Nead KT, et al. Sirt1 regulates adipose tissue inflammation. Diabetes. 2011;60(12):3235-45.

181. Yao H, Chung S, Hwang J-w, Rajendrasozhan S, Sundar IK, Dean DA, et al. Sirt1 protects against emphysema via foxo3-mediated reduction of premature senescence in mice. The Journal of clinical investigation. 2012;122(122 (6)):2032-45.

182. Zhang Z, Lowry SF, Guarente L, Haimovich B. Roles of sirt1 in the acute and restorative phases following induction of inflammation. Journal of Biological Chemistry. 2010;285(53):41391-401.

183. Kawahara TLA, Michishita E, Adler AS, Damian M, Berber E, Lin M, et al. Sirt6 links histone h3 lysine 9 deacetylation to nf-κb-dependent gene expression and organismal life span. Cell. 136(1):62-74. doi: 10.1016/j.cell.2008.10.052.

184. Rothgiesser KM, Erener S, Waibel S, Lüscher B, Hottiger MO. Sirt2 regulates nf-κb-dependent gene expression through deacetylation of p65 lys310. Journal of cell science. 2010;123(24):4251-8.

185. Barzilai N, Huffman DM, Muzumdar RH, Bartke A. The critical role of metabolic pathways in aging. Diabetes. 2012;61(6):1315-22.

186. Fontana L, Partridge L, Longo VD. Extending healthy life span—from yeast to humans. science. 2010;328(5976):321-6.

187. Kenyon CJ. The genetics of ageing. Nature. 2010;464(7288):504-12.

188. Takahashi Y, Kipnis D, Daughaday W. Growth hormone secretion during sleep. Journal of Clinical Investigation. 1968;47(9):2079.

189. Greenwood FC, Landon J. Growth hormone secretion in response to stress in man. Nature. 1966;210(5035):540-1. Epub 1966/04/30. PubMed PMID: 5960526.

190. Khatib N, Gaidhane S, Gaidhane AM, Khatib M, Simkhada P, Gode D, et al. Ghrelin: Ghrelin as a regulatory peptide in growth hormone secretion. J Clin Diagn Res. 2014;8(8):MC13-7. Epub 2014/10/11. doi: 10.7860/jcdr/2014/9863.4767. PubMed PMID: 25302229; PubMed Central PMCID: PMCPMC4190751.

191. Kim TW, Jeong JH, Hong SC. The impact of sleep and circadian disturbance on hormones and metabolism. Int J Endocrinol. 2015;2015:591729. Epub 2015/04/11. doi: 10.1155/2015/591729. PubMed PMID: 25861266; PubMed Central PMCID: PMCPMC4377487.

192. Kato Y, Murakami Y, Sohmiya M, Nishiki M. Regulation of human growth hormone secretion and its disorders. Intern Med. 2002;41(1):7-13. Epub 2002/02/13. PubMed PMID: 11838603.

193. Fontana L, Partridge L, Longo VD. Extending healthy life span—from yeast to humans. Science. 2010;328(5976):321.

194. Foukas LC, Bilanges B, Bettedi L, Pearce W, Ali K, Sancho S, et al. Long-term p110α pi3k inactivation exerts a beneficial effect on metabolism. EMBO molecular medicine. 2013;5(4):563-71.

195. Ortega-Molina A, Efeyan A, Lopez-Guadamillas E, Muñoz-Martin M, Gómez-López G, Cañamero M, et al. Pten positively regulates brown adipose function, energy expenditure, and longevity. Cell metabolism. 2012;15(3):382-94.

196. Schumacher B, van der Pluijm I, Moorhouse MJ, Kosteas T, Robinson AR, Suh Y, et al. Delayed and accelerated aging share common longevity assurance mechanisms. PLoS Genet. 2008;4(8):e1000161. Epub 2008/08/16. doi: 10.1371/journal.pgen.1000161. PubMed PMID: 18704162; PubMed Central PMCID: PMCPMC2493043.

197. Brenner S. The genetics of caenorhabditis elegans. Genetics. 1974;77(1):71-94. Epub 1974/05/01. PubMed PMID: 4366476; PubMed Central PMCID: PMCPMC1213120.

198. Stiernagle T. Maintenance of c. Elegans. C elegans. 1999;2:51-67.

199. Ward S, Carrel JS. Fertilization and sperm competition in the nematodecaenorhabditis elegans. Developmental biology. 1979;73(2):304-21.

200. Hodgkin J, Doniach T. Natural variation and copulatory plug formation in caenorhabditis elegans. Genetics. 1997;146(1):149-64.

201. Klass MR. Aging in the nematode caenorhabditis elegans: Major biological and environmental factors influencing life span. Mech Ageing Dev. 1977;6(6):413-29. Epub 1977/11/01. PubMed PMID: 926867.

202. Friedman DB, Johnson TE. A mutation in the age-1 gene in caenorhabditis elegans lengthens life and reduces hermaphrodite fertility. Genetics. 1988;118(1):75-86.

203. Kenyon C, Chang J, Gensch E, Rudner A, Tabtiang R. A c. Elegans mutant that lives twice as long as wild type. Nature. 1993;366(6454):461-4. Epub 1993/12/02. doi: 10.1038/366461a0. PubMed PMID: 8247153.

204. Apfeld J, Kenyon C. Cell nonautonomy of c. Elegans daf-2 function in the regulation of diapause and life span. Cell. 1998;95(2):199-210.

205. Gems D, Sutton AJ, Sundermeyer ML, Albert PS, King KV, Edgley ML, et al. Two pleiotropic classes of daf-2 mutation affect larval arrest, adult behavior, reproduction and longevity in caenorhabditis elegans. Genetics. 1998;150(1):129-55.

206. Kenyon C. The plasticity of aging: Insights from long-lived mutants. Cell. 2005;120(4):449-60.

207. Cohen E, Bieschke J, Perciavalle RM, Kelly JW, Dillin A. Opposing activities protect against age-onset proteotoxicity. Science. 2006;313(5793):1604-10.

208. Weinkove D, Halstead JR, Gems D, Divecha N. Long-term starvation and ageing induce age-1/pi 3-kinase-dependent translocation of daf-16/foxo to the cytoplasm. BMC Biol. 2006;4(1):1.

209. Tullet JM, Hertweck M, An JH, Baker J, Hwang JY, Liu S, et al. Direct inhibition of the longevity-promoting factor skn-1 by insulin-like signaling in c. Elegans. Cell. 2008;132(6):1025-38.

210. Tissenbaum HA. Genetics, life span, health span, and the aging process in caenorhabditis elegans. The Journals of Gerontology Series A: Biological Sciences and Medical Sciences. 2012;67(5):503-10.

211. Murshid A, Eguchi T, Calderwood SK. Stress proteins in aging and life span. International Journal of Hyperthermia. 2013;29(5):442-7.

212. Joshi PM, Riddle MR, Djabrayan NJV, Rothman JH. Caenorhabditis elegans as a model for stem cell biology. Developmental Dynamics. 2010;239(5):1539-54. doi: 10.1002/dvdy.22296.

213. Dmitrieva NI, Burg MB. High nacl promotes cellular senescence. Cell Cycle. 2007;6(24):3108-13.

214. Herndon LA, Schmeissner PJ, Dudaronek JM, Brown PA, Listner KM, Sakano Y, et al. Stochastic and genetic factors influence tissue-specific decline in ageing c. Elegans. Nature. 2002;419(6909):808-14.

215. Golden TR, Beckman KB, Lee AH, Dudek N, Hubbard A, Samper E, et al. Dramatic age-related changes in nuclear and genome copy number in the nematode caenorhabditis elegans. Aging Cell. 2007;6(2):179-88.

216. Meyer JN, Boyd WA, Azzam GA, Haugen AC, Freedman JH, Van Houten B. Decline of nucleotide excision repair capacity in aging caenorhabditis elegans. Genome Biol. 2007;8(5):R70. Epub 2007/05/03. doi: 10.1186/gb-2007-8-5-r70. PubMed PMID: 17472752; PubMed Central PMCID: PMCPMC1929140.

217. Maures TJ, Greer EL, Hauswirth AG, Brunet A. The h3k27 demethylase utx-1 regulates c. Elegans lifespan in a germline-independent, insulin-dependent manner. Aging Cell. 2011;10(6):980-90.

218. Edwards C, Canfield J, Copes N, Rehan M, Lipps D, Bradshaw PC. D-beta-hydroxybutyrate extends lifespan in c. Elegans. Aging (Albany NY). 2014;6(8):621-44. Epub 2014/08/17. PubMed PMID: 25127866; PubMed Central PMCID: PMCPMC4169858.

219. Chow DK, Glenn CF, Johnston JL, Goldberg IG, Wolkow CA. Sarcopenia in the caenorhabditis elegans pharynx correlates with muscle contraction rate over lifespan. Exp Gerontol. 2006;41(3):252-60.

220. Kurz CL, Tan MW. Regulation of aging and innate immunity in c. Elegans. Aging Cell. 2004;3(4):185-93.

221. Kurz CL, Chauvet S, Andrès E, Aurouze M, Vallet I, Michel GP, et al. Virulence factors of the human opportunistic pathogen serratia marcescens identified by in vivo screening. The EMBO journal. 2003;22(7):1451-60.

222. Laws TR, Harding SV, Smith MP, Atkins TP, Titball RW. Age influences resistance of caenorhabditis elegans to killing by pathogenic bacteria. FEMS microbiology letters. 2006;234(2):281-7.

223. Houthoofd K, Braeckman BP, Lenaerts I, Brys K, Matthijssens F, De Vreese A, et al. Daf-2 pathway mutations and food restriction in aging caenorhabditis elegans differentially affect metabolism. Neurobiology of aging. 2005;26(5):689-96.

224. Yasuda K, Ishii T, Suda H, Akatsuka A, Hartman PS, Goto S, et al. Age-related changes of mitochondrial structure and function in caenorhabditis elegans. Mechanisms of ageing and development. 2006;127(10):763-70.

225. Regmi SG, Rolland SG, Conradt B. Age-dependent changes in mitochondrial morphology and volume are not predictors of lifespan. Aging (Albany NY). 2014;6(2):118.

226. Morcos M, Du X, Pfisterer F, Hutter H, Sayed AA, Thornalley P, et al. Glyoxalase-1 prevents mitochondrial protein modification and enhances lifespan in caenorhabditis elegans. Aging Cell. 2008;7(2):260-9.

227. Fletcher B, Dillard C, Tappel A. Measurement of fluorescent lipid peroxidation products in biological systems and tissues. Analytical biochemistry. 1973;52(1):1-9.

228. Chio K, Tappel AL. Synthesis and characterization of the fluorescent products derived from malonaldehyde and amino acids. Biochemistry. 1969;8(7):2821-7.

229. Davis Jr BO, Anderson GL, Dusenbery DB. Total luminescence spectroscopy of fluorescence changes during aging in caenorhabditis elegans. Biochemistry. 1982;21(17):4089-95.

230. Klass MR. Aging in the nematode caenorhabditis elegans: Major biological and environmental factors influencing life span. Mechanisms of ageing and development. 1977;6:413-29.

231. Gerstbrein B, Stamatas G, Kollias N, Driscoll M. In vivo spectrofluorimetry reveals endogenous biomarkers that report healthspan and dietary restriction in caenorhabditis elegans. Aging Cell. 2005;4(3):127-37.

232. Garigan D, Hsu A-L, Fraser AG, Kamath RS, Ahringer J, Kenyon C. Genetic analysis of tissue aging in caenorhabditis elegans: A role for heat-shock factor and bacterial proliferation. Genetics. 2002;161(3):1101-12.

233. Coburn C, Allman E, Mahanti P, Benedetto A, Cabreiro F, Pincus Z, et al. Anthranilate fluorescence marks a calcium-propagated necrotic wave that promotes organismal death in c. Elegans. PLoS biology. 2013;11(7):e1001613.

234. Ahringer J. Reverse genetics. 2006.

235. Carralot J-P, Ogier A, Boese A, Genovesio A, Brodin P, Sommer P, et al. A novel specific edge effect correction method for rna interference screenings. Bioinformatics. 2012;28(2):261-8.

236. Samuel TK, Sinclair JW, Pinter KL, Hamza I. Culturing caenorhabditis elegans in axenic liquid media and creation of transgenic worms by microparticle bombardment. JoVE (Journal of Visualized Experiments). 2014;(90):e51796-e.

237. Sutphin GL, Kaeberlein M. Measuring caenorhabditis elegans life span on solid media. Journal of visualized experiments: JoVE. 2009;(27).

238. Hamilton B, Dong Y, Shindo M, Liu W, Odell I, Ruvkun G, et al. A systematic rnai screen for longevity genes in c. Elegans. Genes & development. 2005;19(13):1544-55.

239. Scholer LV, Moller TH, Norgaard S, Vestergaard L, Olsen A. Isolating genes involved with genotoxic drug response in the nematode caenorhabditis elegans using genome-wide rnai screening. Methods Mol Biol. 2012;920:27-38. Epub 2012/09/04. doi: 10.1007/978-1-61779-998-3_3. PubMed PMID: 22941594.

240. Houtkooper RH, Mouchiroud L, Ryu D, Moullan N, Katsyuba E, Knott G, et al. Mitonuclear protein imbalance as a conserved longevity mechanism. Nature. 2013;497(7450):451-7. Epub 2013/05/24. doi: 10.1038/nature12188. PubMed PMID: 23698443; PubMed Central PMCID: PMCPMC3663447.

241. Wang J, Robida-Stubbs S, Tullet JM, Rual JF, Vidal M, Blackwell TK. Rnai screening implicates a skn-1-dependent transcriptional response in stress resistance and longevity deriving from translation inhibition. PLoS Genet. 2010;6(8). Epub 2010/08/12. doi: 10.1371/journal.pgen.1001048. PubMed PMID: 20700440; PubMed Central PMCID: PMCPMC2916858.

CHAPTER 2:

METABOLOME AND PROTEOME CHANGES WITH AGING IN *CAENORHABDITIS ELEGANS*

2.1 Abstract

To expand the understanding of aging in the model organism *Caenorhabditis elegans*, global quantification of metabolite and protein levels in young and aged nematodes was performed using mass spectrometry. With age there was a decreased abundance of proteins functioning in transcription termination, mRNA degradation, mRNA stability, protein synthesis, and proteasomal function. Furthermore there was altered S-adenosyl methionine metabolism as well as a decreased abundance of the S-adenosyl methionine synthetase (SAMS-1) protein. Other aging-related changes included alterations in free fatty acid levels and composition, decreased levels of protein arginine methyltransferase-3 (PRMT-3) and poly(ADP-ribose) polymerase-1 (PME-1), a shift in the cellular redox state, an increase in sorbitol content, alterations in free amino acid levels, and indications of altered muscle function and sarcoplasmic reticulum Ca^{2+} homeostasis. There were also decreases in pyrimidine and purine metabolite levels, most markedly nitrogenous bases. Supplementing the culture medium with cytidine (a pyrimidine nucleoside) or hypoxanthine (a purine base) increased lifespan suggesting that aging-induced alterations in RNA or ribonucleotide metabolism may be limiting lifespan. An age-related increase in body size, lipotoxicity from ectopic yolk lipoprotein accumulation, and mitochondrial electron transport chain dysfunction altering the cellular NAD^+/NADH ratio may

explain many of these changes. In addition, dietary restriction in aged worms resulting from sarcopenia of the pharyngeal pump likely decreases the abundance of SAMS-1, possibly leading to decreased phosphatidylcholine levels, larger lipid droplets, and ER and mitochondrial stress. The complementary use of proteomics and metabolomics yielded unique insights into the molecular processes altered with age in *C. elegans*.

2.2 Introduction

The nematode *Caenorhabditis elegans* is used extensively as a model organism for investigating the molecular mechanisms of aging. The popularity of *C. elegans* as an aging model is largely due to its short lifespan (approximately 1.5 – 4 weeks depending on the temperature of incubation), and the ease at which it can be cultivated under laboratory conditions. *C. elegans* aging is characterized by a severe loss of muscle mass and function (sarcopenia), which gradually interferes with movement and the ingestion of food [1]. In addition aging results in an increased size of lipid droplets (LD) as egg yolk lipoproteins continue to be produced after reproduction ceases [2], and the appearance of enlarged dysfunctional mitochondria within cells [3]. Accordingly, aged *C. elegans* experience a dramatic decline in mitochondrial oxygen consumption, and ATP and ADP content, starting as early as the onset of adulthood [4, 5]. Aged *C. elegans* have also been shown to experience a loss of proteostasis and an accumulation of protein aggregates [6, 7], as well as oxidatively damaged proteins and lipids [8, 9]. Macromolecular damage in the form of the non-enzymatic formation of advanced glycation end-products are a part of normal *C. elegans* aging, with the reactive molecule methylglyoxal likely playing a role in limiting the *C. elegans* lifespan.

In 1988 the first genetic mutation resulting in increased longevity, the *C. elegans* phosphoinositide 3-kinase gene *age-1,* was identified [10]. Since that time, knowledge of genetic factors affecting the aging process has greatly expanded, and a search of the GenAge database (http://genomics.senescence.info/genes/) currently lists 741 *C. elegans* genes known to impact lifespan. Two conserved signaling pathways known to increase lifespan have been characterized in *C. elegans* [11-15]; one involves disruption of the insulin/IGF-1 receptor, DAF-2 (abnormal dauer formation-2) signaling pathway, while the other involves activation of the NAD^+-dependent histone deacetylase SIR-2.1. *C. elegans* loss-of-function mutations in *daf*-2 have an extended lifespan, which is dependent on the activation of the transcription factor DAF-16 (homologous to human FOXO proteins) [16-18]. Dietary restriction is one of the most consistent methods for producing lifespan extension in model organisms, activates DAF-16 through a decrease in PI3K/AKT signaling [19]. Activation of SIR-2.1, the *C. elegans* homolog of human SIRT1 also results in lifespan extension through partially overlapping mechanisms, including activation of DAF-16 [20].

The genetic dissection of the *C. elegans* aging process has progressed in part due to the widespread application of transcriptome analysis [21] and through the ease with which RNAi gene knockdown experiments can be performed [22]. Despite these advancements in the field, there have been few global proteomic investigations of the *C. elegans* aging process, and even fewer metabolomic investigations of aging. Based on our previous findings regarding the role that dietary metabolites play in *C. elegans* lifespan extension and in an effort to add to the understanding of aging in this model organism [23-25], we chose to employ a mass spectroscopy-based approach to global endogenous metabolite identification in young versus aged *C. elegans*. We also pursued a mass spectrometry-based heavy isotope labeling approach

for global protein quantification, with the goal of contextualizing the results from both "–omic" investigations using the *C. elegans* aging literature.

2.3 Materials and Methods

2.3.1 Chemicals and Strains

The SLE1 HT115(DE3) *Escherichia coli* bacterial strain was used as described in [26]. $^{15}N_4$-$^{13}C_6$-arginine was purchased from Thermo Scientific Pierce. $^{15}N_2$-$^{13}C_6$-lysine was purchased from Cambridge Isotope Laboratories, Incorporated.

2.3.2 *C. elegans* Culture

Between assays, *glp-4(bn2) C. elegans* (strain SS104) were grown at 15 °C on 10 cm NGM (nematode growth medium) plates containing a lawn of HT115 (DE3) *E. coli*. Prior to use in the assays, several plates of *C. elegans* were washed into a 750 mL liquid culture of *glp-4(bn2) C. elegans* containing HT115(DE3) *E. coli* (6.9 X 10^9 CFU/mL) and grown at 15 °C using standard liquid culturing techniques [27]. After becoming gravid adults, nematodes from this culture were used for experimentation.

2.3.3 Alkaline Bleach Synchronization

A liquid culture was chilled for 10 minutes on ice, and pelleted by centrifugation (~1150 x *g* for 4 minutes). The majority of the supernatant was carefully decanted, leaving behind a concentrated slurry of nematodes. Eggs were collected by alkaline bleach synchronization as follows: 6% NaOCl (Clorox®) was combined with 5 M NaOH in a 2:1 ratio by volume, and added to the concentrated slurry in a ratio of 0.4 mL of alkaline bleach solution per 1 mL of

slurry. The resulting *C. elegans* suspension was then shaken for 4–7 minutes until the carcasses dissolved, as monitored by microscopy, leaving behind only eggs. The egg-containing solution was then diluted 5-fold with 0.1 M NaCl, and centrifuged at ~1,150 x *g* for 2 minutes at room temperature. The supernatant was removed by aspiration, and the resulting pellet of eggs was washed 3 times by the addition of a similar volume 0.1 M NaCl, and centrifuged at ~1,150 x *g* for 2 minutes at room temperature. The final pellet of eggs was then used to establish age-synchronized liquid cultures.

2.3.4 Metabolomics Culturing and Sample Preparation

Eggs obtained by alkaline bleach synchronization were used to start two 1.5 L liquid cultures, containing HT115(DE3) *E. coli* (6.9 X 10^9 CFU/mL), and grown at 25 °C to induce sterility in the *glp-4(bn2) C. elegans*. On the fourth and tenth days of culture, one of the 1.5 L cultures was filtered through a 10 micron filter to separate *C. elegans* from bacteria. The collected nematodes were then washed into 1.5 L of M9 buffer and shaken for 20 minutes to allow the *C. elegans* time to empty the contents of their intestinal tract. The *C. elegans* M9 suspension was then divided among 500 mL bottles and centrifuged at ~1,100 x *g* for 4 minutes at room temperature. The supernatants were aspirated and the resulting pellets were combined in 50 mL of M9 buffer. At this point, three 1 mL portions of the suspension were set aside for protein determination assays (described in a section below). The remaining suspension was divided among five 15 mL conical vials and centrifuged at ~1,100 x *g* for 4 minutes at room temperature. The supernatants were aspirated and the pellets were frozen in liquid nitrogen. The pellets were then each ground to a fine powder using a pre-cooled mortar and pestle. The individual ground pellets were suspended in 5 mL of 80% methanol, and the resulting slurries

were sonicated on ice using a Heat Systems Ultrasonics W-380 sonicator (5-second pulses, 50% duty cycle, max power, 12 pulses total). Each slurry was centrifuged at 10,000 x *g* for 30 minutes at 4 °C, and the resulting supernatant was saved on ice. The pellets were then washed twice more in a similar manner, once with 5 mL of HPLC grade water and once with 70% ethanol, and the resulting supernatants were combined with the 80% methanol supernatant on ice. The remaining pellets were then suspended in 5 mL of chloroform and shaken at 250 rpm for 15 minutes at 37 °C. A separate syringe fitted with a 0.45 micron filter was used to collect the bottom organic layer of each conical vial, which was then saved separately on ice. The five polar fractions (combined methanol, water, and ethanol supernatants), and the five nonpolar fractions (chloroform supernatants) were each dried in a centrifugal vacuum evaporator at 50 °C for 2.5 hours. The samples from days 4 and 10 (5 polar and 5 nonpolar samples each) were sent to the University of Illinois Biotechnology Center for metabolite identification using GC-MS, and normalization based on total protein content.

To guarantee that the *C. elegans* grown until day 10 did not deplete their bacterial food source or accumulate an unwanted amount of waste products in the culture media, on the sixth day the nematodes were pelleted by centrifugation at ~1,100 x *g* for 4 minutes at room temperature and the supernatant was removed by decanting and by aspiration. The *C. elegans* were then suspended in 1.5 L of fresh S-medium containing HT115(DE3) *E. coli* (6.9 X 10^9 CFU/mL), and returned to incubation at 25 °C.

2.3.5 Protein Assay

The total *C. elegans* protein content of each sample was assayed using a similar protocol as described by Braeckman *et al*. [28]. Briefly, 1 mL of a sample was snap frozen in liquid

nitrogen and stored at -10 °C until analysis. For the analysis, 500 µL of the sample was transferred to a new 2 mL microcentrifuge tube and sonicated on ice using a Heat Systems Ultrasonics W-380 sonicator (5-second pulses, 50% duty cycle, max power, 12 pulses total). A 1.5 mL portion of 1:1 ethanol:acetone was added, vortexed briefly, and incubated at 4 °C for 30 minutes to facilitate protein precipitation. The tube was then centrifuged at 15,000 x *g* for 10 minutes at room temperature. The supernatant was decanted and the tube was left open and inverted on a paper towel for 5 – 10 minutes while the pellet dried. The pellet was then suspended in 180 µL of 1 N NaOH, vortexed, and incubated at 70 °C for 25 minutes to degrade any remaining lipids within the sample. A 1.26 mL portion of deionized water was added to dilute the NaOH and 360 µL of 10% sodium dodecyl sulfate (SDS) was added to facilitate the solubilization of the proteins. The tube was then mixed by inversion and centrifuged at 1,500 x *g* for 2 minutes at room temperature. The protein content of the supernatant was then analyzed by the BCA protein assay (Pierce) according to the manufacturer's protocol, using bovine serum albumin protein standards with a similar pH and SDS content as the assayed samples.

2.3.6 Proteomics Culturing

Cultures of SLE1 HT115(DE3) *E. coli*, containing a pAG608 plasmid for dsRNA generation targeting the *orn-1* gene, were grown overnight with vigorous shaking at 37 °C in M9 media (12.8 mg/mL Na_2HPO_4, 3 mg/mL KH_2PO_4, 0.5 mg/mL NaCl, 1 mg/L NH_4Cl, 2 mg/mL glucose, 49.4 µg/mL $MgSO_4 \cdot 7H_2O$, 1.52 µg/mL $CaCl_2 \cdot 2H_2O$, 1 µg/mL thiamine, 1 µg/mL $FeSO_4 \cdot 7H_2O$, and 100 µg/mL of ampicillin). For bacteria grown for isotope labeling, 50 µg/mL $^{15}N_4$-$^{13}C_6$-arginine and 50 µg/mL $^{15}N_2$-$^{13}C_6$-lysine were incorporated into the buffer (final concentration), otherwise 50 µg/mL unlabeled arginine and 50 µg/mL unlabeled lysine were

used. After ~16 hours ($OD_{600\ nm}$ = ~1), dsRNA expression was induced by the addition 1 mM IPTG (final concentration). The bacteria were then incubated for an additional 4 hours at 37 °C with shaking, and collected by pelleting at 3,000 x *g* for 20 minutes.

For both the labeled and unlabeled samples, *C. elegans* were grown as follows: eggs were obtained by alkaline bleach synchronization and used to start a 100 mL liquid culture containing SLE1 HT115(DE3) *E. coli* (6.9 x 10^9 CFU/mL). Isotope label-incorporated *E. coli* was used exclusively for the *C. elegans* culture designated for label incorporation. The nematodes were grown at 15 °C until the culture contained primarily gravid adults, at which point eggs were obtained by alkaline bleach synchronization. This pattern was repeated through two more generations to ensure adequate incorporation of $^{15}N_4$-$^{13}C_6$-arginine and $^{15}N_2$-$^{13}C_6$-lysine into the nematodes. Eggs from the fourth generation were grown at 25 °C. *C. elegans* containing $^{15}N_4$-$^{13}C_6$-arginine and $^{15}N_2$-$^{13}C_6$-lysine were harvested on the fourth day. *C. elegans* containing unlabeled arginine and lysine were harvested on the tenth day. As with the metabolomics assay, on the sixth day the S-medium and bacteria were replaced (see above).

2.3.7 Proteomics Sample Preparation and LC-MS/MS

Harvesting consisted of pelleting the *C. elegans* at ~1,100 x *g* for 4 minutes at room temperature, aspirating the supernatant, and then suspending the nematodes in M9 buffer. The *C. elegans* were washed twice more using this method and then suspended in ~1 mL of 6:4 M9 buffer/Percoll®. Living and dead nematodes were separated by carefully layering the *C. elegans* suspension on top of 10 mL of ice-cold 6:4 M9 buffer/Percoll®. The nematodes were then centrifuged at 1,500 x *g* for 10 minutes at room temperature (living *C. elegans* pellet to the bottom of the solution; dead *C. elegans* stay suspended at the top). The supernatant (and dead

nematodes) were aspirated, and the resulting pellet was washed twice in 10 mL of M9 buffer (~1,100 x *g* for 4 minutes at room temperature). The pellet was then snap-frozen in liquid nitrogen and ground into a fine powder using a pre-cooled mortar and pestle. The ground *C. elegans* were suspended in 10 mL of the following buffer: 50 mM ammonium bicarbonate at pH 8, 2% SDS, 100 mM dithiothreitol, 150 mM NaCl, and 1x Halt™ Protease Inhibitor (from Life Technologies). The slurry was then sonicated on ice using a Heat Systems Ultrasonics W-380 sonicator (5-second pulses, 50% duty cycle, max power, 12 pulses total). 1 mL samples were taken from each group (day 4 and day 10) for assaying total protein (see above; $n = 3$). The slurries from days 4 and 10 were combined in a 1:1 ratio based on total protein content.

A protein precipitation was performed on the slurry by the addition of 3 volumes of 1:1 ethanol:acetone (incubated for 30 minutes at 4 °C, followed by centrifugation at 15,000 x *g* for 10 minutes at room temperature). The supernatant was decanted, and the sample was allowed to dry before being suspended in our buffer solution (described above). A 15 minute water bath sonication was performed to aid in solubilization of the precipitated proteins. The proteins were then digested using a filter-aided sample preparation (FASP) kit (from Protein Discovery), according to the manufacturer's instructions. Five separate digestions were performed, using approximately 100 μg of protein per digestion. The samples were digested with trypsin at a ratio of 1:100 w/w trypsin:protein, and incubated overnight at 37 °C. The resulting eluted peptides were de-salted using a vacuum manifold and Supelco Discovery® DSC-18 solid phase extraction columns. The de-salted peptides were then dried in a centrifugal vacuum evaporator at 50 °C, and suspended in 20 μL of 0.1% formic acid.

The peptides were pooled and then separated by high performance liquid chromatography (HPLC) using a Dionex Ultimate 3000 HPLC system and a strong cation-exchange (SCX)

column loaded with 5 μm 300 angstrom polySULFOETHYL A-SCX material. Fractions were collected once per minute using a 1 hour gradient (5 mM to 500 mM ammonium formate, pH 3 to pH 6). Fractions selected for mass spectroscopy (LC-MS/MS) were mixed with 250 μL of 98% acetonitrile:2% formic acid and again dried using a centrifugal vacuum evaporator at 50 °C. The dried peptides were then suspended in 200 μL of 50% acetonitrile: 2% formic acid. Tandem mass spectrometric analysis was then performed using a hybrid linear ion trap-Orbitrap instrument (LTQ Orbitrap XL, Thermo).

2.3.8 Analysis

Outliers of metabolite spectral counts were removed using the Tukey boxplot method, and the remaining counts were range scaled [29]. Statistical significance was determined using unpaired two-tailed *t*-tests between the young and aged groups with a threshold of 0.05. Metabolites with *p*-value greater than the threshold were scored as unchanged. Principal component analysis was performed for the identified metabolites using XLSTAT. Metabolic pathways were assigned to each metabolite by manually searching the KEGG database. The pathway designated as "Metabolic Pathways" (map01100) was excluded since it encompasses most other pathway information. Proteomic results were checked for adequate incorporation of the labeled isotopes and RAW files were searched using MaxQuant version 1.4.1.2 (default settings) [30] and *C. elegans* and *E. coli* Uniprot databases. Searched parameters included modifications of cysteine by carbamidomethylation and methionine oxidation as well as modifications corresponding to the weights of incorporated $^{15}N_4$-$^{13}C_6$-arginine, $^{15}N_2$-$^{13}C_6$-lysine, and ^{15}N-$^{13}C_5$-proline. Proteomic statistical analysis was performed using Perseus version 1.4.1.3. Log_2-fold change values were calculated for aged/young (unlabeled/labeled), and centered on a

median of zero. Statistical significance was determined using the Significance B method (Benjamini-Hochberg corrected *p*-value; threshold = 0.05). Associated KEGG pathways were assigned to significantly up- and down-regulated proteins using the STRING database.

2.4 Results

2.4.1 Metabolomic Analysis of *C. elegans* Identifies Widespread Metabolite Changes with Age

One liter liquid cultures of *glp-4(bn2) C. elegans* were grown at 25 °C. This strain of *C. elegans* was chosen because it contains a temperature-sensitive mutant allele of *glp-4* (abnormal germ line proliferation-4), which completely restricts germ cell development when the nematodes are cultured 25 °C [31], maintaining the age-synchronized population throughout the course of the experiment. When cultured at 25 °C, adult *glp-4(bn2) C. elegans* contain ~12 prophase-arrested germ cell nuclei, as opposed to the 700 – 1000 non-arrested nuclei present in wild-type adults. Temperature is a major factor affecting developmental rate and lifespan in *C. elegans*, and in agreement with published findings we found that growth at 25 °C produced a mean liquid culture lifespan of ~10 days (Figure 2.1) [32]. We chose to compare metabolite profiles of young adult nematodes at day 4 of their lifespan with aged nematodes at day 10 of their lifespan (the mean length of their lifespan). Our choice of ages was based on a desire to select an early time point of measurement that would exclude metabolite changes from larval development and a later time point of measurement for investigating metabolite changes from an organism near the end of its lifespan, while still guaranteeing enough surviving *C. elegans* within the culture for adequate measurement.

The assay of metabolites from these two population pools was performed by gas chromatography-mass spectroscopy (GC-MS) and normalized to total protein content. The assay resulted in the successful identification of 186 metabolites within the samples. The data was analyzed by principal component analysis (PCA) to identify major factors affecting the distribution of metabolite levels. When graphed two dimensionally as a plane defined by the two largest factors the young and old samples separated along the primary (*F1*) axis showing that the majority of the underlying variation in metabolites levels was attributable to differences in age (Figure 2.2A). When similarly graphed, the individual metabolites showed separation along the same age-related axis (Figure 2.2B).

Log_2-fold change values were calculated for each metabolite by comparing metabolite levels on day 4 and day 10 and relevant affected pathways were identified by matching metabolites to known *C. elegans* enzymes using the KEGG (Kyoto Encyclopedia of Genes and Genomes) database (http://www.genome.jp/kegg/) [33]. Pathways were assigned to a metabolite if that pathway contained a known *C. elegans* enzyme that either produces or consumes the metabolite (Table 2.1). The total observed change for all pathways was calculated as the sum of the absolute log_2-fold change of each metabolite associated with that pathway (Figure 2.3 and Table 2.2).

2.4.2 Altered Amino Acid Pools with Age Reflect Changes in Cell Volume

The pathway found to be most changed with age was the biosynthesis of amino acids, primarily because of the large degree of overlap within that pathway with other metabolic processes, including the pentose phosphate pathway, S-adenosyl methionine metabolism, the urea cycle, and the citric acid cycle. Of the 24 metabolites identified within this pathway, 14

were significantly altered with age, including 7 free amino acids. A total of 11 identified metabolites were significantly decreased in older nematodes, also giving this pathway a large negative total observed $\log_2$-fold change.

Changes in the relative concentrations of identified free amino acids, including the two aromatic amino acids phenylalanine and tryptophan, which are associated with separate pathways, reflect known age-related changes in nematode cell-to-volume ratios. During larval development, the increase in body size greatly outpaces the increase in cell number. During this period, *C. elegans* body size increases ~32-fold, yet the total cell number increases by only ~3.5-fold [34, 35]. By adulthood, all 959 somatic cells are postmitotic, but the *C. elegans* body size continues to increase [36]. Growth at this point is accomplished entirely by expanding cells volumes, which result in shrinking membrane-surface/cell-volume ratios for individual cells.

This continuous change in cell surface-to-volume has been found to be associated with a specific change in protein content. In 2009, Swire *et al*., performed H^1 NMR on young and old *C. elegans* to assay free amino acid pools and analyzed a previously published transcriptome dataset to determine age-related changes in membrane- and cytoplasm-associated genes [37, 38]. Their conclusion was that cytoplasmic genes showed a large and significant increase in expression during larval development compared to membrane-associated genes. The resulting relative increase in cytoplasmic protein production causes an increased incorporation of hydrophilic amino acid residues compared to hydrophobic residues, and the cellular supply of free amino acids should change to match the demand. Accordingly, their H^1 NMR analysis revealed a general age-related increase in the hydrophilic/hydrophobic ratio of free amino acids, with the extent of increase or decrease of individual amino acids corresponding approximately to their hydrophobicity. We found a similar correlation with the 9 significantly changed free amino

acids we identified (Figure 2.4), with a Pearson product-moment correlation coefficient of -0.665 (p-value = 0.05) using a glycine normalized scale of hydrophobicity [39]. Overall, relatively hydrophobic free amino acids tended to decrease in concentration with age, and the few hydrophilic free amino acids detected tended to increase in concentration, in accordance with the requirements for cells increasing in size.

2.4.3 Purine Metabolite Levels Are Decreased in Older Nematodes

Purine metabolite levels showed the largest total decrease in $\log_2$-fold change with age with adenine, guanine, adenosine, adenosine monophosphate, ribose, ribose 5-phosphate, hypoxanthine, and inosine (a nucleoside consisting of hypoxanthine bound to a ribose sugar) all being decreased by day 10. To validate these results, we chose to further assay hypoxanthine concentrations in young (day 5) and old (day 12) wild type N2 *C. elegans* grown at 20 °C. The selection of our nematode strain and growth conditions, which necessitated the use of 5-fluoro-2′-deoxyuridine (FUdR) to prevent egg-laying, was intended to expose any strain- or condition-specific effects present in our measurements. The administration of FUdR between the L4 and adult developmental stages is an alternative method to maintain the age-synchronous population. FUdR is a nucleotide analog and an inhibitor of DNA synthesis. Since only the germ cells are mitotically active in adult *C. elegans*, FUdR selectively restricts germ cell production. From our measurements, we determined that the hypoxanthine concentration decreased ~30% between days 5 and 12 (Figure 2.5A), which matched our metabolomics results in the direction of change, but with a smaller magnitude. To determine if purine levels may be limiting lifespan, we supplemented hypoxanthine to the culture medium and monitored the lifespan. As shown in Figure 2.6A, 10 mM hypoxanthine supplementation increased lifespan by 18%.

Pyrimidine metabolite levels were also largely decreased with age, however the nitrogenous base cytosine – the sixth most decreased metabolite overall – was not associated with pyrimidine metabolism using our method since *C. elegans* apparently lacks a cytidine phosphorylase enzyme to salvage cytosine bases, so no enzymes are directly associated with cytosine in the KEGG database. If cytosine had been associated with pyrimidine metabolism for calculations of total $\log_2$-fold change calculations, it would have been the fourth most decreased pathway and the fourth most changed pathway overall. To determine if pyrimidine levels may be limiting lifespan, we supplemented cytidine (the ribonucleoside of cytosine) to the culture medium. As shown in Figure 2.6B, 10 mM cytidine increased lifespan by 11%.

The nitrogenous bases showed a distinct age-related decrease in abundance (Figure 2.5B). Uracil, adenine, guanine, and cytosine as well as the nucleoside uridine were each decreased in the older *C. elegans*. Thymine, a nitrogenous base found in DNA, failed to achieve a significant *p*-value when evaluating young and old metabolite levels (*p*-value = 0.076), so it was scored as unchanged during analysis, but it also appeared to decrease with age ($\log_2$-fold change = -3.18). Furthermore, a product of pyrimidine catabolism, specifically dihydrouracil catabolism, β-alanine increased with age. It is unclear if the levels of nitrogenous bases decreased with age as a result of (1) decreased *de novo* synthesis due to decreased S-adenosyl methionine (SAM) levels; (2) decreased ingestion due to the sarcopenic pharyngeal pump; (3) an increased rate of the nucleotide salvage pathway draining nitrogenous base pools; or (4) a decreased rate of RNA and nucleotide degradation, or some combination of these mechanisms. Since supplementing back a purine or a pyrimidine to the culture medium extended lifespan however, the decreased purine and pyrimidine levels that occur with aging appear to be limiting lifespan.

2.4.4 S-Adenosyl Methionine and Altered Lipid Content

Four metabolites were identified as part of cysteine and methionine metabolism and all of these decreased in abundance with age. Of these, three were found to be directly associated with the SAM cycle; specifically, L-methionine and L-homocysteine, and the downstream product 5-methylthioadenosine. SAM is the universal methyl donor in eukaryotic cells, and it is capable of acting as a cofactor in the transfer of methyl groups to DNA, RNA, proteins, and lipids [40]. SAM is an important part of phospholipid metabolism, and is used during the synthesis of phosphatidylcholine (PC), which is a major component of cell membranes [41]. In bacteria, fungi, and mammals, PC is synthesized from choline by the *de novo* choline pathway, also known as the Kennedy pathway [42-44]. Yeast and mammalian liver cells use the CDP-diacylglycerol pathway, which begins with the conversion of phosphatidylserine into phosphatidylethanolamine (PE), and uses SAM to sequentially methylate the molecule into PC [45, 46]. *Plasmodium falciparum* (one of the species of *Plasmodium* that cause malaria) and *C. elegans* have been shown to utilize an alternative method of PC synthesis, known as the phosphomethylethanolamine N-methyltransferase (PEAMT) pathway, which begins with the conversion of serine to phosphoethanolamine [47-49]. *C. elegans* then use two phosphomethylethanolamine N-methyltransferase enzymes, PMT-1 and PMT-2, to sequentially methylate phosphoethanolamine into phosphocholine, which then enters the Kennedy pathway to yield PC.

Lipid droplets (LDs) have been identified within cells of a wide range of species, including humans. In general, LDs consist of a hydrophobic core composed of cholesterol esters and triacylglycerols, surrounded by a phospholipid monolayer that is primarily made of PC and

PE [50]. The LD PC phospholipid monolayer appears to act as a surfactant that prevents LDs from coalescing, and the knockdown of genes involved in PC synthesis has been shown to produce larger LDs [51]. Knockdown of either *C. elegans pmt-1* or S-adenosyl methionine synthetase (*sams-1*), which uses ATP and L-methionine to produce SAM, leads to decreased production of PC and increased LD size [52, 53]. Furthermore, the resulting enlargement of *C. elegans* LDs was found to be associated with impaired reduction of LD size during starvation, presumably due to hindered accessibility of triacylglyceride-hydrolyzing lipases given the changed surface-to-volume ratio of the droplets [53]. Large LDs have been shown to accumulate in *C. elegans* as they age [2], and their ectopic accumulation has been theorized to contribute to the age-related dysfunction in the nematode [54].

We found a decrease in monoacylglycerols with age and a concurrent increase in free fatty acids in older nematodes (Figure 2.7 and Table 2.3). We also found an increased level of glycerol in the older nematodes ($\log_2$-fold change = 1.948; *p*-value = 0.017) and a dramatic increase in the level of the ketone body β-hydroxybutyrate ($\log_2$-fold change = 7.370; *p*-value = 0.003), which can form from excess acetyl-CoA under conditions of either fatty acid breakdown (β-oxidation) or fatty acid synthesis. Interestingly, citrate was also increased in older nematodes ($\log_2$-fold change = 1.973; *p*-value = 0.0003). Mitochondrially derived citrate is exported into the cytoplasm and converted into acetyl-CoA by the enzyme ATP citrate lyase [55], which can then either be used for fatty acid synthesis or ketone body production. The increased levels of free fatty acids in the aged nematodes could be partially due to a decreased rate of fatty acid β-oxidation resulting from mitochondrial dysfunction, in addition to any increased rate of hydrolysis from monoacylglycerols.

2.4.5 D-sorbitol Increases in Aged *C. elegans*

Strikingly, fructose and mannose metabolism was identified as one of the most changed pathways solely due to an increase in a single age-related metabolite – sorbitol (log_2-fold change = 8.316; *p*-value = 0.001). Sorbitol is produced from glucose by aldose reductase (AR) in response to elevated glucose levels [56-58], and both increased sorbitol levels and increased AR activity have been associated with diabetes in multiple species and tissues [59-61]. Sorbitol is strongly hydrophilic, does not readily cross cell membranes, and under conditions of high glucose availability, such as diabetes, it may possibly accumulate to an adequate concentration to cause osmotic stress [56]. AR also uses reduced nicotinamide adenine dinucleotide phosphate (NADPH) as a cofactor, and increased metabolic flux through AR has been identified as a possible source of lowered cellular levels of NADPH [58, 62]. Additionally, sorbitol is converted to fructose by sorbitol dehydrogenase, which uses reduced nicotinamide adenine dinucleotide (NAD^+) as a cofactor, and excess metabolic flux through sorbitol dehydrogenase has been associated with a lowered NAD^+ level [63, 64]. Taken together, the activities of AR and sorbitol dehydrogenase (collectively known as the polyol pathway) may affect intracellular redox state though changes in $NAD(P)^+$/NAD(P)H ratios. Given that cellular redox state is a factor in protecting against oxidative stress, some evidence links the diabetic flux of glucose through the polyol pathway with diminished levels of the reduced antioxidants glutathione and ascorbate [65-68], increased lipid peroxidation, nitrosative stress [67, 68], and DNA damage as identified through the activation of poly(ADP-ribose) polymerase [68]. Other sugars upregulated with age included glucose, galactose, and sucrose as well as glucose-6-phosphate, suggesting that glycolysis could be impaired in the older worms. To validate the observed increase in D-sorbitol levels, and to investigate whether the effect was strain or condition specific, we chose to

assay D-sorbitol levels using the same conditions as stated above for the assay of hypoxanthine (wild-type N2 *C. elegans* grown at 20 °C). Under these conditions, we found a significant ~360% increase in D-sorbitol levels from day 5 to day 12 (Figure 2.8A).

2.4.6 Altered Ascorbate Metabolism and Redox Imbalance with Age

We were able to use some of the identified metabolite levels to estimate a general age-related change in redox state. Ascorbic acid (vitamin C) is capable of behaving as an antioxidant in a cellular environment [69-71]. In its fully oxidized form as dehydroascorbic acid (DHA), it can be reduced by glutathione back to ascorbate, thus making the ratio of DHA to ascorbate an indicator of the available glutathione pool and the general cellular redox state [72]. Figure 2.8B shows a shift from reduced ascorbate to oxidized DHA in older *C. elegans*, with the ratio of DHA/ascorbate increasing 7.65 fold ($\log_2$-fold change = 2.935; *p*-value = 0.0243). Furthermore, both erythronic acid (EA) and N-acetylglucosamine (NAG) were identified among the metabolites of young and old *C. elegans*. NAG is a peptidoglycan monomer and a component of chitin and hyaluronic acid. When oxidized, NAG has been found to degrade into EA [73]. Figure 2.8B shows an increase in the ratio of EA to NAG in older nematodes. The EA/NAG ratio showed a dramatic ~17-fold change from day 4 to day 10 ($\log_2$-fold change = 4.122; *p*-value<0.0001).

The metabolite that decreased in abundance to the greatest extent with age was galactonic acid-1,4-lactone, which in plants is the direct precursor of ascorbate in the ascorbate biosynthesis pathway. However, it is unknown if *C. elegans* can convert galactonic acid-1,4-lactone into ascorbate as bioinformatic analysis did not detect an L-galactonic acid-1,4-lactone dehydrogenase in the *C. elegans* genome [74], but invertebrates may have evolved a unique, as

of yet unidentified enzyme to catalyze this reaction. In support of this hypothesis *C. elegans* has been shown to synthesize both ascorbate and an unidentified hydrogenated lactone precursor to ascorbate, but the ascorbate synthesis pathway appears to be different from the pathways present in animals, plants, or protists, while ascorbate is not synthesized by *E. coli* [74]. In *C. elegans* ascorbate levels were highest in eggs, levels declined throughout larval growth, and were lowest in mixed age adults. In addition ascorbate levels were higher when worms were grown in liquid media compared to when they were cultured on agar plates, but ascorbate levels did not increase when worms were exposed to the free radical generator paraquat [74]. We predict that the decreased level of galactonic acid-1,4-lactone with age is partially due to its conversion into ascorbate, as we measured ascorbate and DHA levels to increase during aging. However, identification of a novel enzyme in *C. elegans* with galactonic acid-1,4-lactone dehydrogenase activity is needed to confirm this hypothesis.

Neither NAD^+ nor NADH were identified in our metabolomics screen, but we were able to use the ratio of pyruvate to lactate as an estimator of relative NAD^+ and NADH concentrations, respectively, as the cellular levels of these metabolites are held in equilibrium by the activity of lactate dehydrogenase [75]. Figure 2.8B also shows this, with the ratio of NAD^+/NADH decreasing approximately 69% from day 4 to day 10 ($\log_2$-fold change = -1.672; *p*-value < 0.0001). While our results are only an estimate, a similar age-related decrease in NAD^+/NADH ratio has been observed in aging Wistar rats [76], and the NAD^+ level was found to be negatively correlated with age in human brain [77] and pelvic skin samples [78]. The decreased NAD^+/NADH could slow glycolysis, mitochondrial fatty acid β-oxidation, and citric acid cycle function possibly explaining some of the metabolite level changes observed with age. We attempted to estimate the relative cellular ratios of $NADP^+$/NADPH using identified levels of

pyruvate and malate, respectively, based on the activity of NADP-malic enzyme [79]. The resulting day 4 and day 10 ratios showed a decline, but the result lacked statistical significance (*p*-value = 0.1417).

2.4.7 Proteomic Investigation

To supplement our metabolomic analysis of young vs. aged *C. elegans*, we performed a global mass spectroscopy-based proteomic investigation under similar conditions (day 4 and day 10 liquid cultures of *glp-4(bn2) C. elegans* grown at 25 °C). To increase our capability for quantitation, we chose to follow the general ^{15}N-^{13}C stable isotope labeling strategy outlined by Larance *et al*. [26]. In short, we grew a lysine- and arginine-auxotrophic strain of *E. coli* (SLE1 HT115) in minimal media supplemented with $^{15}N_4$-$^{13}C_6$-arginine (heavy arginine) and $^{15}N_2$-$^{13}C_6$-lysine (heavy lysine). Three successive generations of *glp-4(bn2) C. elegans* were fed the heavy labeled bacteria, in order to ensure complete incorporation of the heavy isotopes into the nematodes. A potential complication with labeling using this approach is that *orn-1* (ornithine transaminase 1), which is one of the enzymes of the urea cycle, is capable of converting arginine into proline. To prevent the accumulation of heavy-labeled proline from confounding the subsequent analysis, we fed *C. elegans* SLE1 *E. coli* expressing dsRNA targeting *orn-1*. Samples for mass spectroscopy were taken from the fourth generation of heavy isotope-labeled *glp-4(bn2) C. elegans*, grown to day 4 (young sample) in liquid culture at 25 °C. The older sample was taken from a similar RNAi-treated culture grown to day 10, but lacking the heavy isotopes. Following high performance liquid chromatography (HPLC)-mass spectroscopy of the samples and data analysis a total of 1,937 proteins were identified as present in both age groups.

After centering the median of the old/young log_2-fold change, a total of 54 proteins were determined to be significantly increased or decreased in abundance in the aged sample (Figure 2.9 and Table 2.4). To help identify relevant connections to the metabolomics data set, we used the STRING (Search Tool for the Retrieval of Interacting Genes/Proteins) online database (http://www.string-db.org/) to match significant proteins to KEGG database metabolites [80]. We then calculated the total observed change for each pathway as the sum of the absolute log_2-fold change of each identified protein within that pathway (Figure 2.10 and Table 2.5).

2.4.8 Changes Associated with Histone Methylation and Acetylation with Age

In agreement with the observed changes in methionine cycle metabolites, the level of SAMS-1, which catalyzes the synthesis of SAM from ATP and L-methionine, was found to be decreased in aged nematodes (log_2-fold change = -1.837; *p*-value = 1.8×10^{-5}). Since the levels of both substrates for SAMS-1, L-methionine and ATP also decline dramatically with age, it is likely that SAM levels decrease dramatically with age, although we did not detect SAM in our metabolomics analysis. In addition, the level of PRMT-3 (protein arginine methyltransferase 3) was dramatically decreased with age (log_2-fold change = -7.636; *p*-value = 1.8×10^{-20}). This protein possesses SAM-specific monomethyltransferase activity and is capable of transferring a methyl group from SAM onto arginine residues present in histone proteins [81]. Evidence indicates that *C. elegans* lack methylated DNA, suggesting that methylation events primarily modulate gene expression through histone modification [82].

Histone deacetylases are enzymes that remove acetyl groups from lysine residues within core histones. *C. elegans* histone deacetylase-1 (HDA-1), which is orthologous to human HDAC-1, affects gene expression during larval development in many tissues including neurons,

muscles, hypodermis, intestines, and the extracellular matrix. Among its many genetic targets, HDA-1 appears to be a strong repressor of the cysteine protease inhibitor CPI-1 expression (homologous to human cystatin D), and RNAi knockdown of HDA-1 leads to an 8.5-fold increase in CPI-1 levels [83]. We found a ~6.4-fold (2.67 $\log_2$-fold) increase in CPI-1 levels with age, along with a similar increase in several genes known to have a high confidence of co-expression with CPI-1 (correlation > 0.7; STRING database), including C53B7.2, Y62H9A.6, CPG-1, and TTR-51. Interestingly, a bacterial ortholog of TTR-51 was shown to play a role in the degradation of uric acid to allantoin as a part of purine catabolism [84]. Furthermore, we recently found β-hydroxybutyrate (βHB) to inhibit class I histone deacetylases to extend lifespan in *C. elegans*, and it is possible that the endogenous increase of βHB observed in older nematodes inhibits HDA-1 to induce this effect [24], although the level of γ-hydroxybutyrate, another endogenous histone deacetylase inhibitor [85], declined with age.

2.4.9 Poly(ADP-ribose) Polymerase Levels Decrease with Age

The *C. elegans* poly(ADP-ribose) polymerase PME-1 decreased in abundance with age ($\log_2$-fold change = -5.991; *p*-value = 2.9×10^{-13}) (Table 2.4). *C. elegans* PME-1 is orthologous to human PARP1, which functions to detect DNA single-strand breaks and signals to proteins responsible for single-strand break repair [86, 87]. As part of this process, PME-1/PARP-1 uses NAD^+ to attach ADP-ribose monomers to target proteins, forming chains of poly(ADP-ribose). Under conditions of genotoxic stress, PME-1/PARP-1 can significantly reduce cellular NAD^+ reserves [87]. Deletion of PARP-1 in mice has been shown to elevate NAD^+ levels of brown adipose tissue and muscle leading to aerobic respiration and increased SIRT1 activity [88]. The

evidence for both a lowered abundance of PME-1 and a lowered NAD^+/NADH ratio in the aged *C. elegans* suggests that PME-1 may be down-regulated with age to conserve NAD^+ levels.

2.4.10 Decreased Levels of Enzymes Involved in Fatty Acid Synthesis and Breakdown with Age

Three key enzymes involved in fatty acid metabolism showed decreased abundance in aged *C. elegans*, cytosolic $NADP^+$-dependent isocitrate dehydrogenase, an acyl-CoA dehydrogenase, and a putative ER carboxylesterase (Table 2.4). The enzyme IDH-1 (isocitrate dehydrogenase-1) is homologous to human IDH1 and functions in the cytoplasm to convert isocitrate into α-ketoglutarate, reducing an $NADP^+$ cofactor to NADPH in the process. We found decreased abundance of IDH-1 in older *C. elegans* (log_2-fold change = -2.349; *p*-value = 6.8×10^{-8}), which may account for the increased citrate level found in the aged worms. Cytosolic aconitase is a regulator of fatty acid synthesis and is capable of converting citrate into isocitrate, which would otherwise be available for entering the fatty acid synthesis pathway through the activity of ATP citrate lyase [89].

The *C. elegans* enzyme ACDH-13 (acyl CoA dehydrogenase 13) is one member of a family of long-chain-acyl-CoA dehydrogenase enzymes identified to function in the first steps of mitochondrial fatty acid β-oxidation. These enzymes act to form a trans double-bond in fatty acids, reducing the cofactor flavin adenine dinucleotide (FAD^+) in the process. Our observed age-related decrease in ACDH-13 abundance (log_2-fold change = -4.318; *p*-value = 1.75×10^{-5}) may play a role in the increased levels of free fatty acids found in aged *C. elegans*. Interestingly, ACDH-13 is homologous to human acyl-CoA dehydrogenase 9 (ACAD9; BLAST *e*-value = $8.9e^{-28}$; % length = 69.7%). ACAD9 has been determined to be necessary for proper assembly of

the mitochondrial electron transport chain complex I, although no such role has yet been investigated or identified in *C. elegans* [90].

C. elegans C23H4.3 encodes an ortholog of human carboxylesterase-2, which is known to play an important role in xenobiotic metabolism, such as catalyzing the breakdown of amide and ester containing drugs. However, carboxylesterase-2 also plays an important role in lipid metabolism by hydrolyzing long-chain fatty acid esters and thioesters. C23H4.3 levels decreased with age (log2-fold change = -4.487; p-value = 1.37×10^{-5}), so this enzyme does not likely play a role in the aging-induced increase in free fatty acids levels.

With aging, we also found decreased abundance of the RME-2 protein that functions as a yolk receptor on oocytes [91]. Yolk is present in *C. elegans* as vitellogenin lipoprotein particles that carry high levels of cholesterol and other lipids [54]. Yolk is produced in the intestine and must be carried across the body cavity to the gonad, where it binds and provides nourishment for developing oocytes [92]. Following the reproductive period, yolk levels increase and become distributed throughout the body [54], releasing fatty acids and other lipids that may damage tissues contributing to aging-induced physiological dysfunction. The decreased abundance of RME-2 in the gonad with age likely facilitates the non-specific distribution of lipid to other locations resulting in lipotoxicity.

2.4.11 Evidence for Muscle Dysfunction and Altered Ca^{2+} Homeostasis with Aging

Five distinct proteins known to be involved in muscle function were present at a lower abundance in aged nematodes in our analysis; SCA-1 (sarco-endoplasmic reticulum calcium ATPase 1, or SERCA), NRA-2 (nicotinic receptor associated protein 2), MLP-1 (muscle LIM protein 1), MLC-2 (myosin regulatory light chain 2), and AIPL-1 (actin interacting protein 1-like

protein 1) (Table 2.4). The *C. elegans* protein SCA-1 is orthologous to the human SERCA protein ATP2A1, which utilizes the hydrolysis of ATP to pump cytosolic Ca^{2+} into the lumen of the sarcoplasmic reticulum in cardiac and slow twitch skeletal muscle [93, 94]. In *C. elegans*, SCA-1 is expressed in all major muscle types, including body wall, pharyngeal, and uterine muscle [95]. Reduction of SERCA function is associated with muscle dysfunction, and SERCA2 heterozygous mutant mice display deficits of muscle relaxation as a consequence of reduced rates of sarcoplasmic Ca^{2+} sequestration [96]. Another protein involved in Ca^{2+} signaling, CAL-4, one of five *C. elegans* calmodulin homologs, was increased in abundance with age. It is possible that this could occur in response to increased cytoplasmic Ca^{2+} levels resulting from lower SCA-1 activity.

The *C. elegans* gene NRA-2 (ortholog of human nicalin) encodes a transmembrane endoplasmic reticulum protein that functions as a molecular chaperone [97]. It contains an EF-hand motif, so it is likely regulated by changes in Ca^{2+} levels. Expression of NRA-2 occurs largely in neurons, body wall muscle, and pharyngeal muscle, where it helps regulate acetylcholine receptor subunit composition, and RNAi knockdown of NRA-2 expression has been shown to sensitize *C. elegans* touch receptor neurons to Ca^{2+}-mediated necrotic cell death [98]. The next protein decreased in abundance MLP-1 is a LIM domain-containing cysteine-rich protein (CRP) expressed in a wide range of cell types in both larva and adults (including intestine, spermatheca, gonad sheath, hypodermis, body wall muscle, pharynx, and neurons) [99, 100]. In humans, the homologous CSRP (cysteine and glycine-rich protein) family of proteins is expressed in cardiac and skeletal muscle, and predominantly localizes to cardiac Z disc structures [101-103]. Abnormal expression of CSRP has been linked to cardiomyopathy and heart failure in patients [104], and mice with deficient CSRP function exhibit progressive enlargement of

cardiac chambers, thinning of the ventricular walls, and defects in sarcoplasmic reticulum Ca^{2+} storage [101, 105, 106].

MLC-2 is expressed in body wall, vulval, and pharyngeal muscles and together with MLC-1 and MLC-4 make up the three *C. elegans* regulatory myosin light chains. These proteins function as regulators of myosin ATPase activity [107]. In the pharyngeal muscles, MLC-2 is essential for proper muscle function, with 90% of MLC-2 mutants arresting at the L1 larval stage due to pharyngeal defects. Therefore the decreased levels of MLC-2 that occur with age may contribute to pharyngeal sarcopenia. AIPL-1 is a WD40 repeat-containing protein homologous to UNC-78 and functions with UNC-60B/ADF/cofilin to regulate the ordered assembly of actin in muscle myofibrils necessary for proper larval development, but its expression was reported to diminish in adulthood [108] as we have confirmed here by measuring protein level changes.

2.4.12 Changes in RNA Metabolism and Translation with Age

From the proteomics data the pathway with the largest total observed changes with age was RNA degradation (Figure 2.10 and Table 2.5), which is the result of the cumulative observed lower abundance of XRN-2 (5'-3' exoribonuclease 2 homolog) and PAB-2 (poly(A) binding protein 2) (Table 2.4). The exonuclease XRN-2 is involved in transcription termination, where it is capable of dislodging RNA polymerase II from DNA following its binding to 5'-uncapped RNA and degrading the RNA until it reaches the polymerase [109]. Furthermore, XRN-2 also degrades mature microRNAs regulating their cellular levels, and the activity of XRN-2 is necessary for proper larval molting and reproduction [54, 110, 111]. Expression of *xrn-2* is ubiquitous and continues past the larval stages into adulthood. The decreased levels of XRN-2 in aged nematodes may prevent efficient transcription termination and/or RNA

degradation resulting in decreased levels of nucleotides and nucleotide degradation products such as nitrogenous bases, possibly explaining the depleted nitrogenous base levels measured in the metabolome analysis.

Most eukaryotic mRNAs of nuclear origin, including microRNAs, possess poly(A) tails, which consist of a series of adenosine nucleotides up to ~300 bases in length. Poly(A) binding proteins, such as PAB-2, bind along the length of this polyadenylated mRNA region and serve to regulate translation through both their interaction with the 5'-cap eukaryotic initiation factor complex eIF4F and their recruitment of the 40S and 60S ribosomal subunits [104]. Furthermore, depletion of the human poly(A) binding protein PABP decreases mRNA translation in vitro, suggesting that the decreased abundance of PAB-2 with age may decrease protein synthesis, perhaps in response to the reduced capacity of the protein-folding chaperone systems in aged worms.

The proteins ZK512.2 (a probable ATP-dependent DEAD-box RNA helicase DDX55 homolog) and RSP-6 (splicing factor, arginine/serine-rich protein 6) were identified as being present at a significantly lower abundance with age (Table 2.4). *C. elegans* RSP-6 is a splicing factor that contributes to nuclear pre-mRNA processing [106, 110, 111]. However, not much is known regarding the function of ZK512.2, but if its predicted function as an ATP-dependent RNA helicase holds, it may play a role in pre-mRNA splicing or the initiation of translation. The *C. elegans* 60S ribosomal subunit L11 (RPL-11.2) and the 40S ribosomal subunit (RPS-26) as well as DPH-2 (diphthamide biosynthesis protein 2) were observed to be down-regulated with age. Diphthamide is a non-standard amino acid found exclusively in translation elongation factor 2 (eEF2). The conversion of L-histidine to diphthamide, in which DPH-2 participates,

requires four SAM molecules and the transfer of three methyl groups, thus representing a direct link between protein translation and SAM [105].

The proteomics data also suggest that translation of mitochondrial DNA-encoded components of oxidative phosphorylation may be compromised in aged nematodes because there was a decreased abundance of PUS-1, pseudouridine synthase (Table 2.4). PUS-1 is responsible for post-transcriptional modifications of mitochondrial and cytoplasmic tRNA essential for translation. Humans with PUS-1 mutations have mitochondrial myopathy and sideroblastic anemia (MLASA) [112].

2.4.13 Aging Decreased the Abundance of RPN-3, a Regulator of Proteasome Function

The RPN-3 protein was found to be present at lower levels in aged nematodes (Table 2.4). Proper RPN-3 levels are critical for proteasome function as either overexpression or deletion of *rpn-3* disrupted the function of the proteasome [113]. Irisflorentin, an isoflavone isolated from the roots of the traditional Chinese herbal, *Belamcanda chinensis*, was shown to specifically upregulate *rpn-3* expression, which directly increased the chymotrypsin-like activity of the proteasome [114]. The increased proteasome activity led to decreased α-synuclein accumulation and toxicity in a nematode model of Parkinson's disease.

2.5 Discussion

The metabolomics results indicate that aged *C. elegans* contain decreased levels of specific purine and pyrimidine metabolites, altered free amino acid pools (attributable to a decrease in the cell surface-to-volume ratio), altered S-adenosyl methionine metabolism,

increased sorbitol content, increased free fatty acid levels, and a shift in cellular redox balance toward oxidation. Proteomic analysis of *C. elegans* showed age-related decreases in the levels of the protein arginine methyltransferase protein PRMT-3, and a poly(ADP-ribose) polymerase PME-1, decreased abundance of muscle proteins including SCA-1, the *C. elegans* SERCA homolog, suggesting muscle dysfunction. There was also decreased abundance of proteins involved in transcription termination, RNA stability, proteasomal function, and protein synthesis, as well as those involved in the regulation of fatty acid synthesis and breakdown. These two data sets yield important clues regarding the molecular mechanisms of aging-induced physiological dysfunction.

Several groups have investigated *C. elegans* metabolite and protein abundance changes with age. Liang *et al*. performed a mass spectrometry-based proteomic analysis with isotopically labeled protein samples using the iTRAQ (Isobaric Tags for Relative and Absolute Quantitation) technique to study young, middle-aged, and aged N2 *C. elegans* grown at 20 °C (approximately days 3.5, 9, and 14 counting from the first day of culture) [115]. For a comparison, the mean lifespan of *C. elegans* grown at 25 °C, as was done in this report, is approximately 9-10 days, whereas the mean wild-type lifespan at 20 °C lies somewhere between 14 and 21 days with a large degree of variability. Still, there was a large degree of overlap between our results and those using the iTRAQ approach. Liang *et al*. identified a decrease in ribosomal proteins, poly(A) binding protein (PAB-1), myosin-related proteins, and fatty acid synthesis and degradation associated proteins (fatty acid CoA synthetase 2 and acyl CoA dehydrogenase 1) in aged nematodes. Furthermore, Pontoizeau *et al*. performed an NMR-based metabolomic study of *C. elegans* subjected to dietary restriction (a consistent method for extending lifespan in model organisms) and found that the phosphocholine level was significantly lowered by the DR

condition [116]. High phosphocholine levels were also found to be associated with shorter *C. elegans* lifespan. Similarly, high vitamin B12 (cobalamin) and folate levels have been found to shorten *C. elegans* lifespan [117, 118]. Notably, both dietary vitamin B12 and folate are required for the synthesis of tetrahydrofolate, which is a necessary part of the metabolic cycle that produces SAM.

Phenotypically, *C. elegans* aging is defined by sarcopenia (loss of muscle mass and function) [1], the accumulation of ectopic fat as yolk lipoprotein production continues beyond the cessation of egg production [2], and a dramatic collapse of aerobic respiration and ATP content as enlarged dysfunctional mitochondria accumulate within cells [3]. Free fatty acid accumulation outside of adipocytes has been associated with ER stress [119], insulin resistance [120, 121], and cardiomyopathy [122, 123]. Evidence suggests that the accumulation of fatty acids as triglycerides sequestered within LDs acts as a preventative measure against lipotoxicity [54, 119, 124]. Deficiencies in SAM lead to decreased PC levels and enlarged LDs. These enlarged LDs sequester fatty acids and likely protect against lipotoxicity extending *C.* elegans lifespan. However, decreased PC levels are not a prerequisite for enlarged LDs or an extended lifespan as several long-lived *C. elegans* strains have enlarged LDs with increased PC:PE ratios [125]. However, increased PE levels have been linked with longevity as well [126], so the specific subcellular localization of these phospholipids may likely control their effects on lifespan.

We also found an aging-related decline in the *C. elegans* homolog of phospholipase D3, an ER membrane protein that hydrolyzes PC into choline and phosphatidic acid. This enzyme may be down-regulated with age to preserve PC levels to decrease LD size and increase LD surface area so lipases can better remove fatty acids for energy production when pharyngeal

pumping slows and energy substrate levels decline. Alternatively, decreased phospholipase D3 activity could be functioning to decrease TOR function, protein synthesis, and proteotoxicity in aged worms, as TOR requires a bound phosphatidic acid for optimal activity [127]. Furthermore, phospholipase D3 activity has been shown to protect against amyloid-β production in Alzheimer's disease brain [128]. A meta-analysis of metabolomics data from several long-lived *C. elegans* mutants found alterations in PC and niacin levels as a common theme [129]. Additionally, PC accounts for about one-third of the phospholipids in the mitochondrial inner membrane. Research is lacking regarding a direct relationship between PC levels and mitochondrial size, but it would be interesting to determine if the same dynamics of surface-to-volume ratio that result in larger LDs when PC is low would also contribute to the accumulation of enlarged mitochondria that might become damaged and resist degradation through the autophagosomal/lysosomal pathway to produce high amounts of reactive oxygen species contributing to the aging process.

The connection between aging-induced changes in lipid metabolism and ER stress is also especially pertinent. The ER stress response declines with age, which may contribute to the aging process and the development of aging-related disease [130]. The ER stress response is normally activated under conditions of increased protein misfolding, but it can also be induced by decreased PC levels in the ER induced by *sams-1* RNAi [131]. Part of the ER stress response is a down-regulation of protein synthesis, which gradually decreases the total protein content of the ER, increasing the number of free chaperones. Accordingly, the down-regulation in the activity of the translation machinery that is consistently observed in aged *C. elegans* [132] may be partially induced by an aging-related decline in SAMS-1 level, which decreases PC levels in

the ER, which induces ER stress and the ER stress response pathway to slow the rate of protein synthesis.

The finding by Liang *et al*. of an age-related decrease in the levels of myosin-related proteins, as well as our identification of protein changes associated with decreased muscle function seem to fit with the observations of sarcopenia in aged *C. elegans*. In addition to body wall muscle, the *C. elegans* pharyngeal pump is greatly affected by sarcopenia. In *C. elegans,* food is consumed through the rhythmic contraction of a set of 20 muscle cells and 20 neuronal cells, termed the pharyngeal pump located between the mouth and the start of the intestine. As *C. elegans* age, the pumping rate gradually slows, and bacteria will often form a plug within the structure, blocking the passage of food to the intestine. The muscle cells of the pharyngeal pump also lose their shape and organization and by late in the *C. elegans* lifespan the loss of structure and function can be rather extreme [133]. The most common *C. elegans* model of dietary restriction is the *eat-2* mutant, which has slowed pharyngeal pumping resulting in a reduced rate of food intake [134]. Dietary restriction appears to work partially through the inhibition of SAMS-1, which down-regulates the expression of the eIF4H gene *drr-2* [135], and RNAi knockdown of SAMS-1 fails to further extend the lifespan of *eat-2* mutants [136]. Given that vitamin B12 and folate are both necessary for SAM metabolism and are both obtained by *C. elegans* only through diet, loss of pharyngeal pump function in aged *C. elegans* likely results in a late-life dietary restriction phenotype. This sarcopenia-induced dietary restriction in aged worms likely contributes to lowering SAM and PC levels, and increasing the size of LDs in intestine, hypodermis, and muscle [2, 137]. LDs are known to increase in size in aged human muscle as well, perhaps in response to increased fatty acid levels from decreased mitochondrial β-oxidation

rates due to electron transport chain dysfunction [138]. It will be interesting to determine if similar mechanisms exist to regulate LD size in humans and nematodes.

The age-related decrease in monoacylglycerols and increase in free fatty acids and the ketone body βHB have at least two possible non-exclusive explanations. First, the increase in free fatty acids and βHB may be the byproduct of increased LD-directed autophagy, up-regulated either as a mechanism for dealing with increased LD accumulation, or as an attempt to meet energy demands under conditions of dietary restriction. Or second, an up-regulation of fatty acid synthesis may result in an increased conversion of citrate into acetyl-CoA (a fatty acid precursor), which is converted into βHB when present in excess, and the increased citrate levels observed in older *C. elegans* may be indicative of this. The enzyme aconitase can divert metabolism away from fatty acid synthesis by converting citrate into isocitrate, which is then converted into α-ketoglutarate by isocitrate dehydrogenase. Notably, mitochondrial aconitase is highly susceptible to impairment by reactive oxygen species (ROS) [139, 140]. Increases in ROS production or decreased antioxidant capacity within mitochondria could lead to an increase in mitochondrial citrate, which would then be exported to the cytoplasm and made available for fatty acid synthesis. Furthermore, the decreased abundance in IDH-1 levels that we observed would help to promote the use of cytosolic citrate for fatty acid synthesis, since the alternate conversion of citrate to isocitrate and α-ketoglutarate would be restricted. However, fatty acid synthesis relies on NADPH, which may be in short supply when IDH-1 protein levels decline with age. We also previously reported that the dietary supplementation of citrate to *C. elegans* produced ER stress [25].

The mechanisms behind the findings of decreased abundance of the poly(ADP-ribose) polymerase PME-1 with aging are unknown. There are six members of the PME family of *C.*

elegans poly(ADP-ribose) polymerases. Our proteomic analysis only identified two of these proteins, the second of which (PME-5) was unchanged with age, but interestingly poly(ADP-ribosylation) capacity in PBMCs declines with age in humans and rodents [141]. In addition poly(ADP-ribosylation) capacity was shown to be directly proportional to lifespan when comparing 13 species [142] and also very high in human centenarians [143]. This is likely due to the important role that poly(ADP-ribose) polymerases play in genomic stability, but it could also be due to the important role they play in regulating chromatin structure [144].

The increased level of sorbitol with aging is striking in that its accumulation, along with increased flux through the polyol pathway, is associated with diabetes [56, 59-61]. Sorbitol is likely formed as a result of increased glucose levels when glycolysis is slowed due to low NAD^+ levels or possibly due to oxidative damage to glycolytic enzymes such as GAPDH [145] or enolase [146]. The low NAD^+ levels in aged cells would likely slow the conversion of sorbitol to fructose and re-entry into glycolysis, leading to sorbitol build up. As mentioned previously, ectopic fat and lipotoxicity have been associated with the onset of insulin resistance [120, 121], suggesting that the observed alterations in fat metabolism and the accumulation of sorbitol may be linked. However, in some yeasts and fungi, as well as in mammalian kidney cells, sorbitol has been identified as an osmolyte for adjusting the intracellular environment to osmotic stress [147-149]. The age-related increase in sorbitol may be a cellular strategy for combating water loss, or simply to balance the dilution of cellular contents that would occur as *C. elegans* increase their volume as the animal grows in size.

2.6 Conclusions

We observed an age-related change in fatty acid metabolism, a decreased abundance of proteins involved in protein synthesis as well as decreases in the levels of many purine and pyrimidine metabolites, changes in free amino acids likely associated with the decreased surface-to-volume ratio of aged *C. elegans* cells, signs of muscle dysfunction and altered SR Ca^{2+} homeostasis, decreased abundance of SAMS-1 and altered SAM metabolism, indicators of a redox shift toward an oxidizing cellular environment likely due to mitochondrial dysfunction, and a large increase in sorbitol levels. We hypothesize that the ectopic accumulation of lipids possibly through the accumulation of yolk lipid proteins that occurs after the cessation of egg-laying likely contributes to lipotoxicity that may account for some of the observed changes with age. We further hypothesize that the age-related reduction in SAM synthesis may be a consequence of dietary restriction caused by age-related pharyngeal pump dysfunction and may act to counter some of the effects of the lipotoxicity.

2.7 Acknowledgements

We would like to thank Robert Hill for his helpful advice, and Alexander Ulanov at the University of Illinois Metabolomics Center for his technical expertise. We would also like to thank Dr. Jeremiah Tipton at the University of South Florida Proteomics facility for his help with performing HPLC and LC-MS/MS, Dr. Harris Bell-Temin for his assistance while analyzing the proteomics results, and Dr. Angus Lamond at the University of Dundee, UK for providing us with the plasmid-containing SLE1 HT115(DE3) strain of *E. coli*. *C. elegans* strains were obtained from the Caenorhabditis Genetics Center (University of Minnesota, Minneapolis, MN, USA), which is funded by NIH Office of Research Infrastructure Programs (P40 OD010440).

The research was funded in part by NIH grant # AG046769 awarded to PB and through funds provided by the University of South Florida.

2.8 References

1. Glenn CF, Chow DK, David L, Cooke CA, Gami MS, Iser WB, et al. Behavioral deficits during early stages of aging in caenorhabditis elegans result from locomotory deficits possibly linked to muscle frailty. J Gerontol A Biol Sci Med Sci. 2004;59(12):1251-60. doi: 10.1093/gerona/59.12.1251. PubMed PMID: 15699524; PubMed Central PMCID: PMC1458366.

2. Herndon LA, Schmeissner PJ, Dudaronek JM, Brown PA, Listner KM, Sakano Y, et al. Stochastic and genetic factors influence tissue-specific decline in ageing c. Elegans. Nature. 2002;419(6909):808-14. doi: 10.1038/nature01135. PubMed PMID: 12397350.

3. Gerstbrein B, Stamatas G, Kollias N, Driscoll M. In vivo spectrofluorimetry reveals endogenous biomarkers that report healthspan and dietary restriction in caenorhabditis elegans. Aging cell. 2005;4(3):127-37. doi: 10.1111/j.1474-9726.2005.00153.x.

4. Houthoofd K, Braeckman BP, Lenaerts I, Brys K, Matthijssens F, De Vreese A, et al. Daf-2 pathway mutations and food restriction in aging caenorhabditis elegans differentially affect metabolism. Neurobiol Aging. 2005;26(5):689-96. doi: 10.1016/j.neurobiolaging.2004.06.011. PubMed PMID: 15708444.

5. Brys K, Castelein N, Matthijssens F, Vanfleteren JR, Braeckman BP. Disruption of insulin signalling preserves bioenergetic competence of mitochondria in ageing caenorhabditis elegans. BMC Biol. 2010;8(1):91. doi: 10.1186/1741-7007-8-91. PubMed PMID: 20584279; PubMed Central PMCID: PMC2914644.

6. Labbadia J, Morimoto RI. Proteostasis and longevity: When does aging really begin? F1000prime reports. 2014;6(7). doi: 10.12703/P6-7. PubMed Central PMCID: PMCPMC3914504.

7. David DC, Ollikainen N, Trinidad JC, Cary MP, Burlingame AL, Kenyon C. Widespread protein aggregation as an inherent part of aging in c. Elegans. PLoS biology. 2010;8(8):e1000450. doi: 10.1371/journal.pbio.1000450.

8. Ishii N, Goto S, Hartman PS. Protein oxidation during aging of the nematode caenorhabditis elegans. Free Radic Biol Med. 2002;33(8):1021-5. doi: 10.1016/S0891-5849(02)00857-2. PubMed PMID: 12374613.

9. Morcos M, Du X, Pfisterer F, Hutter H, Sayed AA, Thornalley P, et al. Glyoxalase-1 prevents mitochondrial protein modification and enhances lifespan in caenorhabditis elegans. Aging Cell. 2008;7(2):260-9. doi: 10.1111/j.1474-9726.2008.00371.x. PubMed PMID: 18221415.

10. Friedman DB, Johnson TE. A mutation in the age-1 gene in caenorhabditis elegans lengthens life and reduces hermaphrodite fertility. Genetics. 1988;118(1):75-86. PubMed PMID: 8608934; PubMed Central PMCID: PMC1203268.

11. Tissenbaum HA. Genetics, life span, health span, and the aging process in caenorhabditis elegans. J Gerontol A Biol Sci Med Sci. 2012;67(5):503-10. doi: 10.1093/gerona/gls088. PubMed PMID: 22499764; PubMed Central PMCID: PMC3410663.

12. Leavy SA. The last of life: Psychological reflections on old age and death. Psychoanal Q. 2011;80(3):699-715. doi: 10.1002/j.2167-4086.2011.tb00102.x. PubMed PMID: 21874997.

13. Murshid A, Eguchi T, Calderwood SK. Stress proteins in aging and life span. Int J Hyperthermia. 2013;29(5):442-7. doi: 10.3109/02656736.2013.798873. PubMed PMID: 23742046; PubMed Central PMCID: PMC4083487.

14. Kenyon C. The plasticity of aging: Insights from long-lived mutants. Cell. 2005;120(4):449-60. doi: 10.1016/j.cell.2005.02.002. PubMed PMID: 15734678.

15. Cohen E, Bieschke J, Perciavalle RM, Kelly JW, Dillin A. Opposing activities protect against age-onset proteotoxicity. Science. 2006;313(5793):1604-10. doi: 10.1126/science.1124646. PubMed PMID: 16902091.

16. Apfeld J, Kenyon C. Cell nonautonomy of c. Elegans daf-2 function in the regulation of diapause and life span. Cell. 1998;95(2):199-210. doi: 10.1016/S0092-8674(00)81751-1. PubMed PMID: 9790527.

17. Gems D, Sutton AJ, Sundermeyer ML, Albert PS, King KV, Edgley ML, et al. Two pleiotropic classes of daf-2 mutation affect larval arrest, adult behavior, reproduction and longevity in caenorhabditis elegans. Genetics. 1998;150(1):129-55. PubMed PMID: 9725835; PubMed Central PMCID: PMC1460297.

18. Tullet JM, Hertweck M, An JH, Baker J, Hwang JY, Liu S, et al. Direct inhibition of the longevity-promoting factor skn-1 by insulin-like signaling in c. Elegans. Cell. 2008;132(6):1025-38. doi: 10.1016/j.cell.2008.01.030. PubMed PMID: 18358814; PubMed Central PMCID: PMC2367249.

19. Weinkove D, Halstead JR, Gems D, Divecha N. Long-term starvation and ageing induce age-1/pi 3-kinase-dependent translocation of daf-16/foxo to the cytoplasm. BMC Biol. 2006;4(1):1. doi: 10.1186/1741-7007-4-1. PubMed PMID: 16457721; PubMed Central PMCID: PMC1403811.

20. Dali-Youcef N, Lagouge M, Froelich S, Koehl C, Schoonjans K, Auwerx J. Sirtuins: The'magnificent seven', function, metabolism and longevity. Annals of medicine. 2007;39(5):335-45. doi: 10.1080/07853890701408194.

21. Golden TR, Melov S. Gene expression changes associated with aging in c. Elegans. WormBook. 2007:1-12. doi: 10.1895/wormbook.1.127.2. PubMed PMID: 18050504.

22. Ni Z, Lee SS. Rnai screens to identify components of gene networks that modulate aging in caenorhabditis elegans. Briefings in functional genomics. 2010;9(1):53-64. doi: 10.1093/bfgp/elp051.

23. Edwards CB, Copes N, Brito AG, Canfield J, Bradshaw PC. Malate and fumarate extend lifespan in caenorhabditis elegans. PLoS One. 2013;8(3):e58345. doi: 10.1371/journal.pone.0058345. PubMed PMID: 23472183; PubMed Central PMCID: PMC3589421.

24. Edwards C, Canfield J, Copes N, Rehan M, Lipps D, Bradshaw PC. D-beta-hydroxybutyrate extends lifespan in c. Elegans. Aging (Albany NY). 2014;6(8):621-44. PubMed PMID: 25127866; PubMed Central PMCID: PMC4169858.

25. Edwards C, Canfield J, Copes N, Brito A, Rehan M, Lipps D, et al. Mechanisms of amino acid-mediated lifespan extension in caenorhabditis elegans. BMC Genet. 2015;16(1):8. doi: 10.1186/s12863-015-0167-2. PubMed PMID: 25643626; PubMed Central PMCID: PMC4328591.

26. Larance M, Bailly AP, Pourkarimi E, Hay RT, Buchanan G, Coulthurst S, et al. Stable-isotope labeling with amino acids in nematodes. Nat Methods. 2011;8(10):849-51. doi: 10.1038/nmeth.1679. PubMed PMID: 21874007; PubMed Central PMCID: PMC3184259.

27. Stiernagle T. Maintenance of c. Elegans. In: Hope IA, editor. C elegans: A practical approach: Oxford University Press; 1999. p. 51-67.

28. Braeckman BP, Houthoofd K, De Vreese A, Vanfleteren JR. Assaying metabolic activity in ageing caenorhabditis elegans. Mech Ageing Dev. 2002;123(2-3):105-19. doi: 10.1016/S0047-6374(01)00331-1. PubMed PMID: 11718805.

29. van den Berg RA, Hoefsloot HC, Westerhuis JA, Smilde AK, van der Werf MJ. Centering, scaling, and transformations: Improving the biological information content of metabolomics data. BMC Genomics. 2006;7(1):142. doi: 10.1186/1471-2164-7-142. PubMed PMID: 16762068; PubMed Central PMCID: PMC1534033.

30. Cox J, Mann M. Maxquant enables high peptide identification rates, individualized ppb-range mass accuracies and proteome-wide protein quantification. Nature biotechnology. 2008;26(12):1367-72. doi: 10.1038/nbt.1511.

31. Beanan MJ, Strome S. Characterization of a germ-line proliferation mutation in c. Elegans. Development. 1992;116(3):755-66. PubMed PMID: 1289064.

32. Klass MR. Aging in the nematode caenorhabditis elegans: Major biological and environmental factors influencing life span. Mech Ageing Dev. 1977;6(6):413-29. doi: 10.1016/0047-6374(77)90043-4. PubMed PMID: 926867.

33. Kanehisa M, Goto S. Kegg: Kyoto encyclopedia of genes and genomes. Nucleic Acids Res. 2000;28(1):27-30. doi: 10.1093/nar/28.1.27. PubMed PMID: 10592173; PubMed Central PMCID: PMC102409.

34. Sulston JE, Horvitz HR. Post-embryonic cell lineages of the nematode, caenorhabditis elegans. Dev Biol. 1977;56(1):110-56. doi: 10.1016/0012-1606(77)90158-0. PubMed PMID: 838129.

35. Sulston JE, Schierenberg E, White JG, Thomson JN. The embryonic cell lineage of the nematode caenorhabditis elegans. Dev Biol. 1983;100(1):64-119. doi: 10.1016/0012-1606(83)90201-4. PubMed PMID: 6684600.

36. Byerly L, Cassada RC, Russell RL. The life cycle of the nematode caenorhabditis elegans. I. Wild-type growth and reproduction. Dev Biol. 1976;51(1):23-33. doi: 10.1016/0012-1606(76)90119-6. PubMed PMID: 988845.

37. Swire J, Fuchs S, Bundy JG, Leroi AM. The cellular geometry of growth drives the amino acid economy of caenorhabditis elegans. Proc Biol Sci. 2009;276(1668):2747-54. doi: 10.1098/rspb.2009.0354. PubMed PMID: 19439436; PubMed Central PMCID: PMC2839950.

38. Jiang M, Ryu J, Kiraly M, Duke K, Reinke V, Kim SK. Genome-wide analysis of developmental and sex-regulated gene expression profiles in caenorhabditis elegans. Proc Natl Acad Sci U S A. 2001;98(1):218-23. doi: 10.1073/pnas.011520898. PubMed PMID: 11134517; PubMed Central PMCID: PMC14571.

39. Monera OD, Sereda TJ, Zhou NE, Kay CM, Hodges RS. Relationship of sidechain hydrophobicity and alpha-helical propensity on the stability of the single-stranded amphipathic alpha-helix. J Pept Sci. 1995;1(5):319-29. doi: 10.1002/psc.310010507. PubMed PMID: 9223011.

40. Chiang PK, Gordon RK, Tal J, Zeng GC, Doctor BP, Pardhasaradhi K, et al. S-adenosylmethionine and methylation. FASEB J. 1996;10(4):471-80. doi: 10.1096/fj.1530-6860. PubMed PMID: 8647346.

41. Kent C. Eukaryotic phospholipid biosynthesis. Annu Rev Biochem. 1995;64(1):315-43. doi: 10.1146/annurev.bi.64.070195.001531. PubMed PMID: 7574485.

42. Carman GM, Henry SA. Phospholipid biosynthesis in yeast. Annu Rev Biochem. 1989;58(1):635-69. doi: 10.1146/annurev.bi.58.070189.003223. PubMed PMID: 2673019.

43. Lykidis A, Jackowski S. Regulation of mammalian cell membrane biosynthesis. Progress in nucleic acid research and molecular biology. 2000;65:361-93. doi: 10.1016/S0079-6603(00)65010-9.

44. Sohlenkamp C, Lopez-Lara IM, Geiger O. Biosynthesis of phosphatidylcholine in bacteria. Prog Lipid Res. 2003;42(2):115-62. doi: 10.1016/S0163-7827(02)00050-4. PubMed PMID: 12547654.

45. Kanipes MI, Henry SA. The phospholipid methyltransferases in yeast. Biochim Biophys Acta. 1997;1348(1-2):134-41. doi: 10.1016/S0005-2760(97)00121-5. PubMed PMID: 9370325.

46. Vance DE, Walkey CJ, Cui Z. Phosphatidylethanolamine n-methyltransferase from liver. Biochim Biophys Acta. 1997;1348(1-2):142-50. doi: 10.1016/S0005-2760(97)00108-2. PubMed PMID: 9370326.

47. Pessi G, Kociubinski G, Mamoun CB. A pathway for phosphatidylcholine biosynthesis in plasmodium falciparum involving phosphoethanolamine methylation. Proc Natl Acad Sci U S A. 2004;101(16):6206-11. doi: 10.1073/pnas.0307742101. PubMed PMID: 15073329; PubMed Central PMCID: PMC395947.

48. Palavalli LH, Brendza KM, Haakenson W, Cahoon RE, McLaird M, Hicks LM, et al. Defining the role of phosphomethylethanolamine n-methyltransferase from caenorhabditis elegans in phosphocholine biosynthesis by biochemical and kinetic analysis. Biochemistry. 2006;45(19):6056-65. doi: 10.1021/bi060199d. PubMed PMID: 16681378.

49. Brendza KM, Haakenson W, Cahoon RE, Hicks LM, Palavalli LH, Chiapelli BJ, et al. Phosphoethanolamine n-methyltransferase (pmt-1) catalyses the first reaction of a new pathway for phosphocholine biosynthesis in caenorhabditis elegans. Biochem J. 2007;404(3):439-48. doi: 10.1042/BJ20061815. PubMed PMID: 17313371; PubMed Central PMCID: PMC1896273.

50. Bartz R, Li W, Venables B, Zehmer JK, Roth MR, Welti R, et al. Lipidomics reveals that adiposomes store ether lipids and mediate phospholipid traffic. Journal of lipid research. 2007;48(4):837-47. doi: 10.1194/jlr.M600413-JLR200.

51. Krahmer N, Guo Y, Wilfling F, Hilger M, Lingrell S, Heger K, et al. Phosphatidylcholine synthesis for lipid droplet expansion is mediated by localized activation of ctp: Phosphocholine cytidylyltransferase. Cell metabolism. 2011;14(4):504-15. doi: 10.1016/j.cmet.2011.07.013.

52. Li Y, Na K, Lee HJ, Lee EY, Paik YK. Contribution of sams-1 and pmt-1 to lipid homoeostasis in adult caenorhabditis elegans. J Biochem. 2011;149(5):529-38. doi: 10.1093/jb/mvr025. PubMed PMID: 21389045.

53. Ehmke M, Luthe K, Schnabel R, Doring F. S-adenosyl methionine synthetase 1 limits fat storage in caenorhabditis elegans. Genes Nutr. 2014;9(2):386. doi: 10.1007/s12263-014-0386-6. PubMed PMID: 24510589; PubMed Central PMCID: PMC3968293.

54. Ackerman D, Gems D. The mystery of c. Elegans aging: An emerging role for fat. Distant parallels between c. Elegans aging and metabolic syndrome? Bioessays. 2012;34(6):466-71. doi: 10.1002/bies.201100189. PubMed PMID: 22371137.

55. Watson JA, Fang M, Lowenstein JM. Tricarballylate and hydroxycitrate: Substrate and inhibitor of atp: Citrate oxaloacetate lyase. Arch Biochem Biophys. 1969;135(1):209-17. doi: 10.1016/0003-9861(69)90532-3. PubMed PMID: 5362924.

56. Gabbay KH. The sorbitol pathway and the complications of diabetes. N Engl J Med. 1973;288(16):831-6. doi: 10.1056/NEJM197304192881609. PubMed PMID: 4266466.

57. Oates PJ. Polyol pathway and diabetic peripheral neuropathy. Int Rev Neurobiol. 2002;50:325-92. doi: 10.1016/S0074-7742(02)50082-9. PubMed PMID: 12198816.

58. Lorenzi M. The polyol pathway as a mechanism for diabetic retinopathy: Attractive, elusive, and resilient. Journal of Diabetes Research. 2007;2007. doi: 10.1155/2007/61038.

59. Szwergold BS, Kappler F, Brown TR. Identification of fructose 3-phosphate in the lens of diabetic rats. Science. 1990;247(4941):451-4. doi: 10.1126/science.2300805. PubMed PMID: 2300805.

60. Dagher Z, Park YS, Asnaghi V, Hoehn T, Gerhardinger C, Lorenzi M. Studies of rat and human retinas predict a role for the polyol pathway in human diabetic retinopathy. Diabetes. 2004;53(9):2404-11. doi: 10.2337/diabetes.53.9.2404. PubMed PMID: 15331552.

61. Asnaghi V, Gerhardinger C, Hoehn T, Adeboje A, Lorenzi M. A role for the polyol pathway in the early neuroretinal apoptosis and glial changes induced by diabetes in the rat. Diabetes. 2003;52(2):506-11. doi: 10.2337/diabetes.52.2.506. PubMed PMID: 12540628.

62. Barnett PA, Gonzalez RG, Chylack LT, Jr., Cheng HM. The effect of oxidation on sorbitol pathway kinetics. Diabetes. 1986;35(4):426-32. doi: 10.2337/diab.35.4.426. PubMed PMID: 3956880.

63. Williamson JR, Chang K, Frangos M, Hasan KS, Ido Y, Kawamura T, et al. Hyperglycemic pseudohypoxia and diabetic complications. Diabetes. 1993;42(6):801-13. doi: 10.2337/diab.42.6.801. PubMed PMID: 8495803.

64. Lou MF, Dickerson JE, Jr., Garadi R, York BM, Jr. Glutathione depletion in the lens of galactosemic and diabetic rats. Exp Eye Res. 1988;46(4):517-30. doi: 10.1016/S0014-4835(88)80009-5. PubMed PMID: 3133235.

65. Cameron NE, Eaton SE, Cotter MA, Tesfaye S. Vascular factors and metabolic interactions in the pathogenesis of diabetic neuropathy. Diabetologia. 2001;44(11):1973-88. doi: 10.1007/s001250100001. PubMed PMID: 11719828.

66. Obrosova IG, Van Huysen C, Fathallah L, Cao XC, Greene DA, Stevens MJ. An aldose reductase inhibitor reverses early diabetes-induced changes in peripheral nerve function, metabolism, and antioxidative defense. FASEB J. 2002;16(1):123-5. doi: 10.1096/fj.01-0603fje. PubMed PMID: 11709499.

67. Lee AY, Chung SS. Contributions of polyol pathway to oxidative stress in diabetic cataract. FASEB J. 1999;13(1):23-30. doi: 10.1096/fj.1530-6860. PubMed PMID: 9872926.

68. Obrosova IG, Pacher P, Szabo C, Zsengeller Z, Hirooka H, Stevens MJ, et al. Aldose reductase inhibition counteracts oxidative-nitrosative stress and poly(adp-ribose) polymerase activation in tissue sites for diabetes complications. Diabetes. 2005;54(1):234-42. doi: 10.2337/diabetes.54.1.234. PubMed PMID: 15616034; PubMed Central PMCID: PMC2756473.

69. Michels AJ, Frei B. Myths, artifacts, and fatal flaws: Identifying limitations and opportunities in vitamin c research. Nutrients. 2013;5(12):5161-92. doi: 10.3390/nu5125161. PubMed PMID: 24352093; PubMed Central PMCID: PMC3875932.

70. Smith AR, Visioli F, Hagen TM. Vitamin c matters: Increased oxidative stress in cultured human aortic endothelial cells without supplemental ascorbic acid. The FASEB journal. 2002;16(9):1102-4. doi: 10.1096/fj.01-0825fje.

71. Martin A, Frei B. Both intracellular and extracellular vitamin c inhibit atherogenic modification of ldl by human vascular endothelial cells. Arteriosclerosis, thrombosis, and vascular biology. 1997;17(8):1583-90. doi: 10.1161/01.ATV.17.8.1583.

72. Meister A. Glutathione-ascorbic acid antioxidant system in animals. J Biol Chem. 1994;269(13):9397-400. PubMed PMID: 8144521.

73. Jahn M, Baynes JW, Spiteller G. The reaction of hyaluronic acid and its monomers, glucuronic acid and n-acetylglucosamine, with reactive oxygen species. Carbohydr Res. 1999;321(3-4):228-34. doi: 10.1016/S0008-6215(99)00186-X. PubMed PMID: 10614067.

74. Patananan AN, Budenholzer LM, Pedraza ME, Torres ER, Adler LN, Clarke SG. The invertebrate caenorhabditis elegans biosynthesizes ascorbate. Arch Biochem Biophys. 2015;569:32-44. Epub 2015/02/11. doi: 10.1016/j.abb.2015.02.002. PubMed PMID: 25668719; PubMed Central PMCID: PMC4357563.

75. Williamson DH, Lund P, Krebs HA. The redox state of free nicotinamide-adenine dinucleotide in the cytoplasm and mitochondria of rat liver. Biochem J. 1967;103(2):514-27. PubMed PMID: 4291787; PubMed Central PMCID: PMC1270436.

76. Braidy N, Guillemin GJ, Mansour H, Chan-Ling T, Poljak A, Grant R. Age related changes in nad+ metabolism oxidative stress and sirt1 activity in wistar rats. PLoS One. 2011;6(4):e19194. doi: 10.1371/journal.pone.0019194. PubMed PMID: 21541336; PubMed Central PMCID: PMC3082551.

77. Zhu XH, Lu M, Lee BY, Ugurbil K, Chen W. In vivo nad assay reveals the intracellular nad contents and redox state in healthy human brain and their age dependences. Proc Natl Acad Sci U S A. 2015;112(9):2876-81. Epub 2015/03/03. doi: 10.1073/pnas.1417921112. PubMed PMID: 25730862; PubMed Central PMCID: PMC4352772.

78. Massudi H, Grant R, Braidy N, Guest J, Farnsworth B, Guillemin GJ. Age-associated changes in oxidative stress and nad+ metabolism in human tissue. PLoS One. 2012;7(7):e42357. doi: 10.1371/journal.pone.0042357. PubMed PMID: 22848760; PubMed Central PMCID: PMC3407129.

79. Veech RL, Eggleston LV, Krebs HA. The redox state of free nicotinamide-adenine dinucleotide phosphate in the cytoplasm of rat liver. Biochem J. 1969;115(4):609-19. PubMed PMID: 4391039; PubMed Central PMCID: PMC1185185.

80. Franceschini A, Szklarczyk D, Frankild S, Kuhn M, Simonovic M, Roth A, et al. String v9.1: Protein-protein interaction networks, with increased coverage and integration. Nucleic Acids Res. 2013;41(Database issue):D808-15. doi: 10.1093/nar/gks1094. PubMed PMID: 23203871; PubMed Central PMCID: PMC3531103.

81. Takahashi Y, Daitoku H, Yokoyama A, Nakayama K, Kim JD, Fukamizu A. The c. Elegans prmt-3 possesses a type iii protein arginine methyltransferase activity. J Recept Signal Transduct Res. 2011;31(2):168-72. doi: 10.3109/10799893.2011.555768. PubMed PMID: 21385054.

82. Simpson VJ, Johnson TE, Hammen RF. Caenorhabditis elegans DNA does not contain 5-methylcytosine at any time during development or aging. Nucleic acids research. 1986;14(16):6711-9. doi: 10.1093/nar/14.16.6711.

83. Whetstine JR, Ceron J, Ladd B, Dufourcq P, Reinke V, Shi Y. Regulation of tissue-specific and extracellular matrix-related genes by a class i histone deacetylase. Mol Cell. 2005;18(4):483-90. doi: 10.1016/j.molcel.2005.04.006. PubMed PMID: 15893731.

84. Eneqvist T, Lundberg E, Nilsson L, Abagyan R, Sauer-Eriksson AE. The transthyretin-related protein family. Eur J Biochem. 2003;270(3):518-32. doi: 10.1046/j.1432-1033.2003.03408.x. PubMed PMID: 12542701.

85. Klein C, Kemmel V, Taleb O, Aunis D, Maitre M. Pharmacological doses of gamma-hydroxybutyrate (ghb) potentiate histone acetylation in the rat brain by histone deacetylase inhibition. Neuropharmacology. 2009;57(2):137-47. Epub 2009/05/12. doi: 10.1016/j.neuropharm.2009.04.013. PubMed PMID: 19427877.

86. Hegedűs C, Virág L. Inputs and outputs of poly (adp-ribosyl) ation: Relevance to oxidative stress. Redox biology. 2014;2:978-82. doi: 10.1016/j.redox.2014.08.003.

87. Dequen F, Gagnon SN, Desnoyers S. Ionizing radiations in caenorhabditis elegans induce poly(adp-ribosyl)ation, a conserved DNA-damage response essential for survival. DNA Repair (Amst). 2005;4(7):814-25. doi: 10.1016/j.dnarep.2005.04.015. PubMed PMID: 15923155.

88. Bai P, Cantó C, Oudart H, Brunyánszki A, Cen Y, Thomas C, et al. Parp-1 inhibition increases mitochondrial metabolism through sirt1 activation. Cell metabolism. 2011;13(4):461-8. doi: 10.1016/j.cmet.2011.03.004.

89. Zaidi N, Swinnen JV, Smans K. Atp-citrate lyase: A key player in cancer metabolism. Cancer Res. 2012;72(15):3709-14. doi: 10.1158/0008-5472.CAN-11-4112. PubMed PMID: 22787121.

90. Nouws J, Nijtmans L, Houten SM, van den Brand M, Huynen M, Venselaar H, et al. Acyl-coa dehydrogenase 9 is required for the biogenesis of oxidative phosphorylation complex i. Cell metabolism. 2010;12(3):283-94. doi: 10.1016/j.cmet.2010.08.002.

91. Grant B, Hirsh D. Receptor-mediated endocytosis in the caenorhabditis elegans oocyte. Mol Biol Cell. 1999;10(12):4311-26. Epub 1999/12/10. PubMed PMID: 10588660; PubMed Central PMCID: PMC25760.

92. Kimble J, Sharrock WJ. Tissue-specific synthesis of yolk proteins in caenorhabditis elegans. Dev Biol. 1983;96(1):189-96. Epub 1983/03/01. PubMed PMID: 6825952.

93. Shaye DD, Greenwald I. Ortholist: A compendium of c. Elegans genes with human orthologs. PLoS One. 2011;6(5):e20085. doi: 10.1371/journal.pone.0020085. PubMed PMID: 21647448; PubMed Central PMCID: PMC3102077.

94. Prasad V, Okunade GW, Miller ML, Shull GE. Phenotypes of serca and pmca knockout mice. Biochem Biophys Res Commun. 2004;322(4):1192-203. doi: 10.1016/j.bbrc.2004.07.156. PubMed PMID: 15336967.

95. Zwaal RR, Van Baelen K, Groenen JTM, van Geel A, Rottiers V, Kaletta T, et al. The sarco-endoplasmic reticulum ca2+ atpase is required for development and muscle function in caenorhabditis elegans. Journal of Biological Chemistry. 2001;276(47):43557-63. doi: 10.1074/jbc.M104693200.

96. Periasamy M, Reed TD, Liu LH, Ji Y, Loukianov E, Paul RJ, et al. Impaired cardiac performance in heterozygous mice with a null mutation in the sarco(endo)plasmic reticulum ca2+-atpase isoform 2 (serca2) gene. J Biol Chem. 1999;274(4):2556-62. doi: 10.1074/jbc.274.4.2556. PubMed PMID: 9891028.

97. Almedom RB, Liewald JF, Hernando G, Schultheis C, Rayes D, Pan J, et al. An er-resident membrane protein complex regulates nicotinic acetylcholine receptor subunit composition at the synapse. The EMBO journal. 2009;28(17):2636-49. doi: 10.1038/emboj.2009.204.

98. Kamat S, Yeola S, Zhang W, Bianchi L, Driscoll M. Nra-2, a nicalin homolog, regulates neuronal death by controlling surface localization of toxic caenorhabditis elegans deg/enac channels. J Biol Chem. 2014;289(17):11916-26. doi: 10.1074/jbc.M113.533695. PubMed PMID: 24567339; PubMed Central PMCID: PMC4002099.

99. McKay S, Johnsen R, Khattra J, Asano J, Baillie D, Chan S, et al., editors. Gene expression profiling of cells, tissues, and developmental stages of the nematode c. Elegans. Cold Spring Harbor symposia on quantitative biology; 2003: Cold Spring Harbor Laboratory Press.

100. Meissner B, Rogalski T, Viveiros R, Warner A, Plastino L, Lorch A, et al. Determining the sub-cellular localization of proteins within caenorhabditis elegans body wall muscle. PloS one. 2011;6(5):e19937. doi: 10.1371/journal.pone.0019937.

101. Arber S, Hunter JJ, Ross J, Jr., Hongo M, Sansig G, Borg J, et al. Mlp-deficient mice exhibit a disruption of cardiac cytoarchitectural organization, dilated cardiomyopathy, and heart failure. Cell. 1997;88(3):393-403. doi: 10.1016/S0092-8674(00)81878-4. PubMed PMID: 9039266.

102. Weiskirchen R, Gunther K. The crp/mlp/tlp family of lim domain proteins: Acting by connecting. Bioessays. 2003;25(2):152-62. doi: 10.1002/bies.10226. PubMed PMID: 12539241.

103. Henderson JR, Pomies P, Auffray C, Beckerle MC. Alp and mlp distribution during myofibrillogenesis in cultured cardiomyocytes. Cell Motil Cytoskeleton. 2003;54(3):254-65. doi: 10.1002/cm.10102. PubMed PMID: 12589684.

104. Kahvejian A, Svitkin YV, Sukarieh R, M'Boutchou M, Sonenberg N. Mammalian poly (a)-binding protein is a eukaryotic translation initiation factor, which acts via multiple mechanisms. Genes & development. 2005;19(1):104-13. doi: 10.1016/S0008-6215(99)00186-X. PubMed Central PMCID: PMCPMC540229.

105. Liu S, Milne GT, Kuremsky JG, Fink GR, Leppla SH. Identification of the proteins required for biosynthesis of diphthamide, the target of bacterial adp-ribosylating toxins on translation elongation factor 2. Mol Cell Biol. 2004;24(21):9487-97. doi: 10.1128/MCB.24.21.9487-9497.2004. PubMed PMID: 15485916; PubMed Central PMCID: PMC522255.

106. Longman D, Johnstone IL, Caceres JF. Functional characterization of sr and sr-related genes in caenorhabditis elegans. EMBO J. 2000;19(7):1625-37. doi: 10.1093/emboj/19.7.1625. PubMed PMID: 10747030; PubMed Central PMCID: PMC310231.

107. Rushforth AM, White CC, Anderson P. Functions of the caenorhabditis elegans regulatory myosin light chain genes mlc-1 and mlc-2. Genetics. 1998;150(3):1067-77. PubMed PMID: 9799259; PubMed Central PMCID: PMC1460388.

108. Ono S, Nomura K, Hitosugi S, Tu DK, Lee JA, Baillie DL, et al. The two actin-interacting protein 1 genes have overlapping and essential function for embryonic development in caenorhabditis elegans. Molecular biology of the cell. 2011;22(13):2258-69. doi: 10.1091/mbc.E10-12-0934.

109. West S, Gromak N, Proudfoot NJ. Human 5' --> 3' exonuclease xrn2 promotes transcription termination at co-transcriptional cleavage sites. Nature. 2004;432(7016):522-5. Epub 2004/11/27. doi: 10.1038/nature03035. PubMed PMID: 15565158.

110. Kawano T, Fujita M, Sakamoto H. Unique and redundant functions of sr proteins, a conserved family of splicing factors, in caenorhabditiselegans development. Mechanisms of development. 2000;95(1):67-76. doi: 10.1016/S0925-4773(00)00339-7.

111. Cui M, Allen MA, Larsen A, Macmorris M, Han M, Blumenthal T. Genes involved in pre-mrna 3'-end formation and transcription termination revealed by a lin-15 operon muv suppressor screen. Proc Natl Acad Sci U S A. 2008;105(43):16665-70. doi: 10.1073/pnas.0807104105. PubMed PMID: 18946043; PubMed Central PMCID: PMC2571909.

112. Patton JR, Bykhovskaya Y, Mengesha E, Bertolotto C, Fischel-Ghodsian N. Mitochondrial myopathy and sideroblastic anemia (mlasa): Missense mutation in the pseudouridine synthase 1 (pus1) gene is associated with the loss of trna pseudouridylation. J Biol Chem. 2005;280(20):19823-8. Epub 2005/03/18. doi: 10.1074/jbc.M500216200. PubMed PMID: 15772074.

113. Joshi KK, Chen L, Torres N, Tournier V, Madura K. A proteasome assembly defect in rpn3 mutants is associated with rpn11 instability and increased sensitivity to stress. J Mol Biol. 2011;410(3):383-99. Epub 2011/05/31. doi: 10.1016/j.jmb.2011.05.005. PubMed PMID: 21619884; PubMed Central PMCID: PMC3763486.

114. Chen YM, Liu SP, Lin HL, Chan MC, Chen YC, Huang YL, et al. Irisflorentin improves alpha-synuclein accumulation and attenuates 6-ohda-induced dopaminergic neuron degeneration, implication for parkinson's disease therapy. Biomedicine (Taipei). 2015;5(1):4. Epub 2015/02/24. doi: 10.7603/s40681-015-0004-y. PubMed PMID: 25705584; PubMed Central PMCID: PMC4326644.

115. Liang V, Ullrich M, Lam H, Chew YL, Banister S, Song X, et al. Altered proteostasis in aging and heat shock response in c. Elegans revealed by analysis of the global and de novo synthesized proteome. Cell Mol Life Sci. 2014;71(17):3339-61. doi: 10.1007/s00018-014-1558-7. PubMed PMID: 24458371; PubMed Central PMCID: PMC4131143.

116. Pontoizeau C, Mouchiroud L, Molin L, Mergoud-dit-Lamarche A, Dallière N, Toulhoat P, et al. Metabolomics analysis uncovers that dietary restriction buffers metabolic changes associated with aging in caenorhabditis elegans. Journal of proteome research. 2014;13(6):2910-9. doi: 10.1021/pr5000686.

117. Virk B, Correia G, Dixon DP, Feyst I, Jia J, Oberleitner N, et al. Excessive folate synthesis limits lifespan in the c. Elegans: E. Coli aging model. BMC Biol. 2012;10(1):67. doi: 10.1186/1741-7007-10-67. PubMed PMID: 22849329; PubMed Central PMCID: PMC3583181.

118. Watson E, MacNeil LT, Ritter AD, Yilmaz LS, Rosebrock AP, Caudy AA, et al. Interspecies systems biology uncovers metabolites affecting c. Elegans gene expression and life history traits. Cell. 2014;156(4):759-70. doi: 10.1016/j.cell.2014.01.047. PubMed PMID: 24529378; PubMed Central PMCID: PMC4169190.

119. Bosma M, Dapito DH, Drosatos-Tampakaki Z, Huiping-Son N, Huang LS, Kersten S, et al. Sequestration of fatty acids in triglycerides prevents endoplasmic reticulum stress in an in vitro model of cardiomyocyte lipotoxicity. Biochim Biophys Acta. 2014;1841(12):1648-55. doi: 10.1016/j.bbalip.2014.09.012. PubMed PMID: 25251292; PubMed Central PMCID: PMC4342292.

120. Shulman GI. Cellular mechanisms of insulin resistance. J Clin Invest. 2000;106(2):171-6. doi: 10.1172/JCI10583. PubMed PMID: 10903330; PubMed Central PMCID: PMC314317.

121. Griffin ME, Marcucci MJ, Cline GW, Bell K, Barucci N, Lee D, et al. Free fatty acid-induced insulin resistance is associated with activation of protein kinase c theta and alterations in the insulin signaling cascade. Diabetes. 1999;48(6):1270-4. doi: 10.2337/diabetes.48.6.1270.

122. Chiu HC, Kovacs A, Ford DA, Hsu FF, Garcia R, Herrero P, et al. A novel mouse model of lipotoxic cardiomyopathy. J Clin Invest. 2001;107(7):813-22. doi: 10.1172/JCI10947. PubMed PMID: 11285300; PubMed Central PMCID: PMC199569.

123. Yagyu H, Chen G, Yokoyama M, Hirata K, Augustus A, Kako Y, et al. Lipoprotein lipase (lpl) on the surface of cardiomyocytes increases lipid uptake and produces a cardiomyopathy. J Clin Invest. 2003;111(3):419-26. doi: 10.1172/JCI16751. PubMed PMID: 12569168; PubMed Central PMCID: PMC151861.

124. Listenberger LL, Han X, Lewis SE, Cases S, Farese RV, Jr., Ory DS, et al. Triglyceride accumulation protects against fatty acid-induced lipotoxicity. Proc Natl Acad Sci U S A. 2003;100(6):3077-82. doi: 10.1073/pnas.0630588100. PubMed PMID: 12629214; PubMed Central PMCID: PMC152249.

125. Shi X, Li J, Zou X, Greggain J, Rodkaer SV, Faergeman NJ, et al. Regulation of lipid droplet size and phospholipid composition by stearoyl-coa desaturase. J Lipid Res. 2013;54(9):2504-14. Epub 2013/06/22. doi: 10.1194/jlr.M039669. PubMed PMID: 23787165; PubMed Central PMCID: PMC3735947.

126. Rockenfeller P, Koska M, Pietrocola F, Minois N, Knittelfelder O, Sica V, et al. Phosphatidylethanolamine positively regulates autophagy and longevity. Cell Death Differ. 2015;22(3):499-508. Epub 2015/01/13. doi: 10.1038/cdd.2014.219. PubMed PMID: 25571976; PubMed Central PMCID: PMC4326582.

127. Fang Y, Vilella-Bach M, Bachmann R, Flanigan A, Chen J. Phosphatidic acid-mediated mitogenic activation of mtor signaling. Science. 2001;294(5548):1942-5. Epub 2001/12/01. doi: 10.1126/science.1066015. PubMed PMID: 11729323.

128. Cruchaga C, Karch CM, Jin SC, Benitez BA, Cai Y, Guerreiro R, et al. Rare coding variants in the phospholipase d3 gene confer risk for alzheimer's disease. Nature. 2014;505(7484):550-4. Epub 2013/12/18. doi: 10.1038/nature12825. PubMed PMID: 24336208; PubMed Central PMCID: PMC4050701.

129. Patti GJ, Tautenhahn R, Johannsen D, Kalisiak E, Ravussin E, Bruning JC, et al. Meta-analysis of global metabolomic data identifies metabolites associated with life-span extension. Metabolomics. 2014;10(4):737-43. Epub 2014/12/23. doi: 10.1007/s11306-013-0608-8. PubMed PMID: 25530742; PubMed Central PMCID: PMC4267291.

130. Brown MK, Naidoo N. The endoplasmic reticulum stress response in aging and age-related diseases. Front Physiol. 2012;3:263. Epub 2012/08/31. doi: 10.3389/fphys.2012.00263. PubMed PMID: 22934019; PubMed Central PMCID: PMC3429039.

131. Hou NS, Gutschmidt A, Choi DY, Pather K, Shi X, Watts JL, et al. Activation of the endoplasmic reticulum unfolded protein response by lipid disequilibrium without disturbed proteostasis in vivo. Proc Natl Acad Sci U S A. 2014;111(22):E2271-80. Epub 2014/05/21. doi: 10.1073/pnas.1318262111. PubMed PMID: 24843123; PubMed Central PMCID: PMC4050548.

132. Syntichaki P, Troulinaki K, Tavernarakis N. Protein synthesis is a novel determinant of aging in caenorhabditis elegans. Ann N Y Acad Sci. 2007;1119:289-95. Epub 2007/12/07. doi: 10.1196/annals.1404.001. PubMed PMID: 18056976.

133. Chow DK, Glenn CF, Johnston JL, Goldberg IG, Wolkow CA. Sarcopenia in the caenorhabditis elegans pharynx correlates with muscle contraction rate over lifespan. Exp Gerontol. 2006;41(3):252-60. doi: 10.1016/j.exger.2005.12.004. PubMed PMID: 16446070; PubMed Central PMCID: PMC2553216.

134. Lakowski B, Hekimi S. The genetics of caloric restriction in caenorhabditis elegans. Proc Natl Acad Sci U S A. 1998;95(22):13091-6. doi: 10.1073/pnas.95.22.13091. PubMed PMID: 9789046; PubMed Central PMCID: PMC23719.

135. Ching T, Paal AB, Mehta A, Zhong L, Hsu AL. Drr-2 encodes an eif4h that acts downstream of tor in diet-restriction-induced longevity of c. Elegans. Aging cell. 2010;9(4):545-57. doi: 10.1111/j.1474-9726.2010.00580.x.

136. Hansen M, Hsu AL, Dillin A, Kenyon C. New genes tied to endocrine, metabolic, and dietary regulation of lifespan from a caenorhabditis elegans genomic rnai screen. PLoS Genet. 2005;1(1):119-28. doi: 10.1371/journal.pgen.0010017. PubMed PMID: 16103914; PubMed Central PMCID: PMC1183531.

137. Palgunow D, Klapper M, Doring F. Dietary restriction during development enlarges intestinal and hypodermal lipid droplets in caenorhabditis elegans. PloS One. 2012;7(11):e46198. Epub 2012/11/28. doi: 10.1371/journal.pone.0046198. PubMed PMID: 23185233; PubMed Central PMCID: PMC3502458.

138. Crane JD, Devries MC, Safdar A, Hamadeh MJ, Tarnopolsky MA. The effect of aging on human skeletal muscle mitochondrial and intramyocellular lipid ultrastructure. J Gerontol A Biol Sci Med Sci. 2010;65(2):119-28. Epub 2009/12/05. doi: 10.1093/gerona/glp179. PubMed PMID: 19959566.

139. Chen YR, Zweier JL. Cardiac mitochondria and reactive oxygen species generation. Circ Res. 2014;114(3):524-37. doi: 10.1161/CIRCRESAHA.114.300559. PubMed PMID: 24481843; PubMed Central PMCID: PMC4118662.

140. Walden WE. From bacteria to mitochondria: Aconitase yields surprises. Proc Natl Acad Sci U S A. 2002;99(7):4138-40. doi: 10.1073/pnas.082108799. PubMed PMID: 11929988; PubMed Central PMCID: PMC123612.

141. Beneke S, Scherr A, Ponath V, Popp O, Bürkle A. Enzyme characteristics of recombinant poly (adp-ribose) polymerases-1 of rat and human origin mirror the correlation between cellular poly (adp-ribosyl) ation capacity and species-specific life span. Mechanisms of ageing and development. 2010;131(5):366-9. doi: 10.1016/j.mad.2010.04.003.

142. Grube K, Burkle A. Poly(adp-ribose) polymerase activity in mononuclear leukocytes of 13 mammalian species correlates with species-specific life span. Proc Natl Acad Sci U S A. 1992;89(24):11759-63. PubMed PMID: 1465394; PubMed Central PMCID: PMC50636.

143. Muiras ML, Muller M, Schachter F, Burkle A. Increased poly(adp-ribose) polymerase activity in lymphoblastoid cell lines from centenarians. J Mol Med (Berl). 1998;76(5):346-54. PubMed PMID: 9587069.

144. Mangerich A, Burkle A. Pleiotropic cellular functions of parp1 in longevity and aging: Genome maintenance meets inflammation. Oxid Med Cell Longev. 2012;2012:321653. doi: 10.1155/2012/321653. PubMed PMID: 23050038; PubMed Central PMCID: PMC3459245.

145. Samson AL, Knaupp AS, Kass I, Kleifeld O, Marijanovic EM, Hughes VA, et al. Oxidation of an exposed methionine instigates the aggregation of glyceraldehyde-3-phosphate dehydrogenase. J Biol Chem. 2014;289(39):26922-36. Epub 2014/08/03. doi: 10.1074/jbc.M114.570275. PubMed PMID: 25086035; PubMed Central PMCID: PMC4175333.

146. Butterfield DA, Lange ML. Multifunctional roles of enolase in alzheimer's disease brain: Beyond altered glucose metabolism. J Neurochem. 2009;111(4):915-33. Epub 2009/09/29. doi: 10.1111/j.1471-4159.2009.06397.x [doi]. PubMed PMID: 19780894.

147. Burg MB, Ferraris JD. Intracellular organic osmolytes: Function and regulation. J Biol Chem. 2008;283(12):7309-13. doi: 10.1074/jbc.R700042200. PubMed PMID: 18256030; PubMed Central PMCID: PMC2276334.

148. Kiewietdejonge A, Pitts M, Cabuhat L, Sherman C, Kladwang W, Miramontes G, et al. Hypersaline stress induces the turnover of phosphatidylcholine and results in the synthesis of the renal osmoprotectant glycerophosphocholine in saccharomyces cerevisiae. FEMS Yeast Res. 2006;6(2):205-17. doi: 10.1111/j.1567-1364.2006.00030.x. PubMed PMID: 16487344.

149. Garcia-Perez A, Burg MB. Renal medullary organic osmolytes. Physiol Rev. 1991;71(4):1081-115. PubMed PMID: 1924548.

2.9 Figures

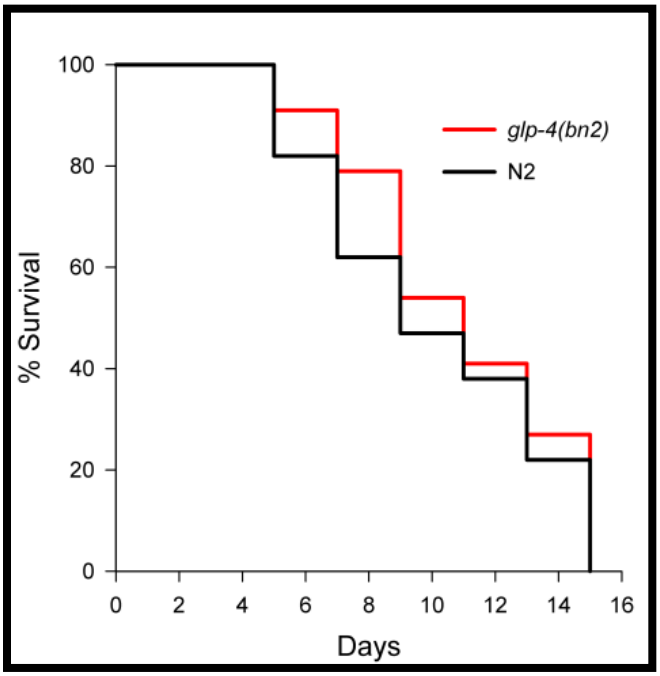

Figure 2.1. When grown at 25 °C, N2 and *glp-4(bn2)* *C. elegans* both have similar mean lifespans. Age-synchronized 100 µL liquid cultures of *C. elegans* were maintained at 25 °C in 96-well plates (n = 4 wells for SS104; n = 2 wells for N2). Nematodes were observed every other day, starting on the third day of culture, using a dissecting microscope, and individual nematodes were scored as either alive or dead based on movement and body rigidity (n = 430 for SS104; n = 306 for N2). The mean lifespan was 10.84 days for *glp-4(bn2)* (standard error ± 0.334 days) and 10.02 days for N2 (standard error ± 0.369 days). The difference between the two mean lifespans was not significantly different (log-rank p-value = 0.185).

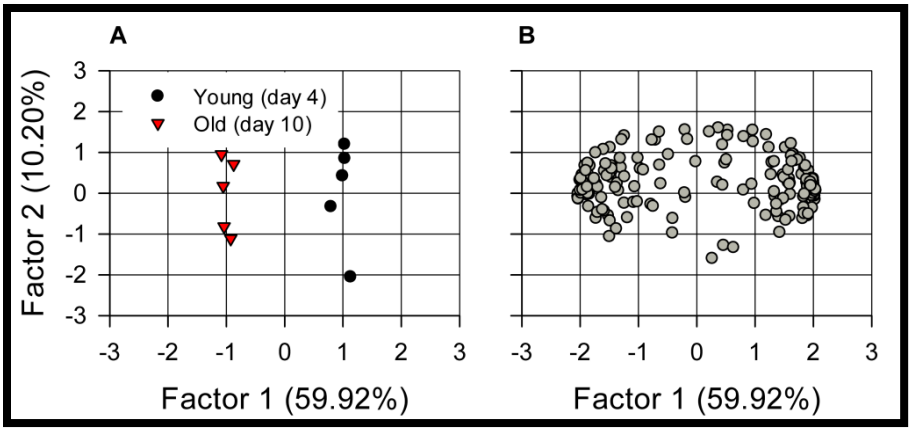

Figure 2.2. Principal component analysis of metabolites shows separation of young and aged samples. (A) When graphed as the 2D relationship between the two top explanatory factors (*F1* = 59.92% of the variation; *F2* = 10.20% of the variation), the scaled young day 5 samples (*n* = 5) and the scaled aged day 10 sample (*n* = 5) are separated primarily linearly along the *F1* axis, showing that the major variation in the distribution of metabolite levels is explained by the difference in ages between the groups. (B) When similarly graphed using the same two factors, the identified metabolites (*n* = 186) visibly congregate at two poles along the *F1* axis.

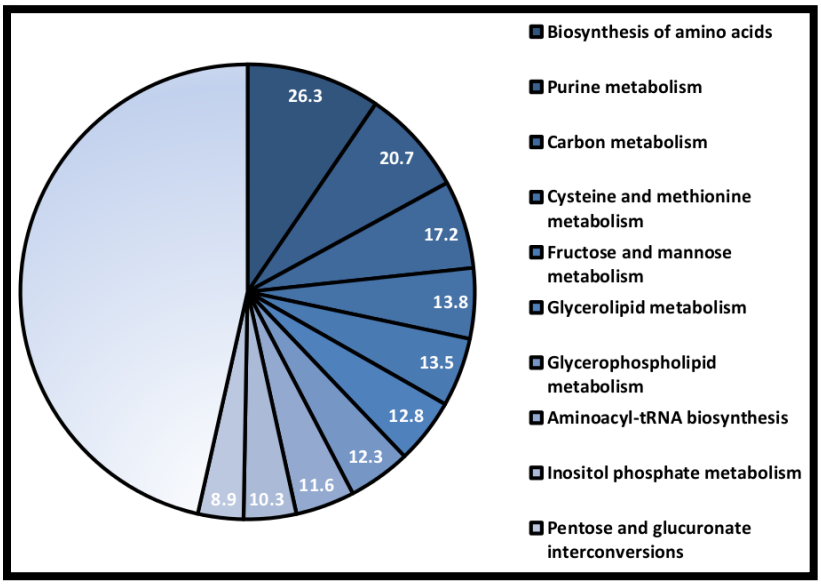

Figure 2.3. Top 10 changed pathways based on metabolome analysis. The total observed change for each identified pathway was calculated as the total of the absolute $\log_2$-fold change for each identified metabolite found within the pathway (*n* = 50 pathways). The top 10 changed pathways are shown in this figure. The width of each pie wedge is equivalent to the percent change of that pathway out of the total absolute $\log_2$-fold change of all pathways. Numbers shown on each pie wedge are the total absolute $\log_2$-fold change for that pathway. The KEGG pathway designated as "Metabolic Pathways" (map01100) was omitted from the list since it encompasses most other pathway information.

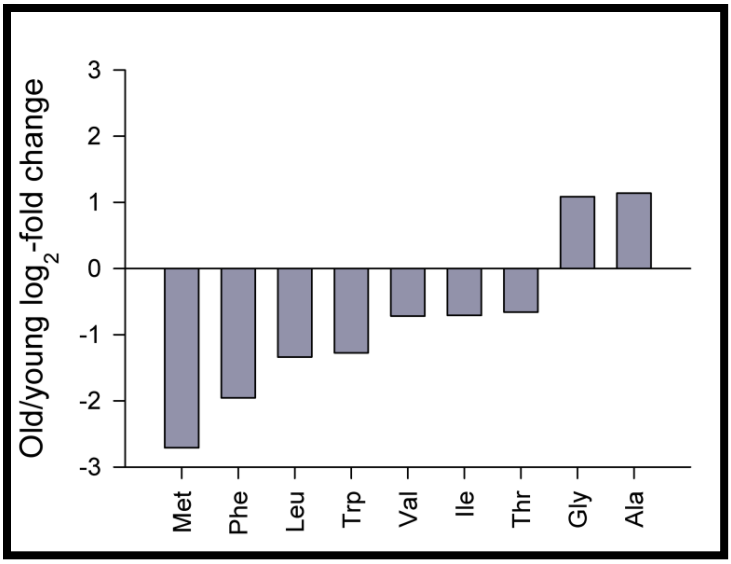

Figure 2.4. Age-related changes in free amino acid levels. The levels of hydrophobic amino acids decreased and the levels of hydrophilic amino acids increased on day 10 compared to day 4 (Pearson correlation -0.67; *p*-value = 0.05). At pH 7.0 the relative hydrophobicity (on a scale from -100 to +100 normalized to glycine) is as follows: Met = 74, Phe = 100, Leu = 97, Trp = 97, Val = 76, Ile = 99, Thr = 13, Gly = 0, Ala = 41.

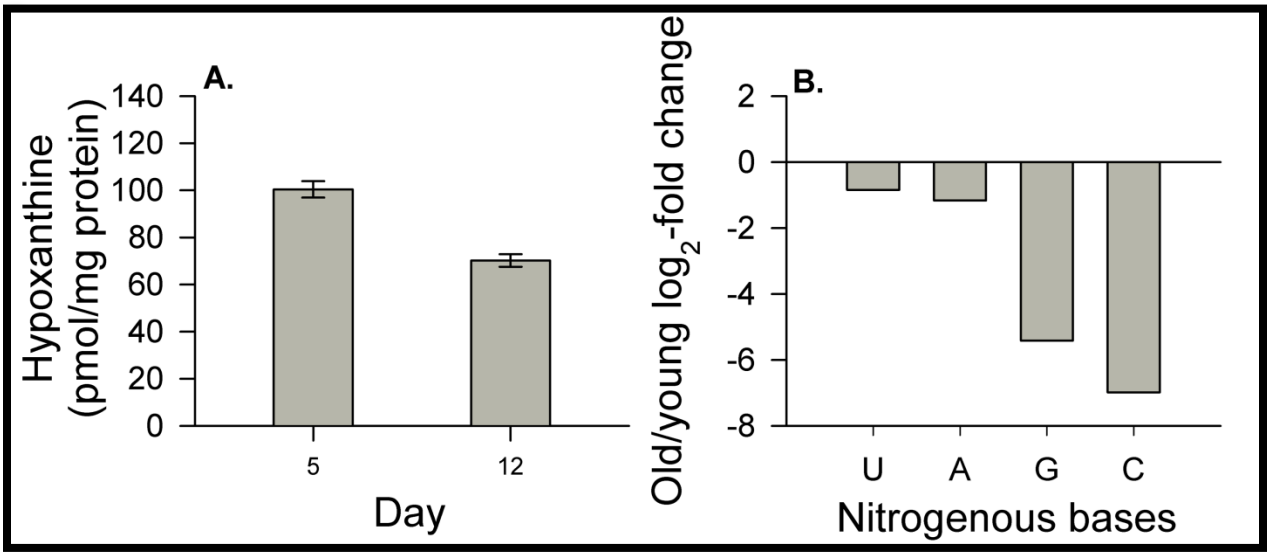

Figure 2.5. Age-related decreases in hypoxanthine and nitrogenous base levels. (A) The concentration of hypoxanthine fell from a mean of 100.37 pmol/mg of protein (SEM ± 3.48) on day 5 (*n* = 6 samples; ~100 nematodes/sample), to a mean of 70.22 pmol/mg of protein (SEM ± 2.65) on day 12 (*n* = 6 samples; ~100 nematodes/sample; unpaired two-tailed t-test *p*-value = 4.2 x 10^{-5}). (B) Uracil, adenine, guanine, and cytosine levels were all decreased with age. Thymine also showed a -3.18 $\log_2$-fold decrease, but the *p*-value of the two-tailed *t*-test between young and aged levels failed to indicate significance (*p*-value = 0.074).

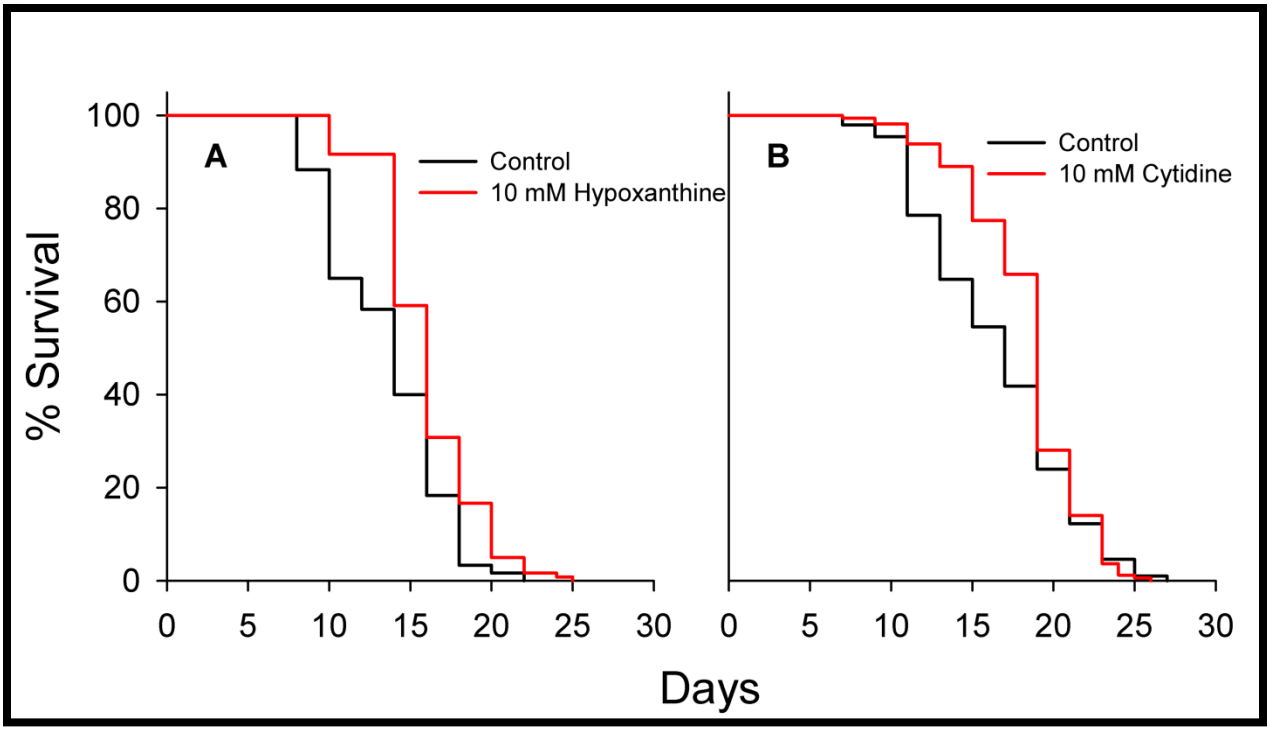

Figure 2.6. Dietary supplementation with 10 mM hypoxanthine extends the lifespan of N2 *C. elegans*. Several liquid cultures were grown for lifespan assays (as described in Edwards *et al*., 2015). (A) The addition of 10 mM hypoxanthine to the S-medium (n = 120 nematodes) resulted in a mean lifespan increase of 18% compared to the untreated N2 control (log-rank p-value < 0.001). (B) The addition of 10 mM cytidine (n = 163 nematodes) resulted in a mean lifespan increase of 11% compared to the untreated N2 control (log-rank p-value = 0.012).

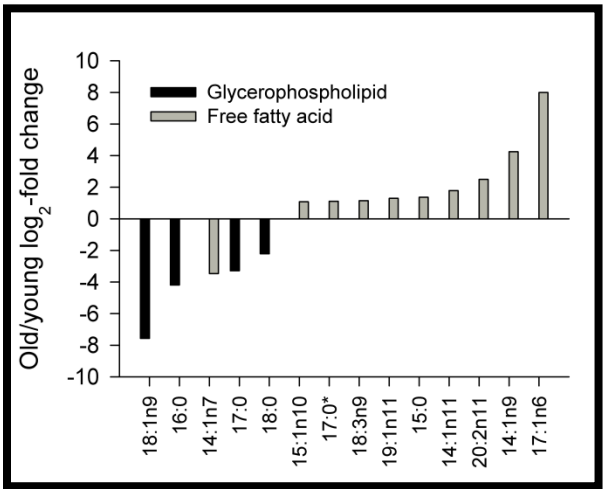

Figure 2.7. Age-related changes in monoacylglycerol and fatty acid levels. Monoacylglycerols primarily decreased with age, while fatty acids primarily increased. For brevity, we've only listed fatty acids with a $\log_2$-fold change above 1 or below -1. For a complete list, see Table S3. *16-methylheptadecanoic acid.

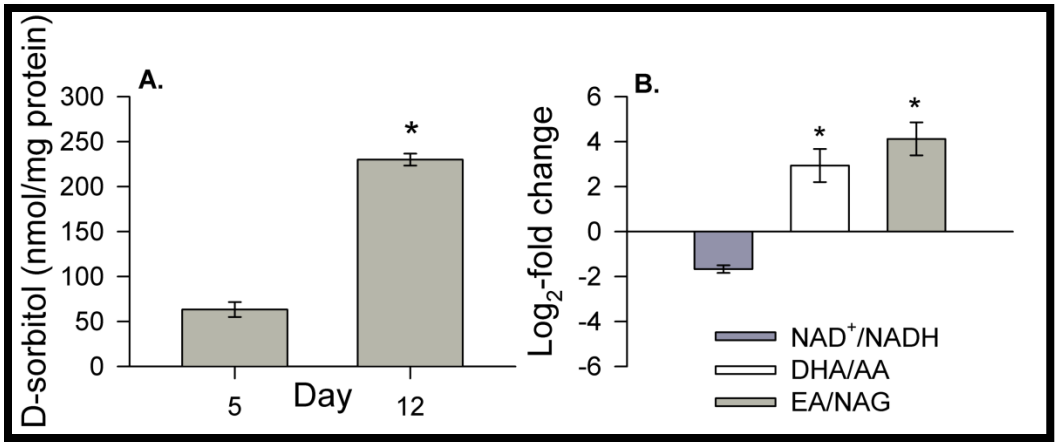

Figure 2.8. Age-related changes in D-sorbitol content and redox state. (A) Whole-nematode D-sorbitol levels increased ~360% from day 5 to day 10 (day 5 mean = 63.28 nmol/mg protein, SEM ± 8.29, n = 4 samples, ~100 nematodes/sample; day 12 mean = 229.95 nmol/mg protein, SEM ± 6.60, n = 4 samples, ~100 nematodes/sample; unpaired two-tailed t-test p-value = 4.19 x 10^{-6}). (B) Aged/young $\log_2$-fold changes for NAD/NADH ($\log_2$-fold change = -1.67; young vs. aged unpaired two-tailed t-test < 0.0001), dehydroascorbic acid/ascorbic acid (DHA/AA; $\log_2$-fold change = 2.94; young vs. aged unpaired two-tailed t-test = 0.024) and erythronic acid (EA)/ N-acetylglucosamine (NAG). NAD and NADH levels were estimated using relative detected levels of pyruvate and lactate.

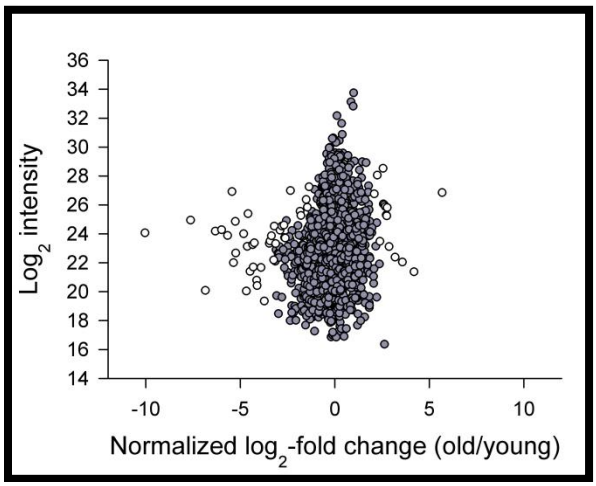

Figure 2.9. Proteomic analysis of young vs. aged *C. elegans* using stable isotope labeling. The y-axis represents the $\log_2$ of the detected abundance, as determined by adding together the total detected intensities of both the heavy ($^{15}N_4$-$^{13}C_6$-arginine and $^{15}N_2$-$^{13}C_6$-lysine) labeled proteins (young day 4 nematodes) and the light non-labeled proteins (aged day 10 nematodes). The x-axis indicates the relative fold-change in abundance of individual proteins from the aged nematodes as compared to the young nematodes. The unfilled circles represent proteins with a significantly changed abundance, as determined by the Significance B method (Benjamini-Hochberg corrected p-value) with a threshold of 0.05. The dark gray circles are proteins without a significant change in abundance.

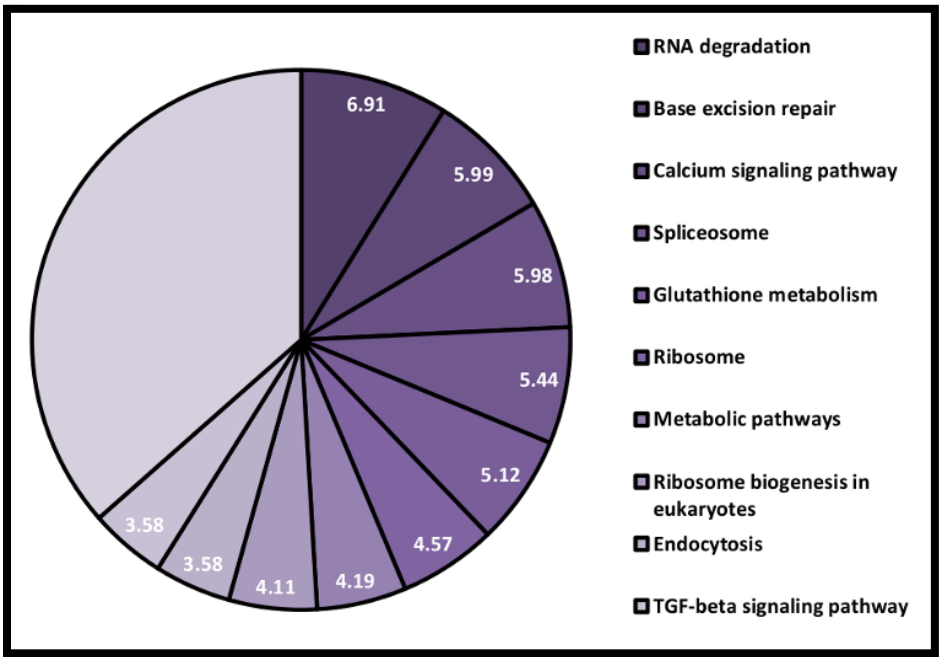

Figure 2.10. The top 10 altered pathways with age based on proteomic analysis. The total observed change for each identified pathway was calculated as the total of the absolute $\log_2$-fold change for each identified protein found within the pathway (n = 20 pathways). The top 10 changed pathways are shown in this figure. The width of each pie wedge is equivalent to the percent change of that pathway out of the total absolute $\log_2$-fold change of all pathways. Numbers shown on each pie wedge are the total absolute $\log_2$-fold change for that pathway.

2.10 Tables

Table 2.1. Pathways assigned to metabolites. The day 10 $\log_2$-fold change was calculated for each metabolite. Metabolites with p-values > 0.05 for day 10 versus day 5 were considered to be unchanged ($\log_2$-fold change = 0). Pathways were assigned to each metabolite by searching the Kyoto Encyclopedia of Genes and Genomes database. A pathway was assigned to a metabolite if that pathway contained a C. elegans enzyme that produces or consumes that metabolite.

Metabolite	KEGG ID	Log2	*p*-value	*C. elegans* Pathways
Galactonic acid-1,4-lactone	C01115	-11.962	0.000	
Hypoxanthine	C00262	-8.323	0.024	Purine metabolism
9-Octadecenoylglycerol		-7.568	0.009	
4-hydroxybutanoic acid	C00989	-7.063	0.001	
5-Methylthioadenosine	C00170	-7.041	0.000	Cysteine and methionine metabolism
Cytosine	C00380	-6.986	0.000	
Xylose	C00181	-6.867	0.002	Pentose and glucuronate interconversions
2-Ketogluconic acid	C15673	-6.512	0.000	
Uridine	C00299	-5.573	0.005	Pyrimidine metabolism
Guanine	C00242	-5.417	0.000	Purine metabolism

Table 2.1 (Continued)

Metabolite	KEGG ID	Log2	*p*-value	*C. elegans* Pathways
3-hydroxypropyl-2-oxo-phosphate	C00111	-5.218	0.000	Glycolysis / Gluconeogenesis
				Fructose and mannose metabolism
				Glycerolipid metabolism
				Inositol phosphate metabolism
				Glycerophospholipid metabolism
				Carbon metabolism
				Biosynthesis of amino acids
6-Hydroxynicotinic acid	C01020	-4.342	0.000	
1-hexadecanoylglycerol		-4.194	0.001	
7-tetradecenoic acid		-3.468	0.000	
Cadaverine	C01672	-3.412	0.001	Glutathione metabolism
2-Aminoadipic acid	C00956	-3.376	0.004	Lysine biosynthesis
				Lysine degradation
				Biosynthesis of amino acids
Ribose	C00121	-3.313	0.000	
1-Heptadecanoylglycerol		-3.289	0.000	
2-hydroxyadipic acid	C02360	-3.276	0.000	
Glycolic acid	C00160	-3.037	0.008	Glyoxylate and dicarboxylate metabolism
Homocysteine	C00155	-2.812	0.017	Cysteine and methionine metabolism
				Biosynthesis of amino acids
Methionine	C00073	-2.709	0.001	Cysteine and methionine metabolism
				Aminoacyl-tRNA biosynthesis
				Biosynthesis of amino acids
3-methyl-3-hydroxybutanoic acid		-2.576	0.000	
Ethyl phosphoric acid		-2.261	0.000	
1-octadecanoylglycerol		-2.214	0.006	
Ribose-5-p	C00117	-2.201	0.004	Pentose phosphate pathway
				Purine metabolism
				Carbon metabolism
				Biosynthesis of amino acids
Inositol-phosphate	C01177	-2.040	0.000	Inositol phosphate metabolism
				Phosphatidylinositol signaling system
Altro-2-Heptulose-7-p		-2.011	0.000	
Phenylalanine	C00079	-1.956	0.000	Phenylalanine metabolism
				Phenylalanine, tyrosine and tryptophan biosynthesis
				Aminoacyl-tRNA biosynthesis
Fumaric acid	C00122	-1.955	0.001	Citrate cycle (TCA cycle)
				Oxidative phosphorylation
				Alanine, aspartate and glutamate metabolism
				Tyrosine metabolism
				Pyruvate metabolism
				Carbon metabolism
Gluconic acid	C00257	-1.925	0.000	Pentose phosphate pathway
				Carbon metabolism
Cholesterol	C00187	-1.912	0.000	Steroid biosynthesis
Mannitol-6-p	C00644	-1.889	0.036	
1,3-Propanediamine	C00986	-1.746	0.000	
Glutaric acid	C00489	-1.621	0.000	
Glucuronic acid	C00191	-1.590	0.023	Pentose and glucuronate interconversions
				Ascorbate and aldarate metabolism
				Starch and sucrose metabolism

Table 2.1 (Continued)

Metabolite	KEGG ID	Log2	*p*-value	*C. elegans* Pathways
				Inositol phosphate metabolism
Nicotinic acid	C00253	-1.508	0.000	Nicotinate and nicotinamide metabolism
Adenosine	C00212	-1.418	0.003	Purine metabolism
Leucine	C00123	-1.338	0.000	Valine, leucine and isoleucine degradation
				Valine, leucine and isoleucine biosynthesis
				Aminoacyl-tRNA biosynthesis
				2-Oxocarboxylic acid metabolism
				Biosynthesis of amino acids
Gulose	C15923	-1.312	0.023	
Lanosterol	C01724	-1.295	0.000	Steroid biosynthesis
Tryptophan	C00078	-1.275	0.001	Tryptophan metabolism
				Aminoacyl-tRNA biosynthesis
Inosine	C00294	-1.259	0.000	Purine metabolism
Pyruvic acid	C00022	-1.218	0.000	Glycolysis / Gluconeogenesis
				Citrate cycle (TCA cycle)
				Alanine, aspartate and glutamate metabolism
				Glycine, serine and threonine metabolism
				Cysteine and methionine metabolism
				Pyruvate metabolism
				Butanoate metabolism
				Carbon metabolism
				Biosynthesis of amino acids
Adenine	C00147	-1.167	0.000	Purine metabolism
Ornithine	C00077	-1.111	0.002	Arginine and proline metabolism
				Glutathione metabolism
				2-Oxocarboxylic acid metabolism
				Biosynthesis of amino acids
Pyroglutamic acid	C01879	-1.091	0.001	Glutathione metabolism
2-hydroxybutanoic acid	C05984	-0.976	0.011	Propanoate metabolism
Maltose	C00208	-0.961	0.000	Starch and sucrose metabolism
Adenosine-5-monophosphate	C00020	-0.954	0.006	Purine metabolism
				FoxO signaling pathway
				mTOR signaling pathway
Malic acid	C00149	-0.929	0.000	Citrate cycle (TCA cycle)
				Pyruvate metabolism
				Glyoxylate and dicarboxylate metabolism
				Carbon metabolism
1-Pentadecanoylglycerol		-0.879	0.000	
Gluconic acid-1,4-lactone	C03107	-0.869	0.048	
Eicosanoic acid	C06425	-0.852	0.000	
Uracil	C00106	-0.843	0.044	Pyrimidine metabolism
				β-Alanine metabolism
				Pantothenate and CoA biosynthesis
Monomethylphosphate		-0.759	0.000	
2-Aminobutyric acid	C02261	-0.752	0.030	
Valine	C00183	-0.719	0.000	Valine, leucine and isoleucine degradation
				Valine, leucine and isoleucine biosynthesis
				Propanoate metabolism
				Pantothenate and CoA biosynthesis
				Aminoacyl-tRNA biosynthesis
				2-Oxocarboxylic acid metabolism

Table 2.1 (Continued)

Metabolite	KEGG ID	Log2	*p*-value	*C. elegans* Pathways
				Biosynthesis of amino acids
Isoleucine	C00407	-0.708	0.001	Valine, leucine and isoleucine degradation
				Valine, leucine and isoleucine biosynthesis
				Aminoacyl-tRNA biosynthesis
				2-Oxocarboxylic acid metabolism
				Biosynthesis of amino acids
Galacturonic acid	C00333	-0.693	0.001	
Threonine	C00188	-0.659	0.000	Glycine, serine and threonine metabolism
				Valine, leucine and isoleucine biosynthesis
				Aminoacyl-tRNA biosynthesis
				Biosynthesis of amino acids
Dodecanoic acid	C02679	-0.655	0.002	
Pyrophosphate	C00013	-0.513	0.000	Oxidative phosphorylation
N-acetylglutamic acid		-0.493	0.048	
Arabitol	C00532	-0.462	0.013	Pentose and glucuronate interconversions
2-Hydroxyglutaric acid	C02630	-0.462	0.003	Butanoate metabolism
5,8,11,14-Eicosatetraenoic acid	C00219	-0.459	0.007	Arachidonic acid metabolism
13-octadecenoic acid		-0.424	0.005	
Heptadecanoic acid		-0.416	0.007	
9-Octadecenoic acid	C01712	-0.414	0.015	
9,12-Octadecadienoic acid		-0.331	0.000	
Tetradecanoic acid	C06424	-0.327	0.000	Fatty acid biosynthesis
Glucose (ambiguous)		-0.229	0.028	
1,6-Anhydroglucose		0	0.068	
11,14,17-Eicosatrienoic acid	C16522	0	0.617	
11-eicosenoic acid	C16526	0	0.564	
12-methyltridecanoic acid		0	0.199	
12-Nonadecenoic acid		0	0.085	
13-eicosenoic acid		0	0.313	
13-Hexadecenoic acid		0	0.126	
13-nonadecenoic acid		0	0.201	
15-eicosenoic acid		0	0.275	
2-Phosphoglycerate	C00631	0	0.075	Glycolysis / Gluconeogenesis
				Glycine, serine and threonine metabolism
				Carbon metabolism
				Biosynthesis of amino acids
3-hydroxybenzoic acid	C00587	0	0.095	
3-phosphoglycerate	C00197	0	0.170	Glycolysis / Gluconeogenesis
				Glycine, serine and threonine metabolism
				Glycerolipid metabolism
				Glyoxylate and dicarboxylate metabolism
				Carbon metabolism
				Biosynthesis of amino acids
4,5-dimethyl-2,6-dihydroxypyrimidine		0	0.083	
4-Aminobutyric acid	C00334	0	0.331	Alanine, aspartate and glutamate metabolism
				Arginine and proline metabolism
				Butanoate metabolism
4-methyl-2-hydroxypentanoic acid		0	0.068	
5,8,11,14,17-Eicosapentaenoic acid		0	0.999	
6,9,12-Octadecatrienoic acid	C06426	0	0.953	
α-glycerophosphorylglycerol		0	0.216	

Table 2.1 (Continued)

Metabolite	KEGG ID	Log2	*p*-value	*C. elegans* Pathways
Aminomalonic acid	C00872	0	0.055	
Aspartic acid	C00049	0	0.586	Alanine, aspartate and glutamate metabolism
				β-Alanine metabolism
				Aminoacyl-tRNA biosynthesis
				Carbon metabolism
				2-Oxocarboxylic acid metabolism
				Biosynthesis of amino acids
				Neuroactive ligand-receptor interaction
b-Aminoisobutyric acid	C05145	0	0.089	Pyrimidine metabolism
Cysteine	C00097	0	0.829	Glycine, serine and threonine metabolism
				Cysteine and methionine metabolism
				Taurine and hypotaurine metabolism
				Glutathione metabolism
				Thiamine metabolism
				Pantothenate and CoA biosynthesis
				Sulfur metabolism
				Aminoacyl-tRNA biosynthesis
				Carbon metabolism
				Biosynthesis of amino acids
Decanoic acid	C01571	0	0.495	
Docosanoic acid	C08281	0	0.475	
Dopamine	C03758	0	0.067	Tyrosine metabolism
				Neuroactive ligand-receptor interaction
Erythritol	C00503	0	0.072	
Ethanolamine	C00189	0	0.555	Glycerophospholipid metabolism
Fructose-6-p	C05345	0	0.525	Glycolysis / Gluconeogenesis
				Pentose phosphate pathway
				Fructose and mannose metabolism
				Starch and sucrose metabolism
				Amino sugar and nucleotide sugar metabolism
				Carbon metabolism
				Biosynthesis of amino acids
Galactose	C00124	0	0.862	Galactose metabolism
Gluconic acid-1,5-lactone	C00198	0	0.490	
Glucuronic acid-6-p		0	0.180	
Glutamic acid	C00025	0	0.631	Alanine, aspartate and glutamate metabolism
				Arginine and proline metabolism
				D-Glutamine and D-glutamate metabolism
				Glutathione metabolism
				Glyoxylate and dicarboxylate metabolism
				Butanoate metabolism
				Porphyrin and chlorophyll metabolism
				Aminoacyl-tRNA biosynthesis
				Nitrogen metabolism
				2-Oxocarboxylic acid metabolism
				Biosynthesis of amino acids
				Neuroactive ligand-receptor interaction
Glyceric acid	C00258	0	0.679	Glycine, serine and threonine metabolism
				Glycerolipid metabolism
				Glyoxylate and dicarboxylate metabolism
Glycerol-3-p	C00093	0	0.183	Glycerolipid metabolism

Table 2.1 (Continued)

Metabolite	KEGG ID	Log2	*p*-value	*C. elegans* Pathways
				Glycerophospholipid metabolism
Hexadecanoic acid	C00249	0	0.395	Fatty acid biosynthesis
				Fatty acid degradation
				Fatty acid metabolism
Lysine	C00047	0	0.083	Lysine degradation
				Aminoacyl-tRNA biosynthesis
Maltotriose	C01835	0	0.075	
N-Acetyl galactosamine	C01132	0	0.180	
N-Acetyl-Lysine		0	0.087	
Octadecanoic acid	C01530	0	0.300	
p-Aminobenzoic acid	C00568	0	0.528	
Proline	C00148	0	0.181	Arginine and proline metabolism
				Aminoacyl-tRNA biosynthesis
				Biosynthesis of amino acids
Ribitol	C00474	0	0.109	
Sedoheptulose	C02076	0	0.434	
Sedoheptulose-7-p	C05382	0	0.080	Pentose phosphate pathway
				Carbon metabolism
				Biosynthesis of amino acids
Serine	C00065	0	0.285	Glycine, serine and threonine metabolism
				Cyanoamino acid metabolism
				Sphingolipid metabolism
				Glyoxylate and dicarboxylate metabolism
				Aminoacyl-tRNA biosynthesis
				Carbon metabolism
				Biosynthesis of amino acids
Succinic acid	C00042	0	0.573	Citrate cycle (TCA cycle)
				Oxidative phosphorylation
				Alanine, aspartate and glutamate metabolism
				Propanoate metabolism
				Butanoate metabolism
				Carbon metabolism
Threonic acid-1,4-lactone		0	0.096	
Thymine	C00178	0	0.074	Pyrimidine metabolism
Trehalose	C01083	0	0.062	Starch and sucrose metabolism
Trehalose-6-p		0	0.392	
Tyrosine	C00082	0	0.064	Ubiquinone and other terpenoid-quinone biosynthesis
				Tyrosine metabolism
				Phenylalanine, tyrosine and tryptophan biosynthesis
				Aminoacyl-tRNA biosynthesis
				Biosynthesis of amino acids
Urea	C00086	0	0.114	
Uridine-5'-monophosphate	C00105	0	0.059	Pyrimidine metabolism
12-methyltetradecanoic acid	C16665	0.219	0.021	
Tridecanoic acid	C17076	0.364	0.018	
9-Heptadecenoic acid		0.377	0.000	
1-Methyl-α-D-glucopyranoside		0.380	0.047	
9-hexadecenoic acid	C08362	0.418	0.000	
15-methyl-11-Hexadecenoic acid		0.437	0.001	
Lactic acid	C00186	0.455	0.000	Glycolysis / Gluconeogenesis
				Pyruvate metabolism

Table 2.1 (Continued)

Metabolite	KEGG ID	Log2	*p*-value	*C. elegans* Pathways
11-Octadecenoic acid	C08367	0.519	0.000	
Glucose-6-p	C00668	0.534	0.004	Glycolysis / Gluconeogenesis
				Pentose phosphate pathway
				Galactose metabolism
				Starch and sucrose metabolism
				Amino sugar and nucleotide sugar metabolism
				Carbon metabolism
8,11,14,17-eicosatetraenoic acid		0.538	0.018	
14-methylpentadecanoic acid		0.550	0.001	
15-methylhexadecanoic acid		0.629	0.000	
11-heptadecenoic acid		0.660	0.001	
2,4,6-Tri-tert.-butylbenzenethiol		0.676	0.008	
11-Hexadecenoic acid		0.729	0.000	
Gluconic acid-6-p		0.764	0.012	
14-methylhexadecanoic acid		0.768	0.000	
9,12-heptadecadienoic acid		0.769	0.001	
Undecanoic acid	C17715	0.846	0.003	
Putrescine	C00134	0.859	0.001	Arginine and proline metabolism
				Glutathione metabolism
Panthotenic acid		0.869	0.002	
6,9,12,15-Octadecatetraenoic acid	C16300	0.876	0.000	
11,14-Octadecadienoic acid		0.892	0.001	
Nonadecanoic acid	C16535	0.975	0.001	
Glycerol-2-p	C02979	0.989	0.000	
Sucrose	C00089	1.063	0.003	Galactose metabolism
				Starch and sucrose metabolism
10-Pentadecenoic acid		1.077	0.000	
Glycine	C00037	1.085	0.000	Glycine, serine and threonine metabolism
				Cyanoamino acid metabolism
				Glutathione metabolism
				Glyoxylate and dicarboxylate metabolism
				Aminoacyl-tRNA biosynthesis
				Carbon metabolism
				Biosynthesis of amino acids
				Neuroactive ligand-receptor interaction
16-methylheptadecanoic acid		1.112	0.000	
Alanine	C00041	1.140	0.006	Alanine, aspartate and glutamate metabolism
				Selenocompound metabolism
				Aminoacyl-tRNA biosynthesis
				Carbon metabolism
				Biosynthesis of amino acids
9,12,15-Octadecatrienoic acid	C06427	1.144	0.004	α-Linolenic acid metabolism
Phosphoric acid	C00009	1.197	0.014	Oxidative phosphorylation
Pyrrole-2-carboxylic acid		1.261	0.000	
11-nonadecenoic acid		1.292	0.000	
Ascorbic acid	C00072	1.334	0.013	
Pentadecanoic acid	C16537	1.365	0.000	
Inositol	C00137	1.459	0.000	Inositol phosphate metabolism
				Ascorbate and aldarate metabolism
				Phosphatidylinositol signaling system
Threonic acid	C01620	1.590	0.000	

Table 2.1 (Continued)

Metabolite	KEGG ID	Log2	*p*-value	*C. elegans* Pathways
11-Tetradecenoic acid		1.785	0.000	
N-Acetyl glucosamine	C00140	1.854	0.004	Amino sugar and nucleotide sugar metabolism
Glycerol	C00116	1.948	0.017	Glycerolipid metabolism
Citric acid	C00158	1.973	0.000	Citrate cycle (TCA cycle)
				Glyoxylate and dicarboxylate metabolism
				Carbon metabolism
				2-Oxocarboxylic acid metabolism
				Biosynthesis of amino acids
b-alanine	C00099	2.017	0.049	Pyrimidine metabolism
				β-Alanine metabolism
				Propanoate metabolism
				Pantothenate and CoA biosynthesis
				Neuroactive ligand-receptor interaction
Glucopyranose (ambiguous)		2.243	0.001	
2-O-Glycerol-alfa-galactopyranoside		2.264	0.000	
Galactopyranose	C00124	2.406	0.015	Galactose metabolism
11,14 Eicosadienoic acid	C16525	2.494	0.000	
Galactofuranose		4.161	0.028	
9-Tetradecenoic acid	C08322	4.243	0.000	
Dehydroascorbic acid	C05422	4.269	0.035	
Erythronic acid		5.976	0.000	
Aminoethyl-glycerol-3-p		6.499	0.006	
N-Acetylglucosylamine		6.683	0.001	
Aminoethyl-phosphate	C00346	7.105	0.006	Glycerophospholipid metabolism
				Sphingolipid metabolism
3-Hydroxybutanoic acid	C01089	7.370	0.003	
3-desoxy-pentitol		7.485	0.000	
6-heptadecenoic acid		7.992	0.001	
Sorbitol	C00794	8.316	0.001	Fructose and mannose metabolism
1-Methyl-β-D-galactopyranoside	C03619	11.188	0.000	

Table 2.2. Metabolomics: total weighted change for all pathways. The absolute weights were calculated for all pathways as the sum of the absolute $\log_2$-fold change of each metabolite within that pathway. Absolute weights for down-regulated pathways and up-regulated pathways were determined as the sum of the absolute negative and positive $\log_2$-fold changes, respectively. Pathways were scored as unchanged if every metabolite within that pathway was scored as unchanged (p-value ≥ 0.05).

Pathways	Absolute Weights
All Pathways	
Biosynthesis of amino acids	26.27
Purine metabolism	20.74
Carbon metabolism	17.25

Table 2.2 (Continued)

Pathways	Absolute Weights
Cysteine and methionine metabolism	13.78
Fructose and mannose metabolism	13.53
Glycerolipid metabolism	12.78
Glycerophospholipid metabolism	12.32
Aminoacyl-tRNA biosynthesis	11.59
Inositol phosphate metabolism	10.31
Pentose and glucuronate interconversions	8.92
Pyrimidine metabolism	8.43
Glycolysis / Gluconeogenesis	7.42
Sphingolipid metabolism	7.11
Glyoxylate and dicarboxylate metabolism	7.02
Citrate cycle (TCA cycle)	6.07
2-Oxocarboxylic acid metabolism	5.85
Pentose phosphate pathway	4.66
Pyruvate metabolism	4.56
Alanine, aspartate and glutamate metabolism	4.31
Starch and sucrose metabolism	4.15
Galactose metabolism	4.00
Propanoate metabolism	3.71
Oxidative phosphorylation	3.66
Pantothenate and CoA biosynthesis	3.58
Phosphatidylinositol signaling system	3.50
Valine, leucine and isoleucine biosynthesis	3.42
Lysine biosynthesis	3.38
Lysine degradation	3.38
Steroid biosynthesis	3.21
Neuroactive ligand-receptor interaction	3.10
Glycine, serine and threonine metabolism	2.96
beta-Alanine metabolism	2.86
Valine, leucine and isoleucine degradation	2.77
Amino sugar and nucleotide sugar metabolism	2.39
alpha-Linolenic acid metabolism	2.29
Arginine and proline metabolism	1.97
Phenylalanine metabolism	1.96
Phenylalanine, tyrosine and tryptophan biosynthesis	1.96
Tyrosine metabolism	1.95
Glutathione metabolism	1.94
Butanoate metabolism	1.68

Table 2.2 (Continued)

Pathways	Absolute Weights
Nicotinate and nicotinamide metabolism	1.51
Tryptophan metabolism	1.27
Selenocompound metabolism	1.14
Ascorbate and aldarate metabolism	1.11
Cyanoamino acid metabolism	1.09
FoxO signaling pathway	0.95
mTOR signaling pathway	0.95
Arachidonic acid metabolism	0.46
Fatty acid biosynthesis	0.33
Up-regulated Pathways	
Fructose and mannose metabolism	8.32
Glycerophospholipid metabolism	7.11
Sphingolipid metabolism	7.11
Carbon metabolism	4.73
Biosynthesis of amino acids	4.20
Galactose metabolism	4.00
Neuroactive ligand-receptor interaction	3.10
Glyoxylate and dicarboxylate metabolism	3.06
Amino sugar and nucleotide sugar metabolism	2.39
alpha-Linolenic acid metabolism	2.29
Aminoacyl-tRNA biosynthesis	2.23
beta-Alanine metabolism	2.02
Pantothenate and CoA biosynthesis	2.02
Propanoate metabolism	2.02
Pyrimidine metabolism	2.02
2-Oxocarboxylic acid metabolism	1.97
Citrate cycle (TCA cycle)	1.97
Glycerolipid metabolism	1.95
Glutathione metabolism	1.94
Starch and sucrose metabolism	1.60
Ascorbate and aldarate metabolism	1.46
Inositol phosphate metabolism	1.46
Phosphatidylinositol signaling system	1.46
Oxidative phosphorylation	1.20
Alanine, aspartate and glutamate metabolism	1.14
Selenocompound metabolism	1.14
Cyanoamino acid metabolism	1.09
Glycine, serine and threonine metabolism	1.09

Table 2.2 (Continued)

Pathways	Absolute Weights
Glycolysis / Gluconeogenesis	0.99
Arginine and proline metabolism	0.86
Pentose phosphate pathway	0.53
Pyruvate metabolism	0.45
Down-regulated Pathways	
Biosynthesis of amino acids	22.07
Purine metabolism	20.74
Cysteine and methionine metabolism	13.78
Carbon metabolism	12.52
Glycerolipid metabolism	10.83
Aminoacyl-tRNA biosynthesis	9.36
Pentose and glucuronate interconversions	8.92
Inositol phosphate metabolism	8.85
Glycolysis / Gluconeogenesis	6.44
Pyrimidine metabolism	6.42
Fructose and mannose metabolism	5.22
Glycerophospholipid metabolism	5.22
Pentose phosphate pathway	4.13
Citrate cycle (TCA cycle)	4.10
Pyruvate metabolism	4.10
Glyoxylate and dicarboxylate metabolism	3.97
2-Oxocarboxylic acid metabolism	3.88
Valine, leucine and isoleucine biosynthesis	3.42
Lysine biosynthesis	3.38
Lysine degradation	3.38
Steroid biosynthesis	3.21
Alanine, aspartate and glutamate metabolism	3.17
Valine, leucine and isoleucine degradation	2.77
Starch and sucrose metabolism	2.55
Oxidative phosphorylation	2.47
Phosphatidylinositol signaling system	2.04
Phenylalanine metabolism	1.96
Phenylalanine, tyrosine and tryptophan biosynthesis	1.96
Tyrosine metabolism	1.95
Glycine, serine and threonine metabolism	1.88
Propanoate metabolism	1.70
Butanoate metabolism	1.68
Ascorbate and aldarate metabolism	1.59

Table 2.2 (Continued)

Pathways	Absolute Weights
Pantothenate and CoA biosynthesis	1.56
Nicotinate and nicotinamide metabolism	1.51
Tryptophan metabolism	1.27
Arginine and proline metabolism	1.11
FoxO signaling pathway	0.95
mTOR signaling pathway	0.95
beta-Alanine metabolism	0.84
Arachidonic acid metabolism	0.46
Fatty acid biosynthesis	0.33
Unchanged Pathways	
D-Glutamine and D-glutamate metabolism	0.00
Fatty acid degradation	0.00
Fatty acid metabolism	0.00
Nitrogen metabolism	0.00
Porphyrin and chlorophyll metabolism	0.00
Sulfur metabolism	0.00
Taurine and hypotaurine metabolism	0.00
Thiamine metabolism	0.00
Ubiquinone and other terpenoid-quinone biosynthesis	0.00

Table 2.3. Glycerophospholipids and fatty acids. Changes in glycerophospholipids (5 out of 54 identified fatty acid-containing metabolites) and fatty acid levels are shown.

Metabolite	KEGG ID	Log2	*p*-value	Free or monoacylglycerol
9-Octadecenoylglycerol		-7.568	0.009	monoacylglycerol
1-hexadecanoylglycerol		-4.194	0.001	monoacylglycerol
7-tetradecenoic acid		-3.468	0.000	free
1-Heptadecanoylglycerol		-3.289	0.000	monoacylglycerol
1-octadecanoylglycerol		-2.214	0.006	monoacylglycerol
1-Pentadecanoylglycerol		-0.879	0.000	monoacylglycerol
Dodecanoic acid	C02679	-0.655	0.002	free
5,8,11,14-Eicosatetraenoic acid	C00219	-0.459	0.007	free
13-octadecenoic acid		-0.424	0.005	free
Heptadecanoic acid		-0.416	0.007	free
9-Octadecenoic acid	C01712	-0.414	0.015	free

Table 2.3 (Continued)

Metabolite	KEGG ID	Log2	*p*-value	Free or monoacylglycerol
9,12-Octadecadienoic acid		-0.331	0.000	free
Tetradecanoic acid	C06424	-0.327	0.000	free
11,14,17-Eicosatrienoic acid	C16522	0	0.617	free
11-eicosenoic acid	C16526	0	0.564	free
12-methyltridecanoic acid		0	0.199	free
12-Nonadecenoic acid		0	0.085	free
13-eicosenoic acid		0	0.313	free
13-Hexadecenoic acid		0	0.126	free
13-nonadecenoic acid		0	0.201	free
15-eicosenoic acid		0	0.275	free
5,8,11,14,17-Eicosapentaenoic acid		0	0.999	free
6,9,12-Octadecatrienoic acid	C06426	0	0.953	free
Decanoic acid	C01571	0	0.495	free
Docosanoic acid	C08281	0	0.475	free
Hexadecanoic acid	C00249	0	0.395	free
Octadecanoic acid	C01530	0	0.300	free
12-methyltetradecanoic acid	C16665	0.219	0.021	free
Tridecanoic acid	C17076	0.364	0.018	free
9-Heptadecenoic acid		0.377	0.000	free
9-hexadecenoic acid	C08362	0.418	0.000	free
15-methyl-11-Hexadecenoic acid		0.437	0.001	free
11-Octadecenoic acid	C08367	0.519	0.000	free
8,11,14,17-eicosatetraenoic acid		0.538	0.018	free
14-methylpentadecanoic acid		0.550	0.001	free
15-methylhexadecanoic acid		0.629	0.000	free
11-heptadecenoic acid		0.660	0.001	free
11-Hexadecenoic acid		0.729	0.000	free
14-methylhexadecanoic acid		0.768	0.000	free
9,12-heptadecadienoic acid		0.769	0.001	free
Undecanoic acid	C17715	0.846	0.003	free
6,9,12,15-Octadecatetraenoic acid	C16300	0.876	0.000	free
11,14-Octadecadienoic acid		0.892	0.001	free
Nonadecanoic acid	C16535	0.975	0.001	free
10-Pentadecenoic acid		1.077	0.000	free
16-methylheptadecanoic acid		1.112	0.000	free
9,12,15-Octadecatrienoic acid	C06427	1.144	0.004	free
11-nonadecenoic acid		1.292	0.000	free
Pentadecanoic acid	C16537	1.365	0.000	free

Table 2.3 (Continued)

Metabolite	KEGG ID	Log2	*p*-value	Free or monoacylglycerol
11-Tetradecenoic acid		1.785	0.000	free
11,14 Eicosadienoic acid	C16525	2.494	0.000	free
9-Tetradecenoic acid	C08322	4.243	0.000	free
6-heptadecenoic acid		7.992	0.001	free

Table 2.4. Proteins showing a significant increase or decrease in abundance with age. Significance was determined using Perseus version 1.4.1.3 based on the Significance B method (Benjamini-Hochberg corrected *p*-value; threshold = 0.05). Log_2-fold change values (aged/young) are sorted from lowest to highest.

Log2-fold change (old/young)	Significance B *p*-value	Protein IDs	Protein name/description	Gene names
-10.045	4.314E-34	G5EDN3	Regulator of chromatid cohesion	tim-1
-7.636	1.787E-20	O02325	Protein methyltransferase	prmt-3
-6.851	1.119E-11	Q93699	Ortholog of human glutathione S-transferase alpha 3	gst-17
-6.324	1.409E-14	O01876	Glutamine/asparagine (Q/N)-rich ('prion') domain protein	pqn-24
-5.991	2.990E-13	Q9N4H4	Poly(ADP-ribose) polymerase pme-1	pme-1
-5.675	4.693E-12	Q22467;B7WN92	CRAL/TRIO and GOLD domain containing protein	ctg-2
-5.440	1.244E-33	Q18409	Probable splicing factor, arginine/serine-rich 6	rsp-6
-5.363	8.971E-08	Q09454	Diphthamide biosynthesis protein 2	dph-2
-5.262	1.385E-10	Q2HQL8	Uncharacterized protein Y43F8B.1	Y43F8B.1
-5.246	1.708E-07	O17157;Q95X81	DEAD-box helicase required for larval development	C24H12.4
-4.828	3.740E-09	O44191	Yolk receptor required for yolk uptake during oogenesis	rme-2
-4.682	5.375E-06	G5ECP5	Uncharacterized protein T02E9.6	T02E9.6
-4.635	3.963E-06	P19626	Myosin regulatory light chain 2 required for pharyngeal pump	mlc-2
-4.592	1.170E-24	O17726	Uncharacterized protein D1086.1	D1086.1
-4.487	1.373E-05	Q93254	Ortholog of human carboxylesterase 2	C23H4.3
-4.345	1.551E-05	Q95QV3;Q94986	Ras-related protein Rab-3 involved in synaptic transmission	rab-3
-4.318	1.754E-05	H2KYN3	Acyl-CoA dehydrogenase domain-containing protein	acdh-13
-4.259	1.882E-07	Q20199	Ortholog of human sperm autoantigenic protein 17	F39H12.3
-4.134	6.792E-05	Q9XXN0;B1V8I7	Pseudouridine synthase, mitochondrial and cytoplasmic	pus-1
-4.111	7.504E-05	Q9U299	5'->3' exoribonuclease 2 involved in transcription termination	xrn-2
-3.907	1.776E-04	Q09488	Ser/thr-protein kinase sma-6 orthologous to TGF-beta receptors	sma-6
-3.734	3.566E-04	P34640;H2FLF4	Probable ATP-dependent RNA helicase DDX55 homolog	ZK512.2
-3.463	2.112E-05	Q09237	Ortholog of human GRB10 interacting GYF protein 2	C18H9.3
-3.424	2.602E-05	Q9BPN8	Uncharacterized protein Y92H12BR.3	Y92H12BR.3

Table 2.4 (Continued)

Log2-fold change (old/young)	Significance B *p*-value	Protein IDs	Protein name/description	Gene names
-3.352	3.803E-05	A5JYX8;O18033	Ortholog of human nicalin; localized to the ER	nra-2
-3.230	1.382E-03	G5EEK8;A8WI68	SR Ca2+ ATPase homolog required for muscle function	sca-1
-3.206	8.032E-05	Q19162	Large ribosomal subunit L11 protein	rpl-11.2
-3.131	1.166E-04	O62416	One of ten lysozyme genes involved in immune function	lys-2
-2.896	3.564E-04	G5EE42	Uncharacterized protein ZK1098.11	ZK1098.11
-2.803	5.432E-04	Q19579;Q19581	Homolog of human polyadenylate-binding protein 1 (PABP 1)	pab-2
-2.689	8.960E-04	Q21874	Ortholog of human sushi domain containing 2 protein	R09E10.5
-2.657	1.028E-03	O17939	Functions in assembly of actin filaments in embryonic muscle	aipl-1
-2.623	1.187E-03	Q19056	Ortholog of human phospholipase D3; ER membrane protein	E04F6.4
-2.349	6.810E-08	H9G2T4;Q21032	Isocitrate dehydrogenase [NADP-dependent]	idh-1
-1.837	1.804E-05	O17680	Probable S-adenosylmethionine synthase 1	sams-1
-1.794	2.731E-05	Q09248	Probable dynactin subunit 2 involved in spindle assembly	dnc-2
-1.515	3.295E-04	Q04908	26S proteasome non-ATPase regulatory subunit 3	rpn-3
-1.454	5.424E-04	Q9GP96;H2KZV8;Q9GP94	LIM domain-containing protein; member of the MLP/CRP family	mlp-1
-1.363	1.107E-03	O45499	40S ribosomal protein S26	rps-26
2.093	9.552E-04	Q9N5N3	Extracellular protein; C. elegans SCP/TAPS domain family member	scl-12
2.249	3.600E-04	Q9XWT3	Uncharacterized protein Y62H9A.6	Y62H9A.6
2.390	6.855E-04	Q18805	Putative secreted TIL-domain protease inhibitor	C53B7.2
2.553	4.445E-05	O62289	TransThyretin-Related family domain-containing protein	ttr-51
2.571	3.896E-05	O44145	PERMeable eggshell	perm-2
2.622	2.669E-05	B9WRT3;O01260	Ortholog of human piezo-type mechanosensitive ion channel component 2	C10C5.1
2.674	1.802E-05	G5EDZ9	Homolog of cysteine protease inhibitors (cystatins)	cpi-1
2.719	1.275E-05	Q17802	Chondroitin proteoglycan 1	cpg-1
2.749	1.009E-05	G5EF93	One of five predicted C. elegans calcium-binding calmodulin homologs	cal-4
2.774	8.287E-06	Q09607	Glutathione S-transferase-36; ortholog of human prostaglandin D synthase	gst-36
2.874	1.550E-04	Q9TZ69	Ortholog of human ubiquitin-conjugating enzyme E2K	ubc-20
3.191	2.759E-05	Q9XVQ3	Uncharacterized protein F15D3.5	F15D3.5
3.577	2.716E-06	Q22038	Ras-like GTP-binding protein rhoA	rho-1
4.191	2.369E-06	Q93289	Uncharacterized protein C27D8.2	C27D8.2
5.679	6.513E-21	Q8WQC4;O18147	Ortholog of human kelch-like family member 18	kel-3

Table 2.5. Proteomics: total weighted change for all pathways. Associated KEGG pathways were identified for significantly up- and down-regulated proteins using the STRING database. The absolute weights were calculated for all pathways as the sum of the absolute $\log_2$-fold change of each protein within that pathway. Absolute weights for down-regulated pathways and

up-regulated pathways were determined as the sum of the absolute negative and positive log_2-fold changes, respectively.

All Pathways	Absolute Weights
All Pathways	
RNA degradation	6.91
Base excision repair	5.99
Calcium signaling pathway	5.98
Spliceosome	5.44
Glutathione metabolism	5.12
Ribosome	4.57
Metabolic pathways	4.19
Ribosome biogenesis in eukaryotes	4.11
Endocytosis	3.58
TGF-beta signaling pathway	3.58
Wnt signaling pathway	3.58
Ubiquitin mediated proteolysis	2.87
mRNA surveillance pathway	2.80
RNA transport	2.80
Drug metabolism - cytochrome P450	2.77
Metabolism of xenobiotics by cytochrome P450	2.77
Phosphatidylinositol signaling system	2.75
Peroxisome	2.35
Citrate cycle (TCA cycle)	2.35
Cysteine and methionine metabolism	1.84
Proteasome	1.51
Up-regulated Pathway	
Endocytosis	3.58
TGF-beta signaling pathway	3.58
Wnt signaling pathway	3.58
Ubiquitin mediated proteolysis	2.87
Glutathione metabolism	2.77
Drug metabolism - cytochrome P450	2.77
Metabolism of xenobiotics by cytochrome P450	2.77
Calcium signaling pathway	2.75
Phosphatidylinositol signaling system	2.75
Down-regulated Pathway	
RNA degradation	6.91
Base excision repair	5.99
Spliceosome	5.44

Table 2.5 (Continued)

All Pathways	Absolute Weights
Ribosome	4.57
Metabolic pathways	4.19
Ribosome biogenesis in eukaryotes	4.11
Calcium signaling pathway	3.23
mRNA surveillance pathway	2.80
RNA transport	2.80
Glutathione metabolism	2.35
Peroxisome	2.35
Citrate cycle (TCA cycle)	2.35
Cysteine and methionine metabolism	1.84
Proteasome	1.51

CHAPTER 3:

AN AUTOMATED 96-WELL PLATE RNAi SCREEN IDENTIFIES EF-HAND MEDIATORS OF Ca^{2+} TOXICITY IN *C. ELEGANS*

3.1 Abstract

Automated high-throughput measurement of *Caenorhabditis elegans* viability is difficult without expensive equipment and presents special challenges. For example, long-term liquid culture microplate-based growth of *C. elegans* suffers from media evaporation, when standard microplate lids or gas-permeable seals are used, or suffers from oxygen limitation when gas-impermeable microplate seals are used. To solve these problems, nematode microplate cultures were covered with oxygen-permeable 12.7 micron fluorinated ethylene–propylene (FEP) Teflon® film, which almost completely prevented media evaporation and allowed for culture for the entire adult lifespan without removal of the film. The optical clarity of the FEP film also allowed for the endogenous fluorescence of the nematodes in each well to be measured easily without film removal as an indicator of viability for high-throughput screening. To this end, the *C. elegans* green fluorescent protein (GFP)-expressing strain BC12907 was identified as having a fluorescence that corresponds to total live nematode volume. Likewise, endogenous anthranilate fluorescence in culture was utilized as an indicator of *C. elegans* death. Anthranilate is released from *C. elegans* gut granules during necrotic cell death resulting in an increase in the blue fluorescence over an ~8 hour period surrounding the death of the nematode. Both GFP and

anthranilate fluorescence measurements were effective for monitoring the increased rate of nematode death when culturing *C. elegans* in a medium containing toxic Ca^{2+} levels. To test the throughput of these assays, a targeted knockdown screen of 191 EF-hand Ca^{2+}-binding domain-containing genes was performed using the toxic Ca^{2+} culture conditions. This led to the identification of 7 genes as potential mediators of Ca^{2+} toxicity.

3.2 Introduction

The nematode *Caenorhabditis elegans* has the potential to be an excellent model organism for high-throughput screening [1-3]. Its small size and high fecundity make it an easy organism to cultivate in the laboratory, and its susceptibility to RNA interference makes it an excellent target for studies involving reverse genetics [2, 4]. *C. elegans* have a nearly transparent body, and the availability of strains expressing inducible fluorescent reporter genes has added to the utility of the organism. We sought to adapt current screening methods to long term investigations of *C. elegans* viability using both liquid culturing techniques and automated fluorescence measurements. We also sought to incorporate the use of the endogenous fluorescent marker of cell death in *C. elegans*, anthranilate, as an additional parameter for assaying survival [5].

Liquid culturing techniques for *C. elegans* have several advantages over solid agar culturing methods. Using liquid cultures, nematodes can be easily transferred by pipette, and the transparency of liquid media allows for a broader range of optically-based assays. These advantages are especially desirable when designing large scale projects, and a set of standardized procedures for liquid culture screening have already been established [6]. As with cell culture, however, liquid cultures of *C. elegans* are subject to evaporation and screens involving liquid

cultures of *C. elegans* in 96- and 384-well plates are prone to well-to-well variations produced by systematic evaporation (edge effect), which is often notably pronounced along the outer wells [7]. Current methods to correct for this evaporation include complex data transformations, incubating plates in humid environments such as sealed containers with wet paper towels, and limiting the duration of screens to just past the *C. elegans* larval stages (~3 – 4 days). Covering 96-well plates with gas impermeable sealing tape and venting every other day to oxygenate the cultures has also been performed with success, but with a maximum of 18 worms per well [8], which is typically not enough animals per well to reliably monitor differences in worm GFP or anthranilate fluorescence in a microplate reader, which was one goal of our current investigation. Therefore, we investigated the efficacy of several gas-permeable microplate sealers at limiting evaporation, and in the process we discovered that fluorinated ethylene–propylene (FEP) Teflon® film is capable of outperforming commercially-available alternatives.

FEP film is permeable to O_2 and CO_2, and acts as strong barrier against both liquids and microbes [9]. The film is also transparent, meaning that optical measurements can occur without its removal. FEP has already been adapted for use in the long-term culture of neural cells, and has successfully been employed at protecting cell cultures from evaporation and contamination for periods longer than 9 months [9]. With proper sealing of the film to microplates, we have used it to dramatically restrict evaporation under arid conditions, and we have maintained liquid cultures of *C. elegans* without the necessity of shaking for aeration for the duration of the approximate mean wild-type lifespan of 21 days.

Due to the utility of assaying *C. elegans* lifespan and the frequency of its use in experimentation [10-12], we also sought to develop a fluorescence-based method for estimating the lifespan of a culture. We pursued the duel strategy of using the bright and ubiquitous

expression of green fluorescent protein (GFP) as a marker of live nematode volume and of using anthranilate fluorescence as an indicator of recent nematode death. To this end, we identified the strain BC12907 as a candidate strain for experimentation. BC12907 have the gene for GFP inserted as a stable transgene, with expression driven by the T09B4.8 promoter. T09B4.8 is the *C. elegans* homolog of the human mitochondrial alanine-glyoxylate aminotransferase 2 gene, and is highly-expressed in cells of the head, hypodermis, nervous system, intestine, and body wall musculature of both larva and adults. The resulting GFP expression pattern creates a bright green fluorescence throughout the majority of the *C. elegans* body. We show that this fluorescence corresponds closely to the volume of individual live nematodes, and that the estimated total nematode volume of a culture closely corresponds to the fluorescence profiles obtained each day from microplate reader measurements.

It has been known for some time that blue fluorescence increases with age in *C. elegans* cultures (peak λ_{ex} = 340 nm and λ_{em} = 430 nm). This fluorescence has been variously associated with increases in substances such as flavins [13], tryptophan metabolites [14], and lipofuscin (the oxidatively cross-linked proteins and lipids found to accumulate in lysosomes) [15, 16]. Like lipofuscin, this fluorescence originates primarily in specialized lysosome-like organelles in *C. elegans*, called gut granules, which are located within intestinal cells [16, 17]. The rise in fluorescence has been reported as biphasic, with a pronounced acceleration occurring after the cessation of the reproductive period when the *C. elegans* mortality rate begins to increase [16]. For these reasons, the age-dependent rise in blue fluorescence has a history of use in *C. elegans* research as a marker of heath and lifespan, and has been reported to be negatively correlated with longevity in both long- and short-lived strains [18, 19].

Whether or not lipofuscin accumulates in *C. elegans* to an appreciable extent remains a matter of debate, but in 2013 Coburn *et al*. used HPLC and genetic analysis to identify the fluorescence substance as anthranilate, in the form of anthranilic acid glucosyl ester [5, 20]. Anthranilate is a fluorescent product of the kynurenine pathway and a downstream metabolite of tryptophan. In *C. elegans*, anthranilate accumulates in the gut granules. Upon activation of the necrotic cell death pathway, increased intracellular Ca^{2+} levels activate Ca^{2+}-dependent cysteine proteases (calpains) [21]. Activated calpains promote lysosomal lysis, which in turn lowers cellular pH and releases lysosomal cathepsin proteases. Coburn *et al*. found that the activity of calpains and cathepsins led to the rupture of *C. elegans* gut granules, and that the altered pH and dilution of anthranilate into the cytosol resulted in a ~400% increase of anthranilate fluorescence during an ~8 hour time period surrounding the death of the organism.

In light of the evidence that cultures of *C. elegans* show an age-dependent increase in blue fluorescence, but individual *C. elegans* only show a sizable increase in the time period following death, the overall blue fluorescence of a culture is likely an aggregate of the recently deceased members. As such, endogenous anthranilate fluorescence is likely a useful metric for the rate of death of *C. elegans* in culture. We show that fluorescence in the blue range (λ_{ex} = 360 nm and λ_{em} = 460 nm) is correlated with the death of *C. elegans* in liquid culture over time. We also show that profiles of anthranilate fluorescence from days 5 to 10 in culture have a tendency for increasing under conditions that decrease GFP fluorescence profiles, further suggesting that an increase in anthranilate fluorescence is associated with a loss of total live nematode volume for a culture. These two finding suggest that under the right conditions, anthranilate fluorescence is likely a useful endogenous parameter for gaining information regarding the viability of a nematode culture.

To demonstrate the above methods, we designed and performed a small-scale screen individually knocking down 191 of the Ca^{2+}-binding EF-hand domain-containing genes [22] in the *C. elegans* genome by feeding RNAi technology and determining the viability of the worms when grown in media containing toxic levels of $CaCl_2$. Through these assays, we identified 7 genes as potential mediators of the Ca^{2+} toxicity.

3.3 Materials and Methods

3.3.1 Evaporation Assay

Every well of six 96-well plates were filled with 100 µL each of S-medium. Three of the plates were covered with commercially available adhesive seals, designed to delay evaporation while allowing the passage of O_2 (Corning® Breathable Sealing tape; AeraSeal® film; and Mepore® film, produced by Mölnlycke Health Care). As positive and negative controls, one plate was left uncovered to represent the maximal rate of evaporation, and one plate was covered using Corning® CoStar™ aluminum sealing tape to prevent the passage of water vapor and O_2. An additional plate was covered with a cut section of 0.0005 inch (12.7 micron) thick FEP Teflon® film, purchased from CS Hyde Company (product # 23-1/2FEP-24), and adhered to the top of the plate by applying rubber cement around the edges (although a 3.5 inch x 0.25 inch rubber band around the edge of the plate also works for FEP membrane attachment). Once sealed, the plates were initially weighed, and then incubated at 20°C and 30% humidity. The plates were weighed every ~24 hours for 12 days, and the change in weight per day for each plate was used to estimate the average loss of media volume per day due to evaporation.

3.3.2 Construction of Gasket-Attached FEP Teflon® Film 96-Well Plate Lids

A scalpel was heated over a Bunsen burner, and used to remove the majority of plastic from the top of 96-well plate lids, leaving only a ~5 mm area around the perimeter. A series of thin, rectangular gaskets were then cut from standard plastic folders. The gaskets were coated on one side with Elmer's Spray Adhesive, and pressed onto cut sections of FEP Teflon® film. Once dried, the gasket-attached FEP film was cut from the larger sheet, and glued to the underside of the prepared 96-well plate lids.

3.3.3 *C. elegans* Culture and Alkaline Bleach Synchronization

Prior to the assays, BC12907 (T09B4.8::GFP) *C. elegans* were cultured on 10 cm NGM agar plates seeded with HT115(DE3) bacteria. When eggs were required to begin a new age-synchronized culture, BC12907 *C. elegans* eggs were attained by alkaline bleach synchronization as follows: 2 mL of 6% NaOCl (Clorox®) were mixed with 1 mL of 5 M NaOH per 7.5 mL of concentrated *C. elegans* suspension, and shaken for 4 – 7 minutes until the carcasses dissolved, as monitored by microscopy, leaving behind eggs. The solution was then diluted 5-fold with 0.1 M NaCl, and centrifuged at ~1150 x *g* for 2 minutes at room temperature. The supernatant was removed by aspiration, and the resulting pellet of eggs was washed 3 times by the addition of ~50 mL of 0.1 M NaCl, and centrifugation at ~1150 x *g* for 2 minutes at room temperature. The final pellet of eggs was suspended in 15 mL of S-medium and egg concentration was determined by averaging the number of eggs counted in ten 10 µL drops.

3.3.4 GFP Fluorescence and Live Nematode Volume

BC12907 *C. elegans* eggs were then used to start a full 96-well plate liquid culture (Corning Costar® plates; black with clear bottoms), with ~100 eggs per well, in 90 µL of S-medium (final volume) containing 10 mg/mL of HT115(DE3) *E. coli* (6.9×10^9 CFU/mL). The plate was then covered with a gasket-attached FEP film lid, and the sides of the plate were wrapped with vinyl tape to prevent evaporation through the air gap between the lid and the base. The plate was incubated at 20°C without shaking, and the nematodes were observed daily through the lid, using a dissecting microscope, in order to track the development of the larva. After the nematodes entered the L4 larval stage (after ~3 days) the lid and tape were temporarily removed and 10 µL of 4 mM 5-fluoro-2′-deoxyuridine (FUdR) was added (400 µM final concentration) to prevent egg-laying. Starting on the fifth day of incubation, a single well was chosen and the GFP fluorescence of that well was measured using a Biotek Synergy 2 microplate reader (λ_{ex} = 485 nm and λ_{em} = 530 nm). The lid and tape were temporarily removed and the number of nematodes within the well was counted by transferring ten 10 µL drops into an empty 10 cm plate and counting the number of *C. elegans* per drop using a dissecting microscope. Fluorescence microscope images were then taken of the drops using an EVOS® microscope (Advanced Microscopy Group) and a λ_{ex} = 470 nm, λ_{em} = 525 nm filter set. Movement of the nematodes was reduced by chilling the plate for a few minutes at -10°C. The image processing software ImageJ was used to measure the length and width in millimeters of each nematode and calibrated based on the scale bar included in the images. The volume for each nematode was calculated as for a cylinder, $Length \times \pi \times 0.5 \times Width^2$, and the total volume of *C. elegans* for the sample was calculated as the *Average Number of Worms* x the *Average Volume*. ImageJ software was also used to measure the total corrected worm fluorescence (TCWF), using the

method for total corrected cell fluorescence outlined in [23]. In short, each image was converted to gray-scale, then every selected *C. elegans* was outlined, and its area and integrated density (IntDen) were recorded. An area of background immediately beside the *C. elegans* was then outlined and the mean gray value for the area was recorded. The TCWF for the *C. elegans* was calculated as *IntDen* – (*Area* x *Mean of Gray Value of Background*).

3.3.5 High Ca^{2+} Toxicity Assays

Eggs were collected from BC12907 *C. elegans* by alkaline bleach synchronization as described above. The eggs were used to start 96-well plate liquid cultures (Corning Costar® microplates; black with clear bottoms), containing ~100 eggs/well with 10 mg/mL of HT115(DE3) *E. coli* (6.9 X 10^9 CFU/mL) in 90 μL total volume of Ca^{2+}-compatible S-medium (made with 10 mM HEPES buffer as a substitute for the standard phosphate buffer to prevent the loss of buffering capacity due to the precipitation of calcium phosphate). The plate was then covered with a gasket-attached FEP film lid, wrapped with vinyl tape, and incubated at 20°C. After the nematodes entered into the L4 larval stage, 5 μL of 7.6 mM FUdR was added to give a final concentration of 400 μM FUdR. On the fifth day, 5 μL of 2 M $CaCl_2$ was added to the treated wells (versus 5 μL of H_2O to the untreated wells) to yield a final concentration of 100 mM $CaCl_2$ in 100 μL of total volume. A Biotek Synergy 2 microplate reader was used to measure GFP fluorescence (λ_{ex} = 485 nm and λ_{em} = 530 nm) and anthranilate fluorescence (λ_{ex} = 360 nm and λ_{em} = 460 nm) every day until the tenth day.

3.3.6 Anthranilate Comparison to Live Nematodes in Culture

Eggs were obtained as described above and used to start a full 96-well plate of liquid culture using a black microplate with a clear bottom. Each well contained ~300 eggs with 10 mg/mL of HT115(DE3) *E. coli* (6.9 X 10^9 CFU/mL) in 90 μL of S-medium. The plate was covered with a gasket-attached FEP film lid, the periphery was sealed with vinyl tape, and the plate was incubated without shaking at 20°C. A separate 96-well plate was prepared with liquid culture in only 10 wells, with a similar bacterial concentration and volume, but with only 1/10th the number of eggs-per-well (~30 eggs/well). The plate was covered, wrapped, and incubated in a similar manner. 10 μL of 4 mM FUdR was added to both plates (400 μM final concentration) upon the larva reaching the L4 stage (~day 3). On the fifth day, by which time the worms had substantially visually reduced the bacterial concentration in each well, anthranilate fluorescence was measured for the full plate of liquid cultures, using a Biotek Synergy 2 microplate reader (λ_{ex} = 360 nm and λ_{em} = 460 nm), and the number of live worms in each well of the remaining 10 wells of culture were counted. The average of this count was then used to estimate the live nematodes per well in the entire plate by multiplying the average number of live *C. elegans* per well by 10. This procedure was then performed on days 6, 7, 9, and 11.

3.3.7 RNAi Gene Knockdown Screen

RNAi clones of 131 EF-hand containing genes were obtained from the Ahringer RNAi library [24]. The other 60 RNAi clones to EF-hand containing genes used in this report were constructed in the laboratory of Dr. Monica Driscoll as outlined in [22]. The EF-hand RNAi library has been used previously to screen for modulators of necrosis [25]. A total of 191 glycerol stocks of HT115(DE3) bacterial clones from the EF-hand RNAi library were used to

start cultures in 500 μL of LB broth, containing 100 μg/mL ampicillin, in the wells of 1 mL deep-well 96-well plates (n = 12; 55 clones were used for the first screen; 191 clones were used for the second and third screens). Additionally, two plates were prepared as controls with HT115(DE3) bacteria lacking an inserted plasmid. The plates were covered with a gasket-attached FEP film lid and the sides were wrapped with vinyl tape. All plates were then incubated at 37°C for 16 hours with shaking. IPTG was then added to all wells at a concentration of 1 mM and incubated at 37°C with shaking for an additional 4 hours to induce dsRNA expression. Afterward, the plates were spun down for 30 minutes to pellet the bacteria and the supernatant was decanted. The resulting pellets were suspended in 90 μL of Ca^{2+} compatible S-medium (see above) containing ~100 eggs/mL. Once mixed, the cultures were transferred to 96-well black, clear-bottom plates. The liquid cultures were then treated as outlined above for the high Ca^{2+} toxicity assay such that half of the plated cultures (n = 6) received 100 mM $CaCl_2$ and the other half received deionized H_2O.

3.3.8 Analysis

Normalized fluorescence profiles were generated by dividing each fluorescence measurement by the fluorescence on the fifth day of liquid culture incubation. Slopes were calculated as (*Normalized Day 10 Fluorescence* – 1)/5. Trapezoidal integration was used to calculate area under curves based on normalized profiles. GraphPad Prism version 5.01 was used to calculate the area under receiver operating characteristic curves, and the strictly standardized mean differences were calculated in Microsoft Excel as $\beta = (\mu_1 - \mu_2)/\sqrt{(\sigma_1^2 + \sigma_2^2)}$. For the six replicates of each RNAi knockdown on each day, the Tukey boxplot method was

used to identify and remove outliers. Graphs and r^2 values were generated in SigmaPlot version 11.0.

3.4 Results

3.4.1 Fluorinated Ethylene–Propylene (FEP) Teflon® Film Limits Evaporation in Long-Term *C. elegans* Liquid Cultures

We began by examining the efficacy of several commercially available adhesive plate sealing films at preventing evaporation. The selected sealers were advertised as being capable of limiting evaporation while allowing gas exchange between the plate and the surrounding environment. Also, inspired by the success of Potter and DeMarse [9] in using 12.7 micron FEP Teflon® film as a protective barrier during long-term neural cell culture, we adapted this non-adhesive film for use with 96-well plates. Figure 3.1 shows the results of a 12-day evaporation assay. A series of 96-well plates were filled with 100 μL per well of S-medium, covered with a specific type of seal, and weighed. The plates were then stored at 20°C in an arid location (an incubator with an internal environment of 30% humidity) for 12 days. The plates were weighed each day to assess the total amount of liquid lost per plate. For comparison, one plate was covered with aluminum sealing tape, which acts as a complete barrier against the transfer of liquid or gas. Of the commercially available sealers, Mepore® film from Mölnlycke Health Care proved to be the most effective, limiting evaporation to just 7.6% (730 μL per plate) per day. However, the application of FEP film, sealed around the outside edges of the plate with rubber cement, was 19 times more effective than Mepore® film, limiting evaporation to just 0.4% per day (38.4 μL for the entire plate, or 0.4 μL per well if distributed evenly), and was nearly as effective as aluminum sealing tape. This low rate of evaporation was for an arid environment,

and represents a much worse case than our average non-regulated incubator humidity of 50–80%.

Given this result, we developed a gasket-attached FEP film lid design that we subsequently employed in our *C. elegans* assays (Figure 3.2), and adhered to plates by sealing the edges with vinyl tape. 12.7 micron FEP film has the extra benefit of being highly permeable to both O_2 and CO_2, and the film is commonly used as a water-proof barrier in dissolved-oxygen probes. FEP is also optically transparent, meaning that it can be left in place during optical measurements of 96-well plates, and it is also impermeable to microbes. As a consequence, we found that liquid cultures of *C. elegans* can grow successfully in a 12.7 micron FEP covered plate for the approximate mean *C. elegans* lifespan (~3 weeks) with only negligible evaporation. Furthermore, the cultures can be maintained without shaking the plate for aeration, as long as the per-well culture volume is not overly deep (we successfully use 100 μL) and the number of *C. elegans* per well is not above 300 nematodes. With shaking, we have successfully used 200 μL volumes.

3.4.2 Fluorescence of the GFP-expressing Strain BC12907 is Associated with Both Number and Volume of Live *C. elegans* in Liquid Culture

The two to three week mean lifespan of wild-type *C. elegans* make them a desirable model for quickly investigating factors that affect health and aging. However, both manual and automated methods for scoring living *C. elegans* currently require microscopy [26-28] and incorporating lifespan analysis into high-throughput screens can be labor intensive [8]. In an effort to simplify the process, we investigated the use of fluorescence markers that might correspond to the quantity of living or dead *C. elegans* in a culture at a variety of ages. As an

initial step, we searched the Caenorhabditis elegans Expression Pattern database (http://gfpweb.aecom.yu.edu/) for promoter::GFP fusion-expressing strains that strongly and ubiquitously exhibit both larval and adult GFP fluorescence. After ordering several candidate strains form the Caenorhabditis Genetics Center, we chose to focus on an especially bright strain, BC12907 *dpy*-5(e907) with GFP expression driven by the promoter for T09B4.8 (a homolog for human mitochondrial *AGXT-2* alanine-glyoxylate aminotransferase-2 gene) as an integrated transgene [29, 30].

Fluorescence microscope images, GFP microplate reader fluorescence measurements, and a visual count were taken of live and dead *C. elegans* from an age-synchronized liquid culture daily for 3 weeks. The image processing software ImageJ was use to estimate the length and width of each imaged live *C. elegans*, which was used to calculate an estimated average body volume for each day, assuming the body shape for *C. elegans* to be approximately cylindrical (Figure 3.3, Figure 3.4, and Figure 3.5). ImageJ was also used to calculate the total corrected worm fluorescence (TCWF) as adapted from [23] for both live and dead *C. elegans*, and was used as an estimate for both group's average relative GFP fluorescence. The total volume of live *C. elegans* for each daily sample was estimated as the average body volume per nematode multiplied by the total number of living nematodes scored in that sample (Figure 3.6). Figure 3.7A shows the positive association between GFP fluorescence measured in the microplate reader and the total estimated *C. elegans* body volume per sample (*volume per nematode* x *live nematodes per sample*). Figure 3.7B shows a similar positive relationship between GFP fluorescence and the total number of live nematodes per sample after the fifth day of the lifespan. Prior to the fifth day (which approximately corresponds to the second day of *C. elegans* adulthood) the small size of the nematodes causes the relationship to degrade.

Fluorescence microscopy revealed *C. elegans* scored as dead to have a non-negligible GFP fluorescence (TCWF/volume), but their average GFP fluorescence was significantly less than that measured in live nematodes (Figure 3.8).

3.4.3 An Altered GFP Fluorescence Profile is a Marker of Shortened Lifespan in *C. elegans* Treated with 100 mM $CaCl_2$.

Lifespan reduction by treatment with high levels of $CaCl_2$ is an easy and inexpensive demonstration of metal toxicity in *C. elegans* [31]. The addition of 100 mM $CaCl_2$ to adult *C. elegans* on the fifth day of culture results in a nearly 40% reduction in mean lifespan, with 98% of the initial fifth-day population dead by the tenth day (Figure 3.9A). We followed the changes in GFP fluorescence from days 5 to 10 for a series of $CaCl_2$-treated and untreated liquid cultures of *C. elegans* (n = 58 for both groups, with ~100 nematodes per well). The resulting mean profiles show a distinct difference in the trajectory of GFP fluorescence for both groups over the course of 5 days (Figure 3.9B). This difference can be quantitated as both slope (from day 5 to day 10), and as the area under the curve (AUC) as shown in Figure 3.9C and Figure 3.9D. Slope and AUC appear to be relatively robust methods of differentiating between treated and untreated samples, with the slopes of both groups showing a strictly standardized mean difference (SSMD) of 2.75, suggesting a strong effect size, and a receiver operating characteristic (ROC) curve area of 0.98 (standard error ± 0.013; p-value < 0.0001), indicating a low false-positive rate for differentiation between the two groups at 3.4%. Likewise, comparison of AUC yields an SSMD of 2.1 and an ROC area of 0.96 (standard error ± 0.024; p-value < 0.0001), with no significant difference in the false-positive rate between the slope and AUC methods of comparing GFP profiles.

3.4.4 GFP Slope and AUC Identify Genetic Targets as Potential Effectors of High Ca^{2+} Toxicity in *C. elegans*.

Using an RNAi library of 191 bacterial clones targeting Ca^{2+}-binding EF-hand-containing genes, we performed a screen for targets that might mediate high Ca^{2+} toxicity in *C. elegans*. RNAi bacterial clones were grown and fed to *C. elegans* in liquid culture and 100 mM $CaCl_2$ was added on the fifth day of the lifespan. The GFP fluorescence profiles from days 5 to 10 were used to calculate mean slopes and AUCs for gene knockdown, which were then evaluated by z-score based on the non-RNAi $CaCl_2$-treated controls. Higher positive z-score values were interpreted as likely representing more live worms in culture during the 5 day period. As expected, slope and AUC calculations produced similar z-scores for individual knockdowns (Figure 3.10).

Initially to test the efficacy of the screen, a subset of 55 RNAi clones were randomly chosen and screened. Then the complete 191 clone $CaCl_2$-treated RNAi gene knockdown library was screened twice, each time with a different 96-well plate location to guard against residual systematic errors due to an edge effect (Table 3.1). An average z-score was calculated for each knockdown from the three screens for both GFP slope and GFP AUC resulting in a refined list of knockdowns associated with a z-score greater than +2 (6 genes based on slope and 11 genes based on AUC). The list was also further refined by calculating the average z-scores for all three screens for the slope and AUC combined in an attempt to identify the strongest overall effects. The resulting list of the RNAi targets with a z-score of greater than +2 was reduced to 7 genes: T04F8.6, ZK673.7 (*tnc-2*), C09H5.7, C04B4.2, C47A4.3, F53F4.14, and K04F1.10 (*irld-40*).

A similar group of RNAi-fed *C. elegans* were screened without $CaCl_2$ to identify any potentially toxic gene knockdowns and to determine if any gene knockdown increased viability independently of the added $CaCl_2$. Results are shown in Table 3.2. In the absence of $CaCl_2$, we show that F53F4.14 knockdown led to a total averaged z-score of 1.66, the second largest value for any gene knockdown. Knockdown of C47A4.3 also led to the ninth highest total averaged z-score of 1.38. This suggests that when these genes are knocked down some of the protection from Ca^{2+} toxicity may be Ca^{2+}-independent and result from a general increase in lifespan. An analysis of the total averaged z-scores for all knockdowns comparing the effect in the presence of $CaCl_2$ to the effect in the absence of $CaCl_2$ only showed a modest correlation ($r^2 = 0.28$). If only examining the averaged GFP AUC z-score results (not the GFP slope z-score results) in the absence of $CaCl_2$, knockdown of the *rsef-1* (Ras and EF-hand domain containing homolog, C33D12.6) gene increased fluorescence over the z-score threshold of 2.0 (z-score=2.20). *C. elegans rsef-1* is an ortholog of human *RAB44*, a member of the Ras oncogene family. Future studies should be conducted to verify the effect of knockdown of *rsef-1* on lifespan.

3.4.5 Increased Anthranilate Fluorescence is Associated with 100 mM $CaCl_2$-treatment of *C. elegans* in Culture

In an effort to benefit from another potentially useful marker of nematode viability for high throughput screening purposes, we examined the utility of measuring anthranilate fluorescence. Anthranilate is a metabolic product of tryptophan that is stored in *C. elegans* intestinal organelles known as gut granules. Upon activation of the necrotic cell death pathway, gut granule membrane integrity is compromised and the resulting change in cellular anthranilate localization (as well as a change in the pH of anthranilate) activates the natural blue fluorescence

of the molecule (peak λ_{ex} = 340 nm and λ_{em} = 430 nm). In culture, individual nematodes experience a ~400% increase in anthranilate-associated fluorescence that begins ~2 hours before death, and ends ~6 hours after death [5]. The 8 hours total spike in fluorescence can be measured as a trend toward increasing blue fluorescence over the lifespan of an entire *C. elegans* culture, presumably as an aggregate of the fluorescence of recently dead members. Accordingly, the fluorescence of *C. elegans* liquid cultures is inversely associated with the number of living nematodes over time (r^2 = 0.95; Pearson correlation = -0.97; Figure 3.11).

We measured the blue fluorescence on days 5 through 10 during the high Ca^{2+} RNAi screen described above using a blue fluorescence filter set (λ_{ex} = 360 nm and λ_{em} = 460 nm) under the assumption that a shallower slope and a smaller AUC than controls would be indicative of a lower rate of death for the cultured *C. elegans*. The resulting differences in fluorescence profiles for slope and AUC (Figures 3.12A) revealed a promising degree of sensitivity for the differentiation between treated and untreated cultures (an ROC area of 0.95 ± 0.2 for slope comparisons, and 0.97 ± 0.1 for AUC comparisons), but a moderate effect size as indicated by SSMD calculations (1.2 for both slope and AUC). Furthermore, the variation in anthranilate profiles among the $CaCl_2$-treated RNAi knockdowns was small in comparison to the non-RNAi group (Figure 3.13), and while the majority of knockdowns had lower slopes and smaller AUCs than the mean $CaCl_2$-treated controls, none of the knockdowns achieved a z-score greater than 2 standard deviations from the control mean (Table 3.3). However, averaging the absolute z-scores for anthranilate fluorescence for each gene knockdown with the z-scores for GFP fluorescence yielded a similar ordering of knockdowns with respect to overall effect with all 7 hits from the GFP screen being in the top 8 hits in the averaged data set (Table 3.1). Interestingly, the relationship between GFP fluorescence and anthranilate fluorescence followed

the hypothesized pattern (smaller GFP fluorescence slopes and AUCs were associated with larger anthranilate fluorescence slopes and AUCs), but there was large variation between the two parameters for individual gene knockdowns (r^2 = 0.29; Figure 3.12B).

We then performed a similar screen, once again monitoring anthranilate fluorescence, but this time adding deionized water instead of $CaCl_2$ to the wells to determine the Ca^{2+} dependence of the viability measurements (Table 3.4). The knockdown yielding the largest increase in viability according to this analysis (total averaged z-score = -1.66), although not reaching the -2 cutoff for being classified as a hit, was the C24H11.2 serine/threonine protein phosphatase gene. Strikingly many of the same knockdowns were observed to be among the best at increasing viability as determined by decreased anthranilate fluorescence in the presence and absence of $CaCl_2$, suggesting that knockdown of these clones may extend lifespan independently of the $CaCl_2$. These knockdown clones include Y105E8A.7 (*eat-18*), C02F4.2 (*tax-6* or calcineurin A), C47C12.4 (mitochondrial rho GTPase *miro-2*), Y9D1A.2 (predicted RNA helicase) and C36E6.5 (myosin light chain *mlc-2*). Supporting this data, RNAi to calcineurin A (*tax-6*) is known to extend lifespan [32]. It is also likely that *eat-18* and *mlc-2* knockdowns increase lifespan through dietary restriction as these genes are known to be essential for normal pharyngeal pumping. A little unexpectedly, there was almost no overall correlation when comparing the total average z-scores from anthranilate fluorescence measurements in the absence and presence of $CaCl_2$ (r^2 = 0.04). In addition, when comparing the total averaged z-scores for the GFP measurements versus those from the anthranilate measurements in the absence of $CaCl_2$, there was also not much correlation (r^2 = 0.03; Pearson correlation = 0.17). However, one noticeable feature was the presence of the proline dehydrogenase gene, B0513.5 near the top of both lists, suggesting increased viability with this knockdown. When examining the total averaged z-score

including GFP and anthranilate as shown on Table 3.2, in addition to the proline dehydrogenase gene knockdown, the knockdowns giving the biggest increases in viability in the absence of $CaCl_2$ included the mitochondrial rho GTPase *miro-2*, and *cal-1*, one of five *C. elegans* calmodulin homologs.

3.5 Discussion

3.5.1 Novel Methods for Long Term Culture and Automated Monitoring of Worm Viability

We successfully adapted a method previously used in the long term culture of neural cells for use in maintaining microplate cultures of *C. elegans* nematodes. Once sealed onto a microplate, 12.7 micron FEP Teflon® film acts as a waterproof barrier that allows O_2 and CO_2 to permeate well enough to maintain aerobic cultures. From our comparisons, we determined that FEP film greatly outperforms several common commercially available brands of waterproof plate sealers at reducing evaporation in arid environments. We were reliably able to maintain *C. elegans* cultures at 20°C for the approximate length of a *C. elegans* lifespan (3 weeks) without substantial evaporation. Furthermore, with moderate liquid culture volumes (below ~150 µL per well in 96-well plates), we were able to grow cultures of between 100 and 300 nematodes without shaking the microplate for aeration and only removing the FEP film when adding reagents to the wells. The optical transparency of FEP film also allowed us to take periodic fluorescence measurements of liquid cultures while leaving the film in place, which greatly reduces the potential introduction of contamination into the cultures.

By simply browsing the Caenorhabditis elegans Expression Pattern database (http://gfpweb.aecom.yu.edu/), we were able to identify multiple strains of *C. elegans* with

ubiquitous expression of GFP in both larva and adults. We chose to work with one particular strain, BC12907, due to its large magnitude of fluorescence. We found that the overall GFP fluorescence of BC12907 positively corresponds to the approximate total volume of live nematodes in liquid culture as determined by both microscopy and microplate reader measurements. We used this fluorescence measurement as an approximation of the volume of worms in a culture, but presumably it could also be used as a normalizing factor for comparing other parameters across multiple cultures. These findings likely apply to any *C. elegans* strain exhibiting bright and ubiquitous fluorescence in adulthood and should not be limited to the BC12907 strain.

3.5.2 An Automated RNAi Screen Identifies Mediators of Ca^{2+}-Induced Worm Death

We then setup a small scale screen to examine the profile of GFP fluorescence over time and compared normal and toxic conditions. We used 100 mM $CaCl_2$ treatment as an established model of metal toxicity in *C. elegans* [33], but high Ca^{2+} may also induce a type of premature aging in the nematodes, as a Ca^{2+} wave spreads down the intestine as part of the normal organismal death program [5]. To avoid issues such as low total fluorescence, the potential interfering aspects of initially high *E. coli* concentrations, and altered developmental rates in toxic conditions, we chose to start $CaCl_2$ treatment and GFP fluorescence measurements on the fifth day of each culture. Daily GFP fluorescence measurements from the start of treatment until the tenth day of culture revealed fluorescence profiles that matched expectations. The 100 mM $CaCl_2$-treated group exhibited significantly decreased slopes and AUCs compared to untreated nematodes ($p < 0.0001$ for both parameters), which suggests a decrease in the total volume of

live *C. elegans* in the treated cultures due to a higher rate of death. RNAi knockdowns from a library of EF-hand domain-containing genes resulted in the improvement of these two metrics (increased GFP slope and AUC) by more than 2 standard deviations (z-score greater than 2) for 7 RNAi clones.

Further investigation is needed for the 7 genes targeted by these clones as many of these genes likely play a role in mediating Ca^{2+}-induced toxicity in *C. elegans*. Notably, of these seven, three are uncharacterized and lack a strong human homolog (T04F8.6, C04B4.2, and F53F4.14), although F53F4.14 shows a weak homology with human UPF0667 protein C1orf55. However, results suggest that a portion of the viability afforded by F53F4.14 knockdown was independent of the presence of $CaCl_2$. Two genes (C47A4.3 and C09H5.7) encode catalytic subunits of serine/threonine-protein phosphatases that are homologous to those from human protein phosphatase 1 (PP1-β and PP1-γ respectively), protein complexes implicated in a broad range of activities, including mitosis, muscle contraction, glycogen metabolism, protein synthesis, and the progression of apoptosis [34, 35]. However, the increased viability observed with C47A4.3 knockdown may also be partially independent of $CaCl_2$. Another protein phosphatase gene, Y40H4A.2, a *C. elegans* homolog of the catalytic subunit of human *PP1-α*, was also nearly a hit in our screen monitoring GFP fluorescence (total averaged z-score of 1.79 in Table 3.1), but did not make the final list due to the z-score criteria of 2 chosen to avoid false positives. Therefore, protein phosphatases may play an especially important role in mediating Ca^{2+}-induced worm death, but this is not all that surprising since 21% (41 out of the 191) of the genes targeted in the EF-hand RNAi library are predicted to be protein phosphatases or subunits of these complexes. This is highly overrepresented as protein phosphatase genes only compose around 1% of the genes in the *C. elegans* genome.

One of the hits K04F1.10 (*irld-40* or Insulin/EGF-Receptor L Domain protein) contains an EGF receptor domain. EGF receptor signaling has been shown to control lifespan in *C. elegans* through Ca^{2+}/IP_3 receptor and phospholipase C-3 (PLC-3) dependent mechanisms [36]. Another phospholipase C isoform, *plc-2* (Y75B12B.6), was very close to being a hit in our screen monitoring GFP fluorescence (total averaged z-score of 1.77 as shown in Table 3.1). The remaining hit in the screen, ZK673.7 (*tnc-2*, encodes a pharyngeal-specific form of troponin C. It is conceivable that knockdown of *tnc-2* could interfere with contraction of the *C. elegans* pharyngeal pump, which would in turn slow the ingestion of $CaCl_2$ from the surrounding media, thus lessening the severity of Ca^{2+}-induced toxicity. It is striking that knockdown of the *pat-10*/*tnc-1* gene (F54C1.7) encoding body wall muscle troponin C had the opposite effect, strongly trending toward increasing worm death in the presence of $CaCl_2$.

3.5.3 Anthranilate Fluorescence as a Marker of Worm Death

Anthranilate fluorescence likely serves as an endogenous indicator of worms that have recently died in culture and attempts to utilize anthranilate fluorescence in a similar manner as GFP fluorescence initially looked promising. 100 mM $CaCl_2$-treated cultures had profiles of daily anthranilate fluorescence with slopes and AUCs significantly greater than untreated cultures, suggesting a higher rate of *C. elegans* death, which is in agreement with our GFP results. RNAi knockdown of EF-hand-containing genes on average produced fluorescence profiles with lower slopes and AUCs, indicative of a decreased rate of death, but the magnitude of the effect proved to be small. None of the calculated slopes or AUCs showed an improvement beyond 2 standard deviations from the mean, although averaging the z-scores from these parameters with the z-scores obtained from GFP measurements indicated the 7 hits when only

measuring GFP are all included in the top 8 hits when averaging both data sets together. The additional averaged top hit in this set of 8 genes is the W08D2.7, the *mtr-4* RNA helicase gene (see Table 3.1). It is possible that the anthranilate fluorescence of a culture, being an aggregate of only the recently-dead members, is not as sensitive of an indicator of toxicity as is the GFP-based fluorescence of live nematode volume. In hindsight, anthranilate fluorescence might also not have been ideal for use with assays of Ca^{2+}-induced toxicity and knockdowns of Ca^{2+}-binding genes. The release of anthranilate from *C. elegans* gut granules, which is a necessary precursor to the ~400% burst of fluorescence, is reliant on functional Ca^{2+} signaling within the nematode [5]. Possible manipulation of that signaling through both high Ca^{2+} levels and the knockdown of Ca^{2+}-binding genes may alter the release of anthranilate from the intestinal gut granules and compromise its use as an indicator of organismal death.

3.5.4 Bacterial Autofluorescence Significantly Contributes to Microplate Reader Fluorescence Measurements

A downside to the use of microplate reader measurements for high-throughput screening with *C. elegans* is the reliance on bacteria as a food source, especially for traditional feeding RNAi-based assays. *E. coli* exhibits autofluorescence in both the blue and green fluorescence ranges, which greatly undermines efforts to accurately assess GFP and anthranilate fluorescence using microplate-based detection methods. To make matters worse, depending on the concentration of bacteria present and the size and number of live nematodes in culture, the autofluorescence of *E. coli* can completely dominate the fluorescence measurements obtained. Additionally, this autofluorescence often increases for a given concentration of *E. coli* over the course of several days as the bacteria adjust to the conditions of the S-medium (see Figure 3.14).

We initially attempted to design protocols for correcting measurements to compensate for the fluorescence of bacteria in *C. elegans* liquid cultures using bacterial standards of known concentrations and the absorbance at 600 nm of the culture (which is equivalent to an OD_{600} nm measurement for bacterial turbidity). These efforts were complicated by the changing absorbance of *E. coli* over time in S-medium and by the changing contribution of *C. elegans* to 600 nm absorbance as they increased in size with age (data not shown). Ultimately, we settled on adjusting the initial concentration of bacteria and *C. elegans* in our cultures such that the wells were nearing a visual clearance of bacteria during the first fluorescence measurement on day 5 of the lifespan. The major drawback to this compromise is that the worms may likely have undergone dietary restriction during the of the fluorescence measurements. *C. elegans* is quite hardy and can live its entire adulthood without food as long as it is well-fed during the larval stages [37]. But, *E. coli* can also easily be re-added to the wells in between fluorescence measurements. The restoration of *C. elegans* to the fully fed state would likely reverse any temporary effects that the dietary restriction had on metabolism or stress resistance as the effects of dietary restriction have been shown to be reversible [38]. A goal of future work is to develop automated techniques to measure viability of worms feeding *ad libitum*. Perhaps this could be accomplished by growing *E. coli* in media that minimizes autofluorescence or by using a *C. elegans* strain expressing a different fluorescent protein, one which emits at a wavelength where *E. coli* autofluorescence does not so readily interfere with the measurements.

3.6 Conclusion

We demonstrated that liquid cultures of *C. elegans* can be maintained for long term with negligible evaporation by covering and sealing microplates with 12.7 micron FEP Teflon® film.

The film permits the passage of gasses, which when combined with a low culture volume per well allows for adequate aeration without shaking. The transparency of FEP also permits optical measurements to be performed on the sealed plates. Daily measurement of the green fluorescence of the GFP-expressing strain BC12907 was shown to correspond to the total volume of live nematodes per well and is reflective of the viability of the entire culture under conditions of Ca^{2+}-induced toxicity. Through the analysis of the loss of GFP fluorescence following $CaCl_2$ addition and by screening an RNAi knockdown library of genes containing an EF-hand Ca^{2+}-binding motif, we were able to identify gene knockdowns having a z-score greater than 2.0 to identify genes that potentially mediate Ca^{2+} toxicity. Anthranilate fluorescence, although clearly showing promise as an indicator of nematode death, did not show as large of changes in fluorescence on average in the knockdown clones following $CaCl_2$ addition as compared to the changes observed in GFP fluorescence. Therefore the anthranilate measurements were not as informative in identifying clones protecting from Ca^{2+} toxicity.

3.7 Acknowledgements

We would like to thank Dr. Monica Driscoll for providing us RNAi clones of EF-hand-containing genes not present in the Ahringer RNAi library. We would like to thank Alyssa Paraggio, Mariam Saifee, and Iosif Barjuca for helping maintain *C. elegans* cultures. We would also like to thank Dr. Meera Nanjundan for coordinating the use of the BioTek Synergy 2 microplate reader, and Robert Hill for helpful advice and providing assistance with the fluorescence microscopy. *C.* elegans strains were obtained from the *Caenorhabditis* Genetics Center (University of Minnesota, Minneapolis, MN, USA), which is funded by NIH Office of Research Infrastructure Programs (P40 OD010440). The research was funded in part by NIH

grant # AG046769 awarded to PB and through funds provided by the University of South Florida.

3.8 References

1. Maher KN, Catanese M, Chase DL. Large-scale gene knockdown in c. Elegans using dsrna feeding libraries to generate robust loss-of-function phenotypes. Journal of visualized experiments : JoVE. 2013;(79):e50693-e.

2. Hamilton B, Dong Y, Shindo M, Liu W, Odell I, Ruvkun G, et al. A systematic rnai screen for longevity genes in c. Elegans. Genes & development. 2005;19(13):1544-55.

3. Leung CK, Wang Y, Malany S, Deonarine A, Nguyen K, Vasile S, et al. An ultra high-throughput, whole-animal screen for small molecule modulators of a specific genetic pathway in caenorhabditis elegans. PloS one. 2013;8(4):e62166.

4. Bargmann CI. High-throughput reverse genetics: Rnai screens in caenorhabditis elegans. Genome Biol. 2001;2(2):1005.1-3.

5. Coburn C, Allman E, Mahanti P, Benedetto A, Cabreiro F, Pincus Z, et al. Anthranilate fluorescence marks a calcium-propagated necrotic wave that promotes organismal death in c. Elegans. PLoS biology. 2013;11(7):e1001613.

6. Ahringer J. Reverse genetics. WormBook. 2006. doi: 10.1895/wormbook.1.47.1.

7. Carralot JP, Ogier A, Boese A, Genovesio A, Brodin P, Sommer P, et al. A novel specific edge effect correction method for rna interference screenings. Bioinformatics. 2012;28(2):261-8. doi: 10.1093/bioinformatics/btr648. PubMed PMID: 22121160.

8. Solis GM, Petrascheck M. Measuring caenorhabditis elegans life span in 96 well microtiter plates. Journal of visualized experiments : JoVE. 2011;(49). doi: 10.3791/2496. PubMed Central PMCID: PMCPMC3197298.

9. Potter SM, DeMarse TB. A new approach to neural cell culture for long-term studies. Journal of neuroscience methods. 2001;110(1):17-24.

10. Edwards CB, Copes N, Brito AG, Canfield J, Bradshaw PC. Malate and fumarate extend lifespan in caenorhabditis elegans. PloS one. 2013;8(3):e58345.

11. Edwards C, Canfield J, Copes N, Rehan M, Lipps D, Bradshaw PC. D-beta-hydroxybutyrate extends lifespan in c. Elegans. Aging (Albany NY). 2014;6(8):621.

12. Edwards C, Canfield J, Copes N, Brito A, Rehan M, Lipps D, et al. Mechanisms of amino acid-mediated lifespan extension in caenorhabditis elegans. BMC genetics. 2015;16(1):8.

13. Davis Jr BO, Anderson GL, Dusenbery DB. Total luminescence spectroscopy of fluorescence changes during aging in caenorhabditis elegans. Biochemistry. 1982;21(17):4089-95.

14. Bhat S, Babu P. Mutagen sensitivity of kynureninase mutants of the nematode caenorhabditis elegans. Molecular and General Genetics MGG. 1980;180(3):635-8.

15. Klass MR. Aging in the nematode caenorhabditis elegans: Major biological and environmental factors influencing life span. Mechanisms of ageing and development. 1977;6:413-29.

16. Gerstbrein B, Stamatas G, Kollias N, Driscoll M. In vivo spectrofluorimetry reveals endogenous biomarkers that report healthspan and dietary restriction in caenorhabditis elegans. Aging cell. 2005;4(3):127-37.

17. Hermann GJ, Schroeder LK, Hieb CA, Kershner AM, Rabbitts BM, Fonarev P, et al. Genetic analysis of lysosomal trafficking in caenorhabditis elegans. Molecular biology of the cell. 2005;16(7):3273-88.

18. Hosokawa H, Ishii N, Ishida H, Ichimori K, Nakazawa H, Suzuki K. Rapid accumulation of fluorescent material with aging in an oxygen-sensitive mutant mev-1 of caenorhabditis elegans. Mechanisms of ageing and development. 1994;74(3):161-70.

19. Garigan D, Hsu A-L, Fraser AG, Kamath RS, Ahringer J, Kenyon C. Genetic analysis of tissue aging in caenorhabditis elegans: A role for heat-shock factor and bacterial proliferation. Genetics. 2002;161(3):1101-12.

20. Coburn C, Gems D. The mysterious case of the c. Elegans gut granule: Death fluorescence, anthranilic acid and the kynurenine pathway. Frontiers in genetics. 2013;4.

21. Yamashima T. Ca 2+-dependent proteases in ischemic neuronal death: A conserved 'calpain–cathepsin cascade'from nematodes to primates. Cell calcium. 2004;36(3):285-93.

22. Zhang W. Molecular and genetic dissection of neuronal necrotic-like death in caenorhabditis elegans: Rutgers University-Graduate School-New Brunswick; 2009.

23. McCloy RA, Rogers S, Caldon CE, Lorca T, Castro A, Burgess A. Partial inhibition of cdk1 in g2 phase overrides the sac and decouples mitotic events. Cell Cycle. 2014;13(9):1400-12.

24. Kamath RS, Martinez-Campos M, Zipperlen P, Fraser AG, Ahringer J. Effectiveness of specific rna-mediated interference through ingested double-stranded rna in caenorhabditis elegans. Genome Biology. 2001;2(1):Research0002. Epub 2001/02/24. doi: 10.1186/gb-2000-2-1-research0002. PubMed PMID: 11178279; PubMed Central PMCID: PMC17598.

25. Kamat S, Yeola S, Zhang W, Bianchi L, Driscoll M. Nra-2, a nicalin homolog, regulates neuronal death by controlling surface localization of toxic caenorhabditis elegans deg/enac channels. Journal of Biological Chemistry. 2014;289(17):11916-26. Epub 2014/02/26. doi: 10.1074/jbc.M113.533695. PubMed PMID: 24567339; PubMed Central PMCID: PMC4002099.

26. Mathew MD, Mathew ND, Ebert PR. Wormscan: A technique for high-throughput phenotypic analysis of caenorhabditis elegans. PloS one. 2012;7(3):e33483.

27. Xian B, Shen J, Chen W, Sun N, Qiao N, Jiang D, et al. Wormfarm: A quantitative control and measurement device toward automated caenorhabditis elegans aging analysis. Aging cell. 2013;12(3):398-409.

28. Stroustrup N, Ulmschneider BE, Nash ZM, López-Moyado IF, Apfeld J, Fontana W. The caenorhabditis elegans lifespan machine. Nature methods. 2013;10(7):665-70.

29. Hunt-Newbury R, Viveiros R, Johnsen R, Mah A, Anastas D, Fang L, et al. High-throughput in vivo analysis of gene expression in caenorhabditis elegans. PLoS biology. 2007;5(9):e237.

30. McKay S, Johnsen R, Khattra J, Asano J, Baillie D, Chan S, et al., editors. Gene expression profiling of cells, tissues, and developmental stages of the nematode c. Elegans. Cold Spring Harbor symposia on quantitative biology; 2003: Cold Spring Harbor Laboratory Press.

31. Wang D, Liu P, Yang Y, Shen L. Formation of a combined ca/cd toxicity on lifespan of nematode caenorhabditis elegans. Ecotoxicology and Environmental Safety. 2010;73(6):1221-30. Epub 2010/06/29. doi: 10.1016/j.ecoenv.2010.05.002. PubMed PMID: 20580433.

32. Mair W, Morantte I, Rodrigues AP, Manning G, Montminy M, Shaw RJ, et al. Lifespan extension induced by ampk and calcineurin is mediated by crtc-1 and creb. Nature. 2011;470(7334):404-8. Epub 2011/02/19. doi: 10.1038/nature09706. PubMed PMID: 21331044; PubMed Central PMCID: PMC3098900.

33. Wang D, Wang Y, Shen L. Confirmation of combinational effects of calcium with other metals in a paper recycling mill effluent on nematode lifespan with toxicity identification evaluation method. Journal of Environmental Science (China). 2010;22(5):731-7. Epub 2010/07/09. PubMed PMID: 20608510.

34. Tournebize R, Andersen SS, Verde F, Doree M, Karsenti E, Hyman AA. Distinct roles of pp1 and pp2a-like phosphatases in control of microtubule dynamics during mitosis. The EMBO journal. 1997;16(18):5537-49.

35. Fong NM, Jensen TC, Shah AS, Parekh NN, Saltiel AR, Brady MJ. Identification of binding sites on protein targeting to glycogen for enzymes of glycogen metabolism. Journal of Biological Chemistry. 2000;275(45):35034-9.

36. Iwasa H, Yu S, Xue J, Driscoll M. Novel egf pathway regulators modulate c. Elegans healthspan and lifespan via egf receptor, plc-gamma, and ip3r activation. Aging Cell. 2010;9(4):490-505. Epub 2010/05/26. doi: 10.1111/j.1474-9726.2010.00575.x. PubMed PMID: 20497132.

37. Kaeberlein TL, Smith ED, Tsuchiya M, Welton KL, Thomas JH, Fields S, et al. Lifespan extension in caenorhabditis elegans by complete removal of food. Aging Cell. 2006;5(6):487-94. Epub 2006/11/04. doi: 10.1111/j.1474-9726.2006.00238.x. PubMed PMID: 17081160.

38. Mair W, Goymer P, Pletcher SD, Partridge L. Demography of dietary restriction and death in drosophila. Science. 2003;301(5640):1731-3.

3.9 Figures

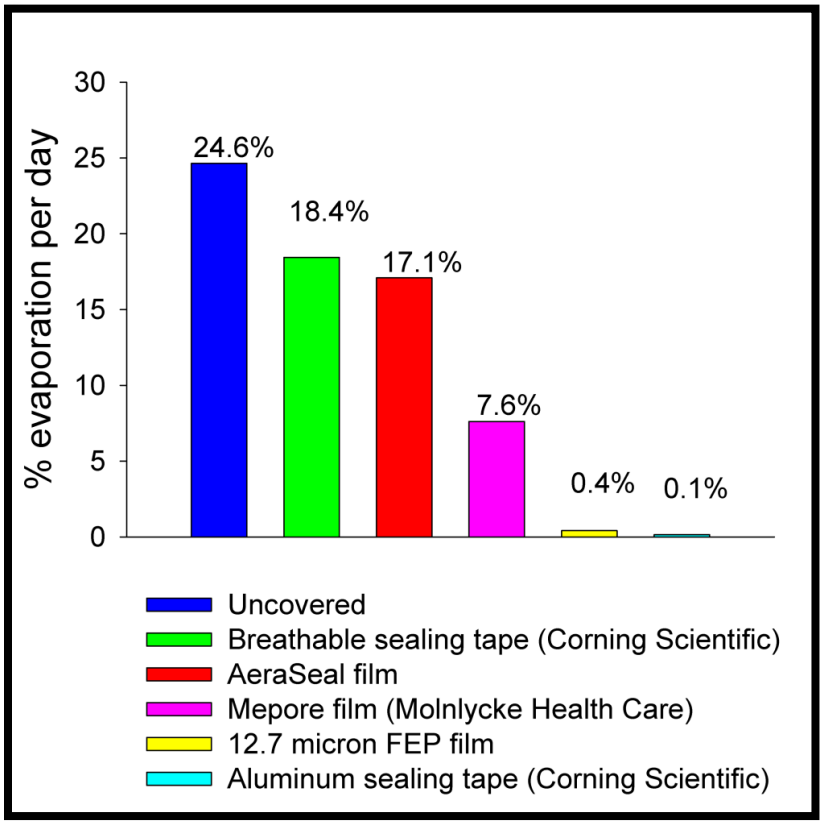

Figure 3.1. Effects of different 96-well plate seals on the rate of evaporation. Five different methods were examined for sealing 96-well plates. Each plate was filled with an approximate mass of 9.6 g of S-media, and incubated in an arid environment (30% humidity). The average percent evaporation per day was calculated by measuring the difference in weight of each plate per day over a period of 12 days. FEP® Teflon film allowed the least amount of evaporation of the gas-permeable seals.

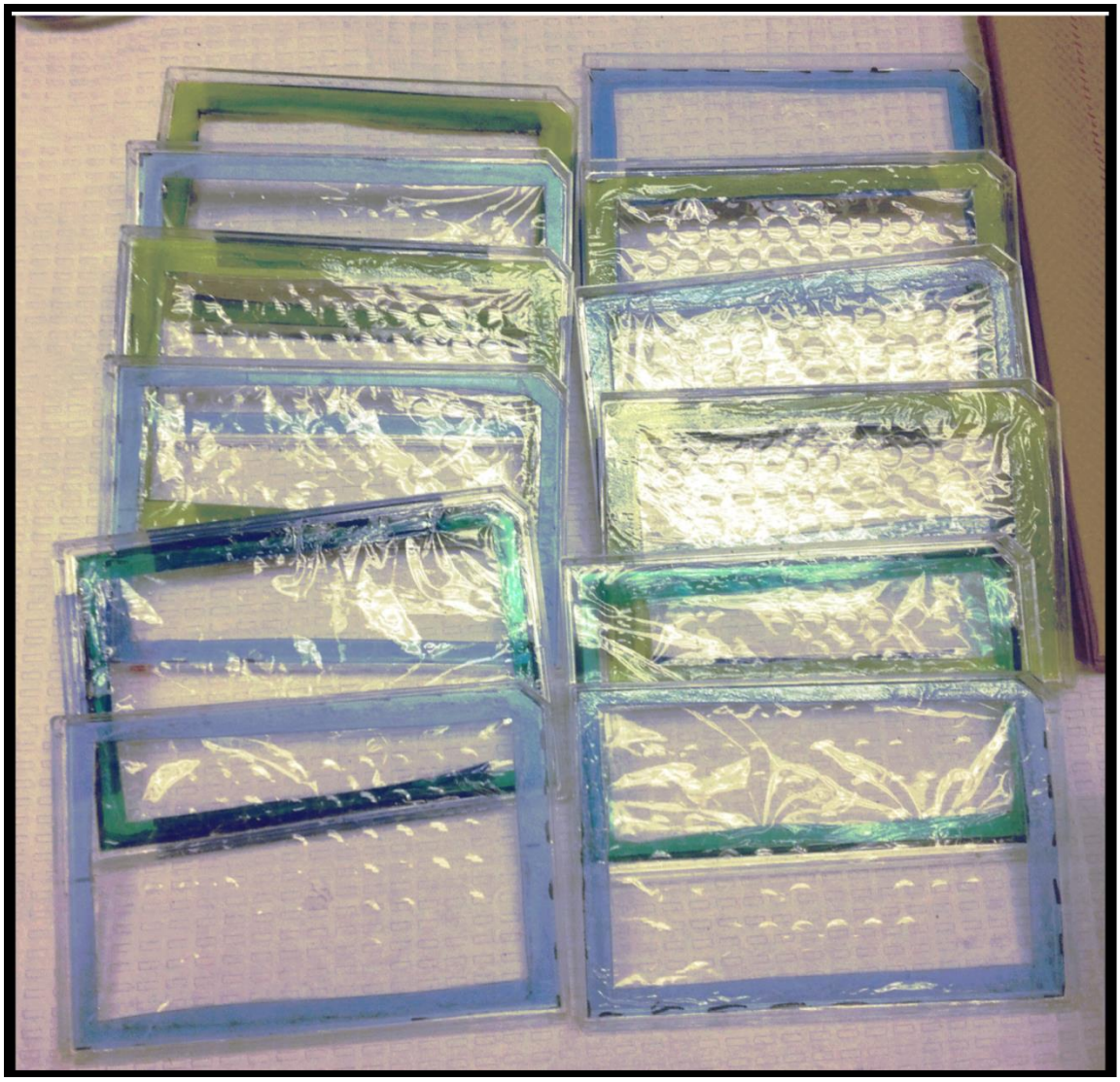

Figure 3.2. Photograph of gasket-attached FEP film lids. The lids were constructed fixing a rectangular gasket (cut from sheets of thick plastic) to a square of FEP film with adhesive. The gasket-film combinations were then glued onto the underside of 96-well plate lids, from which the majority of the top plastic surface had been removed with a hot scalpel. Once placed on top of a microplate, air flow could be completely restricted to the plate, except by passage through the FEP film by, by wrapping the outside edges of the plates with vinyl tape. The durability of FEP film makes it amenable to cleaning by washing with deionized water, and sterilization by cleansing with 70% ethanol. Cleaned plates could then be dried in a sterile environment and reused.

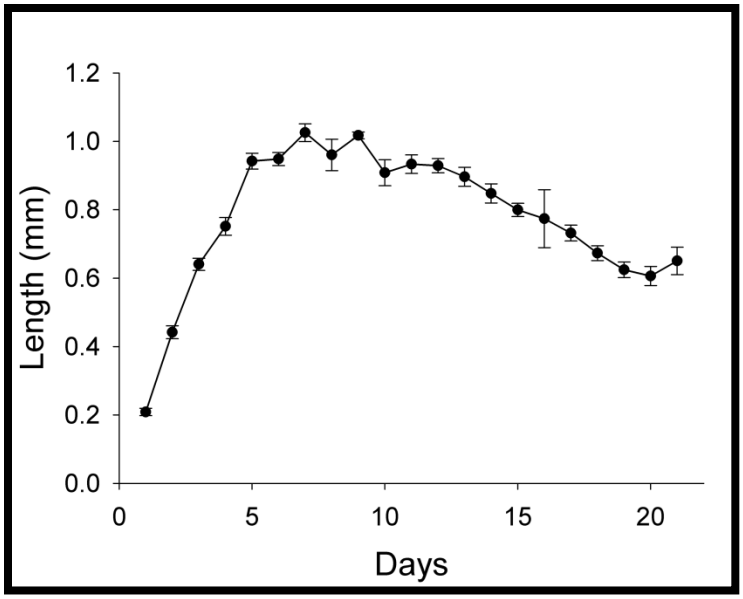

Figure 3.3. The average length (mm) of live *C. elegans* in liquid culture. Each day the image processing software ImageJ was used to calculate the lengths of *C. elegans* in liquid culture based on photographs of microscope images. For each daily series of images a microscope-generated scale bar of 1 mm was used to calibrate the length measurements. The number of worms measured each day varied between 3 and 13, with a mode of 8. Error bars represent the standard error of the mean.

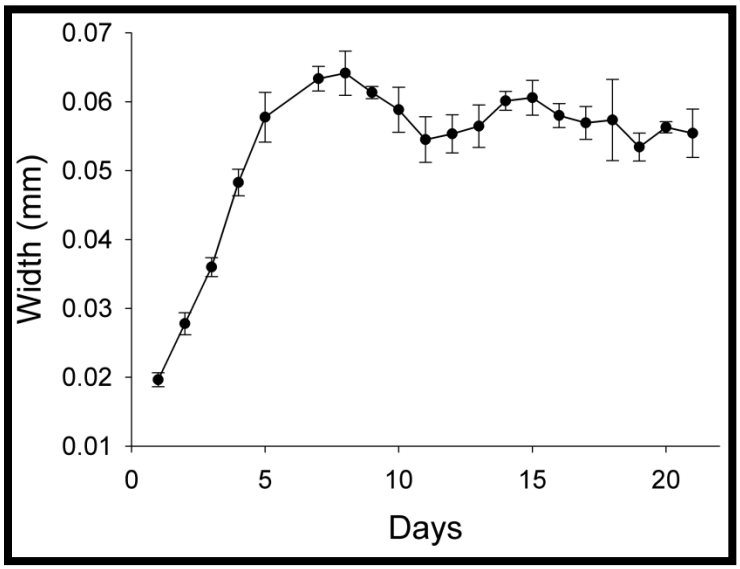

Figure 3.4. The average width (mm) of live *C. elegans* in liquid culture. As with the length measurements, the average *C. elegans* width for each day was determined by using ImageJ to measure the width of multiple nematodes. ImageJ measurements were done on microscope-generated images containing a 1 mm scale bar for daily software calibration. The number of worms measured each day varied between 3 and 13, with a mode of 8. Error bars represent the standard error of the mean.

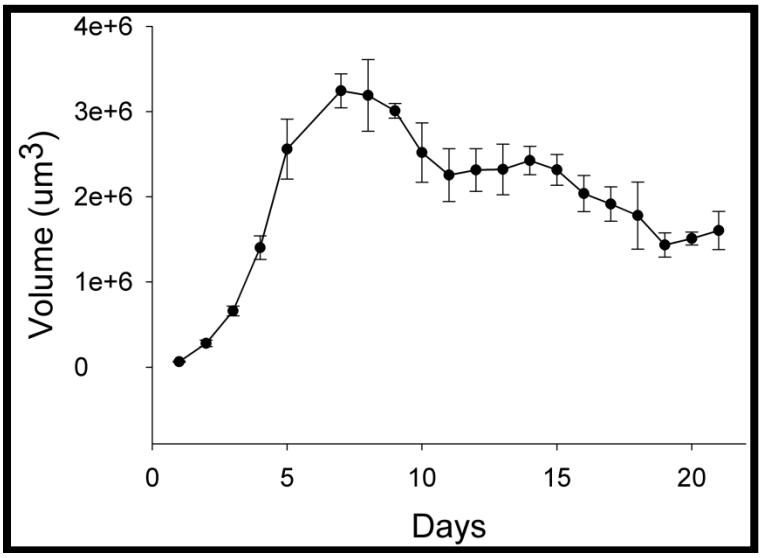

Figure 3.5. The estimated volume (µm^3) of individual live *C. elegans* in liquid culture. The daily estimate of the average volume of a *C. elegans* from that sample was calculate using the average length and average width from that day (*length* x π x 0.5 x *width*^{2}). This estimate assumes an approximately cylindrical *C. elegans* body shape. Error bars represent the standard error of the mean.

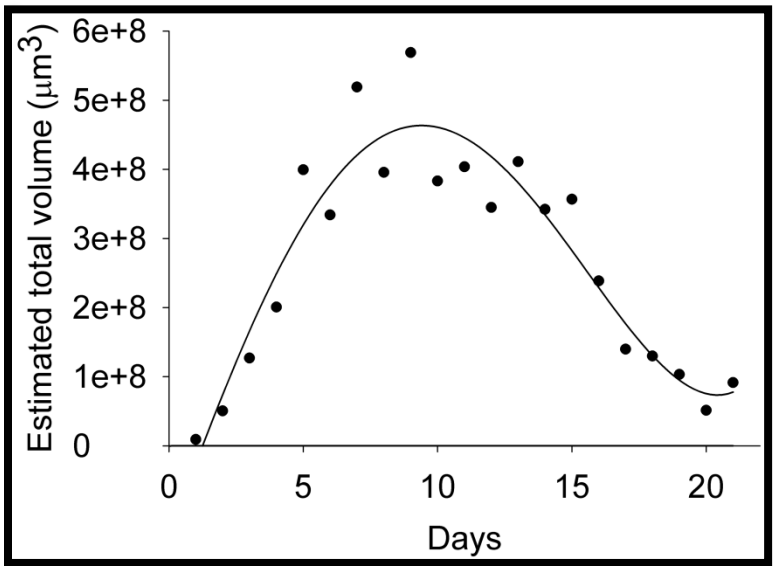

Figure 3.6. The rise and fall of the cumulative volume of live *C. elegans* in culture over the course of 21 days. On each day, the total volume of live *C. elegans* in that sample (corresponding to an estimate of the total mass of nematodes in that sample) was estimated by multiplying the estimated volume of a *C. elegans* worm in that sample by the number of live worms counted in that sample. The black line represents the fourth order polynomial trend line ($20222x^4$-$622952x^3$-$342367x^2$+$104484730x$-128931789).

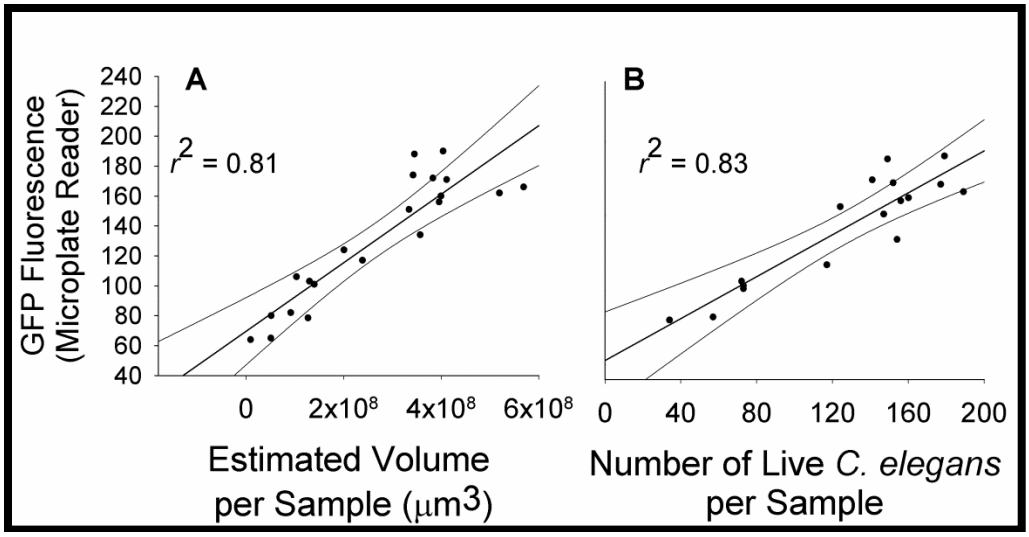

Figure 3.7. Association between GFP and both the number and volume of *C. elegans* in liquid culture. Individual samples were assessed from day 1 (24 hours after alkaline bleach synchronization) to day 23 in liquid cultures of *C. elegans*. (A) Total estimated volume per sample (μm^3) was calculated as the average volume per nematode on each day (*length* x π x ½ *width*^{2}) multiplied by the number of live worms scored in that day's sample (*volume* x *number of live C. elegans*). There is a strong positive association between GFP fluorescence (λ_{ex} = 485 nm and λ_{em} = 530 nm) and the total estimated volume per sample for each day (r^2 = 0.81; Pearson correlation = 0.90). (B) Similarly, as the total number of live nematodes per sample declined over the 23 day period, GFP fluorescence and the number of live worms per sample showed a strong positive association (r^2 = 0.83; Pearson correlation=0.91), but only for *C. elegans* from day 5 and beyond. Before day 5, the high number of live *C. elegans* per sample and the small size of the nematodes did not fit the same linear trend.

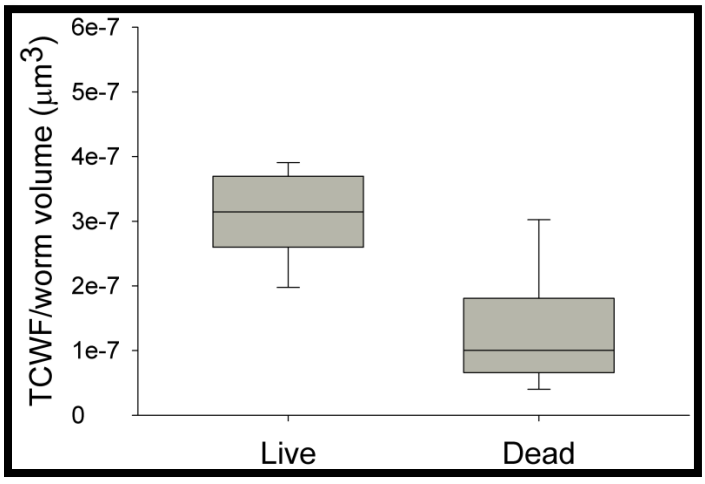

Figure 3.8. Dead *C. elegans* possess a lower degree of GFP fluorescence. The average GFP fluorescence per nematode (λ_{ex}=470 nm and λ_{em}=525 nm) for the entire 21 day period, for both live and dead *C. elegans*, was estimated by averaging the TCWF/volume for both groups ($p < 0.001$).

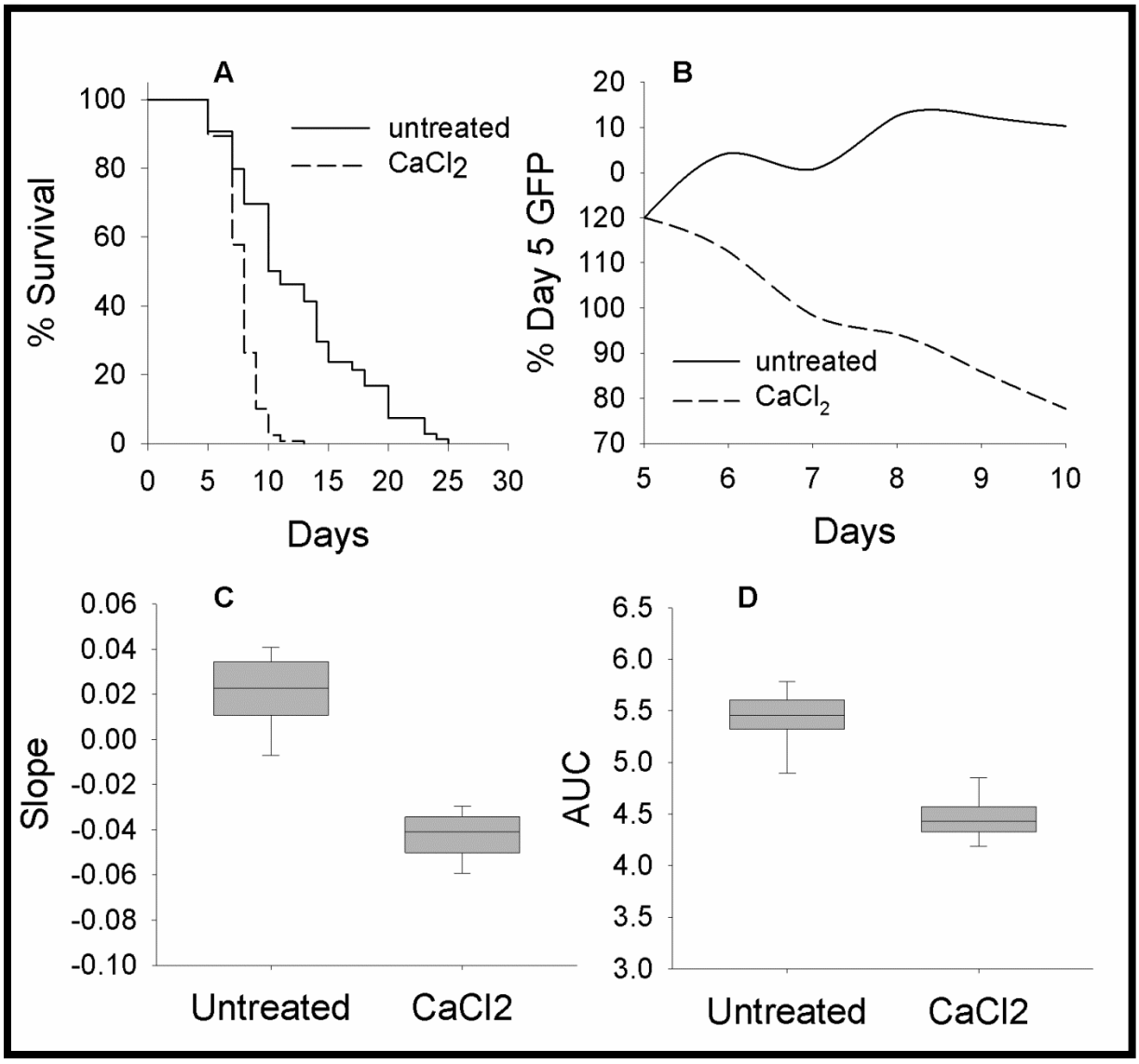

Figure 3.9. 100 mM $CaCl_2$ treatment decreases lifespan and alters the GFP profile of BC12907 *C. elegans*. (A) 100 mM $CaCl_2$ treatment at day 5 (day 2 of adulthood) decreased mean lifespan by 37% compared to the untreated control (7.8 days mean $CaCl_2$-treated lifespan; 12.4 days mean untreated lifespan; Log-Rank $p < 0.001$). (B) Mean GFP fluorescence (λ_{ex} = 485 nm and λ_{em} = 530 nm) profiles expressed as percent of day 5 fluorescence. $CaCl_2$-treatment resulted in a pronounced decrease in GFP fluorescence over the 5 day period as compared to the untreated samples. The dotted lines represent the upper and lower 99% confidence intervals for both groups (n = 58 wells for both groups; ~100 nematodes per well). (C) Boxplot comparison of the slopes for each of the $CaCl_2$-treated and untreated samples, calculated as (GFP Day 10 – GFP Day 5)/5 ($p < 0.0001$). (D) Boxplot comparison of the area under the curve (AUC) for each of the $CaCl_2$-treated and untreated samples ($p < 0.0001$).

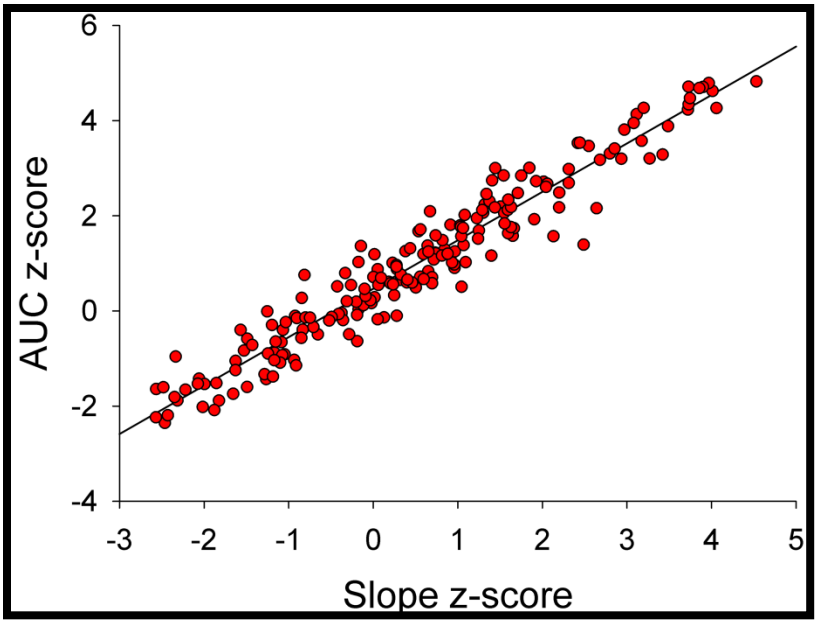

Figure 3.10. Consistency between z-scores of slopes and AUCs. The differences among z-scores of slopes and AUCs among $CaCl_2$-treated RNAi gene knockdowns compared to non-RNAi $CaCl_2$-treated nematodes varies linearly across the observed range (r^2 = 0.93; Pearson correlation=0.97). This linear relationship indicates a high degree of similarity between the two methods of describing GFP fluorescence profiles (λ_{ex}=485 nm and λ_{em}=530 nm).

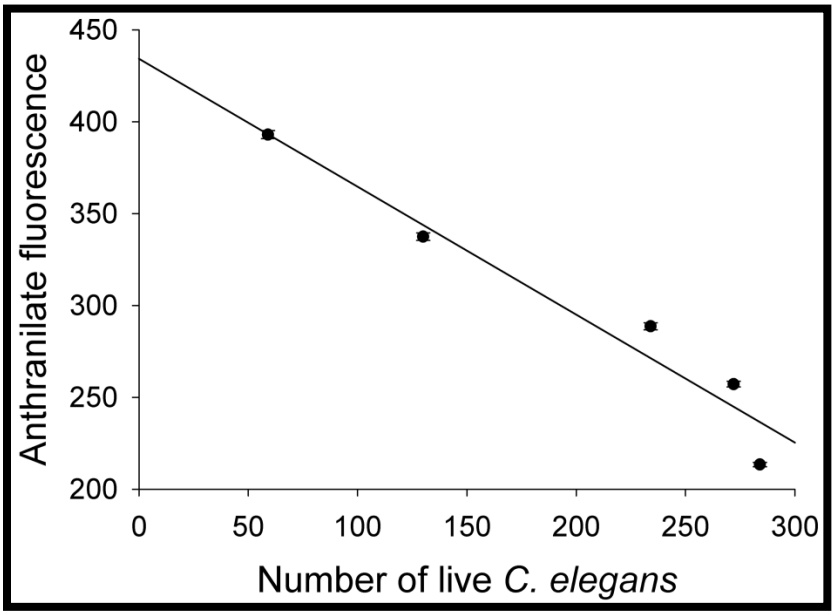

Figure 3.11. Anthranilate fluorescence increases with decreasing nematode population over time. The number of live *C. elegans* in liquid culture decreased over a period of 7 days (day 5 – day 11) as blue fluorescence increased (λ_{ex}=360 nm and λ_{em}=460 nm; n = 10 wells for visual scoring of live nematodes; n = 96 wells for fluorescence measurements by the microplate reader). Error bars represent the standard error of the mean.

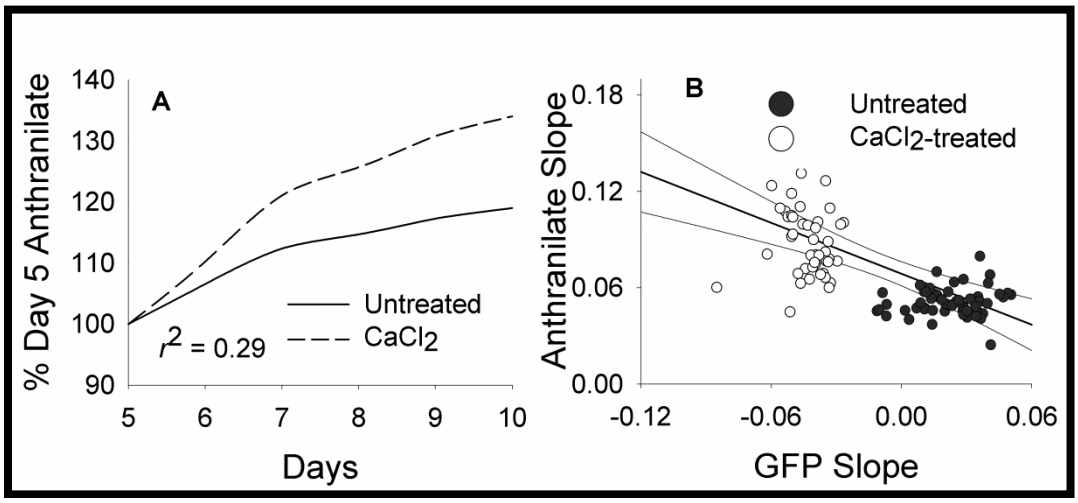

Figure 3.12. Anthranilate Fluorescence Profile. (A) The change in anthranilate fluorescence (λ_{ex} = 360 nM and λ_{em} = 460 nm) on each day, from days 5 through 10, normalized to the fluorescence on day 5 for each group (n = 58 wells; ~100 nematodes per well). Anthranilate fluorescence increased with time in both groups, but increased at a faster rate in the group treated with 100 mM $CaCl_2$, presumably as an indication of an increased rate of death for the *C. elegans* in those cultures. (B) The relationship between the slope of GFP fluorescence and the slope of anthranilate fluorescence (r^2 = 0.29; Pearson correlation = -0.54; n = 58 wells; ~100 worms per well). Lower GFP fluorescence slopes, which correspond to a faster decrease of live *C. elegans* volume in culture, tend to have greater anthranilate slopes, although a large degree of variation per well was observed between the two parameters.

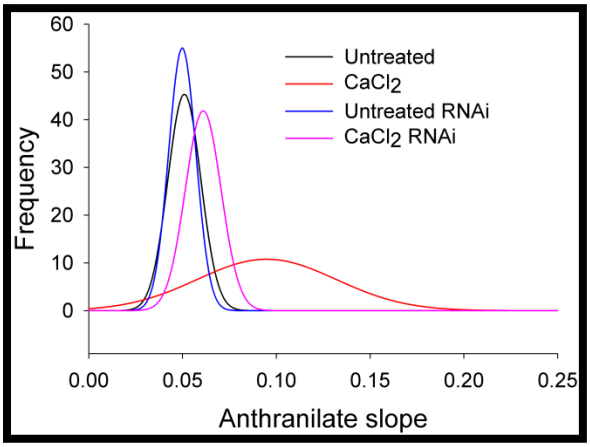

Figure 3.13. RNAi gene knockdowns treated with $CaCl_2$ have reduced variation compared to $CaCl_2$-treated controls. A comparison of the normal curves for each of the four treatment groups. RNAi gene knockdown *C. elegans* exhibited only ~26% of the variation (σ = 0.0095) of the non-RNAi $CaCl_2$-treated controls (σ = 0.0371). Furthermore, all but one of the 191 $CaCl_2$-treated RNAi knockdowns exhibited a lower anthranilate fluorescence slope than the mean of the non-RNAi $CaCl_2$-treated control.

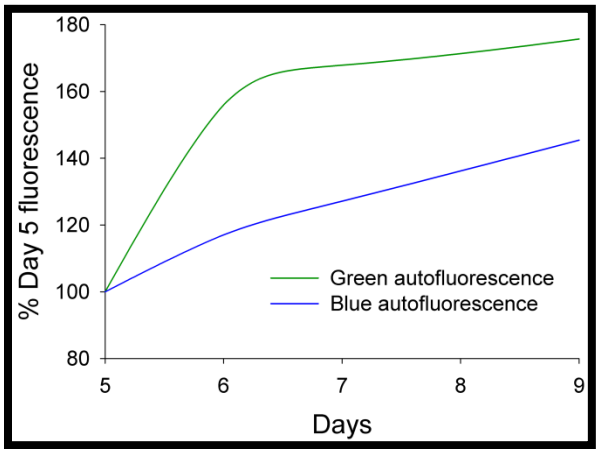

Figure 3.14. Bacterial autofluorescence. The bacterial autofluorescence in the green (λ_{ex}=485 nm and λ_{em}=530 nm) and blue ranges (λ_{ex}=360 nm and λ_{em}=460 nm) for 10 mg/mL *E. coli* tend to increase over the first several days in S-media cultures.

3.10 Tables

Table 3.1. GFP viability measurements to find EF-hand effectors of high Ca^{2+} toxicity in *C. elegans*. To determine hits the z-score for both GFP slope and GFP AUC were calculated (n = 6 wells per RNAi clone; ~100 nematodes per well; λ_{ex}=485 nm and λ_{em}=530 nm). Averages were calculated as the average z-score of the three screens utilizing 191 genes, 191 genes, and 55 genes, respectively. For GFP measurements, higher z-scores indicate increased viability. When calculating the total averaged z-scores including anthranilate, the z-scores from GFP were added to (-1) times the z-scores for anthranilate slope and anthranilate AUC since negative z-scores indicate increased viability in the anthranilate measurements. Z-scores highlighted in yellow are greater than ± 2 standard deviations from the mean of the control.

Gene name	GFP - $CaCl_2$ added			Total averaged z-score including anthranilate	Gene description
	Averaged AUC z-score	Averaged slope z-score	Total averaged z-score		
T04F8.6	2.63	2.43	2.53	1.41	Similar to F59A2.6
C09H5.7	2.56	2.15	2.35	1.32	Serine/threonine protein phosphatase
ZK673.7	2.50	2.05	2.27	1.56	Troponin C
F53F4.14	2.13	2.34	2.23	1.28	Similar to F36H12.3 (major sperm protein)
C47A4.3	2.28	2.13	2.21	1.42	Serine/threonine protein phosphatase
C04B4.2	2.25	2.03	2.14	1.32	Similar to C04B4.4 and LIN-66
K04F1.10	2.36	1.89	2.12	1.31	IRLD-40 (Insulin/EGF-Receptor L Domain protein)
W08D2.7	2.16	1.78	1.97	1.35	yeast MTR (mRNA transport) homolog
Y40H4A.2	2.25	1.50	1.88	1.08	Serine/threonine-protein phosphatase
Y75B12B.6	2.08	1.66	1.87	1.08	Phospholipase C
C03A7.13	2.08	1.53	1.81	1.22	UDP-glucuronosyl/UDP-glucosyltransferase domain containing protein
C27B7.6	1.93	1.57	1.75	1.27	Putative serine/threonine-protein phosphatase

Table 3.1 (Continued)

Gene name	GFP - $CaCl_2$ added			Total averaged z-score including anthranilate	Gene description
	Averaged AUC z-score	Averaged slope z-score	Total averaged z-score		
T06E6.1	1.78	1.64	1.71	1.14	Similar to human WDR-74
F11C7.4	1.96	1.44	1.70	1.27	Drosophila Crumbs homolog
F38H4.9	1.79	1.57	1.68	1.24	LET-92 homolog of protein phosphatase PP2AC
B0513.5	1.53	1.84	1.68	0.98	Proline dehydrogenase, mitochondrial
B0348.4	1.84	1.41	1.62	0.72	Egg Laying defective; EGL-8 encodes a phospholipase C beta
F23B12.1	1.65	1.58	1.61	0.97	Serine/threonine protein phosphatase
C56G7.1	1.67	1.37	1.52	0.89	MLC-4 Myosin Light Chain
C54E10.2	1.46	1.31	1.39	0.88	NCS-5 (Neuronal Calcium Sensor family)
F23B12.7	1.54	1.24	1.39	0.85	Homolog of human CAATT-binding protein
C36E6.5	1.29	1.43	1.36	1.25	MLC-2 Myosin Light Chain
F58G11.1	1.64	1.07	1.35	0.86	LETM1 (Leucine zipper, EF-hand, Transmembrane mitochondrial protein) homolog
Y73B3A.12	1.55	1.13	1.34	1.08	CAL-6 encodes an ortholog of human calmodulin-like 3
Y69E1A.4	1.50	1.11	1.30	0.95	Serine/threonine protein phosphatase
F40F9.8	1.52	1.07	1.30	0.89	CAL-7 encodes an ortholog of human calmodulin-like 4
Y67H2A.4	1.39	1.20	1.29	0.60	MICU-1 (MItochondrial Calcium Uptake protein)
T08D2.1	1.40	0.99	1.20	0.93	Transmembrane emp24 domain-containing protein
K08E3.3	1.35	1.03	1.19	0.75	TOCA (Transducer Of Cdc42-dependent Actin assembly) homolog
F42G8.8	1.57	0.80	1.18	0.88	Serine/threonine protein phosphatase
F08B6.3	1.14	1.17	1.15	0.82	CALU-2 (CALUmenin (calcium-binding protein) homolog)
T27C10.4	1.39	0.88	1.13	0.80	BTB and MATH domain containing
T04F3.4	1.48	0.77	1.13	0.57	Multiple coagulation factor deficiency protein 2 homolog
T07G12.1	1.34	0.89	1.11	0.80	CAL-4 (CALmodulin related genes)
F55A3.7	0.84	1.38	1.11	0.95	FACT complex subunit SPT16 homolog
C34D4.2	1.32	0.87	1.09	0.74	Serine/threonine protein phosphatase
C44C1.3	1.06	1.10	1.08	0.69	NCS-1 (Neuronal Calcium Sensor family)
ZK856.8	1.17	0.99	1.08	0.91	Calcium-binding protein p22 homolog
ZC477.2	1.33	0.76	1.05	0.88	Serine/threonine-protein phosphatase
F13G11.2	1.00	1.05	1.03	0.74	IRLD-4 (Insulin/EGF-Receptor L Domain protein)
K08F11.5	0.64	1.40	1.02	1.03	Mitochondrial Rho GTPase Miro-1
C24H10.5	1.27	0.72	1.00	0.65	CAL-5 (CALmodulin related genes)
ZK1248.3	1.19	0.80	0.99	0.53	Eps15 (endocytosis protein) Homologous Sequence
C33D12.6	0.98	0.95	0.97	0.80	RSEF-1 encodes an ortholog of human RAB44
4R79.2	0.96	0.89	0.92	0.65	Similar to RSEF-1
T22D1.5	1.07	0.75	0.91	0.70	Probable serine/threonine protein phosphatase 2A regulatory subunit
W09C3.6	0.93	0.89	0.91	0.88	GSP-3 (GLC7 (yeast Glc Seven) like Phosphatase)
F25B3.4	1.05	0.76	0.91	0.63	Serine/threonine protein phosphatase
F58E6.1	1.16	0.65	0.91	0.56	Signal transducer and activator of transcription b
M18.5	1.01	0.80	0.90	0.46	DDB1 (UV-Damaged DNA Binding protein) homolog
R05G6.8	0.86	0.93	0.90	0.96	Phospholipase C
Y51H4A.17	1.05	0.61	0.83	0.66	STAT transcription factor family
C36E6.3	1.01	0.61	0.81	0.81	MLC-1 Myosin Light Chain
C06A1.5	1.00	0.60	0.80	0.91	RNA Polymerase II (B) subunit
K11C4.5	0.77	0.82	0.80	0.70	Uncoordinated UNC-68; Ryanodine receptor homolog
F43C9.2	0.95	0.65	0.80	0.87	Homologous to Isoform 1 of Calcium-binding protein 4
F55C10.1	0.71	0.88	0.80	0.69	Calcineurin B

Table 3.1 (Continued)

Gene name	GFP - $CaCl_2$ added				Gene description
	Averaged AUC z-score	Averaged slope z-score	Total averaged z-score	Total averaged z-score including anthranilate	
K07C5.1	0.96	0.50	0.73	0.75	ARX-2; ARp2/3 complex component
Y37A1B.1	0.67	0.76	0.71	0.39	LST-3 (Lateral Signaling Target); ortholog of human CCAR2
C02F4.2	0.68	0.67	0.68	0.88	Calcineurin A/TAX-6
C47C12.4	0.62	0.70	0.66	0.87	Mitochondrial Rho GTPase Miro-2
Y116A8C.36	0.85	0.46	0.66	0.56	ITSN (intersectin) family
T25B9.2	0.81	0.48	0.65	0.52	Serine/threonine protein phosphatase
T10H9.8	0.73	0.56	0.64	0.67	Similar to CAL-4
K03E6.3	0.73	0.55	0.64	0.57	NCS-3 (Neuronal Calcium Sensor family)
M02A10.3	0.71	0.53	0.62	0.44	SLI-1 (Suppressor of LIneage defect); Cbl family of ubiquitin ligases
K10B3.10	0.56	0.69	0.62	0.60	Spectrin
F44A6.1	0.80	0.44	0.62	0.58	Nucleobindin homolog
T12D8.6	0.69	0.52	0.61	0.67	MLC-5 (Myosin Light Chain)
C24H11.1	0.78	0.42	0.60	0.65	Serine/threonine protein phosphatase
M02B7.6	0.87	0.29	0.58	0.41	CAL-3 (CALmodulin related genes)
C18E9.1	0.83	0.33	0.58	0.62	CAL-2 (CALmodulin related genes)
C29E4.14	0.72	0.42	0.57	0.61	Multiple coagulation factor deficiency protein 2 homolog
C44B12.2	0.69	0.42	0.55	0.47	Osteonectin (SPARC) related
T04F3.2	0.73	0.37	0.55	0.60	similar to SPARC-related modular calcium-binding protein 2
F31B12.1	0.60	0.49	0.55	0.37	PhosphoLipase C
F25B3.3	0.76	0.33	0.54	0.62	Rap Guanine nucleotide Exchange Factor homolog
ZK354.9	0.68	0.40	0.54	0.38	Serine/threonine protein phosphatase
M03F4.7	0.83	0.25	0.54	0.51	Calumenin (calcium-binding protein) homolog
R09H10.6	0.52	0.56	0.54	0.56	R09H10.6 Similar to F23F1.2
K03A1.4	0.74	0.34	0.54	0.77	Similar to Calmodulin-1
K04C1.4	0.75	0.31	0.53	0.55	MLC-6 (Myosin Light Chain)
Y39B6A.38	0.44	0.60	0.52	0.60	REPS (RalBP1-associated Eps domain-containing protein) homolog
F29F11.6	0.68	0.36	0.52	0.54	GSP-1 (GLC7 (yeast Glc Seven) like Phosphatase)
C54E4.2	0.54	0.48	0.51	0.72	Similar to Testican-3
F56D1.6	0.64	0.38	0.51	0.69	Calexcitin
C56C10.9	0.56	0.46	0.51	0.57	Similar to human 45 kDa calcium-binding protein
Y73C8B.5	0.67	0.35	0.51	0.57	Similar to calmodulin-3
Y43F4B.3	0.36	0.64	0.50	0.60	Set-25 (SET (trithorax/polycomb) domain containing)
T09B4.4	0.64	0.36	0.50	0.48	Similar to Calmodulin-like protein 4
E02A10.3	0.63	0.29	0.46	0.47	Similar to calmodulin
F53G12.3	0.67	0.23	0.45	0.57	DUOX-2 (DUal OXidase)
ZC116.3	0.46	0.42	0.44	0.52	Probable cubilin
T09F5.10	0.36	0.45	0.40	0.37	Similar to F36D3.16
F59D6.7	0.32	0.44	0.38	0.64	Calcineurin B homolog
Y45F10A.6	0.33	0.37	0.35	0.43	TBC (Tre-2/Bub2/Cdc16) domain family
H10E21.4	0.30	0.34	0.32	0.60	Calmodulin-like protein 6
K08E3.10	0.49	0.15	0.32	0.43	MLC-7 (Myosin Light Chain)
K01A2.11	0.31	0.33	0.32	0.54	Calcium Binding protein homolog
F33C8.4	0.33	0.22	0.27	0.53	Similar to Y41D4A.7
W02B9.1	0.26	0.28	0.27	0.63	Hammerhead embryonic lethal; cadherin homolog

Table 3.1 (Continued)

Gene name	GFP - $CaCl_2$ added			Total averaged z-score including anthranilate	Gene description
	Averaged AUC z-score	Averaged slope z-score	Total averaged z-score		
R08F11.1	0.22	0.32	0.27	0.37	Non-lysosomal glucosylceramidase
C16H3.1	0.37	0.15	0.26	0.55	NCS-7 (Neuronal Calcium Sensor family)
B0252.3	0.30	0.22	0.26	0.50	Putative transporter B0252.3
F55A11.4	0.17	0.33	0.25	0.45	Calcium-binding mitochondrial carrier protein SCaMC-2 homolog; non-coding
K02F3.2	0.46	0.03	0.25	0.35	Probable calcium-binding mitochondrial carrier K02F3.2; Similar to Aralar1
ZK1151.1	0.22	0.27	0.24	0.63	Variable abnormal morphology
F16F9.3	0.32	0.16	0.24	0.33	F16F9.3
T10G3.5	0.14	0.33	0.24	0.39	EEA1 (Early Endosome Antigen, Rab effector) homolog
Y47G6A.27	0.12	0.35	0.23	0.24	Mitochondrial Rho GTPase Miro-3
C06G1.5	0.32	0.12	0.22	0.26	Serine/threonine-protein phosphatase 2A regulatory subunit
R08D7.5	0.16	0.26	0.21	0.46	Human Centrin-2 homolog
F17E5.2	0.05	0.34	0.20	0.44	Probable calcium-binding mitochondrial carrier F17E5.2; SCaMC-2
W06H8.1	0.29	0.08	0.18	0.64	RME-1 (Receptor Mediated Endocytosis); EH domain containing protein
C50C3.5	0.20	0.13	0.16	0.48	Similar to calmodulin 1
R08C7.8	0.50	-0.19	0.16	0.36	Serine/threonine-protein phosphatase
M03C11.8	0.22	0.09	0.15	0.45	Putative SMARCAL1-like protein; Protein archease-like
Y32G9A.6	0.31	0.00	0.15	0.45	NPHP-2 (NePHronoPhthisis (human kidney disease) homolog)
C48A7.1	0.32	-0.02	0.15	0.34	Egg Laying defective
T21H3.3	0.16	0.08	0.12	0.39	Calmodulin
C13C12.1	0.21	0.01	0.11	0.37	CAL-1 (CALmodulin related genes)
W04D2.1	0.14	0.05	0.10	0.26	Actinin
C07A9.5	-0.07	0.23	0.08	0.36	Similar to alpha-actinin-2
Y71H2AL.1	0.24	-0.09	0.08	0.17	PBO-1 (PBOc defective (defecation)) calcineurin B homolog
Y49E10.3	0.24	-0.14	0.05	0.35	Protein Phosphatase
C11G6.4	0.02	0.04	0.03	0.29	NHR-28 (Nuclear Hormone Receptor family)
F25H2.2	0.08	-0.02	0.03	0.21	SNX-27 (Sorting NeXin)
T02G5.2	0.14	-0.14	0.00	0.36	EF-hand calcium-binding domain-containing protein 7
T04D3.2	-0.07	0.07	0.00	0.40	SDZ-30 (SKN-1 Dependent Zygotic transcript)
Y26E6A.2	0.10	-0.16	-0.03	0.09	F-box protein
T03F1.5	0.01	-0.07	-0.03	0.37	GSP-4 (GLC7 (yeast Glc Seven) like Phosphatase)
T02C5.5	0.22	-0.29	-0.03	0.23	Uncoordinated; UNC-2 encodes a calcium channel alpha subunit
K03A1.2	0.05	-0.12	-0.04	0.25	lron-7 (eLRR (extracellular Leucine-Rich Repeat) ONly)
C24H11.2	-0.05	-0.07	-0.06	0.24	Serine/threonine protein phosphatase
F26B1.5	0.00	-0.14	-0.07	0.34	Serine/threonine protein phosphatase
Y105E8A.7	0.01	-0.18	-0.09	0.56	EAT-18 (EATing: abnormal pharyngeal pumping)
F56C9.1	-0.14	-0.10	-0.12	0.37	GSP-2 (GLC7 (yeast Glc Seven) like Phosphatase)
R10E11.6	0.20	-0.45	-0.13	0.36	Similar to Synergin-gamma
R08A2.2	-0.06	-0.27	-0.16	0.25	Serine/threonine protein phosphatase
F53F8.1	-0.01	-0.33	-0.17	0.24	Kruppel-Like Factor (zinc finger protein)
T09A5.1	-0.12	-0.23	-0.17	0.42	Calexcitin
C06A1.3	0.03	-0.39	-0.18	0.17	Putative serine/threonine-protein phosphatase
C48B4.2	0.01	-0.47	-0.23	0.34	Rhomboid (Drosophila) related

Table 3.1 (Continued)

Gene name	GFP - $CaCl_2$ added			Total averaged z-score including anthranilate	Gene description
	Averaged AUC z-score	Averaged slope z-score	Total averaged z-score		
F21A3.5	-0.12	-0.44	-0.28	0.22	PRDE-1 (PiRNA-DEpendent silencing defective) casein kinase-1 homolog
F55A11.1	-0.31	-0.25	-0.28	0.28	Similar to Multiple coagulation factor deficiency protein 2
B0563.7	-0.10	-0.49	-0.29	0.18	Similar to calmodulin
DH11.1	-0.15	-0.44	-0.29	0.24	Putative glutaminase
C56A3.6	-0.02	-0.57	-0.30	0.23	Mitochondrial calcium uptake protein-3 (MICU-3)
ZK328.1	-0.22	-0.43	-0.33	0.23	CYK-3 (CYtoKinesis defect); Ubiquitin C-terminal hydrolase
C50C3.2	-0.32	-0.46	-0.39	0.14	Spectrin alpha chain
B0511.1	-0.27	-0.56	-0.42	0.23	FK506-Binding protein family
T16G12.7	-0.37	-0.47	-0.42	0.20	Serine/threonine protein phosphatase
ZK899.5	-0.41	-0.43	-0.42	0.25	ZK899.5
B0336.11	-0.21	-0.63	-0.42	0.13	HPO-28 (Hypersensitive to POre- forming toxin)
ZK686.2	-0.32	-0.58	-0.45	0.08	Putative ATP-dependent RNA helicase ZK686.2
ZK1307.8	-0.45	-0.46	-0.45	0.12	Glucosidase 2 subunit beta
F56C11.1	-0.40	-0.56	-0.48	0.27	Blistered cuticle; BLI-3 (DUal OXidase)
Y75B8A.30	-0.34	-0.63	-0.49	-0.12	Protein phosphatase
B0511.1	-0.51	-0.48	-0.49	0.08	FK506-Binding protein family
Y9D1A.2	-0.61	-0.41	-0.51	0.22	Putative RNA helicase
C23G10.1	-0.58	-0.49	-0.54	-0.08	Putative serine/threonine-protein phosphatase C23G10.1
F12A10.5	-0.50	-0.59	-0.54	0.13	CAL-8 (CALmodulin related genes)
K10F12.3	-0.43	-0.70	-0.57	0.10	Phospholipase C Like
R13A5.11	-0.53	-0.70	-0.62	-0.08	Serine/threonine protein phosphatase
C36F7.2	-0.65	-0.58	-0.62	0.10	SWAH-1 (SoWAH (Drosophila) homolog)
T05F1.1	-0.62	-0.70	-0.66	-0.07	NRA-2 (Nicotinic Receptor Associated) nicalin homolog
C47D12.1	-0.62	-0.71	-0.66	-0.09	TRRAP-like (transcription/transformation domain-associated protein)
C34C12.3	-0.68	-0.68	-0.68	0.04	Protein Phosphatase
F10G8.5	-0.54	-0.85	-0.70	0.06	NCS-2 (Neuronal Calcium Sensor family)
F09F7.2	-0.57	-0.82	-0.70	0.06	MLC-3 Myosin Light Chain
F23H11.8	-0.51	-0.91	-0.71	-0.06	Phosphatase with EF hands
K07G5.4	-0.61	-0.83	-0.72	-0.02	K07G5.4
F25H2.8	-0.81	-0.65	-0.73	0.00	UBC-25 (UBiquitin Conjugating enzyme)
C25A1.9	-0.68	-0.78	-0.73	-0.10	RSA-1 (Regulator of Spindle Assembly); protein phosphatase 2A (PP2A) regulatory subunit
F23F1.2	-0.61	-0.89	-0.75	-0.01	Similar to R09H10.6
C36C9.6	-0.78	-0.73	-0.76	-0.34	C36C9.6
T09E8.2	-0.84	-0.69	-0.76	-0.11	High Incidence of Males (increased X chromosome loss) HIM-17
W09G10.3	-0.53	-1.15	-0.84	-0.05	NCS-6 (Neuronal Calcium Sensor family)
F54G8.2	-0.92	-0.76	-0.84	-0.11	Diacylglycerol Kinase
F19B10.1	-0.91	-0.84	-0.88	-0.06	MEL-26 binding protein
T03F1.11	-0.83	-1.08	-0.95	-0.13	Similar to CALM-1
F58G1.3	-0.89	-1.04	-0.96	-0.19	Serine/threonine protein phosphatase
Y48B6A.6	-1.01	-0.95	-0.98	-0.10	EFHD-1 (EF Hand calcium binding protein)
ZK938.1	-0.85	-1.12	-0.99	-0.28	Serine/threonine protein phosphatase
F52H3.6	-0.77	-1.21	-0.99	-0.21	Serine/threonine protein phosphatase
F22D6.9	-0.93	-1.09	-1.01	-0.07	Serine/threonine protein phosphatase
T25G3.4	-1.11	-1.07	-1.09	-0.22	Probable glycerol-3-phosphate dehydrogenase,

Table 3.1 (Continued)

Gene name	GFP - $CaCl_2$ added			Total averaged z-score including anthranilate	Gene description
	Averaged AUC z-score	Averaged slope z-score	Total averaged z-score		
					mitochondrial
F21A10.1	-1.04	-1.20	-1.12	-0.31	NCS-4 (Neuronal Calcium Sensor family)
F30A10.1	-1.16	-1.26	-1.21	-0.18	CALM-1 (CALMyrin (Calcium and Integrin Binding protein) homolog)
M04F3.4	-1.49	-0.95	-1.22	-0.26	Probable cysteine protease
F54C1.7	-1.19	-1.37	-1.28	-0.23	PAT-10 (Paralysed Arrest at Two-fold) Body wall muscle troponin C

Table 3.2. The effect of EF-hand gene knockdowns in the absence of $CaCl_2$ on GFP measurement z-scores. The conditions were the same as in S1 Table except deionized water was added to the wells instead of $CaCl_2$.

Gene names	GFP - no $CaCl_2$			Total averaged z-score including anthranilate	Gene description
	Averaged AUC z-score	Averaged slope z-score	Total averaged z-score		
C33D12.6	2.20	1.29	1.75	0.84	RSEF-1 encodes an ortholog of human RAB44
F53F4.14	1.39	1.94	1.66	0.79	Similar to F36H12.3 (major sperm protein)
K03E6.3	1.82	1.41	1.62	0.15	NCS-3 (Neuronal Calcium Sensor family)
B0513.5	1.38	1.83	1.61	1.39	Proline dehydrogenase, mitochondrial
M03F4.7	1.88	1.28	1.58	0.18	Calumenin (calcium-binding protein) homolog
F55A11.1	1.86	1.26	1.56	0.29	Similar to Multiple coagulation factor deficiency protein 2
C34D4.2	1.45	1.58	1.51	0.58	Serine/threonine protein phosphatase
K03A1.4	1.63	1.19	1.41	0.13	Similar to Calmodulin-1
C47A4.3	1.38	1.37	1.38	0.84	Serine/threonine protein phosphatase
T07G12.1	1.62	0.90	1.26	0.56	CAL-4 (CALmodulin related genes)
K10B3.10	1.64	0.77	1.21	0.10	Spectrin
F33C8.4	1.67	0.74	1.21	0.02	Similar to Y41D4A.7
F58G11.1	1.13	1.27	1.20	0.58	LETM1 (Leucine zipper, EF-hand, Transmembrane mitochondrial protein) homolog
T10G3.5	1.06	1.31	1.19	0.31	EEA1 (Early Endosome Antigen, Rab effector) homolog
C13C12.1	1.44	0.92	1.18	0.98	CAL-1 (CALmodulin related genes)
E02A10.3	1.49	0.83	1.16	0.75	Similar to calmodulin
C47C12.4	1.47	0.84	1.15	1.26	Mitochondrial Rho GTPase Miro-2
B0348.4	1.04	1.25	1.14	0.55	Egg Laying defective; EGL-8 encodes a phospholipase C beta
K02F3.2	1.22	0.92	1.07	0.25	Probable calcium-binding mitochondrial carrier K02F3.2; Similar to Aralar1
F43C9.2	1.37	0.75	1.06	0.32	Homologous to Isoform 1 of Calcium-binding protein 4
T12D8.6	1.34	0.78	1.06	0.37	MLC-5 (Myosin Light Chain)
ZC477.2	0.99	1.12	1.06	0.58	Serine/threonine-protein phosphatase
C04B4.2	1.08	1.03	1.06	0.46	Similar to C04B4.4 and LIN-66
C06G1.5	1.44	0.65	1.05	0.18	Serine/threonine-protein phosphatase 2A regulatory subunit
R08F11.1	1.26	0.81	1.03	0.44	Non-lysosomal glucosylceramidase
F53G12.3	1.29	0.66	0.98	0.38	DUOX-2 (DUal OXidase)

Table 3.2 (Continued)

Gene names	GFP - no $CaCl_2$			Total averaged z-score including anthranilate	Gene description
	Averaged AUC z-score	Averaged slope z-score	Total averaged z-score		
C09H5.7	0.94	0.94	0.94	0.47	Serine/threonine protein phosphatase
Y69E1A.4	0.88	0.96	0.92	0.75	Serine/threonine protein phosphatase
C44C1.3	1.01	0.80	0.90	0.38	NCS-1 (Neuronal Calcium Sensor family)
T06E6.1	0.70	1.09	0.89	0.30	Similar to human WDR-74
F16F9.3	0.98	0.77	0.87	0.26	F16F9.3
F58E6.1	1.05	0.69	0.87	0.60	Signal transducer and activator of transcription b
F23B12.1	0.91	0.82	0.86	-0.26	Serine/threonine protein phosphatase
4R79.2	0.88	0.83	0.85	0.51	Similar to RSEF-1
C16H3.1	1.03	0.56	0.79	0.13	NCS-7 (Neuronal Calcium Sensor family)
C54E4.2	1.23	0.32	0.78	0.56	Similar to Testican-3
T09B4.4	1.26	0.27	0.76	-0.09	Similar to Calmodulin-like protein 4
T03F1.5	1.22	0.28	0.75	0.36	GSP-4 (GLC7 (yeast Glc Seven) like Phosphatase)
Y75B12B.6	0.56	0.93	0.74	0.45	Phospholipase C
K04F1.10	0.72	0.71	0.72	0.63	IRLD-40 (Insulin/EGF-Receptor L Domain protein)
W09C3.6	1.02	0.41	0.71	0.21	GSP-3 (GLC7 (yeast Glc Seven) like Phosphatase)
F25B3.4	0.60	0.82	0.71	0.03	Serine/threonine protein phosphatase
Y40H4A.2	0.84	0.55	0.70	0.26	Serine/threonine-protein phosphatase
F56C11.1	0.98	0.39	0.68	0.24	Blistered cuticle; BLI-3 (DUal OXidase)
T04F3.2	1.00	0.35	0.68	-0.27	similar to SPARC-related modular calcium-binding protein 2
F25H2.2	1.09	0.21	0.65	0.24	SNX-27 (Sorting NeXin)
F26B1.5	1.13	0.14	0.64	0.72	Serine/threonine protein phosphatase
Y73B3A.12	0.61	0.65	0.63	0.28	CAL-6 encodes an ortholog of human calmodulin-like 3
ZK673.7	0.42	0.83	0.63	0.14	Troponin C
T09F5.10	0.92	0.33	0.62	-0.26	Similar to F36D3.16
C03A7.13	0.40	0.83	0.62	0.61	UDP-glucuronosyl/UDP-glucosyltransferase domain containing protein
K07C5.1	0.98	0.24	0.61	0.85	ARX-2; ARp2/3 complex component
F42G8.8	0.54	0.66	0.60	0.67	Serine/threonine protein phosphatase
T08D2.1	0.40	0.72	0.56	0.38	Transmembrane emp24 domain-containing protein
Y43F4B.1	0.54	0.47	0.50	-0.07	Set-25 (SET (trithorax/polycomb) domain containing)
F11C7.4	0.46	0.52	0.49	0.59	Drosophila Crumbs homolog
Y116A8C.36	0.65	0.23	0.44	0.58	ITSN (intersectin) family
F55A11.4	0.38	0.46	0.42	0.44	Calcium-binding mitochondrial carrier protein SCaMC-2 homolog; non-coding
F13G11.2	0.85	-0.03	0.41	0.36	IRLD-4 (Insulin/EGF-Receptor L Domain protein)
C18E9.1	0.63	0.18	0.40	0.15	CAL-2 (CALmodulin related genes)
T04F8.6	0.12	0.60	0.36	0.55	Similar to F59A2.6
C02F4.2	0.32	0.34	0.33	0.91	Calcineurin A/TAX-6
F40F9.8	0.23	0.39	0.31	-0.09	CAL-7 encodes an ortholog of human calmodulin-like 4
C50C3.5	0.41	0.12	0.26	0.09	Similar to calmodulin 1
K07G5.4	0.52	-0.03	0.25	-0.10	K07G5.4
ZK856.8	0.48	-0.07	0.20	0.50	Calcium-binding protein p22 homolog
C27B7.6	0.23	0.14	0.19	0.11	Putative serine/threonine-protein phosphatase
T21H3.3	0.15	0.21	0.18	0.21	Calmodulin
F17E5.2	0.26	0.10	0.18	0.08	Probable calcium-binding mitochondrial carrier F17E5.2; SCaMC-2
M02A10.3	0.25	0.11	0.18	-0.44	SLI-1 (Suppressor of LIneage defect); Cbl family of ubiquitin ligases
K11C4.5	0.30	0.00	0.15	-0.01	Uncoordinated UNC-68; Ryanodine receptor homolog

Table 3.2 (Continued)

Gene names	GFP - no $CaCl_2$			Total averaged z-score including anthranilate	Gene description
	Averaged AUC z-score	Averaged slope z-score	Total averaged z-score		
T05F1.1	0.41	-0.18	0.12	-0.20	NRA-2 (Nicotinic Receptor Associated) nicalin homolog
T09A5.1	0.33	-0.11	0.11	0.15	Calexcitin
K08F11.5	-0.22	0.38	0.08	-0.15	Mitochondrial Rho GTPase Miro-1
C56A3.6	0.47	-0.35	0.06	-0.35	Mitochondrial calcium uptake protein-3 (MICU-3)
C54E10.2	0.24	-0.14	0.05	0.15	NCS-5 (Neuronal Calcium Sensor family)
Y67H2A.4	0.10	-0.01	0.05	-0.34	MICU-1 (MItochondrial Calcium Uptake protein)
ZK1151.1	0.24	-0.17	0.04	0.30	Variable abnormal morphology
ZK1307.8	0.01	0.03	0.02	-0.24	Glucosidase 2 subunit beta
C36C9.6	-0.04	0.08	0.02	-0.06	C36C9.6
R09H10.6	-0.17	0.21	0.02	0.15	R09H10.6 Similar to F23F1.2
B0252.3	0.16	-0.14	0.01	0.05	Putative transporter B0252.3
F59D6.7	0.11	-0.15	-0.02	0.06	Calcineurin B homolog
F58G1.3	0.18	-0.23	-0.02	-0.17	Serine/threonine protein phosphatase
Y37A1B.1	-0.07	0.02	-0.03	-0.16	LST-3 (Lateral Signaling Target); ortholog of human CCAR2
T04D3.2	0.00	-0.08	-0.04	0.62	SDZ-30 (SKN-1 Dependent Zygotic transcript)
T04F3.4	-0.04	-0.06	-0.05	0.07	Multiple coagulation factor deficiency protein 2 homolog
ZK1248.3	-0.02	-0.09	-0.06	0.16	Eps15 (endocytosis protein) Homologous Sequence
H10E21.4	-0.04	-0.10	-0.07	0.45	Calmodulin-like protein 6
Y71H2AL.1	-0.14	0.00	-0.07	-0.53	PBO-1 (PBOc defective (defecation)) calcineurin B homolog
F31B12.1	-0.20	0.05	-0.07	0.57	PhosphoLipase C
Y39B6A.38	-0.21	0.04	-0.08	0.00	REPS (RalBP1-associated Eps domain-containing protein) homolog
K01A2.11	0.00	-0.20	-0.10	0.46	Calcium Binding protein homolog
M18.5	-0.13	-0.08	-0.11	-0.12	DDB1 (UV-Damaged DNA Binding protein) homolog
W08D2.7	-0.17	-0.04	-0.11	-0.01	yeast MTR (mRNA transport) homolog
F23B12.7	-0.18	-0.07	-0.12	0.33	Homolog of human CAATT-binding protein
C07A9.5	0.10	-0.36	-0.13	0.40	Similar to alpha-actinin-2
F56D1.6	0.13	-0.40	-0.13	-0.40	Calexcitin
F29F11.6	-0.21	-0.09	-0.15	-0.04	GSP-1 (GLC7 (yeast Glc Seven) like Phosphatase)
T02G5.2	0.02	-0.32	-0.15	0.01	EF-hand calcium-binding domain-containing protein 7
F55C10.1	-0.14	-0.20	-0.17	0.31	Calcineurin B
Y32G9A.6	-0.19	-0.17	-0.18	0.05	NPHP-2 (NePHronoPhthisis (human kidney disease) homolog)
C56C10.9	-0.05	-0.31	-0.18	0.09	Similar to human 45 kDa calcium-binding protein
F53F8.1	0.20	-0.57	-0.19	-0.09	Kruppel-Like Factor (zinc finger protein)
K04C1.4	-0.13	-0.30	-0.21	-0.20	MLC-6 (Myosin Light Chain)
DH11.1	0.02	-0.49	-0.23	-0.19	Putative glutaminase
Y75B8A.30	-0.19	-0.30	-0.25	-0.27	Protein phosphatase
T22D1.5	-0.33	-0.17	-0.25	-0.21	Probable serine/threonine protein phosphatase 2A regulatory subunit
F08B6.3	-0.46	-0.05	-0.25	0.15	CALU-2 (CALUmenin (calcium-binding protein) homolog)
C25A1.9	-0.10	-0.41	-0.25	-0.91	RSA-1 (Regulator of Spindle Assembly); protein phosphatase 2A (PP2A) regulatory subunit
W02B9.1	-0.17	-0.38	-0.27	0.34	Hammerhead embryonic lethal; cadherin homolog
Y47G6A.27	-0.59	0.01	-0.29	-1.13	Mitochondrial Rho GTPase Miro-3
W04D2.1	-0.39	-0.21	-0.30	-0.52	Actinin
T25B9.2	-0.25	-0.36	-0.31	-0.04	Serine/threonine protein phosphatase
F23F1.2	0.00	-0.61	-0.31	-0.27	Similar to R09H10.6

Table 3.2 (Continued)

Gene names	GFP - no $CaCl_2$			Total averaged z-score including anthranilate	Gene description
	Averaged AUC z-score	Averaged slope z-score	Total averaged z-score		
B0511.1	-0.08	-0.58	-0.33	0.06	FK506-Binding protein family
C06A1.5	-0.42	-0.29	-0.36	0.12	RNA Polymerase II (B) subunit
K08E3.3	-0.35	-0.37	-0.36	-0.03	TOCA (Transducer Of Cdc42-dependent Actin assembly) homolog
C24H11.1	-0.32	-0.44	-0.38	-0.02	Serine/threonine protein phosphatase
R05G6.8	-0.66	-0.14	-0.40	0.06	Phospholipase C
B0563.7	-0.13	-0.67	-0.40	-0.20	Similar to calmodulin
T02C5.5	-0.62	-0.19	-0.41	-0.09	Uncoordinated; UNC-2 encodes a calcium channel alpha subunit
F09F7.2	-0.28	-0.55	-0.42	0.05	MLC-3 Myosin Light Chain
Y26E6A.2	-0.51	-0.35	-0.43	-0.70	F-box protein
C36E6.5	-0.87	-0.04	-0.45	0.22	MLC-2 Myosin Light Chain
ZK328.1	-0.34	-0.59	-0.46	-0.18	CYK-3 (CYtoKinesis defect); Ubiquitin C-terminal hydrolase
C36E6.3	-0.69	-0.35	-0.52	-0.70	MLC-1 Myosin Light Chain
F12A10.5	-0.25	-0.79	-0.52	-0.24	CAL-8 (CALmodulin related genes)
K03A1.2	-0.71	-0.36	-0.53	-0.31	lron-7 (eLRR (extracellular Leucine-Rich Repeat) ONly)
Y45F10A.6	-0.54	-0.55	-0.55	-0.33	TBC (Tre-2/Bub2/Cdc16) domain family
ZK899.5	-0.74	-0.39	-0.57	-0.07	ZK899.5
K08E3.10	-0.59	-0.58	-0.58	-0.59	MLC-7 (Myosin Light Chain)
C06A1.3	-0.52	-0.73	-0.63	-0.40	Putative serine/threonine-protein phosphatase
F30A10.1	-0.37	-0.88	-0.63	-0.03	CALM-1 (CALMyrin (Calcium and Integrin Binding protein) homolog)
C47D12.1	-0.53	-0.74	-0.63	-0.40	TRRAP-like (transcription/transformation domain-associated protein)
F23H11.8	-0.42	-0.87	-0.65	-0.52	Phosphatase with EF hands
F38H4.9	-0.71	-0.62	-0.66	-0.07	LET-92 homolog of protein phosphatase PP2AC
M03C11.8	-0.59	-0.74	-0.67	-0.22	Putative SMARCAL1-like protein; Protein archease-like
C23G10.1	-0.53	-0.82	-0.68	-0.66	Putative serine/threonine-protein phosphatase C23G10.1
T10H9.8	-0.92	-0.49	-0.70	-0.71	Similar to CAL-4
F10G8.5	-0.48	-0.95	-0.71	-0.45	NCS-2 (Neuronal Calcium Sensor family)
Y49E10.3	-0.49	-0.96	-0.72	-0.58	Protein Phosphatase
C48B4.2	-0.47	-0.99	-0.73	-0.18	Rhomboid (Drosophila) related
C24H11.2	-0.75	-0.73	-0.74	0.53	Serine/threonine protein phosphatase
ZK938.1	-0.65	-0.85	-0.75	-0.60	Serine/threonine protein phosphatase
F54C1.7	-0.62	-0.89	-0.75	-0.39	PAT-10 (Paralysed Arrest at Two-fold) Body wall muscle troponin C
C50C3.2	-0.45	-1.10	-0.78	-0.45	Spectrin alpha chain
ZC116.3	-0.82	-0.74	-0.78	0.02	Probable cubilin
C44B12.2	-0.72	-0.85	-0.78	-0.53	Osteonectin (SPARC) related
F25B3.3	-1.03	-0.57	-0.80	-0.39	Rap Guanine nucleotide Exchange Factor homolog
ZK686.2	-0.79	-0.81	-0.80	-0.35	Putative ATP-dependent RNA helicase ZK686.2
F21A3.5	-0.85	-0.76	-0.81	-0.05	PRDE-1 (PiRNA-DEpendent silencing defective) casein kinase-1 homolog
R08A2.2	-0.82	-0.96	-0.89	-0.14	Serine/threonine protein phosphatase
R08C7.8	-0.82	-0.97	-0.89	0.06	Serine/threonine-protein phosphatase
C56G7.1	-1.09	-0.71	-0.90	-0.21	MLC-4 Myosin Light Chain
F55A3.7	-1.06	-0.76	-0.91	-0.17	FACT complex subunit SPT16 homolog
T16G12.7	-0.86	-1.00	-0.93	-0.44	Serine/threonine protein phosphatase
T03F1.11	-0.75	-1.11	-0.93	-0.22	Similar to CALM-1
K10F12.3	-0.70	-1.19	-0.95	-0.31	Phospholipase C Like

Table 3.2 (Continued)

Gene names	GFP - no $CaCl_2$			Total averaged z-score including anthranilate	Gene description
	Averaged AUC z-score	Averaged slope z-score	Total averaged z-score		
R08D7.5	-0.92	-0.99	-0.95	-0.35	Human Centrin-2 homolog
W06H8.1	-1.02	-0.89	-0.96	-0.89	RME-1 (Receptor Mediated Endocytosis); EH domain containing protein
C11G6.4	-1.18	-0.83	-1.00	-0.45	NHR-28 (Nuclear Hormone Receptor family)
F52H3.6	-0.82	-1.20	-1.01	-0.66	Serine/threonine protein phosphatase
Y73C8B.5	-1.17	-0.85	-1.01	-0.57	Similar to calmodulin-3
C48A7.1	-1.22	-0.94	-1.08	-0.40	Egg Laying defective
T09E8.2	-1.08	-1.09	-1.08	-0.51	High Incidence of Males (increased X chromosome loss) HIM-17
F22D6.9	-0.88	-1.29	-1.09	-0.78	Serine/threonine protein phosphatase
F56C9.1	-1.05	-1.14	-1.09	-0.30	GSP-2 (GLC7 (yeast Glc Seven) like Phosphatase)
F19B10.1	-0.93	-1.28	-1.11	-0.97	MEL-26 binding protein
Y9D1A.2	-1.12	-1.13	-1.12	0.14	Putative RNA helicase
R13A5.11	-1.07	-1.18	-1.13	-0.51	Serine/threonine protein phosphatase
C29E4.14	-1.45	-0.80	-1.13	-0.85	Multiple coagulation factor deficiency protein 2 homolog
R10E11.6	-1.00	-1.25	-1.13	-0.28	Similar to Synergin-gamma
F44A6.1	-1.36	-0.93	-1.15	-0.95	Nucleobindin homolog
ZK354.9	-1.07	-1.23	-1.15	-0.70	Serine/threonine protein phosphatase
Y48B6A.6	-0.94	-1.37	-1.15	-0.51	EFHD-1 (EF Hand calcium binding protein)
F54G8.2	-1.12	-1.24	-1.18	-0.37	Diacylglycerol Kinase
C36F7.2	-1.09	-1.29	-1.19	-0.33	SWAH-1 (SoWAH (Drosophila) homolog)
T25G3.4	-1.12	-1.42	-1.27	-0.74	Probable glycerol-3-phosphate dehydrogenase, mitochondrial
F21A10.1	-1.08	-1.47	-1.27	-0.80	NCS-4 (Neuronal Calcium Sensor family)
F25H2.8	-1.01	-1.55	-1.28	-0.43	UBC-25 (UBiquitin Conjugating enzyme)
C24H10.5	-1.53	-1.07	-1.30	-0.55	CAL-5 (CALmodulin related genes)
Y105E8A.7	-1.33	-1.36	-1.35	0.01	EAT-18 (EATing: abnormal pharyngeal pumping)
Y51H4A.17	-1.69	-1.01	-1.35	-1.00	STAT transcription factor family
W09G10.3	-0.87	-1.88	-1.38	-0.50	NCS-6 (Neuronal Calcium Sensor family)
B0511.1	-1.11	-1.71	-1.41	-0.81	FK506-Binding protein family
C34C12.3	-1.24	-1.64	-1.44	-0.37	Protein Phosphatase
M02B7.6	-1.68	-1.23	-1.45	-0.55	CAL-3 (CALmodulin related genes)
T27C10.4	-1.89	-1.14	-1.51	-1.09	BTB and MATH domain containing
B0336.11	-1.44	-2.02	-1.73	-0.37	HPO-28 (Hypersensitive to POre- forming toxin)
M04F3.4	-2.24	-2.14	-2.19	-1.31	Probable cysteine protease

Table 3.3. Anthranilate measurements to find EF-hand effectors of high Ca^{2+} toxicity in *C. elegans*. The conditions were the same as in S1 Table except anthranilate fluorescence was monitored instead of GFP. The more negative the z-score the less anthranilate is present indicating a higher viability.

Gene Name	Anthranilate- $CaCl_2$ added			Gene Description
	Averaged AUC z-score	Averaged Slope z-score	Total Averaged z-score	
Y105E8A.7	-1.23	-1.17	-1.20	EAT-18 (EATing: abnormal pharyngeal pumping)

Table 3.3 (Continued)

Gene Name	Anthranilate- $CaCl_2$ added			Gene Description
	Averaged AUC z-score	Averaged Slope z-score	Total Averaged z-score	
C36E6.5	-1.16	-1.12	-1.14	MLC-2 Myosin Light Chain
W06H8.1	-1.17	-1.01	-1.09	RME-1 (Receptor Mediated Endocytosis); EH domain containing protein
C02F4.2	-1.13	-1.02	-1.08	Calcineurin A/TAX-6
C47C12.4	-1.07	-1.08	-1.07	Mitochondrial Rho GTPase Miro-2
K08F11.5	-1.11	-0.98	-1.04	Mitochondrial Rho GTPase Miro-1
ZK1151.1	-1.07	-0.98	-1.03	Variable abnormal morphology
R05G6.8	-1.06	-0.99	-1.02	Phospholipase C
C06A1.5	-1.04	-1.00	-1.02	RNA Polymerase II (B) subunit
F56C11.1	-1.05	-0.98	-1.01	Blistered cuticle; BLI-3 (DUal OXidase)
T09A5.1	-1.15	-0.88	-1.01	Calexcitin
K03A1.4	-1.08	-0.92	-1.00	Similar to Calmodulin-1
W02B9.1	-1.08	-0.90	-0.99	Hammerhead embryonic lethal; cadherin homolog
Y9D1A.2	-1.03	-0.87	-0.95	Putative RNA helicase
F43C9.2	-0.96	-0.93	-0.94	Homologous to Isoform 1 of Calcium-binding protein 4
C54E4.2	-0.96	-0.89	-0.93	Similar to Testican-3
ZK899.5	-0.86	-0.97	-0.92	ZK899.5
C48B4.2	-0.93	-0.87	-0.90	Rhomboid (Drosophila) related
F59D6.7	-0.96	-0.83	-0.89	Calcineurin B homolog
B0511.1	-1.00	-0.77	-0.88	FK506-Binding protein family
H10E21.4	-0.95	-0.82	-0.88	Calmodulin-like protein 6
F22D6.9	-0.92	-0.84	-0.88	Serine/threonine protein phosphatase
F56D1.6	-0.96	-0.80	-0.88	Calexcitin
F56C9.1	-0.89	-0.83	-0.86	GSP-2 (GLC7 (yeast Glc Seven) like Phosphatase)
F30A10.1	-0.91	-0.80	-0.86	CALM-1 (CALMyrin (Calcium and Integrin Binding protein) homolog)
ZK673.7	-0.89	-0.82	-0.85	Troponin C
W09C3.6	-0.87	-0.83	-0.85	GSP-3 (GLC7 (yeast Glc Seven) like Phosphatase)
C16H3.1	-0.84	-0.85	-0.84	NCS-7 (Neuronal Calcium Sensor family)
R10E11.6	-0.86	-0.82	-0.84	Similar to Synergin-gamma
F11C7.4	-0.75	-0.93	-0.84	Drosophila Crumbs homolog
F55A11.1	-0.86	-0.80	-0.83	Similar to Multiple coagulation factor deficiency protein 2
Y73B3A.12	-0.80	-0.85	-0.83	CAL-6 encodes an ortholog of human calmodulin-like 3
F09F7.2	-0.89	-0.76	-0.82	MLC-3 Myosin Light Chain
F54C1.7	-0.87	-0.77	-0.82	PAT-10 (Paralysed Arrest at Two-fold) Body wall muscle troponin C
F10G8.5	-0.90	-0.73	-0.82	NCS-2 (Neuronal Calcium Sensor family)
C36E6.3	-0.87	-0.76	-0.82	MLC-1 Myosin Light Chain
C36F7.2	-0.88	-0.74	-0.81	SWAH-1 (SoWAH (Drosophila) homolog)
T16G12.7	-0.86	-0.76	-0.81	Serine/threonine protein phosphatase
F38H4.9	-0.82	-0.80	-0.81	LET-92 homolog of protein phosphatase PP2AC
F12A10.5	-0.87	-0.74	-0.80	CAL-8 (CALmodulin related genes)
T04D3.2	-0.89	-0.71	-0.80	SDZ-30 (SKN-1 Dependent Zygotic transcript)
C50C3.5	-0.82	-0.78	-0.80	Similar to calmodulin 1
F55A3.7	-0.89	-0.70	-0.80	FACT complex subunit SPT16 homolog
C27B7.6	-0.84	-0.74	-0.79	Putative serine/threonine-protein phosphatase
ZK328.1	-0.83	-0.75	-0.79	CYK-3 (CYtoKinesis defect); Ubiquitin C-terminal hydrolase
F33C8.4	-0.84	-0.73	-0.78	Similar to Y41D4A.7
T03F1.5	-0.79	-0.77	-0.78	GSP-4 (GLC7 (yeast Glc Seven) like Phosphatase)
DH11.1	-0.77	-0.77	-0.77	Putative glutaminase

Table 3.3 (Continued)

Gene Name	Anthranilate- $CaCl_2$ added			Gene Description
	Averaged AUC z-score	Averaged Slope z-score	Total Averaged z-score	
K10F12.3	-0.83	-0.71	-0.77	Phospholipase C Like
Y48B6A.6	-0.80	-0.74	-0.77	EFHD-1 (EF Hand calcium binding protein)
K07C5.1	-0.83	-0.70	-0.77	ARX-2; ARp2/3 complex component
C56A3.6	-0.71	-0.81	-0.76	Mitochondrial calcium uptake protein-3 (MICU-3)
M03C11.8	-0.81	-0.70	-0.76	Putative SMARCAL1-like protein; Protein archease-like
K01A2.11	-0.79	-0.72	-0.75	Calcium Binding protein homolog
C34C12.3	-0.83	-0.68	-0.75	Protein Phosphatase
F19B10.1	-0.81	-0.70	-0.75	MEL-26 binding protein
B0252.3	-0.78	-0.71	-0.75	Putative transporter B0252.3
W09G10.3	-0.74	-0.75	-0.75	NCS-6 (Neuronal Calcium Sensor family)
F26B1.5	-0.75	-0.74	-0.75	Serine/threonine protein phosphatase
Y32G9A.6	-0.75	-0.74	-0.74	NPHP-2 (NePHronoPhthisis (human kidney disease) homolog)
F23F1.2	-0.77	-0.71	-0.74	Similar to R09H10.6
ZK856.8	-0.78	-0.70	-0.74	Calcium-binding protein p22 homolog
T12D8.6	-0.80	-0.67	-0.73	MLC-5 (Myosin Light Chain)
F25H2.8	-0.78	-0.68	-0.73	UBC-25 (UBiquitin Conjugating enzyme)
F21A3.5	-0.77	-0.69	-0.73	PRDE-1 (PiRNA-DEpendent silencing defective) casein kinase-1 homolog
T02G5.2	-0.76	-0.69	-0.72	EF-hand calcium-binding domain-containing protein 7
W08D2.7	-0.62	-0.82	-0.72	yeast MTR (mRNA transport) homolog
ZC477.2	-0.72	-0.72	-0.72	Serine/threonine-protein phosphatase
R08D7.5	-0.79	-0.64	-0.72	Human Centrin-2 homolog
M04F3.4	-0.73	-0.69	-0.71	Probable cysteine protease
Y43F4B.1	-0.76	-0.64	-0.70	Set-25 (SET (trithorax/polycomb) domain containing)
F53G12.3	-0.72	-0.67	-0.70	DUOX-2 (DUal OXidase)
ZK1307.8	-0.68	-0.72	-0.70	Glucosidase 2 subunit beta
C24H11.1	-0.74	-0.65	-0.70	Serine/threonine protein phosphatase
T10H9.8	-0.69	-0.70	-0.69	Similar to CAL-4
T03F1.11	-0.64	-0.74	-0.69	Similar to CALM-1
F25B3.3	-0.69	-0.69	-0.69	Rap Guanine nucleotide Exchange Factor homolog
F17E5.2	-0.77	-0.60	-0.69	Probable calcium-binding mitochondrial carrier F17E5.2; SCaMC-2
Y39B6A.38	-0.69	-0.66	-0.68	REPS (RalBP1-associated Eps domain-containing protein) homolog
B0336.11	-0.72	-0.63	-0.68	HPO-28 (Hypersensitive to POre- forming toxin)
K07G5.4	-0.76	-0.58	-0.67	K07G5.4
C50C3.2	-0.75	-0.59	-0.67	Spectrin alpha chain
C18E9.1	-0.71	-0.61	-0.66	CAL-2 (CALmodulin related genes)
T08D2.1	-0.70	-0.62	-0.66	Transmembrane emp24 domain-containing protein
R08A2.2	-0.66	-0.65	-0.66	Serine/threonine protein phosphatase
T04F3.2	-0.64	-0.67	-0.66	similar to SPARC-related modular calcium-binding protein 2
T21H3.3	-0.70	-0.61	-0.66	Calmodulin
B0563.7	-0.64	-0.67	-0.65	Similar to calmodulin
C29E4.14	-0.74	-0.56	-0.65	Multiple coagulation factor deficiency protein 2 homolog
B0511.1	-0.68	-0.62	-0.65	FK506-Binding protein family
F53F8.1	-0.72	-0.58	-0.65	Kruppel-Like Factor (zinc finger protein)
Y49E10.3	-0.70	-0.60	-0.65	Protein Phosphatase
F55A11.4	-0.66	-0.62	-0.64	Calcium-binding mitochondrial carrier protein SCaMC-2 homolog; non-coding
T25G3.4	-0.68	-0.61	-0.64	Probable glycerol-3-phosphate dehydrogenase, mitochondrial
Y73C8B.5	-0.65	-0.62	-0.64	Similar to calmodulin-3

Table 3.3 (Continued)

Gene Name	Anthranilate- $CaCl_2$ added			Gene Description
	Averaged AUC z-score	Averaged Slope z-score	Total Averaged z-score	
C13C12.1	-0.63	-0.64	-0.63	CAL-1 (CALmodulin related genes)
C07A9.5	-0.81	-0.45	-0.63	Similar to alpha-actinin-2
F54G8.2	-0.68	-0.57	-0.63	Diacylglycerol Kinase
C33D12.6	-0.69	-0.57	-0.63	RSEF-1 encodes an ortholog of human RAB44
C03A7.13	-0.69	-0.56	-0.63	UDP-glucuronosyl/UDP-glucosyltransferase domain containing protein
C56C10.9	-0.66	-0.59	-0.62	Similar to human 45 kDa calcium-binding protein
C47A4.3	-0.68	-0.57	-0.62	Serine/threonine protein phosphatase
ZK686.2	-0.59	-0.64	-0.61	Putative ATP-dependent RNA helicase ZK686.2
ZC116.3	-0.65	-0.56	-0.61	Probable cubilin
Y69E1A.4	-0.57	-0.62	-0.60	Serine/threonine protein phosphatase
K11C4.5	-0.65	-0.54	-0.59	Uncoordinated UNC-68; Ryanodine receptor homolog
F55C10.1	-0.57	-0.61	-0.59	Calcineurin B
K10B3.10	-0.64	-0.53	-0.58	Spectrin
R09H10.6	-0.59	-0.58	-0.58	R09H10.6 Similar to F23F1.2
F23H11.8	-0.62	-0.54	-0.58	Phosphatase with EF hands
F58G1.3	-0.64	-0.51	-0.58	Serine/threonine protein phosphatase
F52H3.6	-0.57	-0.58	-0.57	Serine/threonine protein phosphatase
T06E6.1	-0.53	-0.62	-0.57	Similar to human WDR-74
F29F11.6	-0.67	-0.47	-0.57	GSP-1 (GLC7 (yeast Glc Seven) like Phosphatase)
F42G8.8	-0.58	-0.56	-0.57	Serine/threonine protein phosphatase
K04C1.4	-0.67	-0.47	-0.57	MLC-6 (Myosin Light Chain)
R08C7.8	-0.62	-0.48	-0.55	Serine/threonine-protein phosphatase
T10G3.5	-0.54	-0.56	-0.55	EEA1 (Early Endosome Antigen, Rab effector) homolog
C11G6.4	-0.61	-0.48	-0.55	NHR-28 (Nuclear Hormone Receptor family)
K08E3.10	-0.56	-0.53	-0.55	MLC-7 (Myosin Light Chain)
T09E8.2	-0.60	-0.49	-0.54	High Incidence of Males (increased X chromosome loss) HIM-17
K03A1.2	-0.53	-0.55	-0.54	lron-7 (eLRR (extracellular Leucine-Rich Repeat) ONly)
C24H11.2	-0.54	-0.54	-0.54	Serine/threonine protein phosphatase
C25A1.9	-0.55	-0.53	-0.54	RSA-1 (Regulator of Spindle Assembly); protein phosphatase 2A (PP2A) regulatory subunit
F44A6.1	-0.59	-0.49	-0.54	Nucleobindin homolog
C48A7.1	-0.58	-0.48	-0.53	Egg Laying defective
T05F1.1	-0.60	-0.45	-0.52	NRA-2 (Nicotinic Receptor Associated) nicalin homolog
C06A1.3	-0.60	-0.44	-0.52	Putative serine/threonine-protein phosphatase
F21A10.1	-0.62	-0.41	-0.51	NCS-4 (Neuronal Calcium Sensor family)
Y45F10A.6	-0.49	-0.52	-0.50	TBC (Tre-2/Bub2/Cdc16) domain family
K03E6.3	-0.55	-0.46	-0.50	NCS-3 (Neuronal Calcium Sensor family)
T02C5.5	-0.57	-0.44	-0.50	Uncoordinated; UNC-2 encodes a calcium channel alpha subunit
C04B4.2	-0.48	-0.52	-0.50	Similar to C04B4.4 and LIN-66
K04F1.10	-0.49	-0.50	-0.50	IRLD-40 (Insulin/EGF-Receptor L Domain protein)
F08B6.3	-0.51	-0.48	-0.49	CALU-2 (CALUmenin (calcium-binding protein) homolog)
M03F4.7	-0.51	-0.46	-0.48	Calumenin (calcium-binding protein) homolog
T22D1.5	-0.54	-0.43	-0.48	Probable serine/threonine protein phosphatase 2A regulatory subunit
C47D12.1	-0.54	-0.43	-0.48	TRRAP-like (transcription/transformation domain-associated protein)
T07G12.1	-0.44	-0.52	-0.48	CAL-4 (CALmodulin related genes)
Y51H4A.17	-0.50	-0.46	-0.48	STAT transcription factor family
R08F11.1	-0.56	-0.40	-0.48	Non-lysosomal glucosylceramidase
F40F9.8	-0.43	-0.52	-0.48	CAL-7 encodes an ortholog of human calmodulin-like 4

Table 3.3 (Continued)

Gene Name	Anthranilate- $CaCl_2$ added			Gene Description
	Averaged AUC z-score	Averaged Slope z-score	Total Averaged z-score	
T27C10.4	-0.50	-0.45	-0.48	BTB and MATH domain containing
T09B4.4	-0.47	-0.47	-0.47	Similar to Calmodulin-like protein 4
E02A10.3	-0.47	-0.47	-0.47	Similar to calmodulin
Y116A8C.36	-0.43	-0.50	-0.46	ITSN (intersectin) family
R13A5.11	-0.42	-0.50	-0.46	Serine/threonine protein phosphatase
K02F3.2	-0.45	-0.46	-0.46	Probable calcium-binding mitochondrial carrier K02F3.2; Similar to Aralar1
F13G11.2	-0.55	-0.36	-0.45	IRLD-4 (Insulin/EGF-Receptor L Domain protein)
ZK938.1	-0.48	-0.37	-0.42	Serine/threonine protein phosphatase
W04D2.1	-0.46	-0.38	-0.42	Actinin
F16F9.3	-0.39	-0.44	-0.41	F16F9.3
F25H2.2	-0.42	-0.37	-0.39	SNX-27 (Sorting NeXin)
C23G10.1	-0.40	-0.38	-0.39	Putative serine/threonine-protein phosphatase C23G10.1
C34D4.2	-0.29	-0.49	-0.39	Serine/threonine protein phosphatase
C44B12.2	-0.36	-0.41	-0.39	Osteonectin (SPARC) related
T25B9.2	-0.38	-0.40	-0.39	Serine/threonine protein phosphatase
4R79.2	-0.48	-0.28	-0.38	Similar to RSEF-1
C54E10.2	-0.41	-0.35	-0.38	NCS-5 (Neuronal Calcium Sensor family)
F58G11.1	-0.38	-0.37	-0.37	LETM1 (Leucine zipper, EF-hand, Transmembrane mitochondrial protein) homolog
F25B3.4	-0.28	-0.44	-0.36	Serine/threonine protein phosphatase
T09F5.10	-0.41	-0.25	-0.33	Similar to F36D3.16
F23B12.1	-0.20	-0.44	-0.32	Serine/threonine protein phosphatase
F53F4.14	-0.33	-0.31	-0.32	Similar to F36H12.3 (major sperm protein)
K08E3.3	-0.52	-0.11	-0.31	TOCA (Transducer Of Cdc42-dependent Actin assembly) homolog
F23B12.7	-0.10	-0.53	-0.31	Homolog of human CAATT-binding protein
C06G1.5	-0.36	-0.24	-0.30	Serine/threonine-protein phosphatase 2A regulatory subunit
C24H10.5	-0.28	-0.32	-0.30	CAL-5 (CALmodulin related genes)
C44C1.3	-0.33	-0.26	-0.30	NCS-1 (Neuronal Calcium Sensor family)
T04F8.6	-0.29	-0.29	-0.29	Similar to F59A2.6
C09H5.7	-0.25	-0.33	-0.29	Serine/threonine protein phosphatase
Y75B12B.6	-0.38	-0.20	-0.29	Phospholipase C
B0513.5	-0.28	-0.29	-0.29	Proline dehydrogenase, mitochondrial
Y40H4A.2	-0.25	-0.31	-0.28	Serine/threonine-protein phosphatase
Y71H2AL.1	-0.38	-0.16	-0.27	PBO-1 (PBOc defective (defecation)) calcineurin B homolog
M02A10.3	-0.31	-0.22	-0.26	SLI-1 (Suppressor of LIneage defect); Cbl family of ubiquitin ligases
C56G7.1	-0.33	-0.19	-0.26	MLC-4 Myosin Light Chain
Y75B8A.30	-0.22	-0.28	-0.25	Protein phosphatase
Y47G6A.27	-0.36	-0.14	-0.25	Mitochondrial Rho GTPase Miro-3
M02B7.6	-0.21	-0.28	-0.25	CAL-3 (CALmodulin related genes)
F58E6.1	-0.29	-0.15	-0.22	Signal transducer and activator of transcription b
ZK354.9	-0.20	-0.21	-0.21	Serine/threonine protein phosphatase
Y26E6A.2	-0.27	-0.13	-0.20	F-box protein
F31B12.1	-0.19	-0.17	-0.18	PhosphoLipase C
ZK1248.3	-0.14	-0.01	-0.08	Eps15 (endocytosis protein) Homologous Sequence
Y37A1B.1	-0.10	-0.05	-0.08	LST-3 (Lateral Signaling Target); ortholog of human CCAR2
C36C9.6	-0.08	-0.07	-0.07	C36C9.6
M18.5	-0.15	0.10	-0.03	DDB1 (UV-Damaged DNA Binding protein) homolog
T04F3.4	-0.10	0.05	-0.02	Multiple coagulation factor deficiency protein 2 homolog

Table 3.3 (Continued)

Gene Name	Anthranilate- $CaCl_2$ added			Gene Description
	Averaged AUC z-score	Averaged Slope z-score	Total Averaged z-score	
Y67H2A.4	0.09	0.09	0.09	MICU-1 (MItochondrial Calcium Uptake protein)
B0348.4	0.28	0.08	0.18	Egg Laying defective; EGL-8 encodes a phospholipase C beta

Table 3.4. The effect of EF-hand gene knockdowns in the absence of $CaCl_2$ on anthranilate measurement z-scores. The conditions were the same as in S3 Table except deionized water was added to the wells instead of $CaCl_2$.

Gene name	Anthranilate- no $CaCl_2$			Gene description
	Averaged AUC z-score	Averaged slope z-score	Total averaged z-score	
C24H11.2	-1.88	-1.73	-1.81	Serine/threonine protein phosphatase
C02F4.2	-1.80	-1.19	-1.50	Calcineurin A/TAX-6
Y9D1A.2	-1.51	-1.30	-1.40	Putative RNA helicase
C47C12.4	-1.29	-1.45	-1.37	Mitochondrial Rho GTPase Miro-2
Y105E8A.7	-1.09	-1.63	-1.36	EAT-18 (EATing: abnormal pharyngeal pumping)
T04D3.2	-1.28	-1.27	-1.27	SDZ-30 (SKN-1 Dependent Zygotic transcript)
F31B12.1	-1.24	-1.20	-1.22	PhosphoLipase C
B0513.5	-1.26	-1.08	-1.17	Proline dehydrogenase, mitochondrial
K07C5.1	-0.94	-1.24	-1.09	ARX-2; ARp2/3 complex component
K01A2.11	-0.98	-1.07	-1.03	Calcium Binding protein homolog
R08C7.8	-0.73	-1.29	-1.01	Serine/threonine-protein phosphatase
B0336.11	-1.07	-0.89	-0.98	HPO-28 (Hypersensitive to POre- forming toxin)
H10E21.4	-1.06	-0.89	-0.97	Calmodulin-like protein 6
W02B9.1	-0.80	-1.12	-0.96	Hammerhead embryonic lethal; cadherin homolog
C07A9.5	-0.73	-1.11	-0.92	Similar to alpha-actinin-2
C36E6.5	-1.09	-0.71	-0.90	MLC-2 Myosin Light Chain
ZC116.3	-0.99	-0.65	-0.82	Probable cubilin
ZK856.8	-0.78	-0.83	-0.80	Calcium-binding protein p22 homolog
F26B1.5	-0.89	-0.71	-0.80	Serine/threonine protein phosphatase
F55C10.1	-0.83	-0.74	-0.79	Calcineurin B
C13C12.1	-0.55	-1.00	-0.77	CAL-1 (CALmodulin related genes)
F23B12.7	-0.85	-0.70	-0.77	Homolog of human CAATT-binding protein
F42G8.8	-0.66	-0.84	-0.75	Serine/threonine protein phosphatase
T04F8.6	-0.80	-0.69	-0.74	Similar to F59A2.6
Y116A8C.36	-0.70	-0.74	-0.72	ITSN (intersectin) family
F21A3.5	-0.63	-0.80	-0.71	PRDE-1 (PiRNA-DEpendent silencing defective) casein kinase-1 homolog
F11C7.4	-0.80	-0.60	-0.70	Drosophila Crumbs homolog
C34C12.3	-0.58	-0.81	-0.70	Protein Phosphatase
R08A2.2	-0.59	-0.63	-0.61	Serine/threonine protein phosphatase
C03A7.13	-0.80	-0.39	-0.60	UDP-glucuronosyl/UDP-glucosyltransferase domain containing protein
C06A1.5	-0.58	-0.60	-0.59	RNA Polymerase II (B) subunit
Y69E1A.4	-0.51	-0.67	-0.59	Serine/threonine protein phosphatase
ZK1151.1	-0.40	-0.75	-0.57	Variable abnormal morphology
R10E11.6	-0.46	-0.69	-0.57	Similar to Synergin-gamma

Table 3.4 (Continued)

Gene name	Anthranilate- no $CaCl_2$			Gene description
	Averaged AUC z-score	Averaged slope z-score	Total averaged z-score	
F55A3.7	-0.52	-0.62	-0.57	FACT complex subunit SPT16 homolog
F30A10.1	-0.36	-0.77	-0.56	CALM-1 (CALMyrin (Calcium and Integrin Binding protein) homolog)
F08B6.3	-0.33	-0.77	-0.55	CALU-2 (CALUmenin (calcium-binding protein) homolog)
C36F7.2	-0.66	-0.42	-0.54	SWAH-1 (SoWAH (Drosophila) homolog)
K04F1.10	-0.64	-0.43	-0.53	IRLD-40 (Insulin/EGF-Receptor L Domain protein)
F38H4.9	-0.41	-0.63	-0.52	LET-92 homolog of protein phosphatase PP2AC
R05G6.8	-0.27	-0.78	-0.52	Phospholipase C
F09F7.2	-0.34	-0.70	-0.52	MLC-3 Myosin Light Chain
F56C9.1	-0.40	-0.59	-0.50	GSP-2 (GLC7 (yeast Glc Seven) like Phosphatase)
T03F1.11	-0.29	-0.68	-0.49	Similar to CALM-1
C56G7.1	-0.60	-0.36	-0.48	MLC-4 Myosin Light Chain
F55A11.4	-0.42	-0.51	-0.47	Calcium-binding mitochondrial carrier protein SCaMC-2 homolog; non-coding
B0511.1	-0.51	-0.38	-0.44	FK506-Binding protein family
F54G8.2	-0.27	-0.60	-0.44	Diacylglycerol Kinase
F25H2.8	-0.27	-0.58	-0.42	UBC-25 (UBiquitin Conjugating enzyme)
ZK899.5	-0.48	-0.36	-0.42	ZK899.5
ZK1248.3	-0.62	-0.16	-0.39	Eps15 (endocytosis protein) Homologous Sequence
W09G10.3	-0.24	-0.53	-0.39	NCS-6 (Neuronal Calcium Sensor family)
C48B4.2	-0.26	-0.47	-0.37	Rhomboid (Drosophila) related
C56C10.9	-0.44	-0.28	-0.36	Similar to human 45 kDa calcium-binding protein
E02A10.3	-0.09	-0.60	-0.35	Similar to calmodulin
C54E4.2	-0.20	-0.49	-0.35	Similar to Testican-3
M02B7.6	-0.37	-0.32	-0.35	CAL-3 (CALmodulin related genes)
C24H11.1	-0.36	-0.32	-0.34	Serine/threonine protein phosphatase
F58E6.1	-0.51	-0.14	-0.32	Signal transducer and activator of transcription b
K10F12.3	-0.33	-0.31	-0.32	Phospholipase C Like
K08E3.3	-0.35	-0.26	-0.30	TOCA (Transducer Of Cdc42-dependent Actin assembly) homolog
F13G11.2	-0.08	-0.53	-0.30	IRLD-4 (Insulin/EGF-Receptor L Domain protein)
C47A4.3	-0.26	-0.34	-0.30	Serine/threonine protein phosphatase
R09H10.6	-0.29	-0.27	-0.28	R09H10.6 Similar to F23F1.2
Y32G9A.6	-0.39	-0.17	-0.28	NPHP-2 (NePHronoPhthisis (human kidney disease) homolog)
C48A7.1	-0.47	-0.08	-0.27	Egg Laying defective
R08D7.5	-0.24	-0.29	-0.26	Human Centrin-2 homolog
T21H3.3	-0.57	0.08	-0.24	Calmodulin
C54E10.2	-0.12	-0.36	-0.24	NCS-5 (Neuronal Calcium Sensor family)
M03C11.8	-0.36	-0.11	-0.23	Putative SMARCAL1-like protein; Protein archease-like
T02C5.5	-0.67	0.21	-0.23	Uncoordinated; UNC-2 encodes a calcium channel alpha subunit
T25B9.2	-0.27	-0.17	-0.22	Serine/threonine protein phosphatase
T08D2.1	-0.67	0.28	-0.20	Transmembrane emp24 domain-containing protein
T09A5.1	-0.19	-0.19	-0.19	Calexcitin
C24H10.5	-0.15	-0.23	-0.19	CAL-5 (CALmodulin related genes)
T04F3.4	-0.30	-0.07	-0.19	Multiple coagulation factor deficiency protein 2 homolog
T02G5.2	-0.17	-0.18	-0.18	EF-hand calcium-binding domain-containing protein 7
4R79.2	-0.28	-0.07	-0.17	Similar to RSEF-1
Y75B12B.6	-0.51	0.19	-0.16	Phospholipase C
F59D6.7	0.00	-0.28	-0.14	Calcineurin B homolog
Y48B6A.6	0.02	-0.28	-0.13	EFHD-1 (EF Hand calcium binding protein)
C11G6.4	-0.08	-0.11	-0.10	NHR-28 (Nuclear Hormone Receptor family)

Table 3.4 (Continued)

Gene name	Anthranilate- no $CaCl_2$			Gene description
	Averaged AUC z-score	Averaged slope z-score	Total averaged z-score	
R13A5.11	-0.04	-0.17	-0.10	Serine/threonine protein phosphatase
ZK328.1	0.08	-0.29	-0.10	CYK-3 (CYtoKinesis defect); Ubiquitin C-terminal hydrolase
ZK686.2	0.07	-0.26	-0.09	Putative ATP-dependent RNA helicase ZK686.2
W08D2.7	0.07	-0.26	-0.09	yeast MTR (mRNA transport) homolog
ZC477.2	-0.13	-0.06	-0.09	Serine/threonine-protein phosphatase
B0252.3	-0.27	0.09	-0.09	Putative transporter B0252.3
Y39B6A.38	-0.09	-0.08	-0.09	REPS (RalBP1-associated Eps domain-containing protein) homolog
F29F11.6	-0.09	-0.07	-0.08	GSP-1 (GLC7 (yeast Glc Seven) like Phosphatase)
T09E8.2	0.08	-0.20	-0.06	High Incidence of Males (increased X chromosome loss) HIM-17
T16G12.7	1.00	-1.10	-0.05	Serine/threonine protein phosphatase
F12A10.5	0.02	-0.10	-0.04	CAL-8 (CALmodulin related genes)
C27B7.6	0.04	-0.10	-0.03	Putative serine/threonine-protein phosphatase
F25B3.3	-0.11	0.09	-0.01	Rap Guanine nucleotide Exchange Factor homolog
B0563.7	0.00	-0.02	-0.01	Similar to calmodulin
F53F8.1	-0.11	0.11	0.00	Kruppel-Like Factor (zinc finger protein)
C09H5.7	-0.10	0.11	0.01	Serine/threonine protein phosphatase
F17E5.2	0.26	-0.22	0.02	Probable calcium-binding mitochondrial carrier F17E5.2; SCaMC-2
F54C1.7	0.23	-0.18	0.03	PAT-10 (Paralysed Arrest at Two-fold) Body wall muscle troponin C
B0348.4	0.08	-0.01	0.03	Egg Laying defective; EGL-8 encodes a phospholipase C beta
T03F1.5	0.22	-0.15	0.04	GSP-4 (GLC7 (yeast Glc Seven) like Phosphatase)
F58G11.1	0.07	0.02	0.04	LETM1 (Leucine zipper, EF-hand, Transmembrane mitochondrial protein) homolog
C33D12.6	0.49	-0.35	0.07	RSEF-1 encodes an ortholog of human RAB44
Y73B3A.12	-0.13	0.29	0.08	CAL-6 encodes an ortholog of human calmodulin-like 3
C50C3.5	0.14	0.05	0.09	Similar to calmodulin 1
K03A1.2	0.01	0.17	0.09	lron-7 (eLRR (extracellular Leucine-Rich Repeat) ONly)
F53F4.14	0.25	-0.06	0.09	Similar to F36H12.3 (major sperm protein)
C18E9.1	0.15	0.07	0.11	CAL-2 (CALmodulin related genes)
Y45F10A.6	0.01	0.21	0.11	TBC (Tre-2/Bub2/Cdc16) domain family
Y73C8B.5	0.05	0.18	0.12	Similar to calmodulin-3
C50C3.2	-0.01	0.25	0.12	Spectrin alpha chain
C04B4.2	-0.01	0.26	0.13	Similar to C04B4.4 and LIN-66
T07G12.1	0.42	-0.15	0.13	CAL-4 (CALmodulin related genes)
M18.5	0.07	0.20	0.14	DDB1 (UV-Damaged DNA Binding protein) homolog
C36C9.6	0.09	0.20	0.14	C36C9.6
C44C1.3	0.17	0.12	0.14	NCS-1 (Neuronal Calcium Sensor family)
DH11.1	0.27	0.03	0.15	Putative glutaminase
F25H2.2	0.34	-0.02	0.16	SNX-27 (Sorting NeXin)
R08F11.1	0.28	0.04	0.16	Non-lysosomal glucosylceramidase
C47D12.1	0.14	0.18	0.16	TRRAP-like (transcription/transformation domain-associated protein)
Y40H4A.2	0.11	0.23	0.17	Serine/threonine-protein phosphatase
T22D1.5	0.17	0.19	0.18	Probable serine/threonine protein phosphatase 2A regulatory subunit
C06A1.3	0.12	0.25	0.18	Putative serine/threonine-protein phosphatase
K11C4.5	0.34	0.01	0.18	Uncoordinated UNC-68; Ryanodine receptor homolog
K04C1.4	0.19	0.17	0.18	MLC-6 (Myosin Light Chain)
F10G8.5	0.51	-0.14	0.19	NCS-2 (Neuronal Calcium Sensor family)
F56C11.1	0.34	0.06	0.20	Blistered cuticle; BLI-3 (DUal OXidase)
T25G3.4	0.23	0.17	0.20	Probable glycerol-3-phosphate dehydrogenase, mitochondrial

Table 3.4 (Continued)

Gene name	Anthranilate- no $CaCl_2$			Gene description
	Averaged AUC z-score	Averaged slope z-score	Total averaged z-score	
B0511.1	0.33	0.08	0.21	FK506-Binding protein family
F53G12.3	0.32	0.11	0.21	DUOX-2 (DUal OXidase)
F23F1.2	0.44	0.02	0.23	Similar to R09H10.6
ZK354.9	0.17	0.33	0.25	Serine/threonine protein phosphatase
C44B12.2	0.26	0.28	0.27	Osteonectin (SPARC) related
T06E6.1	-0.08	0.66	0.29	Similar to human WDR-74
W09C3.6	0.43	0.15	0.29	GSP-3 (GLC7 (yeast Glc Seven) like Phosphatase)
Y37A1B.1	0.40	0.18	0.29	LST-3 (Lateral Signaling Target); ortholog of human CCAR2
Y75B8A.30	0.43	0.17	0.30	Protein phosphatase
F52H3.6	0.30	0.30	0.30	Serine/threonine protein phosphatase
F58G1.3	0.40	0.24	0.32	Serine/threonine protein phosphatase
F21A10.1	0.48	0.16	0.32	NCS-4 (Neuronal Calcium Sensor family)
T12D8.6	0.44	0.21	0.32	MLC-5 (Myosin Light Chain)
ZK673.7	0.14	0.54	0.34	Troponin C
C34D4.2	0.26	0.43	0.34	Serine/threonine protein phosphatase
F16F9.3	0.31	0.39	0.35	F16F9.3
K08F11.5	0.48	0.29	0.39	Mitochondrial Rho GTPase Miro-1
F23H11.8	0.73	0.05	0.39	Phosphatase with EF hands
F43C9.2	0.79	0.05	0.42	Homologous to Isoform 1 of Calcium-binding protein 4
M04F3.4	0.43	0.42	0.42	Probable cysteine protease
Y49E10.3	0.42	0.45	0.43	Protein Phosphatase
K07G5.4	0.56	0.33	0.44	K07G5.4
ZK938.1	0.54	0.37	0.45	Serine/threonine protein phosphatase
F22D6.9	0.62	0.33	0.47	Serine/threonine protein phosphatase
F40F9.8	0.12	0.85	0.48	CAL-7 encodes an ortholog of human calmodulin-like 4
ZK1307.8	0.38	0.61	0.50	Glucosidase 2 subunit beta
T05F1.1	0.53	0.50	0.51	NRA-2 (Nicotinic Receptor Associated) nicalin homolog
C16H3.1	0.75	0.32	0.53	NCS-7 (Neuronal Calcium Sensor family)
K02F3.2	0.73	0.40	0.57	Probable calcium-binding mitochondrial carrier K02F3.2; Similar to Aralar1
C29E4.14	0.42	0.72	0.57	Multiple coagulation factor deficiency protein 2 homolog
T10G3.5	0.38	0.77	0.58	EEA1 (Early Endosome Antigen, Rab effector) homolog
K08E3.10	0.25	0.95	0.60	MLC-7 (Myosin Light Chain)
C23G10.1	0.67	0.61	0.64	Putative serine/threonine-protein phosphatase C23G10.1
Y43F4B.1	0.73	0.57	0.65	Set-25 (SET (trithorax/polycomb) domain containing)
F25B3.4	0.71	0.59	0.65	Serine/threonine protein phosphatase
Y51H4A.17	0.73	0.59	0.66	STAT transcription factor family
T27C10.4	0.60	0.73	0.66	BTB and MATH domain containing
F56D1.6	0.80	0.54	0.67	Calexcitin
C06G1.5	0.93	0.43	0.68	Serine/threonine-protein phosphatase 2A regulatory subunit
T10H9.8	0.57	0.86	0.71	Similar to CAL-4
Y67H2A.4	0.49	0.95	0.72	MICU-1 (MItochondrial Calcium Uptake protein)
W04D2.1	0.74	0.75	0.74	Actinin
F44A6.1	0.58	0.92	0.75	Nucleobindin homolog
C56A3.6	0.69	0.84	0.77	Mitochondrial calcium uptake protein-3 (MICU-3)
F19B10.1	0.90	0.74	0.82	MEL-26 binding protein
W06H8.1	0.94	0.72	0.83	RME-1 (Receptor Mediated Endocytosis); EH domain containing protein
C36E6.3	0.80	0.96	0.88	MLC-1 Myosin Light Chain
T09B4.4	1.00	0.88	0.94	Similar to Calmodulin-like protein 4

Table 3.4 (Continued)

Gene name	Anthranilate- no $CaCl_2$			Gene description
	Averaged AUC z-score	Averaged slope z-score	Total averaged z-score	
Y26E6A.2	0.84	1.10	0.97	F-box protein
F55A11.1	0.93	1.03	0.98	Similar to Multiple coagulation factor deficiency protein 2
Y71H2AL.1	0.81	1.17	0.99	PBO-1 (PBOc defective (defecation)) calcineurin B homolog
K10B3.10	1.11	0.90	1.00	Spectrin
M02A10.3	0.83	1.28	1.06	SLI-1 (Suppressor of LIneage defect); Cbl family of ubiquitin ligases
T09F5.10	1.09	1.21	1.15	Similar to F36D3.16
K03A1.4	1.15	1.16	1.15	Similar to Calmodulin-1
F33C8.4	1.48	0.84	1.16	Similar to Y41D4A.7
T04F3.2	1.20	1.22	1.21	similar to SPARC-related modular calcium-binding protein 2
M03F4.7	1.16	1.27	1.22	Calumenin (calcium-binding protein) homolog
K03E6.3	1.40	1.23	1.31	NCS-3 (Neuronal Calcium Sensor family)
F23B12.1	1.34	1.43	1.38	Serine/threonine protein phosphatase
C25A1.9	1.83	1.30	1.57	RSA-1 (Regulator of Spindle Assembly); protein phosphatase 2A (PP2A) regulatory subunit
Y47G6A.27	1.78	2.15	1.96	Mitochondrial Rho GTPase Miro-3

CHAPTER 4:

DEVELOPMENT OF HIGHT-THROUGHPUT RNAi SCREENS FOR THE IDENTIFICATION OF GENE KNOCKDOWNS THAT INCREASE OXYGEN CONSUMPTION, ATP, AND REDOX STATUS IN *CAENORHABDITIS ELEGANS*

4.1 Abstract

Caenorhabditis elegans exhibit a dramatic decrease in aerobic metabolism with age as evidenced by large declines in ATP content, oxygen consumption, and reductive capacity during the first week of their adult lifespan. Assays for measuring these changes during high throughput RNAi feeding screens are complicated by the co-culturing of *C. elegans* with its bacterial food source. With the exception of a few fluorescent protein sensors, *C. elegans*-specific measurements of metabolic activity currently require the use of axenic media or the killing or removal of bacteria, which currently preclude the use of feeding RNAi. Therefore, we have developed a high-throughput 96-well feeding RNAi method that allows for a fluorescent or luminescent measurement of a specific *C. elegans* enzymatic activity or metabolite level. These methods were facilitated by the finding that treatment of dsRNA-expressing bacteria with 40% or more of acetone or ethanol maintained a high level of gene knockdown in *C. elegans*, while denaturing bacterial proteins. However, this bacterial solvent treatment prevented *C. elegans* larval development, so to allow development 5-10% live *E. coli* were provided, which were later

killed by the addition of the antibiotic ciprofloxacin allowing for specific measurement of *C. elegans* metabolic activity. To demonstrate the utility of these methods RNAi screening of 2,688 X-chromosome genes was performed followed by either oxygen consumption analysis with fluorescent oxygen-sensing microplates, fluorescent measurement of redox status using the redox-sensitive indicator resazurin, or luminescent determination of ATP levels following freeze-thaw through the use of firefly luciferase.

4.2 Introduction

Several major conserved longevity-promoting signaling pathways have been characterized in the nematode *Caenorhabditis elegans* [1-5]. One pathway involves the activation of the NAD^+-dependent histone deacetylase SIR-2.1, and another involves disruption of insulin/IGF-1 receptor, DAF-2 (abnormal dauer formation-2) signaling. Loss-of-function mutations in the *C. elegans* DAF-2 gene confer an extended lifespan through the activation of the transcription factor DAF-16, which is homologous to human FOXO genes [6-8] and through the activation of SKN-1, the C. elegans homolog of mammalian Nrf2. Dietary restriction, which is currently the most consistent and universal method for producing lifespan extension in model organisms, decreases PI3K/AKT signaling, in turn activating DAF-16 [9]. Furthermore, although it functions through a separate upstream mechanism, the SIR-2.1-dependent lifespan extension pathway partially overlaps with the DAF-2/DAF-16 pathway, including the activation of DAF-16 [10].

Mitochondrial function decreases dramatically during the first week of adulthood in *C. elegans*. The rate of oxygen consumption falls steeply over this interval, accompanied by a similar drop in cellular ATP content [11-13]. Wild-type N2 *C. elegans* maintain slightly higher

oxygen consumption levels with age when cultured under conditions of dietary restriction, and long-lived *daf-2* mutants similarly possess higher cellular ATP levels. The calorimetric/respirometric (C/R) ratio, which is a measure of the heat produced per oxygen consumed, correlates to the degree of proton leakage across the inner mitochondrial membrane [14], and is also lower in *daf-2* mutants during the first two weeks of adulthood, indicating a tighter coupling between electron transport and ATP production [13]. In contrast, *daf-16* mutant *C. elegans* exhibit slightly lower rates of oxygen consumption during this time frame compared to wild-type N2 and they similarly show decreased cellular ATP levels.

Both Braeckman *et al*. [12] and Houthoofd *et al*. [13] have successfully used the colorimetric redox-sensitive viability dye XTT to assay the metabolic reductive capacity of *C. elegans*, demonstrating that XTT reductive capacity declines with age. Encouraged by this finding, we investigated the ability of *C. elegans* to reduce another redox-sensitive viability dye resazurin, which is irreversibly converted into the fluorescent compound resorufin upon chemical reduction. Resazurin has a long history of use as a bacterial viability indicator, dating back to at least 1929, being used to test for bacterial contamination in milk [15]. We found that the reductive capacity, as indicated by resazurin reduction, also exhibits a similar decline with age.

C. elegans are especially susceptible to RNA interference (RNAi) of gene expression, making them a desirable model organism for studies involving reverse genetics [16, 17]. Genes affecting lifespan have been identified in *C. elegans* using high-throughput screening approaches [18], however genes affecting individual age-related changes have been much less studied. The prospect of performing a high-throughput RNAi screen looking for changes in metabolic attributes is complicated by the usual presence of live dsRNA-expressing bacteria in the media of *C. elegans* during typical RNAi feeding studies. Live bacteria potentially contribute to

measurements assaying aerobic respiration, ATP content, and enzymatic activity. Both ultraviolet light (UV) and γ-irradiation killing of bacteria have been developed as methods for performing RNAi with metabolically inactive bacteria [19], but these treatments potentially damage the dsRNA present making the RNAi-mediated gene knockdown less effective. In addition, we found UV-treatment to be difficult to scale to the quantities necessary for high-throughput screening and resulted in inconsistent effects on bacterial reductive capacity (data not shown). Therefore, we set out to find an alternative method to kill *E. coli* and preserve RNAi knockdown potential and to investigate the feasibility of developing high-throughput assays for assaying age-related changes in *C. elegans* oxygen consumption, ATP content, and reductive capacity using dead *E. coli* as an RNAi source.

4.3 Materials and Methods

4.3.1 *C. elegans* Culture

Prior to individual experiments, *C. elegans* were grown at 20 °C in 10 cm dishes containing nematode growth medium (NGM) and streaked with HT115(DE3) *E. coli*. To prepare *C. elegans* for experimentation, eggs were obtained by alkaline bleach synchronization. In short, nematodes were washed off plates with 0.1 M NaCl and combined with a 2:1 mixture of 5 M NaOH and 6% Clorox bleach, in a ratio of 0.4 mL of alkaline-bleach solution per 1 mL of suspended nematodes. The mixture was then rocked for 4 – 7 minutes until the *C. elegans* carcasses dissolved as monitored by microscopy. The resulting eggs were then diluted 5-fold with 0.1 M NaCl, pelleted by centrifugation at 1150 x *g* for 2 minutes at room temperature, and the supernatant was aspirated. The egg pellet was then washed three times each with 50 mL of 0.1 M NaCl, using centrifugation at 1150 x *g* for 2 minutes at room temperature and aspiration to

remove the supernatant. The final pellet was suspended in 15 mL of fresh S-medium (containing the appropriate concentration of antifungal or antibiotic drugs), and then left to rock overnight at 20 °C. The next day (approximately 12 hours later) the concentration of live L1 larvae were determined by counting the number of nematodes in ten 10 μL drops.

For all assays utilizing *C. elegans*, the nematodes were cultured in 100 μL of S-medium in black, clear-bottom CoStar® 96-well plates with bacteria and antifungal and antibiotic drugs present at appropriate concentrations. The plates were covered with 12.7 micron (0.0005 inch) FEP Teflon (CS Hyde Company) membrane gasket-attached lids sealed along the edges of the plates with vinyl tape. All assays consisted of either N2 or BC12907 *C. elegans* (both purchased from the Caenorhabditis Genetics Center at the University of Minnesota). The strain BC12907 *dpy*-5(e907) expresses an integrated GFP transgene driven by the T09B4.8 promoter. T09B4.8 is a homolog of the human mitochondrial *AGXT-2* (alanine-glyoxylate aminotransferase-2) gene [20, 21]. Unpublished data from our lab has shown that the bright and ubiquitous GFP fluorescence of the BC12907 strain corresponds well to live *C. elegans* volume per well after the fifth day of culture (Chapter 3).

4.3.2 Viability Assay

The redox-sensitive viability dye resazurin (7-Hydroxy-3H-phenoxazin-3-one 10-oxide; obtained from Acros Organics) was added to 96-well plate liquid cultures at a concentration of 20 μM per well and then incubated in the dark for 90 minutes at 20 °C. Resazurin is converted to the fluorescent compound resorufin through an irreversible reduction, which was assayed at the end of the incubation period by measuring the fluorescence ($\lambda_{ex}/\lambda_{em}$ 528/590 nm filter set) in a BioTek Synergy 2 microplate reader.

4.3.3 Low-throughput ATP Assays

For bacteria and *C. elegans*, microcentrifuge tube samples were prepared by submerging the tubes in liquid nitrogen followed by a 5 minute thaw at 37 °C and sonication on ice using a Heat Systems Ultrasonics W-380 sonicator (5-second pulses, 50% duty cycle, max power, 12 pulses total). The samples were then briefly vortexed and transferred to the wells of white, solid-bottom 96-well plates at 50 μL per sample. An equal volume of CellTiter Glo® (Promega), a reagent for ATP determination consisting of a mixture of luciferin and luciferase was added to each well. The plates were shaken for 2 minutes and then incubated at room temperature for 10 minutes. ATP content was determined by measuring the luminescence in a BioTek Synergy 2 microplate reader and comparing it to a standard curve made using the measurements from a similarly prepared series of ATP standards.

4.3.4 Clark Oxygen Electrode Measurements

The rate of oxygen consumption for bacteria and *C. elegans* was determined by placing 300 μL of a sample into the chamber of a Clark oxygen electrode (MT200A chamber, Strathkelvin Instruments). The level of dissolved oxygen in the sealed chamber was then recorded over the span of 10 minutes and the rate of the decline in dissolved oxygen was determined per minute using a linear segment of the recording.

4.3.5 *C. elegans* Protein Assay

The total protein of *C. elegans* samples was determined by using a similar method as described by Braeckman *et al*. [12]. In short, a 1 mL sample to be assayed was frozen in liquid

nitrogen and then stored at -10 °C until analysis. For the protein assay 500 µL of the thawed sample was transferred to a fresh 2 mL microcentrifuge tube and sonicated on ice using a Heat Systems Ultrasonics W-380 sonicator (5-second pulses, 50% duty cycle, max power, 12 pulses total). Three times the volume of 1:1 ethanol:acetone was added to promote protein precipitation, vortexed briefly, and incubated at 4 °C for 30 minutes. The tube was then centrifuged at 15,000 x *g* for 10 minutes at room temperature to pellet the protein precipitates. The resulting supernatant was decanted and the microcentrifuge tube was left open and inverted on a paper towel in an isolated enclosure for 5 – 10 minutes while any remaining ethanol:acetone evaporated. The protein was then suspended in 180 µL of 1 N NaOH, vortexed, and incubated at 70 °C for 25 minutes to degrade any remaining lipids within the sample. 1.26 mL of deionized water was added to dilute the NaOH, and 360 µL of 10% sodium dodecyl sulfate (SDS) was added to assist in solubilizing the proteins. The contents of the tube were then mixed by inversion and centrifuged at 1,500 x *g* for 2 minutes at room temperature. The protein concentration of the supernatant was analyzed by the BCA assay (Pierce) according to the manufacturer's protocol using bovine serum albumin protein standards with a similar pH and SDS content as the assayed samples.

4.3.6 Measuring Total Corrected Worm Fluorescence (TCWF)

Fluorescence microscope images were taken of GFP-expressing BC12907 *C. elegans* in drops of S-medium by using an EVOS® microscope (Advanced Microscopy Group) and a λex/λem 470/525 nm filter set. The *C. elegans* were chilled prior to microscopy by placing the slide at -10 °C for a few minutes to reduce movement. The image analysis software ImageJ was used to manually calculate an estimate of the relative green fluorescence of individual nematodes

by using the method for total corrected cell fluorescence outlined by McCloy *et al*., [22]. Briefly, each image was converted to gray-scale; each *C. elegans* in the image was outlined and its area and integrated density (*IntDen*) were recorded. An empty area of the image immediately beside that *C. elegans* was then outlined, and the mean gray value for that area was recorded. The total corrected worm fluorescence (TCWF) for that *C. elegans* was then calculated as *IntDen* – (*Area* X *Mean of Gray Value of Background*).

4.3.7 Preparation of 9:1 mix of dead:live HT115(DE3) *E. coli*

E. coli was suspended in 40% acetone/60% 0.1 M NaCl (v/v) at a concentration of 6.9 x 10^9 cells/mL and incubated for 2 hours at 37 °C. The bacteria was then pelleted by centrifugation at 3,000 x *g* for 30 minutes at 4 °C and the supernatant was decanted. The pellet was then allowed to dry in an isolated enclosure for ~30 minutes before being suspended in fresh S-medium (containing the appropriate antifungal or antibiotic drugs). Nine portions of the bacteria were then mixed with one portion (v/v) of a suspension of an identical concentration of live HT115(DE3) *E. coli* to yield a 9:1 mix.

For the RNAi genome screen, individual clones were grown in 500 μL of LB, in 1.3 mL 96-well deep-well plates (Thermo Scientific Nunc #260251 or #260252) covered with sealed FEP Teflon gasket-attached membrane lids, and shaken at 37 °C for 24 hours. Optimal growth time was determined by optical density measurements at 600 nm and dilution plating so as to produce a minimum of >1.24 x 10^9 cells/mL. The expression of dsRNA was then induced by the addition of a 1 mM concentration of isopropyl β-D-1-thiogalactopyranoside (IPTG) followed by a 4 hour incubation at 37 °C with shaking. 500 μL of 100% acetone was then added to each well (~50% acetone final concentration) and the plates were incubated. Given the large volume of

plates being prepared for the high-throughput screen, incubating the plates with acetone in closed incubators at 37 °C for 2 hours, as we had done in preliminary experiments, was determined to be unsafe. As such, plates were covered with 96-well plate lids and then placed in a container covered with aluminum foil inside of a sealed fumehood overnight (~16 hours). On the following day, the bacteria were pelleted in the wells of the 96-well plates by centrifugation at ~1,000 x *g* for 30 minutes at 4 °C. The supernatant was decanted, and the plates were allowed to dry in an isolated enclosure for ~30 minutes. The bacteria were then suspended in 90 μL of S-medium (pH 6.0) containing ~200 BC12907 *C. elegans* L1 larvae, 4 μg/mL of fluconazole, 50 μg/mL of ciprofloxacin, and 6.9 x 10^8 cells/mL of fresh, live HT115(DE3) *E. coli* (lacking a plasmid). The individual cultures were then transferred to black, clear-bottom CoStar® 96-well plates.

4.3.8 Setup of the High Throughput RNAi Screen

Bacteria and L1 larvae were prepared in black, clear-bottom CoStar® 96-well plates as described above. The plates were then covered with oxygen permeable 12.7 micron FEP Teflon gasket-attached membrane lids and sealed around the edges of the plate with vinyl tape. The plates were then incubated at 20 °C and the growth of nematodes within the plates was checked by microscopy. Because RNAi treatment can potentially alter the growth rate of *C. elegans*, it was not practical to use the visual confirmation that individual cultures had entered the L4/adult stage before adding 5-fluorodeoxyuridine (FUdR) to sterilize the nematodes. Therefore, a single time point was chosen for treatment that should allow the majority of cultures to reach the proper developmental stage. A 10 μL portion of FUdR (400 μg/mL final concentration; 100 μL final culture volume) was added on the fourth day of culture with the reasoning that any second-

generation hatched larva would arrest and die in the presence of the drug. The plates were then assayed on the sixth day of culture. The X chromosome RNAi clones present in the original Ahringer RNAi library, consisting of 2,688 clones, was investigated in triplicate for each of three separate RNAi screens. This resulted in the use of 28 plates for each replicate, 84 plates for each assay, and 252 plates overall.

4.3.9 ATP Assay for the RNAi High Throughput Screen

CellTiter Glo® was added at 10 μL per well to plates from the RNAi genome screen (prepared as described above). The plates were then immediately placed in a shallow pan of liquid nitrogen in order to freeze the contents of the wells. The plates were then incubated at 37 °C for 20 minutes to thaw the samples, and then placed at 20 °C for 10 minutes to equilibrate to room temperature. The luminescence of each plate was measured in a BioTek Synergy 2 microplate reader, with a white plain index card placed below the clear-bottom plates to aid in luminescence detection. ATP standards were measured using an identical protocol in order to convert the measurements to pmol ATP.

4.3.10 Redox Assay for the RNAi High Throughput Screen

Resazurin was added at a final concentration of 20 μM per well along with 1 mM of the protease inhibitor phenylmethanesulfonyl fluoride (PMSF) to plates from the RNAi genome screen (prepared as described above). The plates were then immediately placed in a shallow pan of liquid nitrogen in order to freeze the contents of the wells. Following the freeze, the plates were incubated for 20 minutes at 37 °C to thaw the samples, and then incubated at 90 minutes at

room temperature (20 °C). The fluorescence of each plate was measured in a BioTek Synergy 2 microplate reader using an λex/λem 528/590 nm filter set.

4.3.11 Oxygen Saturation Assay for the RNAi High Throughput Screen

On day 6 of the lifespan the contents of each well for each 96-well plate from the RNAi screen was transferred to a freshly opened 96-well OXOPlate® (PreSens, Regensburg, Germany). The plates were incubated in the dark at 20 °C for 30 minutes. Following this step, the oxygen saturation of each well was measured according to the manufacturer's instructions, using a BioTek Synergy 2 microplate reader with an λex/λem 528/590 nm filter set for the reference dye, and an λex/λem 528/620 nm filter set for the indicator dye. Calibration and conversion to nmol O_2 saturation was performed according to the manufacturer's instructions using oxygen-free and highly-oxygenated deionized water.

4.3.12 Data Analysis for the High-throughput Screen

The measurements taken from the OXOPlates® were first converted to nmol O_2 based on the manufacturer's instructions, otherwise inter-plate normalization was performed on the raw measurements from each plate in each screen by calculating the robust z-score for each well. Robust z-score calculations use the median measured value of each plate (as opposed to the mean) and the median absolute deviation (MAD) of each plate (as opposed to the standard deviation), with the formula $z\text{-}score = (x - \text{MEDIAN})/\text{MAD}$. This method is more robust against outliers than the standard z-score and compensates for per-plate variation by exploiting the assumption that the majority of RNAi knockdowns should not have a significant effect on the attribute measured.

For each RNAi knockdown the both the mean robust z-score and standard error of the mean (SEM) were calculated based on the three replicates. The upper and lower 95% confidence intervals (CI) were calculated by respectively adding and subtracting 1.96 x SEM from the mean. A *p*-value was also calculated for each knockdown by performing an unpaired two-tailed *t*-test between the knockdown and the theoretical population mean robust z-score of zero. A knockdown was scored as a hit in the screen if its lower 95% CI was greater than 2 (in the case of ATP content and reductive capacity) or less than -2 (in the case of O_2 saturation), and if its *p*-value was less than 0.05.

Receiver operating characteristic (ROC) calculations were performed in GraphPad Prism® version 5.01. Otherwise all calculations and statistical tests were performed using either SigmaPlot® version 11.0 or Microsoft Excel 2010.

4.4 Results

4.4.1 Acetone Treatment Kills Bacteria and Preserves RNAi Knockdown

One of the major complicating factors when performing high-throughput respiratory assays or metabolic assays of *C. elegans* is typically the presence of their food source – living bacteria. In an attempt to overcome this complication, we attempted to find a convenient method of culturing *C. elegans* in liquid culture with dead HT115(DE3) *E. coli*, while still guaranteeing adequate larval development and adequate gene knockdown when performing RNAi feeding studies. As part of this search, we subjected HT115(DE3) *E. coli* cultures to 111 different treatment conditions (selected by surveying protocols from the literature), varying the treatment time and temperature. We then washed and pelleted the individual bacterial cultures, suspended them in S-medium at a concentration appropriate for *ad libitum* feeding of *C. elegans* liquid

cultures (6.9 x 10^9 cells/mL), and assayed bacterial viability with the redox-sensitive dye resazurin (Table 4.1). We also performed a similar screen of treatment conditions using HT115(DE3) *E. coli* containing an L4440 plasmid designed to target green fluorescent protein (GFP) for RNAi knockdown. We washed and pelleted the bacteria and used it to feed *ad libitum* age-synchronized GFP-expressing (strain BC12907) *C. elegans* in liquid culture for 3 days at 20 °C. We then determined the effectiveness of gene knockdown using fluorescence microscopy and calculated the total corrected worm fluorescence (TCWF) based on the method described by McCloy *et al*. (Table 4.2) [22]. During the examination of the data from the different treatment conditions, we noticed that nematode size and developmental stage varied among the treatments (Table 4.3). Since TCWF is partially dependent on nematode size, we normalized our measurements to size, as determined by the image area in pixels, using the image processing software ImageJ (Table 4.4). From these measurements we were able to determine that although heat-treatment of *E. coli* (exposure to temperatures at or above 50 °C) seems to be an effective method for killing the bacteria, it appears to disrupt or degrade the dsRNA content of the bacteria preventing efficient gene knockdown upon consumption by the nematodes. Furthermore, based on these comparisons we decided to focus our attention on acetone treatment as a possible method for rapidly killing *E. coli* while preserving dsRNA for RNAi, although ethanol treatment appeared promising as well.

We performed an additional assay measuring the extent of GFP RNAi knockdown based on the minimum effective acetone treatment conditions as indicated by the bacterial resazurin-based viability screen (40% acetone treatment for 2 hours at 37 °C). As shown in Figure 4.1A, RNAi against GFP resulted in a ~75 – 80% decrease in GFP fluorescence in the BC12907 strain of *C. elegans* fed both the acetone-treated and non-treated *E. coli* (two-way Holm-Sidak analysis

of variance *p*-value < 0.001 for GFP RNAi vs. control). However, acetone treated bacteria appeared to cause delayed *C. elegans* larval development as indicated by a smaller mean area/nematode as indicated by ImageJ software analysis (Figure 4.1B; two-way Holm-Sidak analysis of variance *p*-value < 0.001 for acetone-treated vs. non-treated *E. coli*). Compensating for the differences in nematode size, as seen in Figure 4.1C, indicates an RNAi induced decrease in GFP fluorescence from the acetone-treated bacteria is still comparable to that from the non-treated *E. coli* (~80% of fluorescence in *C. elegans* fed non-treated *E. coli*; two-way Holm-Sidak analysis of variance *p*-value = 0.122 for acetone-treated vs. non-treated *E. coli*). An additional check of bacterial lethality for our treatment conditions can be seen in Figure 4.1D, showing a 60 minute timecourse using resazurin as a viability indicator. Furthermore, dilution plating of similarly acetone-treated HT115(DE3) *E. coli* (40% and higher) on LB agar-containing plates failed to produce bacterial colonies (data not shown).

4.4.2 Fluconazole Prevents Fungal Contamination of Liquid *C. elegans* Cultures without Affecting Mean Lifespan

Besides the issue of restricted *C. elegans* larval development when grown using acetone-treated *E. coli* as food, we observed that dead *E. coli* are especially susceptible to microbial contamination in liquid S-medium cultures. Figure 4.2A shows one instance of microbial contamination that occurred when using 40% acetone-treated (2 hours at 37 °C) HT115(DE3) *E. coli* that were washed and suspended at an *ad libitum* concentration and then cultured in S-medium for one week. The *C. elegans* and *E. coli* suspensions were maintained at 20 °C in 96-well plates sealed with oxygen permeable FEP Teflon membranes. The seal was only briefly removed once every 24 hours to apply resazurin to several of the wells to assay viability. Due to

the transparency of FEP Teflon, the resulting fluorescence viability measurements were performed without removing the seal. As is observed in Figure 4.2, the microbial contamination is refractory to antibiotic treatment (kanamycin in this instance) but minimized by the presence of FUdR. Similar occurrences of microbial growth were detected in the presence of other antibiotics such as ampicillin (50 – 200 μg/mL) and streptomycin (50 – 200 μg/mL), a 1X concentration of commercial algaecide (Silvertrine® containing colloidal silver; data not shown), and surprisingly, the antifungals amphotericin B (5 – 25 μg/mL) and nystatin (concentration range; data not shown). Even though FUdR, which arrests mitotically active cells is commonly used in age-synchronized *C. elegans* cultures to prevent egg laying, its presence in the media before the L4 larval stage (~3 – 4 days at 20 °C) restricts development. The sporadic microbial contamination was often easily detectable by the third day of culture, which led us to believe that FUdR treatment on its own was not an adequate solution for preventing contamination.

Amphotericin B has a history of use as an antifungal agent in mammalian cell and *C. elegans* cultures [23, 24]. However, likely due to the ease at which amphotericin B precipitates from aqueous solutions, we found that it did not adequately prevent microbial contamination under our growth conditions. Therefore, we performed a screen of 26 different antifungal agents to test their effectiveness at preventing microbial contamination in S-medium solutions of dead *E. coli* (Table 4.5). In short, a 96-well plate containing S-medium and 40% acetone-treated *E. coli* was left exposed to the open air for 30 minutes. Afterwards, the appropriate concentration of the various antifungal drugs was added to wells in triplicate and the plate was sealed with an FEP Teflon-containing lid fastened with vinyl tape. The plate was then incubated at 20 °C and on the seventh day a resazurin viability assay was performed. The presence of a high viability-associated resazurin fluorescence on the seventh day within the control (no antifungal drug)

wells and much lower or absent fluorescence (comparable to wells containing only S-medium) in almost all of the other antifungal drug-containing wells supports our suspicion that amphotericin B was failing to prevent sporadic fungal contamination within *C. elegans* liquid cultures.

Of the 26 antifungal drugs tested, eight were selected based on antifungal capability and low predicted toxicity and added to liquid cultures containing *ad libitum* levels of live HT115(DE3) *E. coli* and age-synchronized wild-type N2 *C. elegans* in an attempt to determine if any of the antifungal agents significantly perturbed *C. elegans* lifespan. Figure 4.2B shows the Kaplan-Meier survival curves of the eight antifungal agents along with an antifungal-free control culture. Of these, three appeared to significantly affect *C. elegans* mean lifespan Methylene blue and acriflavine increased lifespan, while sodium benzoate decreased lifespan (Table 4.6). The remaining five antifungal agents showed no effect on mean survival time (fluconazole, ketoconazole, malachite green, propionic acid, and sodium sulfite). Due to its established history of safe and non-toxic clinical use in humans [25-29], we decided to pursue the use of 4 μg/mL fluconazole as an inhibitor of fungal contamination in *C. elegans* liquid cultures containing dead *E. coli*.

4.4.3 The Addition of a Small Amount of Live *E. coli* to the Acetone-Killed *E. coli* Promotes Full *C. elegans* Larval Development

We next investigated whether the failure of the *C. elegans* to develop to adulthood when fed acetone-treated *E. coli* was due to the loss of soluble bacterial metabolites during the wash step prior to suspending the bacteria in S-medium. As an alternative protocol, we incubated HT115(DE3) *E. coli* for 2 hours at 37 °C suspended in 100% acetone and then allowed the acetone to evaporate completely in a fume hood at room temperature. The bacteria were then

suspended to a concentration of 6.9 x 10^9 cells/mL in S-medium containing 4 μg/mL fluconazole and ~100 L1 age-synchronized N2 *C. elegans*. After 3 days in culture at 20 °C, no nematodes had developed to adulthood (scored based on a length greater than 1 mm as determined by microscopy). The majority of the *C. elegans* were between 0.3 and 0.5 mm (data not shown). Therefore the acetone treatment appears to be leading to the degradation of a nutrient required for nematode development.

Next we sought to determine the minimum percentage of live non-treated *E. coli* that would promote full larval development in the majority of *C. elegans* culture. A series of liquid *C. elegans* cultures was prepared using age-synchronized L1 larvae, 4 μg/mL fluconazole, and 6.9 x 10^9 cells/mL of combined HT115(DE3) *E. coli*. The bacterial content of each culture was prepared as a mixture of live *E. coli* and 40% acetone-treated *E. coli*, in percentages of 1% - 10% live bacteria (in increments of 1%). The cultures were then sealed with FEP Teflon membrane-containing lids secured with vinyl tape. After 3 days of incubation at 20 °C, nematode development was scored by measuring *C. elegans* length through microscopy and the use of ImageJ analysis software. The culture containing 96% acetone-treated *E. coli* and 4% live *E. coli* was the culture with the lowest percentage of live bacteria that contained mostly adult *C. elegans* after 3 days. As a point of reference, 4% *E. coli* corresponds to 2.76 x 10^8 cells/mL of live bacteria. Kenyon *et al*. [30] found that *C. elegans* fed only 2.6 x 10^8 arrested at the L1 larval stage. Given that our *C. elegans* developed to adulthood at this concentration of live bacteria suggests that the nematodes are likely still capable of obtaining nutrients from the acetone-treated *E. coli*, with the small amount of live *E. coli* providing the other source of the developmentally-essential nutrient.

A second test of GFP knockdown by RNAi was performed using acetone-treated HT115(DE3) *E. coli* supplemented with 10% live *E. coli* (6.9×10^8 cells/mL live *E.coli*). The higher concentration of live *E. coli* was chosen as a buffer to ensure proper larval development. Similarly-treated 1:9 live:dead HT115(DE3) *E. coli* lacking a plasmid as well as non-treated dsRNA-expressing bacteria were prepared as controls. Age-synchronized L1 larval (strain BC12907) *C. elegans* were grown in culture for 3 days at 20 °C using the bacteria as a food source and their resulting GFP fluorescence was measured using fluorescence microscopy and the TCWF was calculated (Figure 4.3A). The average nematode size at day 3 (Figure 4.3B) as determined by the pixel area showed no significant difference among the types of bacteria tested as determined by unpaired two-tailed t-tests and one-way analysis of variance comparisons (*p*-value > 0.05). The TCWF/area of *C. elegans* fed treated and non-treated dsRNA-expressing *E. coli* (Figure 4.3C and 4.3D) showed a statistically significant decrease in GFP fluorescence (*p*-value < 0.05 with one-way analysis of variance using Dunn's method), even though the GFP fluorescence of both RNAi-fed groups only decreased by ~40% compared to the non-RNAi fed controls.

4.4.4 Ciprofloxacin Treatment Kills Stationary Phase *E. coli* but a Resazurin Signal Persists

Liquid S-medium is a nutrient-poor growth environment for *E. coli* and once placed in this medium *E. coli* likely enters stationary phase. Once in stationary phase, bacteria tend to become more resistant to the activity of antibiotics, many of which are bactericidal due to their interference with mechanisms of cell growth or division, such as protein translation or cell wall synthesis. Antibiotic compounds of the quinolone family, however, have been shown to be

effective against stationary phase bacteria [31-33], with ciprofloxacin and ofloxacin specifically showing high potency. We examined ciprofloxacin and ofloxacin as options for removing the residual metabolic activity of the remaining live bacteria in the *C. elegans* liquid cultures. Figure 4.4A shows the ATP content of fresh, live HT115 (DE3) *E. coli* suspended in S-medium at a concentration of 6.9 x 10^9 cells/mL and treated with either 50 μg/mL ciprofloxacin, 50 μg/mL ofloxacin, or left non-treated and assayed after 0, 12, or 24 hours. The presence of ciprofloxacin or ofloxacin in the media, which are most soluble in aqueous solutions at a low pH, necessitated the adjustment of the pH of the S-medium to 6.0, still well within the range for optimal growth [34]. The ATP content for the ciprofloxacin and ofloxacin treated bacteria decreased by 32% and 37% respectively of the initial non-treated time point at 12 hours and decreased by 18% and 25% respectively at 24 hours. Furthermore, streaking *E. coli* from both treatments onto antibiotic-free LB agar plates after 48 hours of treatment did not result in the formation of colonies after an overnight incubation at 37 °C, whereas streaking similar non-treated *E. coli* resulted in a lawn of growth.

We then performed lifespan analysis of N2 *C. elegans* cultured under similar conditions (6.9 x 10^9 cells/mL of *E. coli* in S-medium containing 4 μg/mL fluconazole and incubated at 20 °C) as shown in Figure 4.4B. The log-rank *p*-value showed a difference among the groups (p = 0.026). Pair-wise comparison using the Holm-Sidak method showed a significant difference between the control lifespan (mean of 15.2 days ± 0.4; n = 141 nematodes), and the ofloxacin-treated lifespan (mean of 14.1 days ± 0.4; n = 147 nematodes; p-value = 0.0103), but not between the control lifespan and the ciprofloxacin-treated lifespan (mean of 14.7 days ± 0.4; n = 209; p-value = 0.572). Given the lack of statistical effect on *C. elegans* lifespan, we chose ciprofloxacin for additional investigation. Figure 4.4C shows the effect of 50 μg/mL

ciprofloxacin on the viability of 6.9 x 10^9 cells/mL HT115(DE3) *E. coli* in S-medium with 4 μg/mL fluconazole incubated for 8 days at 20 ˚C. Viability was measured at intervening time points using resazurin. On the eighth day of treatment ciprofloxacin-treated *E. coli* displayed a 75% reduction in viability signal as opposed to the 49% reduction of signal observed for non-treated *E. coli*. However, by the eighth day the ciprofloxacin-treated *E. coli* still responded to the dye to a significantly greater extent than samples containing only S-medium and 4 μg/mL fluconazole (~9.2 fold higher). A similar experiment using 6.9 x 10^8 cells/mL of HT115(DE3) *E. coli* (10% of the previous concentration and an equal amount as used in Figure 4.3) gave a similar profile for 50 μg/mL ciprofloxacin treatment with an approximately 5-fold lower viability signal. However, at 153 hours (~6.4 days) the ciprofloxacin-treated *E. coli* displayed a viability signal comparable to that of the S-medium only control (unpaired two-tailed t-test *p*-value = 0.066; $n = 3$) and it remained comparable at 192 hours (8 days; unpaired two-tailed t-test *p*-value = 0.090; $n = 3$). As expected, an investigation of lower concentrations of ciprofloxacin-treated *E. coli* (9% to 1% of the full 6.9 x 10^8 cells/mL concentration) revealed a similar pattern of indistinguishability of the resazurin reduction signal compared to the control by ~6.4 days post antibiotic treatment (data not shown). Therefore, it appears that the presence of ciprofloxacin can completely kill the bacteria by the sixth day if the percent of live bacteria in the culture is 10% or less.

Interestingly, an investigation of the rate of aerobic respiration of non-treated and ciprofloxacin-treated *E. coli* at similar concentrations (6.9 x 10^9 cells/mL and 6.9 x 10^8 cells/mL) revealed that respiration is minimal for live *E. coli* in 100 μL S-medium cultures (Figure 4.5). A one-way analysis of variance of the respiratory rate of all groups revealed no significant difference between live *E. coli* in culture and an S-medium-only control (*p*-value = 0.202).

Given that 50 μg/mL ciprofloxacin-treated *E. coli* showed a roughly 5-fold drop in ATP content after 24 hours, failed to form colonies after 48 hours, but continued to reduce resazurin for ~6 days at 6.9 x 10^8 cells/mL and for at least 8 days at 6.9 x 10^9 cells/mL was unexpected and may represent a gradual decay of functional enzymatic activity in dead or dying *E. coli*. Furthermore, we found that *C. elegans* develop fully to adulthood when fed a 9:1 dead:live mix of HT115(DE3) *E. coli* as used in Figure 4.3 (6.21 x 10^9 cells/mL of 40% acetone-treated *E. coli* and 6.9 x 10^8 cells/mL of fresh, live *E. coli*) and treated with 50 μg/mL ciprofloxacin while in the L1 larval stage. Therefore these culture conditions were chosen and day 6 was chosen for measurements for RNAi screens demonstrating the feasibility of this approach.

4.4.5 Screens for ATP content, Oxygen Consumption, and Reductive Capacity

C. elegans experience a dramatic decline in oxygen consumption and ATP content over their adult lifespan [11-13]. Our results with N2 *C. elegans* support this respiratory decline with ATP exhibiting a steep decline starting on the third day of culture (approximately the first day of adulthood) as measured per nematode (Figure 4.6A) and per ng of *C. elegans* protein (Figure 4.6B). When oxygen consumption was normalized per nematode, we found the rate of oxygen consumption to start to decline sharply by the seventh day of culture (Figure 4.6C), but when normalized per ng of *C. elegans* protein, it started to decline sharply on the third day of culture (Figure 4.6D). Inspired by the success reported by Braeckman *et al*., using the redox-sensitive viability dye XTT to assay metabolic reductive capacity, which was found to decline with age [12], we sought to apply the viability dye resazurin, which has the advantage of a fluorescent signal, for a similar purpose. Figures 4.6E and 4.6F show the results of assaying resazurin reduction on days 4 through 8 using samples of age-synchronized N2 *C. elegans* that were

physically disrupted by freezing in liquid nitrogen, thawing, and then sonication. Our findings were similar to those found by Braeckman *et al*. with worms showing a decrease in reductive capacity with age as evidenced by the rate of resazurin reduction falling sharply beginning with the first measurement as assayed per nematode (Figure 4.6E) and per ng *C. elegans* protein (Figure 4.6F). We also found that intact nematodes reduced resazurin well at young ages, but not quite as well as freeze-thawed nematodes at older ages. This suggests that resazurin may have limited permeability though the cuticle of the nematode and the decreased rate of pharyngeal pumping in aged nematodes might contribute to a decreased resazurin reduction signal independent of the redox status of the worm.

Because of our success in developing a functional RNAi feeding protocol that uses dsRNA-expressing bacteria that are dead by day 6 of the lifespan, we decided to examine the feasibility of performing high-throughput screens to identify genes preventing the age-related decline in aerobic respiration, ATP content, and redox status. We began by attempting to modify our ATP and redox measurements, which require the disruption of the *C. elegans* cuticle, for high-throughput screening. Figure 4.7 shows the results of ATP assays performed following several different disruption methods involving rapid freezing and/or boiling. From these results we decided that a single freeze/thaw cycle using liquid nitrogen was adequate to disrupt the *C. elegans* cuticle for ATP analysis. We then examined quality of our overall method of differentiating between physiologically relevant levels of ATP by examining 3-day-old and 6-day-old BC12907 *C. elegans*, both grown on a 9:1 dead:live mix of 40% acetone-treated and non-treated HT115(DE3) *E. coli* (6.9×10^9 cells/mL total) in S-medium with 4 μg/mL fluconazole and 50 μg/mL ciprofloxacin. Prior to these assays the nematodes were washed three times with 0.1 M NaCl and then added at a concentration of ~200 nematodes/well to 96-well

plates containing 9:1 dead:live bacteria that had been incubated for 6 days in S-medium (prepared with 4 μg/mL fluconazole and 50 μg/mL ciprofloxacin; n = 60 wells for each plate). CellTiter Glo® was added to both plates, which were then placed in a shallow pan of liquid nitrogen until entirely frozen. The plates were then thawed at 37 °C for 20 minutes and then placed at room temperature (20 °C) for 10 minutes. Figure 4.8A shows a comparison of the pmol ATP distribution for both groups as determined by well luminescence. An analysis of the potential quality of this assay method for investigating values within the tested physiological range was performed by calculation of the strictly standardized mean difference (SSMD) between the two groups. The resulting SSMD value for the use of this assay with *C. elegans* was β = 2.180 (Table 4.7 and Table 4.8 for a summary and an interpretation of SSMD values [35]). SSMD value interpretation depends on a subjective assessment of the strength of the controls; however, based on the calculated β value, the assay is rated as either "good" for a strong pair of controls, or "excellent" for a moderate pair of controls. An investigation of the receiver operating characteristic (ROC) yielded an area under the curve (AUC) of 0.998 ± 0.002 (Table 4.8), indicating a high capacity to differentiate between the day 3 and day 6 groups with a minimal error rate. Interestingly, normalizing the pmol ATP measurements to the GFP fluorescence of each well (an indication of the total nematode volume per well; Figure 4.8B) slightly lowered the SSMD and ROC values (β = 1.652; AUC = 0.932 ± 0.024) possibly due to the high green autofluorescence of concentrated bacteria at their initial concentration of 6.9×10^9 cells/mL.

We used a similar method to investigate the potential for high-throughput measurements of redox status. Again we used 3-day-old and 6-day-old *C. elegans* that were washed and plated at a concentration of ~200 nematodes/well in 96-well plates containing a 9:1 dead:live mix of

40% acetone-treated and non-treated HT115(DE3) *E. coli* (6.9×10^9 cells/mL total) that had been incubated for 6 days in S-medium (prepared with 4 μg/mL fluconazole and 50 μg/mL ciprofloxacin; n = 60 wells for each plate). Resazurin was added to each well at a final concentration of 20 μM with 1 mM PMSF to inhibit proteases activated by the subsequent freeze-thaw step. The plates were then immediately frozen in a shallow pan of liquid nitrogen and allowed to thaw and equilibrate to room temperature as described above. The plates were then incubated at room temperature for an additional 90 minutes before measuring fluorescence. The results (shown in Figure 4.8C) were analyzed by calculating the SSMD for the 3 and 6-day-old *C. elegans* indicating a scoring of "excellent" for the assay for controls assessed to be moderate, strong, or very strong ($\beta = 5.809$), and the ROC was determined to have an AUC of 1.00 ± 0.00 indicating a complete capacity to differentiate between the two groups. Normalizing the measurements to GFP fluorescence, however, completely negated the utility of the assay (reversing the relative measurements of the 3- and 6-day-old groups; $\beta = -8.297$; Figure 4.8D).

The oxygen-sensing 96-well OXOPlates® (from PreSens) have been used successfully for the assay of *C. elegans* respiration [36]. We used OXOPlates® to measure the oxygen saturation per well of 3 and 6-day-old *C. elegans* grown as indicated above. Prior to assaying oxygen saturation, the nematodes were combined in OXOPlates® with 9:1 dead:live HT115 (DE3) *E. coli* that had been incubated for 6 days in S-medium (prepared with 4 μg/mL fluconazole and 50 μg/mL ciprofloxacin; n = 60 wells for each plate; ~200 nematodes/well). The plates were allowed to equilibrate for 30 minutes at room temperature (20 °C) and then measured according to the manufacturer's instructions. Figure 4.8E shows the difference between the 3 and 6-day-old *C. elegans*. In this assay lower nmol oxygen saturation corresponds to a higher rate of oxygen consumption. SSMD and ROC were calculated as before indicating a

robust assay (β = 3.197; "excellent" for moderate or strong controls, and "good" for very strong controls) with complete ability to differentiate between the assayed groups (AUC = 1.00 ± 0.00). In contrast to the previous two assays, normalizing the measurements to the GFP fluorescence of the *C. elegans* slightly increased the quality of the oxygen saturation assay (β = 3.960; Figure 4.8F).

Given these results we used our novel method to investigate ATP content, oxygen consumption, and redox status of 6-day-old *C. elegans* fed dsRNA-expressing bacterial clones from X chromosome plates of the Ahringer *C. elegans* RNAi genome library (2,688 clones total; supplied by Source BioScience) to individually knockdown gene expression. For each assay, *C. elegans* (strain BC12907) were grown from the L1 stage for 6 days at 20 °C in 96-well plate liquid cultures containing 4 μg/mL fluconazole, 50 μg/mL ciprofloxacin, and a 9:1 dead:live mixture of HT115(DE3) *E. coli* (prepared as previously described) and performed in triplicate. On the sixth day GFP fluorescence was measured in a microplate reader to give the option for normalizing measurements to *C. elegans* GFP fluorescence (data not used in our analysis). Depending on the assay, measurements were then taken as described above (OXOplate® measurements for oxygen saturation determination or a liquid nitrogen freeze/thaw cycle followed by either CellTiter Glo® for ATP level analysis or resazurin reduction for redox measurements). Figure 4.9A, 4.9B, and 4.9C show the distribution of measurements for each of the three screens. Hits were determined for each screen by calculating the mean and 95% confidence interval associated with the z-score for each gene knockdown as well as the unpaired two-tailed t-test *p*-value of each knockdown compared to a theoretical population z-score mean of zero. A knockdown was determined to be a hit if its lower 95% confidence interval was more than 2 standard deviations above the mean (for ATP content and reductive capacity), or if its

upper 95% confidence interval was 2 standard deviations below the mean (for oxygen saturation) and if it had an associated *p*-value less than 0.05 (Figure 4.9D, 4.9E, and 4.9F). In other words, hits were selected that showed a significant increase in ATP content, oxygen consumption, or reductive capacity – similar to a younger *C. elegans* phenotype – on the sixth day of liquid culture.

The results from our 3 RNAi screens of 2,688 clones targeting genes on the *C. elegans* X chromosome identified 55 total gene knockdowns identified as hits. Of these hits, 10 gene knockdowns were associated with increased ATP content, 8 gene knockdowns were associated with increased oxygen consumption, and 37 gene knockdowns were associated with increased reductive capacity (representing 0.37%, 0.30%, and 1.38% of the total number of genes screened, respectively).

4.4.6 Genetic Mediators of ATP Content, Oxygen Consumption, and Reductive Capacity

The genes identified as hits from the three screens are relatively diverse in function (Table 4.9). To further investigate the roles of these genes, we used the STRING (Search Tool for the Retrieval of Interacting Genes/Proteins) online database (http://www.string-db.org/) to identify gene ontology categories (GO) enriched in the hits for each screen (Table 4.10). There were not enough genes selected from the oxygen consumption screen for any of the gene ontology categories to reach statistical significance ($\alpha < 0.05$), but 16 GO categories were found to be enriched among the ATP content screen hits, and 50 GO categories were significantly enriched among the reductive capacity screen hits. For both of these screens, categories relating to the negative regulation of cellular processes were the most representative (10 GO categories

for the ATP content screen, or 62.5% of the categories; and 25 of the GO categories for the reductive capacity screen, or 50% of the categories). Additionally, four cellular component-related GO categories were found to be enriched among the reductive capacity screen hits, all four which are related to vesicles and synapses.

For each hit from the three screens, we used the Human Aging Genomic Resources (HAGR) GenAge database (http://genomics.senescence.info/genes/) to determine reported effects on *C. elegans* lifespan. Of the 55 identified genes, 4 were reported to affect lifespan (*lin-2*, *lin-14*, F42G10.1, and *daf-6*) with all of them showing an anti-longevity effect, meaning that RNAi knockdown or attenuation of function results in an increase in lifespan. For the remaining genes, WormBase (https://www.wormbase.org/) was used to identify the number of orthologous gene members within the same gene class, and the GenAge database was searched to identify individual members of each gene class reported to affect lifespan. Using the total number of known *C. elegans* genes (19,762) and the number of pro- and anti-longevity *C. elegans* genes currently reported through GenAge (474 and 254 respectively), we were able to use χ^2 analysis to identify gene classes that are significantly enriched for both pro- and anti-longevity genes ($\alpha < 0.05$). Five of these remaining hits were found to be members of gene classes that are significantly enriched in anti-longevity genes (*unc-2*, *hpl-1*, *sid-5*, *nac-1*, and *set-12*). No similar genes were found to be members of pro-longevity enriched gene classes. In total, 9 of our 55 hits (16.36%) were found to be either anti-longevity genes, or members of gene classes enriched for anti-longevity genes.

4.5 Discussion

We effectively used the RNAi-mediated knockdown of GFP expression to demonstrate that HT115(DE3) *E. coli* can be effectively killed through the use of a 40% acetone solution in a manner that preserves RNAi-mediated gene knockdown. The use of acetone-treated bacteria as sole food source resulted in the knockdown of GFP expression as determined by fluorescence microscopy, but restricted the proper larval development of the nematodes. We were able to compensate for this restriction by including a small amount of live bacteria to our liquid cultures, which proved to be effective down to 4% of the total bacterial content. Treatment of these mixed dead:live *E. coli* cultures with ciprofloxacin, which is bactericidal against stationary phase bacteria, resulted in a ~5-fold drop in bacterial ATP levels after 48 hours at which time streaking of the ciprofloxacin-treated cultures failed to produce colonies. The ability of the ciprofloxacin-treated bacteria to reduce resazurin decreased but lingered for ~6 days after ciprofloxacin treatment, a full four days past the point at which the culture failed to produce plated bacterial colonies. This continuation of resazurin reductive capacity may represent the residual enzymatic activity of dead or dying *E. coli*. The inclusion of ciprofloxacin from the beginning of an age-synchronized L1 *C. elegans* liquid culture fed with a 9:1 acetone-treated dead:live mixture of *E. coli* still permitted proper larval development. Since larvae develop under these culture conditions, but fail to properly develop on purely acetone-treated *E. coli*, the initial inclusion of live bacteria likely provides an essential nutrient that is destroyed or rendered unusable by the acetone treatment.

Miscellaneous troubleshooting with using resazurin reduction as a marker of viability led to the discovery that long-term cultures of dead *E. coli* in S-medium showed sporadic recovery of viability/reductive capacity. This restored viability was restricted by the inclusion of the DNA

replication inhibitor FUdR in the media, but was otherwise resistant to a variety of antibiotic agents. Despite the use of sterile equipment and reagents and limiting the exposure of cultures and reagents to the open air, the sporadic occurrence of this phenomenon suggested fungal contamination, possibly facilitated by the rich food source of dead bacteria. Amphotericin B and nystatin are antifungal agents with a history of use in *C. elegans* agar and liquid cultures, however the inclusion of these compounds in our S-medium failed to prevent the apparent contamination, possibly due to the limited solubility of the drugs. Therefore, screens of antifungal agents were performed, examining both the efficacy of preventing contamination and their effect on *C. elegans* lifespan. Given the unknown nature of the contaminant we used a long exposure to open air as a positive control. Under these conditions contamination did not occur in the majority of the antifungal-treated samples, while contamination was detectable in the non-treated samples. This is admittedly not completely conclusive evidence of efficacy, but it is highly suggestive of adequate prevention. Given the results of the screen, fluconazole was selected for inclusion in liquid cultures as a nontoxic antifungal agent and has so far proven to be a more effective prophylactic agent against fungal contamination than amphotericin B or nystatin under our liquid culture conditions.

Initial testing of the newly developed high-throughput screening protocol for ATP content, rate of oxygen consumption, and reductive capacity revealed that the physiological change in these parameters between young (day 3) and older (day 6) *C. elegans* is measurable and highly distinguishable, even in the presence of the full initial concentration (6.9×10^9 cells/mL) of the mixture of 9:1 acetone-treated dead:live ciprofloxacin-treated *E. coli*. Unfortunately with this necessary high concentration of bacteria, normalizing the measurements to the amount of nematodes per well, as indicated by total GFP fluorescence, decreased (and in

one instance, completely removed) the sensitivity of the assays likely due to two contributing factors. First, as unpublished work from our lab has suggested, the GFP fluorescence of the BC12907 strain of *C. elegans* does not correlate to total nematode volume per well before at least the fifth day of culture (approximately the first or second day of adulthood), suggesting that the GFP fluorescence measurements of the day 3 sample is likely a poor attribute for normalization. And second, even when dead, *E. coli* can show a very high amount of autofluorescence in the green range, which likely overwhelmed the fluorescence emitted by the nematodes. However, given that our criteria for hit detection for screening consists of identifying gene knockdowns associated with significantly higher measured values, which would exclude knockdowns that proved toxic enough to decrease the number of live nematodes per well and that z-scores are calculated on a per-plate basis to correct for variation among batches, the lack of a normalizing factor for *C. elegans* mass did not dramatically alter the results of our screens. We believe the methods developed here can be applied to dozens of other screening strategies and will be an invaluable contribution to the *C. elegans* research community.

Approximately 1/6th of the hits from the three screens can be classified as either anti-longevity genes, or belonging to gene classes that are significantly enriched for anti-longevity genes. It is noteworthy then that the majority of the identified gene ontology categories are associated with the negative regulation of cellular processes. RNAi knockdown of these genes may be attenuating cellular processes that restrict lifespan. Given that our method for detecting hits was based on the identification of metabolic attributes that most significantly resemble a younger phenotype, we believe it is an acceptable hypothesis that the resulting hits may be enriched for genes that negatively affect lifespan. Many of the lifespan effects reported through the GenAge database are themselves the products of high-throughput screens. Based on our

results, we believe that a more thorough investigation is warranted for the effect of these genes on *C. elegans* lifespan.

4.6 Acknowledgements

We would like to thank Dr. Meera Nanjundan for coordinating the use of the BioTek Synergy 2 microplate reader and Robert Hill for helpful advice and providing assistance with the fluorescence microscopy. *C. elegans* strains were obtained from the Caenorhabditis Genetics Center (University of Minnesota, Minneapolis, MN, USA), which is funded by NIH Office of Research Infrastructure Programs (P40 OD010440). The research was funded in part by NIH grant # AG046769 awarded to PB and through funds provided by the University of South Florida.

4.7 References

1. Kenyon C. The plasticity of aging: Insights from long-lived mutants. Cell. 2005;120(4):449-60. Epub 2005/03/01. doi: 10.1016/j.cell.2005.02.002. PubMed PMID: 15734678.

2. Cohen E, Bieschke J, Perciavalle RM, Kelly JW, Dillin A. Opposing activities protect against age-onset proteotoxicity. Science. 2006;313(5793):1604-10. Epub 2006/08/12. doi: 10.1126/science.1124646. PubMed PMID: 16902091.

3. Leavy SA. The last of life: Psychological reflections on old age and death. Psychoanal Q. 2011;80(3):699-715. Epub 2011/08/31. PubMed PMID: 21874997.

4. Murshid A, Eguchi T, Calderwood SK. Stress proteins in aging and life span. Int J Hyperthermia. 2013;29(5):442-7. Epub 2013/06/08. doi: 10.3109/02656736.2013.798873. PubMed PMID: 23742046; PubMed Central PMCID: PMCPMC4083487.

5. Tissenbaum HA. Genetics, life span, health span, and the aging process in caenorhabditis elegans. J Gerontol A Biol Sci Med Sci. 2012;67(5):503-10. Epub 2012/04/14. doi: 10.1093/gerona/gls088. PubMed PMID: 22499764; PubMed Central PMCID: PMCPMC3410663.

6. Apfeld J, Kenyon C. Cell nonautonomy of c. Elegans daf-2 function in the regulation of diapause and life span. Cell. 1998;95(2):199-210. Epub 1998/10/28. PubMed PMID: 9790527.

7. Gems D, Sutton AJ, Sundermeyer ML, Albert PS, King KV, Edgley ML, et al. Two pleiotropic classes of daf-2 mutation affect larval arrest, adult behavior, reproduction and longevity in caenorhabditis elegans. Genetics. 1998;150(1):129-55. Epub 1998/09/02. PubMed PMID: 9725835; PubMed Central PMCID: PMCPMC1460297.

8. Tullet JM, Hertweck M, An JH, Baker J, Hwang JY, Liu S, et al. Direct inhibition of the longevity-promoting factor skn-1 by insulin-like signaling in c. Elegans. Cell. 2008;132(6):1025-38. Epub 2008/03/25. doi: 10.1016/j.cell.2008.01.030. PubMed PMID: 18358814; PubMed Central PMCID: PMCPMC2367249.

9. Weinkove D, Halstead JR, Gems D, Divecha N. Long-term starvation and ageing induce age-1/pi 3-kinase-dependent translocation of daf-16/foxo to the cytoplasm. BMC Biol. 2006;4:1. Epub 2006/02/07. doi: 10.1186/1741-7007-4-1. PubMed PMID: 16457721; PubMed Central PMCID: PMCPMC1403811.

10. Dali-Youcef N, Lagouge M, Froelich S, Koehl C, Schoonjans K, Auwerx J. Sirtuins: The 'magnificent seven', function, metabolism and longevity. Ann Med. 2007;39(5):335-45. Epub 2007/08/19. doi: 10.1080/07853890701408194. PubMed PMID: 17701476.

11. Braeckman BP, Houthoofd K, De Vreese A, Vanfleteren JR. Apparent uncoupling of energy production and consumption in long-lived clk mutants of caenorhabditis elegans. Curr Biol. 1999;9(9):493-6. Epub 1999/05/20. PubMed PMID: 10330373.

12. Braeckman BP, Houthoofd K, De Vreese A, Vanfleteren JR. Assaying metabolic activity in ageing caenorhabditis elegans. Mech Ageing Dev. 2002;123(2-3):105-19. Epub 2001/11/24. PubMed PMID: 11718805.

13. Houthoofd K, Braeckman BP, Lenaerts I, Brys K, Matthijssens F, De Vreese A, et al. Daf-2 pathway mutations and food restriction in aging caenorhabditis elegans differentially affect metabolism. Neurobiol Aging. 2005;26(5):689-96. Epub 2005/02/15. doi: 10.1016/j.neurobiolaging.2004.06.011. PubMed PMID: 15708444.

14. Dejean L, Beauvoit B, Guerin B, Rigoulet M. Growth of the yeast saccharomyces cerevisiae on a non-fermentable substrate: Control of energetic yield by the amount of mitochondria. Biochim Biophys Acta. 2000;1457(1-2):45-56. Epub 2000/02/29. PubMed PMID: 10692549.

15. Pesch K, Simmert U. Combined assays for lactose and galactose by enzymatic reactions. Milchw Forsch. 1929;8:551.

16. Bargmann CI. High-throughput reverse genetics: Rnai screens in caenorhabditis elegans. Genome Biol. 2001;2(2):REVIEWS1005. Epub 2001/02/22. PubMed PMID: 11182891; PubMed Central PMCID: PMCPMC138903.

17. Leung CK, Wang Y, Malany S, Deonarine A, Nguyen K, Vasile S, et al. An ultra high-throughput, whole-animal screen for small molecule modulators of a specific genetic pathway in caenorhabditis elegans. PLoS One. 2013;8(4):e62166. Epub 2013/05/03. doi: 10.1371/journal.pone.0062166. PubMed PMID: 23637990; PubMed Central PMCID: PMCPMC3639262.

18. Hamilton B, Dong Y, Shindo M, Liu W, Odell I, Ruvkun G, et al. A systematic rnai screen for longevity genes in c. Elegans. Genes Dev. 2005;19(13):1544-55. Epub 2005/07/07. doi: 10.1101/gad.1308205. PubMed PMID: 15998808; PubMed Central PMCID: PMCPMC1172061.

19. Sutphin GL, Kaeberlein M. Measuring caenorhabditis elegans life span on solid media. J Vis Exp. 2009;(27). Epub 2009/06/03. doi: 10.3791/1152. PubMed PMID: 19488025; PubMed Central PMCID: PMCPMC2794294.

20. Hunt-Newbury R, Viveiros R, Johnsen R, Mah A, Anastas D, Fang L, et al. High-throughput in vivo analysis of gene expression in caenorhabditis elegans. PLoS Biol. 2007;5(9):e237. Epub 2007/09/14. doi: 10.1371/journal.pbio.0050237. PubMed PMID: 17850180; PubMed Central PMCID: PMCPMC1971126.

21. McKay SJ, Johnsen R, Khattra J, Asano J, Baillie DL, Chan S, et al. Gene expression profiling of cells, tissues, and developmental stages of the nematode c. Elegans. Cold Spring Harb Symp Quant Biol. 2003;68:159-69. Epub 2004/09/02. PubMed PMID: 15338614.

22. McCloy RA, Rogers S, Caldon CE, Lorca T, Castro A, Burgess A. Partial inhibition of cdk1 in g 2 phase overrides the sac and decouples mitotic events. Cell Cycle. 2014;13(9):1400-12. Epub 2014/03/15. doi: 10.4161/cc.28401. PubMed PMID: 24626186; PubMed Central PMCID: PMCPMC4050138.

23. Solis GM, Petrascheck M. Measuring caenorhabditis elegans life span in 96 well microtiter plates. J Vis Exp. 2011;(49). Epub 2011/03/30. doi: 10.3791/2496. PubMed PMID: 21445049; PubMed Central PMCID: PMCPMC3197298.

24. Merritt C, Seydoux G. Transgenic solutions for the germline. WormBook. 2010:1-21. Epub 2010/02/20. doi: 10.1895/wormbook.1.148.1. PubMed PMID: 20169625.

25. Egunsola O, Adefurin A, Fakis A, Jacqz-Aigrain E, Choonara I, Sammons H. Safety of fluconazole in paediatrics: A systematic review. Eur J Clin Pharmacol. 2013;69(6):1211-21. Epub 2013/01/18. doi: 10.1007/s00228-012-1468-2. PubMed PMID: 23325436; PubMed Central PMCID: PMCPMC3651820.

26. Turner K, Manzoni P, Benjamin DK, Cohen-Wolkowiez M, Smith PB, Laughon MM. Fluconazole pharmacokinetics and safety in premature infants. Curr Med Chem. 2012;19(27):4617-20. Epub 2012/08/11. PubMed PMID: 22876898; PubMed Central PMCID: PMCPMC3522083.

27. Lalla RV, Latortue MC, Hong CH, Ariyawardana A, D'Amato-Palumbo S, Fischer DJ, et al. A systematic review of oral fungal infections in patients receiving cancer therapy. Support Care Cancer. 2010;18(8):985-92. Epub 2010/05/08. doi: 10.1007/s00520-010-0892-z. PubMed PMID: 20449755; PubMed Central PMCID: PMCPMC2914797.

28. Martin MV. The use of fluconazole and itraconazole in the treatment of candida albicans infections: A review. J Antimicrob Chemother. 1999;44(4):429-37. Epub 1999/12/10. PubMed PMID: 10588302.

29. Anaissie EJ, Darouiche RO, Abi-Said D, Uzun O, Mera J, Gentry LO, et al. Management of invasive candidal infections: Results of a prospective, randomized, multicenter study of fluconazole versus amphotericin b and review of the literature. Clin Infect Dis. 1996;23(5):964-72. Epub 1996/11/01. PubMed PMID: 8922787.

30. Hansen M, Chandra A, Mitic LL, Onken B, Driscoll M, Kenyon C. A role for autophagy in the extension of lifespan by dietary restriction in c. Elegans. PLoS Genet. 2008;4(2):e24. Epub 2008/02/20. doi: 10.1371/journal.pgen.0040024. PubMed PMID: 18282106; PubMed Central PMCID: PMCPMC2242811.

31. Zeiler H-J, Voigt W-H, Endermann R. Efficacy of ciprofloxacin and other quinolones on stationary-phase bacteria in vitro and in vivo. Reviews of Infectious Diseases. 1988:S119-S21.

32. Zeiler HJ, Grohe K. The in vitro and in vivo activity of ciprofloxacin. Eur J Clin Microbiol. 1984;3(4):339-43. Epub 1984/08/01. PubMed PMID: 6237902.

33. Zeiler HJ. Evaluation of the in vitro bactericidal action of ciprofloxacin on cells of escherichia coli in the logarithmic and stationary phases of growth. Antimicrob Agents Chemother. 1985;28(4):524-7. Epub 1985/10/01. PubMed PMID: 2934022; PubMed Central PMCID: PMCPMC180297.

34. Khanna N, Cressman CP, 3rd, Tatara CP, Williams PL. Tolerance of the nematode caenorhabditis elegans to ph, salinity, and hardness in aquatic media. Arch Environ Contam Toxicol. 1997;32(1):110-4. Epub 1997/01/01. PubMed PMID: 9002442.

35. Zhang XD. Optimal high-throughput screening. Cambridge. http://dx. doi. org/10.1017/CBO9780511973888; 2011.

36. Fitzenberger E, Boll M, Wenzel U. Impairment of the proteasome is crucial for glucose-induced lifespan reduction in the mev-1 mutant of caenorhabditis elegans. Biochimica et Biophysica Acta (BBA)-Molecular Basis of Disease. 2013;1832(4):565-73.

4.8 Figures

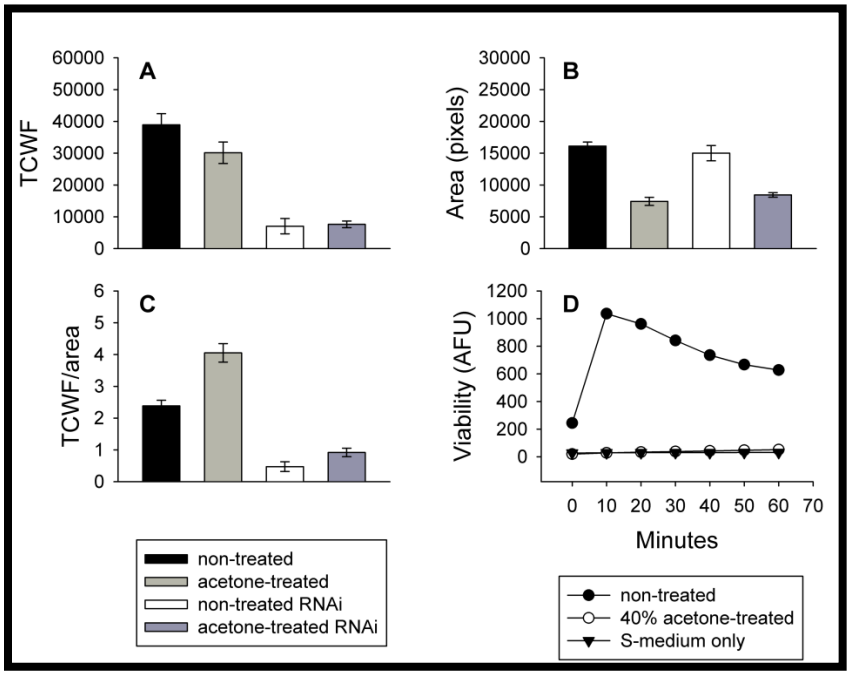

Figure 4.1. Acetone treatment kills *E. coli* and preserves capacity for RNAi knockdown. After screening various treatment conditions, we decided to investigate acetone treatment for killing HT115(DE3) *E. coli* prior to performing RNAi. We pretreated *E. coli* with 40% acetone for 2 hours at 37 °C, before washing, pelleting, and feeding the bacteria to developing GFP-expressing BC12907 *C. elegans*. The nematodes were grown for ~3.5 days and their fluorescence was determined by fluorescence microscopy (λex/λem 470/525 nm filter set) and ImageJ analysis software using the total corrected worm fluorescence method (TCWF). (A) *C. elegans* fed *E. coli* expressing dsRNA targeted to GFP showed a ~75 – 80% decreased in mean GFP fluorescence (n = 10 nematodes from each group; two-way Holm-Sidak ANOVA p-value < 0.001). (B) However, the average size on day ~3.5 of the *C. elegans* fed acetone-treated *E. coli* was approximately 50% smaller than the *C. elegans* fed non-treated *E. coli* (two-way Holm-Sidak ANOVA p-value < 0.001). (C) Correcting for the size differences by dividing average TCWF (which is partially dependent on nematode size) by the average area per nematode, showed a consistent RNAi-induced decrease in GFP fluorescence of ~80% for both acetone-treated and non-treated *E. coli* (two-way Holm-Sidak ANOVA p-value = 0.122). (D) HT115(DE3) *E. coli* treated with 40% acetone for 2 hours at 37 °C, washed and suspended in S-medium at *ad libitum* concentration (6.9 x 10^9 cells/mL), compared to an identical concentration of non-treated live HT115(DE3), and bacteria-free S-medium. Each time point represents the viability as indicated by total fluorescence (in arbitrary fluorescence units) from the respiratory conversion of resazurin to resorufin.

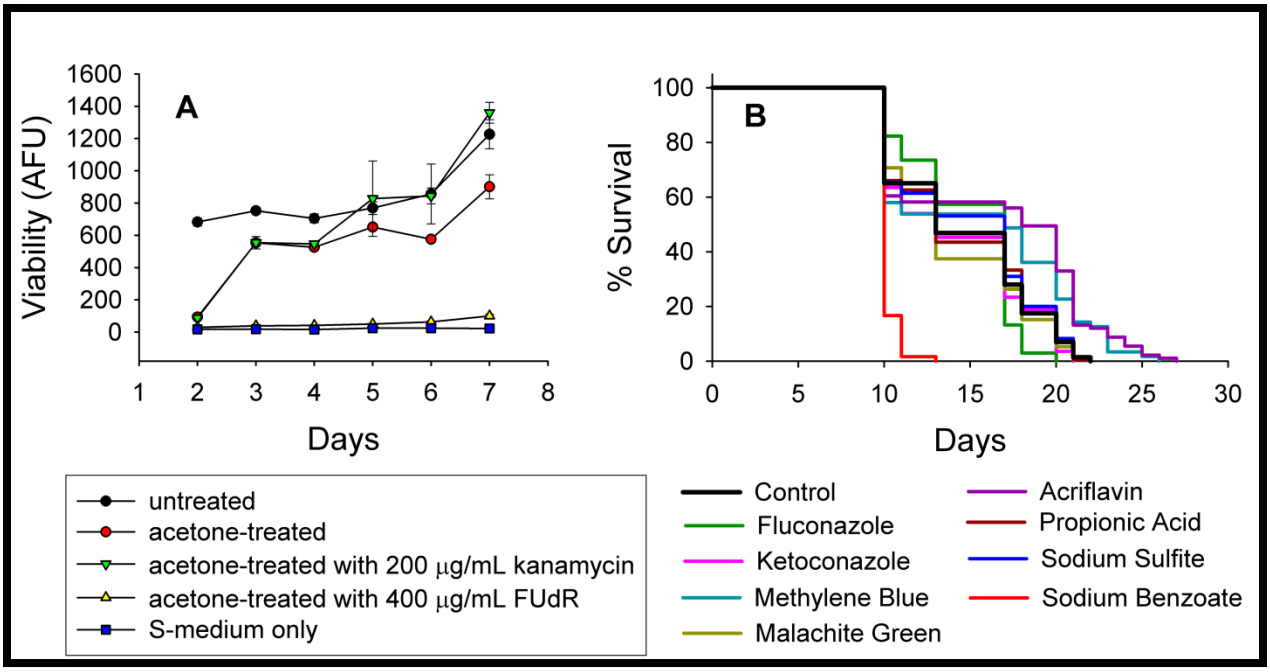

Figure 4.2. Microbial Growth in Liquid is Inhibited by the Presence of Antifungal Drugs. (A) One instance of microbial contamination from a series of microplates sealed with FEP Teflon film and incubated for one week at 20 °C. The wells of the plates contained 100 µL of S-medium with 6.9 x 10^9 cells/mL of 40% acetone-treated HT115(DE3) *E. coli* (incubated with 40% acetone for 2 hours at 37 °C, then washed, pelleted, and suspended in S-medium). Enough wells were treated with either 200 µg/mL kanamycin or 400 µg/mL FUdR for six days of resazurin viability assays to be performed in quadruplicate (n = 24 wells total for each treatment). An identical concentration of fresh live HT115(DE3) *E. coli* was used as a positive control for viability (n = 24) and S-medium was used as a negative control (n = 24). The y-axis represents the presence of respiring microbes, as indicated by the fluorescence of the viability indicator resazurin (λex/λem 528/590 nm filter set), given in arbitrary fluorescence units (AFU). (B) Kaplan-Meier survival curves of age-synchronized *C. elegans* grown in the presence of live HT115(DE3) *E. coli* (6.9 x 10^9 cells/mL) and eight different antifungal drugs. FUdR was added to all groups once the nematodes reached the L4/adult stage in order to prevent egg-laying. Compared to the untreated control (n = 143 nematodes), methylene blue treatment (2 µg/mL) showed a small but significant extension of the mean *C. elegans* lifespan by ~7% ± 4% SEM (log-rank p-value = 0.002; n = 119 nematodes). Acriflavin treatment (7 µg/mL) showed a ~13% ± 5% SEM increase in mean lifespan (log-rank p-value = 0.0000102; n = 91 nematodes), and sodium benzoate showed a ~30% ± 2% SEM decrease in mean lifespan (log-rank p-value < 0.0000001; n = 60 nematodes). The remaining antifungal drugs displayed no significant deviation from the mean control lifespan (log-rank > 0.05).

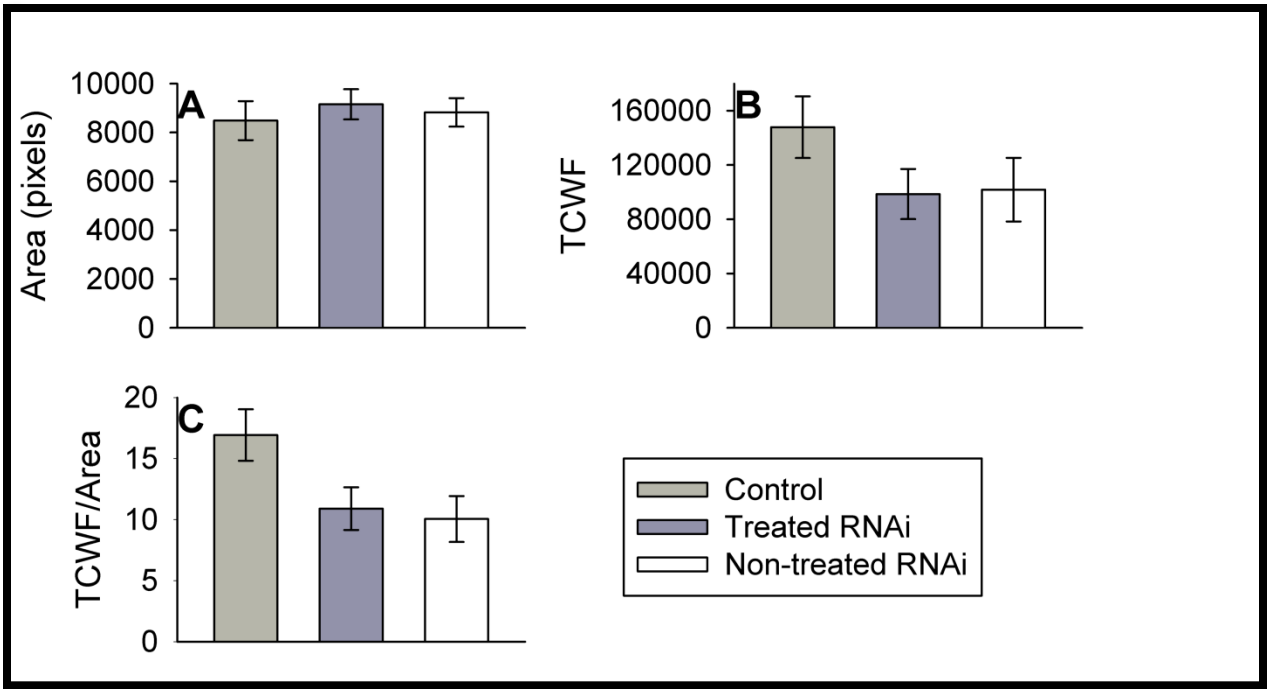

Figure 4.3. Using a 9:1 dead:live mix of HT115(DE3) *E. coli* for RNAi allows full *C. elegans* larval development and preserves ability for gene knockdown. HT115(DE3) *E. coli* expressing dsRNA targeted to GFP was pre-treated with 40% acetone for 2 hours at 37 °C, washed, pelleted, and suspended at 6.21 x 10^9 cells/mL in S-medium containing 4 µg/mL fluconazole, along with 6.9 x 10^8 cells/mL of live HT115(DE3) *E. coli* lacking a plasmid (a 9:1 dead:live total mix of *E. coli*, labeled as "treated RNAi"), and a small population of age-synchronized L1 BC12907 GFP-expressing *C. elegans* (*n* = 18 nematodes). Similar cultures were prepared using either 9:1 dead:live *E. coli* with no plasmid present in either the live or dead portion (labeled as "control"; *n* = 35 nematodes), or 100% (6.9 x 10^9 cells/mL) of plasmid containing bacteria (labeled as "non-treated RNAi"; *n* = 36 nematodes). The cultures were incubated for 3 days at 20 °C, after which *C. elegans* size (in pixels) and GFP fluorescence (as TCWF) were assessed by fluorescence microscopy (λex/λem 470/525 nm filter set) and ImageJ analysis software. (A) The size in pixels was not significantly different among any of the treatment groups, as determined by one-way analysis of variance. (B) The difference in GFP fluorescence (as TCWF) between the RNAi groups (treated RNAi and non-treated RNAi) approached significance (one-way analysis of variance rank *p*-value = 0.073), (C) and attained significance when normalized to the average area in pixels per group (one-way analysis of variance rank *p*-value = 0.013).

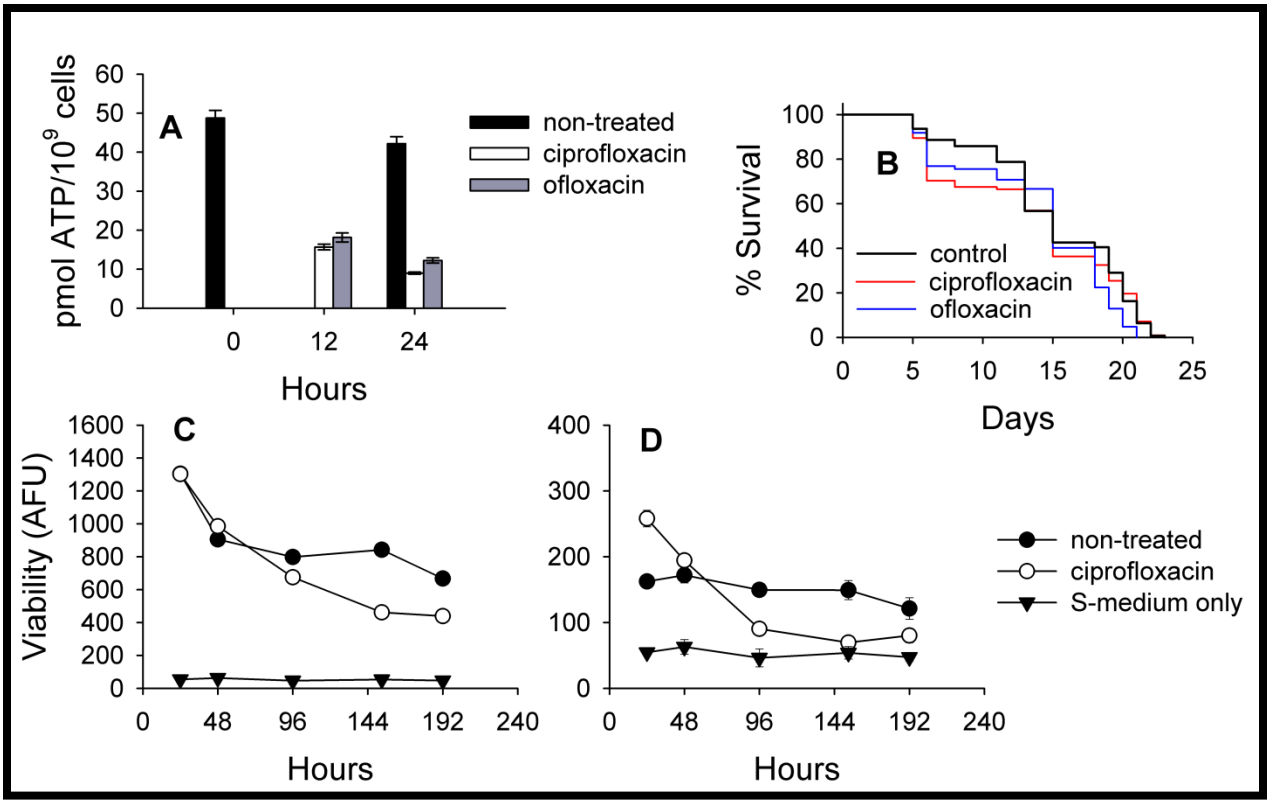

Figure 4.4. Ciprofloxacin treatment reduces both *E. coli* ATP content, and viability as determined by resazurin, and does not affect *C. elegans* lifespan. (A) Live HT115(DE3) *E. coli* were suspended at 6.9 x 10^9 cells/mL in S-medium containing 4 µg/mL fluconazole, treated with either 50 µg/mL ciprofloxacin, 50 µg/mL ofloxacin, or left non-treated (n = 16 per group). ATP was then assayed (using n = 8 per assay) at 0, 12, or 24 hours using CellTiter Glo®. (B) N2 *C. elegans* grown in liquid culture at 20 °C and fed 6.9 x 10^9 cells/mL of live HT115(DE3) *E. coli* were treated with either 50 µg/mL ciprofloxacin (n = 209 nematodes), 50 µg/mL ofloxacin (n = 147 nematodes), or left non-treated (n = 141 nematodes). FUdR was added to all groups once the nematodes reached the L4/adult stage in order to prevent egg-laying. Starting on the fifth day of culture, surviving *C. elegans* were visually scored every 1 – 3 days using a dissecting microscope. The resulting lifespans were then compared using Kaplan-Meier survival curves and log-rank analysis. Pair-wise comparison using the Holm-Sidak method showed that ciprofloxacin treatment was statistically similar to the control (p-value = 0.572), whereas ofloxacin treatment resulted in a significantly shorter lifespan (p-value = 0.0103). (C) Live HT115(DE3) *E. coli* were suspended at 100% concentration (6.9 x 10^9 cells/mL) in S-medium containing 4 µg/mL fluconazole and either treated with 50 µg/mL ciprofloxacin (n = 15) or left non-treated (n = 15). The samples were incubated at 20 °C along with samples of just S-medium with 4 µg/mL fluconazole (n = 15). At five different time points over the course of 8 days, a resazurin viability assay was performed on samples from each group (n = 3 per group). (D) A similar assay was setup using 10% *E. coli* (6.9 x 10^8 cells/mL). By approximately the sixth day, the resulting resazurin fluorescence of the ciprofloxacin-treated group was similar to that of the S-medium only control (p-value > 0.05).

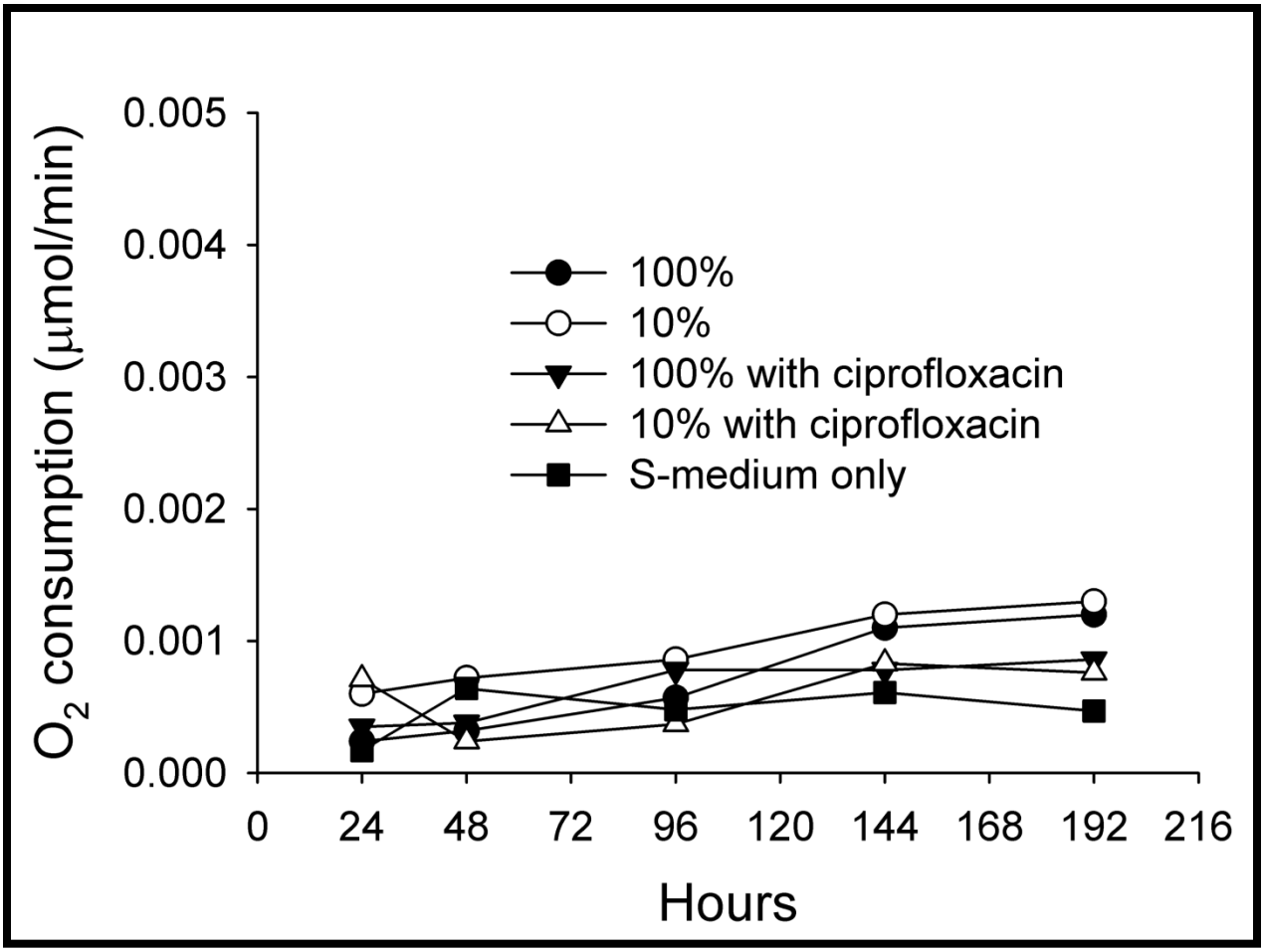

Figure 4.5. HT115(DE3) *E. coli* does not significantly consume oxygen in long-term S-medium cultures. Live HT115(DE3) *E. coli* was suspended at either 100% (6.9 x 10^9 cells/mL) or 10% (6.9 x 10^8 cells/mL) in S-medium with 4 µg/mL fluconazole (n = 15 each), and incubated at 20 °C. S-medium only samples (containing 4 µg/mL fluconazole) were similarly incubated as a negative control (n = 15). For each group, at each time point, three samples were combined in the chamber of a Clark oxygen electrode, and the rate of oxygen consumption was calculated over the course of 10 minutes. A one-way analysis of variance of the respiratory rate of all groups revealed no significant difference between live *E. coli* in culture and an S-medium-only control (p-value = 0.202).

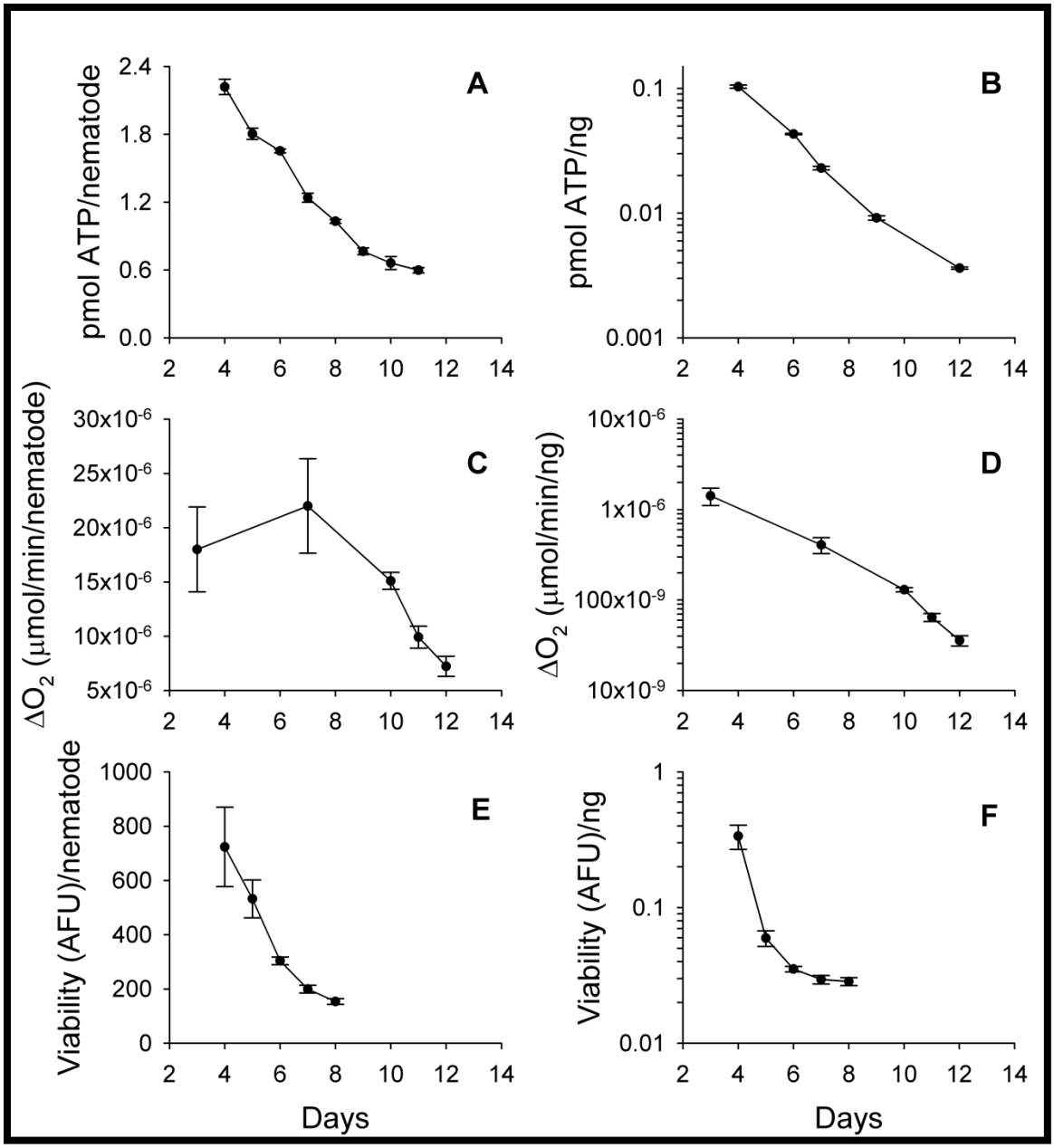

Figure 4.6. Oxygen consumption, ATP content, and reductive capacity decline with age in *C. elegans*. Age-synchronized *C. elegans* were grown in S-medium at 20 °C in 2L flasks with moderate shaking, and fed 6.9 x 10^9 cells/mL HT115(DE3) *E. coli*. Additional bacteria were added over the course of the incubation as deemed necessary by visual examination of the media. FUdR was added once the nematodes reached the L4/adult stage in order to prevent egg-laying. For each time point, a sample was removed from the culture, washed and pelleted 4 times to remove bacteria, and suspended in M9 buffer at a concentration of 2 nematodes/µL. A portion was saved for assaying protein content and the remaining was used for ATP assays (using CellTiter Glo®; panels A and B), oxygen consumption measurements (using a Clark oxygen electrode; panels C and D), and resazurin-based viability measurements (panels E and F). Note: panels B, D, and F are shown with the *y*-axis in log scale.

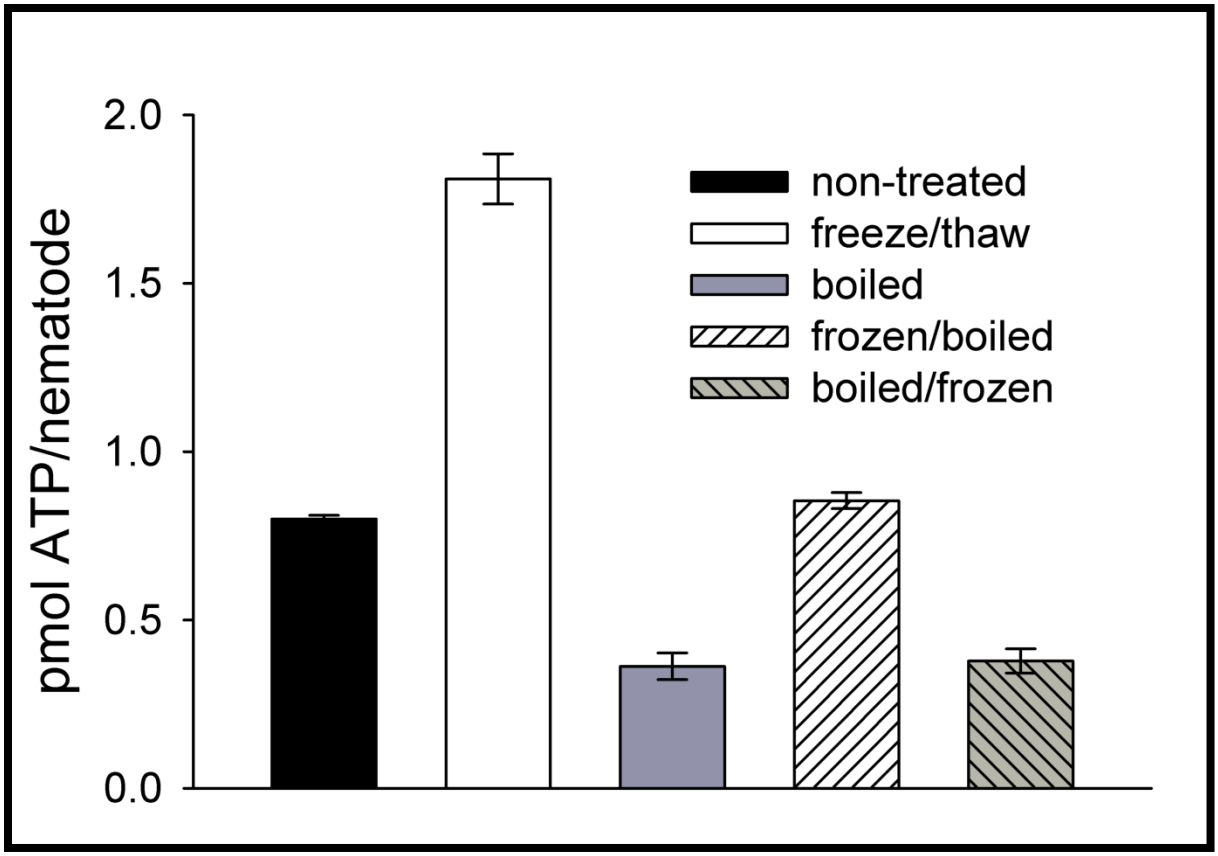

Figure 4.7. Various treatment conditions for disrupting the *C. elegans* cuticle. A liquid culture of age-synchronized N2 *C. elegans* was prepared using L1 larva, 6.9 x 10^9 cells/mL HT115(DE3) *E. coli* and 4 μg/mL fluconazole. On the third day of culture, samples of *C. elegans* were removed and washed 4 times to remove bacteria. The *C. elegans* were then suspended in 100 μL of fresh S-medium at a concentration of 1 nematode/μL, and subjected to either a snap freeze in liquid nitrogen, followed by a 20 minute thaw at 37 °C, followed by 10 minutes of incubation at room temperature at 20 °C (labeled "freeze/thaw"); incubation at 100 °C for 1 minute, followed by cooling to room temperature for 10 minutes (labeled "boiled"); snap frozen in liquid nitrogen, followed by a rapid thaw at 100 °C, where it was then left for 1 minute once liquid, and then allowed to cool for 10 minutes at room temperature (labeled "frozen/boiled"); or incubated at 100 °C for 1 minute, followed by a snap freeze in liquid nitrogen, a 20 minute thaw at 37 °C, and a 10 minute adjustment to room temperature (labeled "frozen/boiled").

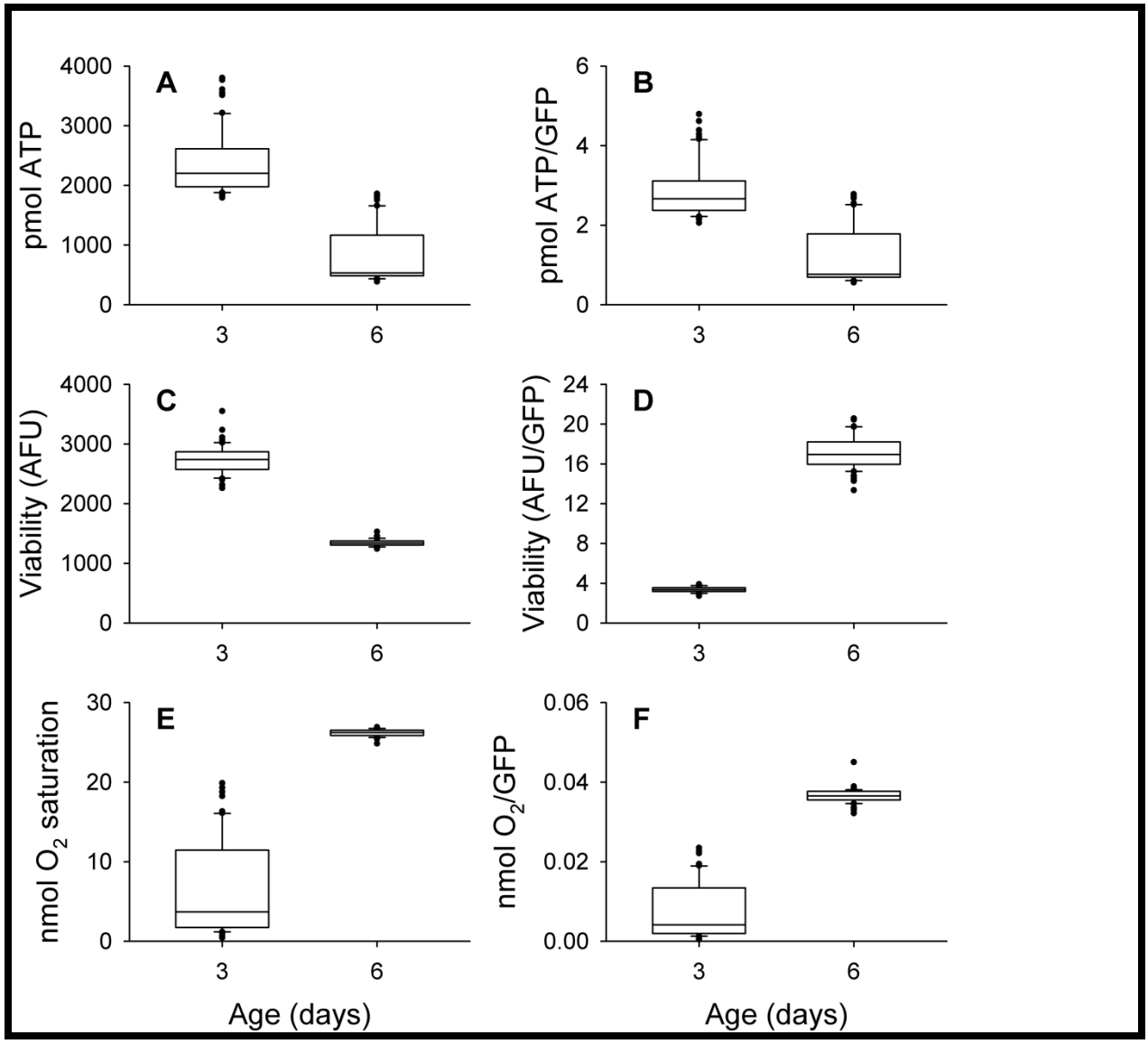

Figure 4.8. Ciprofloxacin-treated 9:1 dead:live mix of *E. coli* allows adequate measurement of ATP content, oxygen saturation, and reductive capacity between 3- and 6-day-old *C. elegans*. Three- and six-day-old BC12907 *C. elegans* were washed free of bacteria, and placed at ~200 nematodes/well in S-medium with 6.9 x 10^9 cell/mL HT115(DE3) *E. coli*, which had been treated for 6 days with 4 μg/mL fluconazole and 50 μg/mL ciprofloxacin. (A) CellTiter-Glo® was used to measure ATP content after a single freeze/thaw cycle in liquid nitrogen. (B) ATP content normalized to the GFP fluorescence of the *C. elegans* gave worse separation between the ATP content of the two groups. (C) Reductive capacity measured by resazurin fluorescence, after a similar freeze/thaw cycle in liquid nitrogen. (D) Reductive capacity normalized to the GFP fluorescence of the *C. elegans*. (E) Rate of oxygen consumption as measured by the level of oxygen saturation in wells of OXOPlates®. (F) Oxygen saturation normalized to *C. elegans* GFP fluorescence.

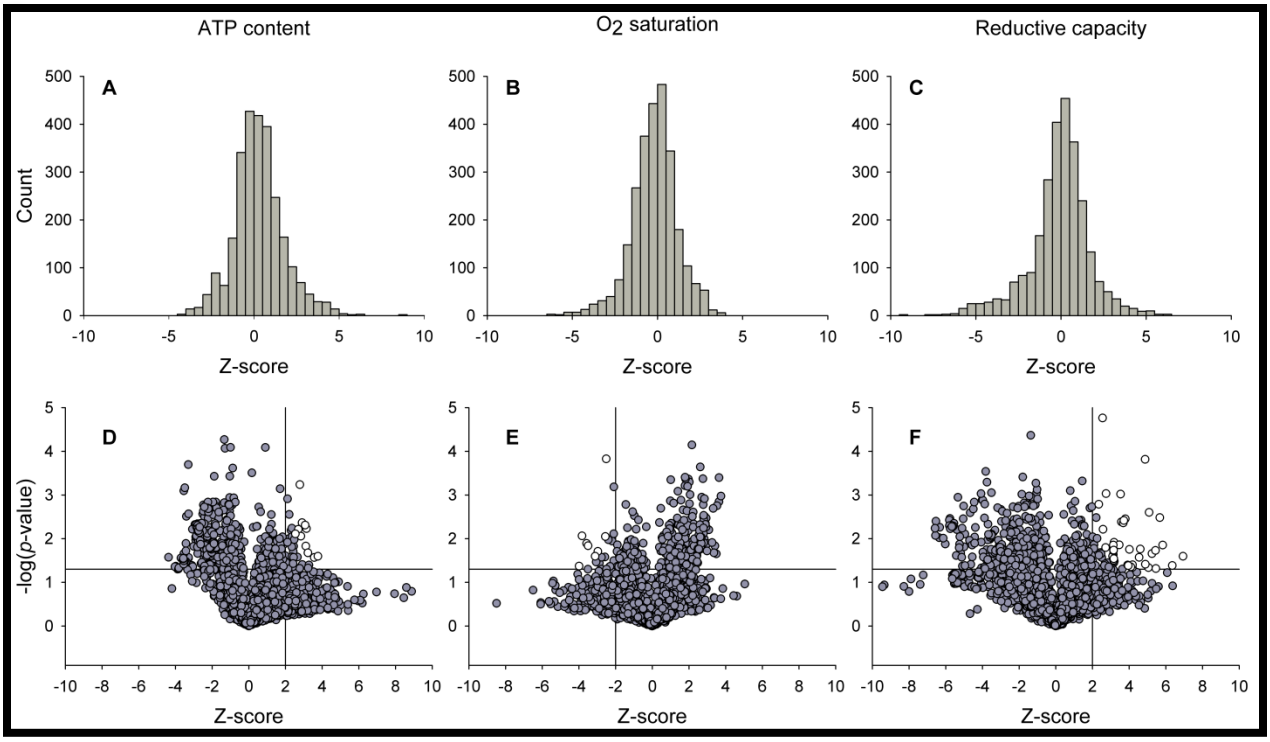

Figure 4.9. An RNAi screen of the X chromosome reveals genes affecting ATP content, oxygen consumption, and reductive capacity. All three screens produced a Gaussian distribution of standardized mean measurements (upper panels A, B, and C). The lower panels (D, E, and F) show individual standardized mean measurements (shaded gray circles), sorted z-score (*x*-axis), and significance indicated by the negative log of the *p*-value obtained by comparing the three replicates for each measurement to the overall theoretical population mean (zero) by an unpaired two-tailed t-test. The vertical line indicates standard deviation value used for hit determination, and the horizontal line indicates the –log associated with a *p*-value threshold of 0.05. Circles shaded in white represent individual standardized mean measurements regarded as hits. In other words, the white shaded circles are gene knockdowns that were more than 2 standard deviations beyond the mean (+2 for ATP content and reductive capacity, and -2 for oxygen saturation) as determined by the 95% confidence interval for that set of measurements, with a *p*-value less than 0.05.

4.9 Tables

Table 4.1. Bacterial viability after various treatments. A total of 111 different treatment conditions were investigated for their potential to kill *E. coli*, varying in chemical treatment, incubation time, and incubation temperature. Prior to the assays, the bacteria were washed and suspended in S-medium at an *ad libitum* feeding concentration. The % control viability column lists the resulting viability as determined by the fluorescence of the reporter dye resazurin (λex/λem 528/590 nm filter set), given as a percentage of the fluorescence of an assayed untreated bacterial control for that specific trial. Statistical significance was investigated by the comparison of each treatment to the untreated bacterial control, and to S-medium lacking bacteria (unpaired two-tailed *t*-test; *p*-values < 0.05 are displayed in bold).

Treatment	Temperature (°C)	Incubation	% Control viability	± SEM	vs. Untreated *E. coli* *p*-value	vs. S-medium Only *p*-value
S-medium only	N/A	N/A	3%	0%	**4.373E-03**	1.000E+00
30% ethanol with 1 mM IPTG	50	3 days	4%	0%	**1.923E-04**	**3.926E-03**
30% ethanol with 25 mM citrate and 10 mM EDTA at pH 5.2	50	3 days	5%	0%	**1.961E-04**	**5.643E-04**
30% ethanol with 25 mM citrate, 10 mM EDTA, and 1 mM IPTG at pH 5.2	50	3 days	5%	0%	**1.971E-04**	**2.132E-04**
untreated	50	24 hrs	6%	0%	**2.195E-05**	**7.673E-05**
25 mM citrate and 10 mM ETDA at pH 5.2	50	24 hrs	7%	0%	**2.495E-05**	**1.024E-05**
100% ethanol	37	2 hrs	7%	0%	**1.038E-04**	**6.744E-06**
46.6% ammonium sulfate with 25 mM citrate and 10 mM EDTA at pH 5.2	50	24 hrs	7%	0%	**2.468E-05**	**5.270E-06**
30% ethanol	50	3 days	7%	0%	**1.981E-04**	**5.187E-05**
46.6% ammonium sulfate with 25 mM citrate and 10 mM EDTA at pH 5.2	37	24 hrs	8%	0%	**2.472E-05**	**3.038E-06**
40% ethanol	37	2 hrs	8%	0%	**1.037E-04**	**4.926E-06**
40% acetone	37	2 hrs	8%	0%	**1.082E-04**	**1.446E-06**
70% acetone	37	2 hrs	8%	0%	**1.098E-04**	**8.890E-07**
30% ethanol	50	3 days	8%	1%	**1.697E-03**	**4.225E-06**
100% acetone	37	2 hrs	8%	0%	**1.087E-04**	**1.267E-06**
70% ethanol	37	2 hrs	8%	0%	**1.072E-04**	**1.932E-06**
100 μM potassium cyanide	50	3 days	8%	1%	**1.680E-03**	**3.207E-05**
30% ethanol with 25 mM citrate, 10 mM EDTA, and 1 mM IPTG at pH 5.2	37	3 days	9%	1%	**1.930E-04**	**3.838E-05**
100 μM potassium cyanide	50	2 days	9%	1%	**2.490E-04**	**6.318E-05**
46.6% ammonium sulfate	50	2 days	9%	1%	**2.773E-04**	**6.466E-06**
30% ethanol	50	2 days	9%	0%	**2.917E-04**	**7.907E-07**
46.6% ammonium sulfate	50	3 days	10%	1%	**1.754E-03**	**1.049E-05**
100 μM zinc sulfate	50	2 days	10%	1%	**2.749E-04**	**8.225E-06**
30% ethanol	20	3 days	12%	2%	**1.627E-03**	**5.077E-03**
40% acetone with 25 mM citrate and EDTA at pH 5.2	37	2 hrs	14%	1%	**1.653E-04**	**3.165E-06**
40% acetone	50	2 hrs	14%	1%	**1.756E-04**	**1.557E-06**
40% acetone	37	2 hrs	14%	1%	**7.964E-07**	**9.892E-04**
40% acetone with 25 mM citrate and EDTA at pH 5.2	50	2 hrs	15%	1%	**2.130E-04**	**3.632E-08**
100 μM zinc sulfate	50	3 days	15%	2%	**1.986E-03**	**9.728E-06**

Table 4.1 (Continued)

Treatment	Temperature (°C)	Incubation	% Control viability	± SEM	vs. Untreated *E. coli* *p*-value	vs. S-medium Only *p*-value
40% ethanol	50	2 hrs	15%	1%	**2.205E-04**	**2.013E-08**
40% ethanol with 25 mM citrate and EDTA at pH 5.2	50	2 hrs	15%	1%	**1.974E-04**	**3.079E-07**
46.6% ammonium sulfate	20	2 days	16%	1%	**2.664E-04**	**5.488E-06**
40% ethanol with 25 mM citrate and EDTA at pH 5.2	37	2 hrs	18%	1%	**1.017E-06**	**4.812E-04**
46.6% ammonium sulfate	4	2 days	19%	1%	**3.965E-04**	**1.268E-07**
30% ethanol with 25 mM citrate and 10 mM EDTA at pH 5.2	37	3 days	19%	1%	**2.897E-04**	**5.640E-08**
46.6% ammonium sulfate with 25 mM citrate and 10 mM EDTA at pH 5.2	50	3 days	20%	2%	**2.062E-06**	**8.844E-04**
30% ethanol	37	3 days	21%	1%	**2.316E-04**	**8.253E-07**
30% ethanol with 1 mM IPTG	37	3 days	24%	1%	**3.176E-04**	**4.929E-08**
46.6% ammonium sulfate with 25 mM citrate, 10 mM EDTA, and 1 mM IPTG at pH 5.2	50	3 days	24%	1%	**2.712E-04**	**2.592E-07**
46.6% ammonium sulfate with 25 mM citrate, 10 mM EDTA, and 1 mM IPTG at pH 5.2	37	3 days	28%	2%	**5.031E-06**	**8.291E-04**
46.6% ammonium sulfate with 25 mM citrate and 10 mM EDTA at pH 5.2	20	24 hrs	30%	1%	**7.111E-08**	**2.422E-08**
46.6% ammonium sulfate with 25 mM citrate and 10 mM EDTA at pH 5.2	37	3 days	30%	2%	**4.052E-06**	**8.514E-05**
46.6% ammonium sulfate with 25 mM citrate and 10 mM EDTA at pH 5.2	4	24 hrs	40%	2%	**4.467E-07**	**9.645E-05**
40% ethanol	37	2 hrs	48%	3%	**3.141E-05**	**3.026E-04**
25 mM citrate and 10 mM ETDA at pH 5.2	37	24 hrs	62%	3%	**3.769E-05**	**2.243E-04**
40% ethanol	20	90 min	69%	7%	**6.891E-03**	**2.588E-03**
40% acetone	20	90 min	75%	3%	**7.049E-04**	**1.219E-04**
46.6% ammonium sulfate	20	3 days	76%	6%	6.622E-02	**3.002E-11**
100% methanol	20	90 min	83%	5%	**2.108E-02**	**4.741E-04**
25 mM citrate and 10 mM ETDA at pH 5.2	4	24 hrs	87%	5%	5.763E-02	**4.855E-04**
25 mM citrate and 10 mM EDTA at pH 5.2	20	2 hrs	89%	5%	8.161E-02	**2.002E-04**
100 μM potassium cyanide	4	2 days	89%	10%	3.129E-01	**2.457E-03**
100 μM potassium cyanide	20	2 days	90%	9%	3.143E-01	**1.700E-03**
untreated	60	20 hrs	90%	5%	1.173E-01	**3.769E-04**
untreated	60	14 hrs	91%	9%	3.332E-01	**1.729E-03**
46.6% ammonium sulfate	4	3 days	91%	9%	3.884E-01	**2.255E-04**
100 μM potassium cyanide	20	3 days	91%	13%	5.370E-01	**3.007E-03**
untreated	60	22 hrs	92%	5%	1.954E-01	**3.035E-04**
100 μM zinc sulfate	20	2 days	92%	6%	2.489E-01	**1.712E-04**
untreated	60	18 hrs	92%	4%	1.139E-01	**9.010E-05**
25 mM citrate and 10 mM EDTA at pH 5.2	4	2 hrs	92%	6%	2.586E-01	**3.286E-04**
untreated	60	16 hrs	93%	5%	2.569E-01	**2.603E-04**
25 mM citrate and 10 mM ETDA at pH 5.2	20	24 hrs	95%	6%	3.824E-01	**3.914E-04**
80% methanol	20	90 min	95%	13%	7.360E-01	**4.695E-03**
1:1 40% ethanol:acetone	20	90 min	96%	5%	4.225E-01	**1.536E-04**
30% ethanol	20	2 days	100%	5%	9.803E-01	**1.791E-05**

Table 4.1 (Continued)

Treatment	Temperature (°C)	Incubation	% Control viability	± SEM	vs. Untreated *E. coli* *p*-value	vs. S-medium Only *p*-value
125 mM propionic acid	20	90 min	106%	8%	5.040E-01	**4.003E-02**
100 μM potassium cyanide	4	3 days	107%	10%	4.713E-01	**4.581E-05**
untreated	4	24 hrs	108%	5%	1.914E-01	**2.078E-04**
25 mM citrate and 10 mM EDTA at pH 5.2	37	2 hrs	109%	7%	2.201E-01	**2.725E-04**
untreated	20	24 hrs	109%	4%	5.254E-02	**5.279E-05**
125 mM lactic acid	20	90 min	110%	8%	3.016E-01	**4.086E-03**
100 μM zinc sulfate	4	2 days	113%	6%	5.238E-02	**3.220E-05**
70% methanol	20	90 min	114%	16%	4.829E-01	**4.984E-03**
40% acetone	4	2 hrs	114%	7%	9.484E-02	**3.112E-04**
40% acetone	20	90 min	116%	9%	1.524E-01	**4.807E-03**
90% methanol	20	90 min	116%	14%	3.121E-01	**1.402E-02**
untreated	37	24 hrs	117%	3%	**1.529E-03**	**1.641E-05**
40% acetone with 25 mM citrate and EDTA at pH 5.2	20	2 hrs	118%	5%	**1.759E-02**	**3.657E-12**
30% ethanol	4	2 days	121%	8%	**2.343E-02**	**1.928E-04**
30% ethanol	4	3 days	122%	11%	6.634E-02	**1.504E-04**
60% ethanol	20	90 min	123%	7%	**1.945E-02**	**1.432E-04**
25 mM citrate and 10 mM EDTA at pH 5.2	50	2 hrs	124%	9%	**2.779E-02**	**5.150E-04**
100 μM zinc sulfate	20	3 days	125%	14%	8.575E-02	**8.399E-04**
40% ethanol	20	90 min	127%	20%	1.831E-01	9.857E-02
100% methanol	20	90 min	131%	18%	1.836E-01	**4.585E-03**
70% ethanol	20	90 min	131%	12%	**4.980E-02**	5.368E-02
6 M urea with 1 mM DTT and 1 mM iodoacetomide	37	2 hrs	132%	17%	**4.923E-02**	**3.805E-05**
100% ethanol with 1 mM DTT and 1mM iodoacetomide	37	2 hrs	138%	17%	5.628E-02	**6.260E-12**
100 μM zinc sulfate	4	3 days	143%	13%	**4.534E-03**	**9.360E-05**
60% acetone	20	90 min	145%	14%	**2.732E-02**	**7.745E-03**
100% acetone with 1 mM DTT and 1 mM iodoacetomide	37	2 hrs	149%	19%	**9.459E-03**	**3.431E-05**
40% acetone	20	2 hrs	151%	9%	**7.485E-04**	**2.349E-04**
50%ethanol	20	90 min	152%	22%	9.691E-02	**5.968E-03**
46.6% ammonium sulfate with 25 mM citrate and 10 mM EDTA at pH 5.2	50	2 hrs	158%	9%	**3.183E-04**	**1.902E-04**
50% acetone	20	90 min	163%	18%	**2.021E-02**	**1.029E-02**
40% ethanol	4	2 hrs	164%	10%	**3.099E-04**	**2.311E-04**
40% ethanol with 25 mM citrate and EDTA at pH 5.2	20	2 hrs	166%	11%	**5.482E-04**	**3.704E-04**
46.6% ammonium sulfate with 25 mM citrate and 10 mM EDTA at pH 5.2	20	2 hrs	179%	10%	**1.032E-04**	**1.979E-04**
46.6% ammonium sulfate with 25 mM citrate and 10 mM EDTA at pH 5.2	37	2 hrs	192%	12%	**1.058E-04**	**2.749E-04**
46.6% ammonium sulfate with 25 mM citrate and 10 mM EDTA at pH 5.2	4	2 hrs	193%	8%	**1.391E-06**	**9.321E-06**
46.6% sodium sulfate	0	2 hrs	197%	35%	**3.863E-03**	**7.719E-04**
40% ethanol with 25 mM citrate and EDTA at pH 5.2	4	2 hrs	205%	9%	**1.035E-06**	**1.012E-05**
40% acetone with 25 mM citrate and EDTA at pH 5.2	4	2 hrs	208%	9%	**2.056E-06**	**2.355E-05**
20% ammonium sulfate	20	2 hrs	215%	47%	**1.743E-02**	**6.640E-03**

Table 4.1 (Continued)

Treatment	Temperature (°C)	Incubation	% Control viability	± SEM	vs. Untreated *E. coli* *p*-value	vs. S-medium Only *p*-value
40% ethanol	20	2 hrs	216%	12%	**1.238E-05**	**1.112E-04**
46.6% ammonium sulfate	0	2 hrs	237%	42%	**1.125E-03**	**8.364E-04**
46.6% sodium sulfate	20	2 hrs	239%	63%	**3.765E-02**	**1.782E-02**
20% sodium sulfate	20	2 hrs	245%	53%	**1.003E-02**	**6.539E-03**
20% sodium sulfate	0	2 hrs	256%	53%	**5.568E-03**	**4.706E-03**
20% ammonium sulfate	0	2 hrs	267%	45%	**2.198E-04**	**2.997E-04**
46.6% ammonium sulfate	20	2 hrs	344%	80%	**6.363E-03**	**9.466E-03**

Table 4.2. Resulting RNAi knockdown of GFP produced from bacteria treated by various conditions. A total of 36 different treatment conditions were investigated using bacteria expressing dsRNA targeted for knockdown of GFP expression. Several conditions were investigated with bacteria lacking the associated plasmid as controls (14 treatments). Prior to the assays, the bacteria were washed and suspended in S-medium at an *ad libitum* feeding concentration. An age-synchronized culture of GFP-expressing *C. elegans* (BC12907 strain) was then grown for ~3.5 days in each of the pre-treated bacterial samples. The resulting *C. elegans* GFP expression was determined by fluorescence microscopy ($\lambda_{ex}/\lambda_{em}$=470/525 nm filter set) and quantitated by calculating the average total corrected worm fluorescence (TCWF) in each sample (n = 3 to 14 nematodes per sample, with a mode of 6 nematodes). The column labeled "% Control TCWF" represents the resulting percentage of average TCWF for each treatment divided by the average TCWF of BC12907 *C. elegans* fed *ad libitum* HT115(DE3) *E. coli* lacking the plasmid for RNAi. The *p*-values are from unpaired two-tailed *t*-test, with *p*-values < 0.05 displayed in bold.

RNAi	Treatment	Temperature (°C)	Incubation	% Control TCWF	± SEM	vs. Control *p*-value	vs. Knockdown *p*-value
Yes	GFP RNAi positive control	N/A	N/A	20%	3%	N/A	N/A
yes	no treatment	60	20 hrs	19%	2%	**4.673E-04**	8.702E-01
yes	propionic acid	20	90 min	17%	11%	**1.261E-03**	8.486E-01
yes	80% methanol	20	90 min	19%	3%	**2.916E-04**	8.308E-01
yes	40% ethanol	20	90 min	21%	6%	**2.956E-04**	8.006E-01
yes	90% methanol	20	90 min	22%	5%	**3.209E-04**	6.879E-01
yes	70% acetone	20	90 min	17%	4%	**2.095E-04**	6.204E-01
yes	60% ethanol	20	90 min	23%	5%	**3.793E-04**	4.988E-01
yes	1:1 40% ethanol:acetone	20	90 min	16%	2%	**4.317E-04**	3.318E-01
no	propionic acid	20	90 min	42%	22%	**3.174E-02**	3.143E-01
yes	no treatment	60	22 hrs	12%	3%	**2.207E-04**	2.987E-01
yes	40% acetone	20	90 min	23%	3%	**5.829E-04**	2.943E-01
yes	50% ethanol	20	90 min	30%	10%	**8.804E-04**	2.807E-01
yes	100% methanol	20	90 min	27%	5%	**5.419E-04**	2.483E-01
yes	70% ethanol	20	90 min	29%	8%	**6.313E-04**	1.729E-01
yes	60% acetone	20	90 min	28%	7%	**5.807E-04**	1.521E-01
yes	50% acetone	20	90 min	29%	8%	**7.102E-04**	1.495E-01
yes	100% methanol	20	90 min	14%	2%	**3.066E-04**	1.384E-01
yes	no treatment	60	14 hrs	7%	3%	**1.401E-04**	9.520E-02
no	100% methanol	20	90 min	43%	13%	**1.157E-02**	9.463E-02

Table 4.2 (Continued)

RNAi	Treatment	Temperature (°C)	Incubation	% Control TCWF	± SEM	vs. Control *p*-value	vs. Knockdown *p*-value
yes	40% acetone	20	90 min	40%	12%	**4.274E-03**	8.461E-02
no	70% ethanol	20	90 min	52%	15%	**4.219E-02**	5.324E-02
yes	30% EtOH with citrate and EDTA, pH 5.2	50	3 days	33%	5%	**2.023E-05**	**4.469E-02**
yes	no treatment	60	16 hrs	11%	2%	**2.525E-04**	**2.385E-02**
no	60% acetone	20	90 min	56%	15%	**3.179E-02**	**1.974E-02**
yes	30% EtOH with citrate, EDTA, and IPTG, pH 5.2	50	3 days	35%	4%	**2.231E-05**	**1.911E-02**
no	80% methanol	20	90 min	56%	15%	**3.924E-02**	**1.829E-02**
no	70% acetone	20	90 min	64%	16%	9.895E-02	**1.645E-02**
yes	46.6% ammonium sulfate with citrate, EDTA, and IPTG, pH 5.2	37	3 days	135%	33%	3.152E-01	**1.285E-02**
no	60% ethanol	20	90 min	42%	11%	**3.195E-02**	**1.204E-02**
no	70% methanol	20	90 min	58%	14%	**3.960E-02**	**9.617E-03**
yes	30% ethanol with citrate, EDTA, and IPTG, pH 5.2	37	3 days	72%	14%	9.487E-02	**8.068E-03**
no	90% methanol	20	90 min	69%	16%	1.463E-01	**5.675E-03**
yes	70% methanol	20	90 min	42%	10%	**6.877E-03**	**4.533E-03**
no	40% acetone	20	90 min	87%	19%	5.388E-01	**3.098E-03**
no	50% acetone	20	90 min	80%	17%	3.619E-01	**2.759E-03**
yes	46.6% ammonium sulfate with citrate and EDTA, pH 5.2	50	3 days	160%	28%	5.946E-02	**2.120E-03**
yes	no treatment	60	18 hrs	8%	1%	**2.618E-04**	**1.717E-03**
yes	30% ethanol with citrate, EDTA, and IPTG, pH 5.2	37	3 days	177%	28%	**2.232E-02**	**1.134E-03**
yes	30% ethanol with IPTG	37	3 days	146%	25%	8.041E-02	**9.557E-04**
yes	30% ethanol	50	3 days	48%	8%	**7.617E-04**	**4.388E-04**
yes	30% ethanol with citrate and EDTA, pH 5.2	37	3 days	121%	17%	2.245E-01	**1.796E-04**
yes	46.6% ammonium sulfate with citrate and EDTA, pH 5.2	37	3 days	174%	22%	**2.320E-03**	**1.592E-04**
yes	lactic acid	20	90 min	103%	20%	8.803E-01	**1.520E-04**
yes	30% ethanol with IPTG	50	3 days	53%	9%	**2.352E-03**	**1.174E-04**
no	50% ethanol	20	90 min	65%	17%	1.787E-01	**7.743E-05**
yes	46.6% ammonium sulfate with citrate, EDTA, and IPTG, pH 5.2	50	3 days	244%	27%	**2.536E-05**	**4.034E-05**
no	lactic acid	20	90 min	106%	19%	7.643E-01	**1.117E-05**
yes	40% ethanol	20	90 min	59%	7%	**6.543E-03**	**7.084E-06**
no	40% ethanol	20	90 min	96%	15%	8.294E-01	**4.440E-10**

Table 4.3. Nematode size and/or developmental rate varies among the bacterial treatments. The size of the nematodes grown in each sample of bacteria was assessed by dividing the average area (in pixels) of the nematodes by the average area (in pixels) of nematodes grown without RNAi, and is listed in the column labeled "% Control Area." The *p*-values are from unpaired two-tailed *t*-test, with *p*-values < 0.05 displayed in bold.

RNAi	Treatment	Temperature (°C)	Incubation	% Control Area	± SEM	vs. Control *p*-value	vs. Knockdown *p*-value
Yes	GFP RNAi positive control	N/A	N/A	44%	5%	N/A	N/A

Table 4.3 (Continued)

RNAi	Treatment	Temperature (°C)	Incubation	% Control Area	± SEM	vs. Control *p*-value	vs. Knockdown *p*-value
yes	no treatment	60	16 hrs	45%	10%	**6.888E-03**	9.553E-01
yes	100% methanol	20	90 min	43%	6%	**6.416E-03**	9.306E-01
yes	no treatment	60	22 hrs	45%	10%	**1.268E-02**	9.163E-01
yes	90% methanol	20	90 min	46%	8%	**1.486E-03**	8.268E-01
yes	40% ethanol	20	90 min	47%	8%	**1.819E-03**	7.809E-01
yes	no treatment	60	18 hrs	48%	9%	**1.745E-03**	6.926E-01
yes	no treatment	60	14 hrs	51%	11%	**2.211E-02**	6.121E-01
no	propionic acid	20	90 min	62%	20%	1.011E-01	3.727E-01
yes	propionic acid	20	90 min	30%	13%	**2.059E-03**	2.767E-01
yes	no treatment	60	20 hrs	56%	9%	**1.096E-02**	2.629E-01
yes	30% ethanol with citrate and EDTA, pH 5.2	50	3 days	52%	5%	**1.749E-04**	2.281E-01
yes	100% methanol	20	90 min	58%	12%	**2.483E-02**	2.086E-01
yes	60% acetone	20	90 min	58%	12%	**1.368E-02**	1.826E-01
yes	1:1 40% ethanol:acetone	20	90 min	65%	12%	1.189E-01	1.719E-01
yes	70% acetone	20	90 min	53%	7%	**3.617E-03**	1.665E-01
yes	80% methanol	20	90 min	55%	8%	**4.840E-03**	1.117E-01
yes	40% acetone	20	90 min	76%	18%	2.418E-01	8.469E-02
yes	50% ethanol	20	90 min	66%	15%	7.130E-02	7.113E-02
yes	50% acetone	20	90 min	65%	12%	**4.977E-02**	6.893E-02
yes	30% ethanol with citrate, EDTA, and IPTG, pH 5.2	50	3 days	65%	7%	**3.764E-03**	5.991E-02
no	70% ethanol	20	90 min	67%	14%	9.090E-02	5.663E-02
yes	46.6% ammonium sulfate with citrate, EDTA, and IPTG, pH 5.2	37	3 days	156%	44%	2.467E-01	**4.487E-02**
no	100% methanol	20	90 min	72%	17%	1.551E-01	**3.513E-02**
yes	60% ethanol	20	90 min	66%	11%	**3.095E-02**	**3.118E-02**
no	90% methanol	20	90 min	105%	23%	8.379E-01	**2.082E-02**
yes	70% methanol	20	90 min	74%	16%	1.840E-01	**1.904E-02**
yes	40% acetone	20	90 min	80%	19%	3.639E-01	**1.713E-02**
yes	70% ethanol	20	90 min	88%	18%	5.539E-01	**1.350E-02**
no	80% methanol	20	90 min	75%	15%	1.791E-01	**1.092E-02**
yes	30% ethanol with IPTG	50	3 days	76%	8%	**2.758E-02**	**6.783E-03**
yes	30% ethanol	50	3 days	78%	9%	5.822E-02	**5.354E-03**
yes	30% ethanol with citrate, EDTA, and IPTG, pH 5.2	37	3 days	81%	12%	1.727E-01	**3.801E-03**
no	70% methanol	20	90 min	78%	14%	2.012E-01	**3.468E-03**
yes	46.6% ammonium sulfate with citrate and EDTA, pH 5.2	50	3 days	166%	26%	**3.340E-02**	**2.561E-03**
no	60% ethanol	20	90 min	101%	27%	9.626E-01	**1.499E-03**
yes	30% ethanol	37	3 days	159%	23%	**1.866E-02**	**1.451E-03**
no	60% acetone	20	90 min	80%	13%	1.969E-01	**1.139E-03**
yes	lactic acid	20	90 min	130%	22%	1.488E-01	**4.374E-04**
no	70% acetone	20	90 min	93%	17%	6.990E-01	**3.752E-04**
yes	40% ethanol	20	90 min	95%	13%	7.347E-01	**2.152E-04**
no	50% ethanol	20	90 min	100%	14%	9.860E-01	**2.954E-05**
yes	30% ethanol with citrate and EDTA, pH 5.2	37	3 days	101%	13%	9.494E-01	**2.358E-05**
no	50% acetone	20	90 min	101%	14%	9.395E-01	**2.203E-05**
yes	30% ethanol with IPTG	37	3 days	102%	12%	8.638E-01	**1.307E-05**
no	40% acetone	20	90 min	110%	17%	5.505E-01	**2.296E-06**
no	lactic acid	20	90 min	118%	17%	2.560E-01	**2.661E-08**

Table 4.3 (Continued)

RNAi	Treatment	Temperature (°C)	Incubation	% Control Area	± SEM	vs. Control *p*-value	vs. Knockdown *p*-value
no	40% ethanol	20	90 min	145%	23%	**3.595E-02**	**1.839E-08**
yes	46.6% ammonium sulfate with citrate and EDTA, pH 5.2	37	3 days	166%	21%	**4.671E-03**	**1.286E-09**
yes	46.6% ammonium sulfate with citrate, EDTA, and IPTG, pH 5.2	50	3 days	265%	24%	**8.050E-07**	**4.268E-16**

Table 4.4. Comparison of size-adjusted GFP fluorescence resulting from each bacterial treatment. Since TCWF partially depends on the size of the measured nematode, we normalized each average TCWF by the associated average nematode area (in pixels). The column labeled "% Control TCWF/Area" represents the percentage resulting from dividing the TCWF/area of each treatment by the TCWF/area of BC12907 *C. elegans* fed *ad libitum* HT115(DE3) *E. coli* lacking the plasmid for RNAi. The *p*-values are from unpaired two-tailed *t*-test, with *p*-values < 0.05 displayed in bold.

RNAi	Treatment	Temperature (°C)	Incubation	% Control TCWF/Area	± SEM	vs. Control *p*-value	vs. Knockdown *p*-value
Yes	GFP RNAi positive control	N/A	N/A	48%	8%	N/A	N/A
yes	60% acetone	20	90 min	48%	5%	**1.026E-07**	9.599E-01
yes	90% methanol	20	90 min	46%	6%	**1.969E-07**	8.603E-01
yes	50% acetone	20	90 min	45%	7%	**2.066E-06**	8.373E-01
no	50% ethanol	20	90 min	44%	16%	**1.534E-02**	8.292E-01
no	60% ethanol	20	90 min	44%	5%	**5.753E-06**	8.278E-01
yes	40% acetone	20	90 min	50%	6%	**7.644E-07**	8.175E-01
yes	100% methanol	20	90 min	51%	6%	**3.986E-06**	7.823E-01
no	propionic acid	20	90 min	52%	9%	**8.763E-05**	7.487E-01
yes	40% ethanol	20	90 min	44%	5%	**2.577E-07**	7.142E-01
yes	propionic acid	20	90 min	42%	9%	**9.331E-06**	7.131E-01
yes	50% ethanol	20	90 min	42%	6%	**1.324E-07**	5.959E-01
yes	30% ethanol with citrate, EDTA, and IPTG, pH 5.2	50	3 days	54%	3%	**5.132E-06**	4.973E-01
yes	40% acetone	20	90 min	32%	7%	**1.290E-05**	4.196E-01
yes	30% ethanol with citrate and EDTA, pH 5.2	50	3 days	63%	7%	**7.122E-04**	3.251E-01
yes	70% methanol	20	90 min	57%	4%	**1.756E-06**	2.883E-01
no	100% methanol	20	90 min	58%	5%	**5.172E-06**	2.613E-01
no	60% acetone	20	90 min	65%	11%	**1.028E-02**	2.232E-01
yes	30% ethanol with IPTG	50	3 days	69%	9%	**1.018E-02**	1.890E-01
yes	30% ethanol	50	3 days	61%	6%	**1.614E-04**	1.792E-01
yes	60% ethanol	20	90 min	35%	4%	**1.709E-09**	1.768E-01
yes	80% methanol	20	90 min	35%	3%	**4.942E-10**	1.694E-01
yes	40% ethanol	20	90 min	61%	5%	**1.130E-04**	1.584E-01
no	70% acetone	20	90 min	69%	9%	**2.367E-03**	1.543E-01
no	40% ethanol	20	90 min	72%	9%	**4.578E-03**	1.203E-01
yes	no treatment	60	20 hrs	34%	3%	**4.700E-08**	1.169E-01
yes	70% acetone	20	90 min	31%	5%	**6.833E-09**	1.036E-01
no	70% methanol	20	90 min	72%	10%	**2.252E-02**	9.179E-02
yes	100% methanol	20	90 min	31%	4%	**1.107E-07**	7.463E-02

Table 4.4 (Continued)

RNAi	Treatment	Temperature (°C)	Incubation	% Control TCWF/Area	± SEM	vs. Control *p*-value	vs. Knockdown *p*-value
no	70% ethanol	20	90 min	80%	15%	2.207E-01	7.119E-02
yes	70% ethanol	20	90 min	30%	3%	**1.467E-11**	5.733E-02
no	50% acetone	20	90 min	80%	7%	**1.597E-02**	**4.956E-02**
no	40% acetone	20	90 min	80%	11%	5.820E-02	**4.478E-02**
yes	no treatment	60	22 hrs	26%	5%	**1.871E-06**	**2.725E-02**
no	80% methanol	20	90 min	72%	7%	**1.022E-03**	**2.664E-02**
yes	30% ethanol with citrate, EDTA, and IPTG, pH 5.2	37	3 days	86%	10%	2.011E-01	**2.611E-02**
no	90% methanol	20	90 min	69%	4%	**4.099E-05**	**2.214E-02**
yes	1:1 40% ethanol:acetone	20	90 min	25%	3%	**6.059E-06**	**1.828E-02**
yes	no treatment	60	16 hrs	24%	4%	**2.169E-07**	**1.490E-02**
yes	lactic acid	20	90 min	83%	8%	**4.690E-02**	**1.152E-02**
yes	46.6% ammonium sulfate with citrate, EDTA, and IPTG, pH 5.2	50	3 days	92%	9%	4.097E-01	**8.875E-03**
yes	46.6% ammonium sulfate with citrate and EDTA, pH 5.2	50	3 days	97%	12%	7.910E-01	**6.139E-03**
yes	46.6% ammonium sulfate with citrate, EDTA, and IPTG, pH 5.2	37	3 days	95%	9%	6.148E-01	**5.766E-03**
yes	no treatment	60	18 hrs	16%	1%	**1.175E-06**	**1.157E-03**
yes	46.6% ammonium sulfate with citrate and EDTA, pH 5.2	37	3 days	106%	9%	5.094E-01	**1.074E-03**
yes	30% ethanol	37	3 days	113%	16%	4.667E-01	**9.452E-04**
yes	no treatment	60	14 hrs	12%	4%	**4.326E-07**	**8.677E-04**
no	lactic acid	20	90 min	90%	7%	1.729E-01	**2.042E-04**
yes	30% ethanol with citrate and EDTA, pH 5.2	37	3 days	120%	12%	1.398E-01	**7.973E-05**
yes	30% ethanol with IPTG	37	3 days	143%	21%	6.858E-02	**1.526E-05**

Table 4.5. Microbial growth is restricted by common antifungal drugs. A total of 26 different antifungal drugs were screened for the presence of microbe growth seven days after a 30 minute exposure to the open air. The drugs were present in triplicate in 100 µL microplate S-medium suspensions of 40% acetone-treated HT115 (DE3) *E. coli* (treated with 40% acetone for 2 hours at 37 °C, washed, pelleted, and suspended in S-medium at a concentration of 6.9 x 10^9 cells/mL). To account for the possible fluorescence of each drug in the wavelength range of the viability dye ($\lambda_{ex}/\lambda_{em}$=528/590 nm filter set), fluorescence measurements were taken before the addition of the dye, and then subtracted from the fluorescence measurement of the assay. The mean fluorescence measurement for each drug is given the column labeled "Mean AFU." An identical concentration of 40% acetone-treated bacteria was used as a positive control for microbial contamination. The % Range was calculated for each drug by subtracting the mean AFU measurement for the S-medium only negative control, and then dividing the remainder by the mean AFU of the positive control – the AFU of the negative control.

Concentration	Antifungal	Mean	SEM	% Range	SEM
2 µg/mL	Miconazole	23.67	1.20	-1%	5%
4 µg/mL	Fluconazole	24.67	0.67	2%	3%
1 µg/mL	Ketoconazole	24.00	0.58	0%	3%
2 µg/mL	Methylene blue	21.33	0.33	-10%	6%

Table 4.5 (Continued)

Concentration	Antifungal	Mean	SEM	% Range	SEM
100 ng/mL	Malachite green	23.67	0.33	-1%	3%
7 µg/mL	Acriflavin	-0.33	2.03	-88%	50%
2 µg/mL	Crystal (gentian) violet	19.33	0.33	-17%	10%
4.1 mg/mL	Phenoxyethanol	25.33	0.33	5%	4%
2.4 mg/mL	2-phenylethanol	26.00	0.58	7%	5%
2 mg/mL	Beta-phenylethylamine	19.67	0.33	-16%	9%
3 µg/mL	Propionic acid	25.33	0.33	5%	4%
200 µg/mL	Cyclosporin A	23.67	0.33	-1%	3%
125 µg/mL	Sodium sulfite	24.00	0.00	0%	2%
150 µg/mL	Sodium benzoate	24.67	0.33	2%	3%
3 mg/mL	Sodium nitrite	15.33	0.33	-31%	18%
3 mg/mL	Potassium sorbate	22.67	0.33	-5%	4%
7.2 mg/mL	Caprylic (octanoic) acid	24.67	0.33	2%	3%
250 µg/mL	Propyl 4-hydroxybenzoate	23.00	0.00	-4%	3%
50 µg/mL	Chitosan	25.67	0.33	6%	4%
4 µg/mL	5-fluorocytosine	23.33	0.33	-2%	3%
1X	Pima-Fix aquarium antifungal	24.67	0.33	2%	3%
1X	Rid-Fungus aquarium antifungal	37.33	11.84	48%	51%
1 mg/mL	Triacetin (triacetyl glycerol)	26.00	2.00	7%	9%
1.4 mg/mL	Dimethylfumarate	25.00	0.00	4%	3%
5.8 mg/mL	Fumaric acid	24.67	0.67	2%	3%
3 mg/mL	Boric acid	24.67	0.67	2%	3%
-	no antifungal	51.67	15.52	100%	79%
-	S-medium only	24.00	0.58	0%	3%

Table 4.6. The mean survival times of *C. elegans* treated with antifungal drugs. Eight of the antifungal drugs were chosen based on lack of microbial growth and predicted low toxicity. These drugs were used to treat age-synchronized N2 *C. elegans* in an assay of lifespan. The mean lifespan survival times, number of nematodes (*n*), and log-rank *p*-values are listed.

Concentration	Antifungal	*n*	Mean Survival Time (days)	SEM	% Control	SEM	Log-rank *p*-value
-	Control	143	14.538	0.339	100%	3%	-
4 µg/mL	Fluconazole	68	14.779	0.383	102%	4%	9.10E-01
1 µg/mL	Ketoconazole	137	14.175	0.351	98%	3%	9.68E-01
2 µg/mL	Methylene Blue	119	15.597	0.496	107%	4%	2.07E-03
100 ng/mL	Malachite Green	171	14.070	0.294	97%	3%	9.68E-01
7 µg/mL	Acriflavin	91	16.407	0.594	113%	5%	1.02E-05
3 µg/mL	Propionic Acid	147	14.429	0.338	99%	3%	9.93E-01
125 µg/mL	Sodium Sulfite	145	14.814	0.349	102%	3%	9.82E-01
150 µg/mL	Sodium Benzoate	60	10.200	0.066	70%	2%	0.00E+00

Table 4.7. Interpretation of SSMD values. Strictly standardized mean difference (SSMD) values are reported as β. The table shows the ranges of β values associated with excellent, good, inferior, and poor assay types, based on the subjectively evaluated strength of the positive and negative controls.

Assay Quality	Moderate Control	Strong Control	Very Strong Control	Extremely Strong Control
Excellent	$\beta \geq 2$	$\beta \geq 3$	$\beta \geq 5$	$\beta \geq 7$
Good	$2 > \beta \geq 1$	$3 > \beta \geq 2$	$5 > \beta \geq 3$	$7 > \beta \geq 5$
Inferior	$1 > \beta \geq 0.5$	$2 > \beta \geq 1$	$3 > \beta \geq 2$	$5 > \beta \geq 3$
Poor	$\beta < 0.5$	$\beta < 1$	$\beta < 2$	$\beta < 3$

Table 4.8. Summary of SSMD values. The SSMD (β value), and the receiver operating characteristic (ROC) area under the curve (AUC) for each assay, with and without normalization to GFP fluorescence.

Attribute Assayed	SSMD	ROC AUC	ROC AUC Standard Error	*p*-value
pmol ATP	2.180	0.998	0.002	< 0.0001
pmol ATP/GFP fluorescence	1.652	0.923	0.024	< 0.0001
viability	5.809	1.000	0.000	< 0.0001
viability/GFP fluorescence	-8.297	1.000	0.000	< 0.0001
nmol O_2 saturation	3.197	1.000	0.000	< 0.0001
nmol O_2 saturation/GFP fluorescence	3.960	1.000	0.000	< 0.0001

Table 4.9. Genes identified as hits in the screens for ATP content, oxygen consumption, and reductive capacity. Genes are sorted by mean robust z-score (highest to lowest for ATP content and reductive capacity; lowest to highest for oxygen saturation), and –log(*p*-values) > 1.3 correspond to *p*-values less than 0.05.

Measured Parameter	Mean z-score	− log(*p*-value)	Gene	Gene Name	Description	Human Homolog
ATP content	3.772	1.598	W07E11.2	flp-3	FMRF-Like Peptide	
ATP content	3.570	1.569	F09E10.8	toca-1	TOCA (Transducer Of Cdc42-dependent Actin assembly) homolog	Isoform 3 of Formin-binding protein 1-like
ATP content	3.225	1.676	C37E2.1	idhb-1	Isocitrate DeHydrogenase Beta	Isocitrate dehydrogenase [NAD] subunit beta, mitochondrial precursor
ATP content	3.146	2.232	T25C12.1	lin-14	abnormal cell LINeage	
ATP content	3.072	2.311	F42G10.1		neprilysin	
ATP content	2.904	2.367	T25C12.4	spp-21	SaPosin-like Protein family	
ATP content	2.841	2.058	F13D11.4		NAD(P) dependent steroid dehydrogenase-like	Sterol-4-alpha-carboxylate 3-dehydrogenase, decarboxylating

Table 4.9 (Continued)

Measured Parameter	Mean z-score	− log(*p*-value)	Gene	Gene Name	Description	Human Homolog
ATP content	2.787	3.238	F46C3.1	pek-1	human PERK kinase homolog	Eukaryotic translation initiation factor 2-alpha kinase 3
ATP content	2.703	2.214	T02C5.5	unc-2	UNCoordinated	voltage-dependent P/Q-type calcium channel subunit alpha-1A isoform 5
ATP content	2.543	2.110	C35C5.8		uncharacterized	
O_2 Saturation	-3.99	1.372	C47C12.6	deg-1	DEGeneration of certain neurons	Amiloride-sensitive sodium channel subunit gamma
O_2 Saturation	-3.83	2.064	C18B12.1		uncharacterized	
O_2 Saturation	-3.58	1.891	Y81B9A.2		uncharacterized	
O_2 Saturation	-3.50	1.838	Y12A6A.1		uncharacterized	
O_2 Saturation	-3.11	1.598	F22E10.1	pgp-12	P-GlycoProtein related	Isoform 2 of Multidrug resistance protein 3
O_2 Saturation	-2.97	1.708	T01B10.1	grd-4	GRounDhog (hedgehog-like family)	
O_2 Saturation	-2.56	2.050	R01E6.3	cah-4	Carbonic AnHydrase	Carbonic anhydrase 7
O_2 Saturation	-2.51	3.827	C11H1.4	prx-1	PeRoXisome assembly factor	Peroxisome biogenesis factor 1
Reductive Capacity	6.35	1.384	K08H2.5		predicted kinase activity and ATP binding activity	Isoform 3 of Tau-tubulin kinase 2
Reductive Capacity	5.83	1.853	C49F8.3		uncharacterized	
Reductive Capacity	5.67	2.482	ZK455.3	npr-9	NeuroPeptide Receptor family	Galanin receptor type 2
Reductive Capacity	5.46	1.316	C36B7.5		Semaphorin-5A	Semaphorin-5A
Reductive Capacity	5.44	1.731	F08G12.8		uncharacterized	
Reductive Capacity	5.25	1.658	C55B6.2	dnj-7	DNaJ domain (prokaryotic heat shock protein)	DnaJ homolog subfamily C member 3
Reductive Capacity	5.09	2.602	F19H6.3		uncharacterized	
Reductive Capacity	5.05	1.337	F55A4.4		pseudogene	
Reductive Capacity	4.88	1.414	H28G03.6	mtm-5	MTM (myotubularin) family	Myotubularin-related protein 13
Reductive Capacity	4.87	3.816	W04G3.6	sulp-7	SULfate Permease family	Isoform 1 of Prestin
Reductive Capacity	4.61	1.762	K08H2.6	hpl-1	HP1 Like (heterochromatin protein)	Chromobox protein homolog 3
Reductive Capacity	4.55	1.572	T21B6.2	pho-7	intestinal acid PHOsphatase	Isoform 2 of Prostatic acid phosphatase
Reductive Capacity	4.19	1.401	T02C5.5	unc-2	UNCoordinated	voltage-dependent P/Q-type calcium channel subunit alpha-1A isoform 5
Reductive Capacity	4.18	1.343	F55A4.5	stau-1	STAUfen (dsRNA binding protein) homolog	double-stranded RNA-binding protein Staufen homolog 1 isoform c
Reductive Capacity	4.02	1.753	K08H2.7		uncharacterized	
Reductive Capacity	3.95	1.383	F14B8.2	sid-5	Systemic RNA Interference Defective	
Reductive Capacity	3.92	1.396	T24C12.3		predicted glycosyl hydrolase	
Reductive Capacity	3.79	2.453	F19H6.6		uncharacterized	
Reductive Capacity	3.72	2.417	F31F6.6	nac-1	NADC (Na+-coupled dicarboxylate transporter) family	Solute carrier family 13 member 2

Table 4.9 (Continued)

Measured Parameter	Mean z-score	− log(*p*-value)	Gene	Gene Name	Description	Human Homolog
Reductive Capacity	3.68	2.361	E01G6.1		predicted serine-type endopeptidase inhibitor activity and chitin binding activity	tissue factor pathway inhibitor (lipoprotein-associated coagulation inhibitor)
Reductive Capacity	3.58	2.385	K09C8.2		uncharacterized	
Reductive Capacity	3.53	3.020	F20D1.1		predicted calcium channel activity	uncharacterized protein
Reductive Capacity	3.46	1.859	F19H6.5		uncharacterized	
Reductive Capacity	3.19	1.482	R04E5.2		may participate in metal homoeostasis	Isoform 1 of Metal transporter CNNM2
Reductive Capacity	3.18	1.915	C49F5.3		uncharacterized	
Reductive Capacity	3.17	1.542	F31F6.5	daf-6	abnormal DAuer Formation	Patched domain-containing protein 3
Reductive Capacity	3.16	1.507	F13D2.1		ortholog of human complement component 5	Complement C5
Reductive Capacity	3.15	1.738	C18B12.1		uncharacterized	
Reductive Capacity	3.15	1.721	F40E10.3	csq-1	CalSeQuestrin	44 kDa protein
Reductive Capacity	3.14	1.635	F49H12.3		potassium channel tetramerization domain containing	Isoform 2 of BTB/POZ domain-containing protein KCTD17
Reductive Capacity	3.14	1.854	T04C10.4	atf-5	ATF (cAMP-dependent transcription factor) family	Cyclic AMP-dependent transcription factor ATF-5
Reductive Capacity	3.10	1.597	F58A3.5	ttr-31	TransThyretin-Related family domain	
Reductive Capacity	2.74	3.031	F17E5.1	lin-2	abnormal cell LINeage	Isoform 1 of Peripheral plasma membrane protein CASK
Reductive Capacity	2.72	1.796	T13G4.5		uncharacterized	
Reductive Capacity	2.58	2.214	K09F5.5	set-12	SET (trithorax/polycomb) domain containing; putative histone H3 lysine-9 methyltransferase	
Reductive Capacity	2.56	4.763	T05A10.1	sma-9	SMAll	Zinc finger protein 853
Reductive Capacity	2.35	2.788	K04G11.1		uncharacterized	

Table 4.10. Gene ontology categories for screen hits. Gene ontology categories enriched for the ATP content and reductive capacity screens. No gene ontology categories were determined to be significant for the oxygen consumption screen.

Measured Parameter	Gene Ontology Type	Gene Ontology ID	Gene Ontology Category	# of Genes	*p*-value
ATP content	cellular processes	GO:0048519	negative regulation of biological process	4	0.000
ATP content	cellular processes	GO:0048523	negative regulation of cellular process	3	0.001
ATP content	cellular processes	GO:2000113	negative regulation of cellular macromolecule biosynthetic process	2	0.001
ATP content	cellular processes	GO:0010558	negative regulation of macromolecule biosynthetic process	2	0.001
ATP content	cellular processes	GO:0031327	negative regulation of cellular biosynthetic process	2	0.001
ATP content	cellular processes	GO:0009890	negative regulation of biosynthetic process	2	0.001
ATP content	cellular processes	GO:0031324	negative regulation of cellular metabolic process	2	0.004
ATP content	cellular processes	GO:0010629	negative regulation of gene expression	2	0.005
ATP content	cellular processes	GO:0007399	nervous system development	2	0.007

Table 4.10 (Continued)

Measured Parameter	Gene Ontology Type	Gene Ontology ID	Gene Ontology Category	# of Genes	*p*-value
ATP content	cellular processes	GO:0048583	regulation of response to stimulus	2	0.009
ATP content	cellular processes	GO:0010605	negative regulation of macromolecule metabolic process	2	0.010
ATP content	cellular processes	GO:0009892	negative regulation of metabolic process	2	0.011
ATP content	cellular processes	GO:0040008	regulation of growth	2	0.016
ATP content	cellular processes	GO:0007610	behavior	2	0.020
ATP content	cellular processes	GO:0055114	oxidation-reduction process	2	0.029
ATP content	cellular processes	GO:1901362	organic cyclic compound biosynthetic process	2	0.048
Reductive Capacity	cellular processes	GO:0048523	negative regulation of cellular process	7	0.000
Reductive Capacity	cellular processes	GO:0048519	negative regulation of biological process	8	0.000
Reductive Capacity	cellular processes	GO:0010605	negative regulation of macromolecule metabolic process	5	0.000
Reductive Capacity	cellular processes	GO:0009892	negative regulation of metabolic process	5	0.000
Reductive Capacity	cellular processes	GO:0031324	negative regulation of cellular metabolic process	4	0.000
Reductive Capacity	cellular processes	GO:0050789	regulation of biological process	12	0.002
Reductive Capacity	cellular processes	GO:0065007	biological regulation	13	0.002
Reductive Capacity	cellular processes	GO:0060255	regulation of macromolecule metabolic process	7	0.003
Reductive Capacity	cellular processes	GO:0000122	negative regulation of transcription from RNA polymerase II promoter	2	0.004
Reductive Capacity	cellular processes	GO:0050794	regulation of cellular process	10	0.004
Reductive Capacity	cellular processes	GO:0019222	regulation of metabolic process	7	0.005
Reductive Capacity	cellular processes	GO:0098656	anion transmembrane transport	2	0.005
Reductive Capacity	cellular processes	GO:0009966	regulation of signal transduction	3	0.005
Reductive Capacity	cellular processes	GO:0045892	negative regulation of transcription, DNA-templated	2	0.007
Reductive Capacity	cellular processes	GO:1902679	negative regulation of RNA biosynthetic process	2	0.007
Reductive Capacity	cellular processes	GO:1903507	negative regulation of nucleic acid-templated transcription	2	0.007
Reductive Capacity	cellular processes	GO:0051253	negative regulation of RNA metabolic process	2	0.007
Reductive Capacity	cellular processes	GO:0010629	negative regulation of gene expression	3	0.008
Reductive Capacity	cellular processes	GO:0051172	negative regulation of nitrogen compound metabolic process	2	0.009
Reductive Capacity	cellular processes	GO:0045934	negative regulation of nucleobase-containing compound metabolic process	2	0.009
Reductive Capacity	cellular processes	GO:0023051	regulation of signaling	3	0.009
Reductive Capacity	cellular processes	GO:0009968	negative regulation of signal transduction	2	0.009
Reductive Capacity	cellular processes	GO:0010646	regulation of cell communication	3	0.009
Reductive Capacity	cellular processes	GO:0023057	negative regulation of signaling	2	0.009
Reductive Capacity	cellular processes	GO:0010648	negative regulation of cell communication	2	0.009
Reductive Capacity	cellular processes	GO:2000113	negative regulation of cellular macromolecule biosynthetic process	2	0.011
Reductive Capacity	cellular processes	GO:0010558	negative regulation of macromolecule biosynthetic process	2	0.011

Table 4.10 (Continued)

Measured Parameter	Gene Ontology Type	Gene Ontology ID	Gene Ontology Category	# of Genes	*p*-value
Reductive Capacity	cellular processes	GO:0031327	negative regulation of cellular biosynthetic process	2	0.011
Reductive Capacity	cellular processes	GO:0009890	negative regulation of biosynthetic process	2	0.011
Reductive Capacity	cellular processes	GO:0043086	negative regulation of catalytic activity	2	0.012
Reductive Capacity	cellular processes	GO:0048585	negative regulation of response to stimulus	2	0.012
Reductive Capacity	cellular processes	GO:0044092	negative regulation of molecular function	2	0.013
Reductive Capacity	cellular processes	GO:0032269	negative regulation of cellular protein metabolic process	2	0.016
Reductive Capacity	cellular processes	GO:0051248	negative regulation of protein metabolic process	2	0.016
Reductive Capacity	cellular processes	GO:0048583	regulation of response to stimulus	3	0.016
Reductive Capacity	cellular processes	GO:0006820	anion transport	2	0.017
Reductive Capacity	cellular processes	GO:0010628	positive regulation of gene expression	2	0.021
Reductive Capacity	cellular processes	GO:0044700	single organism signaling	6	0.021
Reductive Capacity	cellular processes	GO:1902580	single-organism cellular localization	2	0.023
Reductive Capacity	cellular processes	GO:0010468	regulation of gene expression	5	0.023
Reductive Capacity	cellular processes	GO:0007154	cell communication	6	0.024
Reductive Capacity	cellular processes	GO:0080090	regulation of primary metabolic process	5	0.027
Reductive Capacity	cellular processes	GO:0031323	regulation of cellular metabolic process	5	0.028
Reductive Capacity	cellular processes	GO:0010604	positive regulation of macromolecule metabolic process	2	0.035
Reductive Capacity	cellular processes	GO:0034220	ion transmembrane transport	3	0.037
Reductive Capacity	cellular processes	GO:0030001	metal ion transport	2	0.040
Reductive Capacity	cellular processes	GO:0044763	single-organism cellular process	12	0.045
Reductive Capacity	cellular component	GO:0044456	synapse part	2	0.011
Reductive Capacity	cellular component	GO:0031410	cytoplasmic vesicle	2	0.019
Reductive Capacity	cellular component	GO:0031982	vesicle	2	0.019
Reductive Capacity	cellular component	GO:0045202	synapse	2	0.029

CHAPTER 5:

THE SIGNIFICANCE OF THE FACTORS ASSOCIATED WITH AGE-RELATED CHANGES AND OF THE DEVELOPED METHODS

5.1 Summary

This project was divided into two broad and overlapping parts. One consisted of determining the specific genetic, proteomic, and metabolomic factors associated with age-related changes in *C. elegans*. The other consisted of developing novel methods for high-throughput culturing and screening of *C. elegans* to investigate age-related changes. Both parts proved to be fruitful. As with any protocol however, the methods we developed were found to have limitations as well as strengths.

5.2 Identified Genetic Factors

5.2.1 Genes related to Ca^{2+} signaling

Calcium plays a very central role in several parts of *C. elegans* aging. Ca^{2+} is necessary for muscle contraction, where it is released by the sarcoplasm upon muscular innervation and binds to troponin within actin filaments, allowing myosin to bind and pull the filaments, contracting the muscle. As muscle relaxes, Ca^{2+} is then actively pumped back into the sarcoplasm by membrane-bound ATPases. Through our proteomic investigation (Chapter 2), we identified significant age-dependent changes in the expression four *C. elegans* genes related to this entire process. SCA-1 (sarco-endoplasmic reticulum calcium ATPase 1 or SERCA) is

orthologous to the human SERCA protein ATP2A1, which utilizes the hydrolysis of ATP to transport cytosolic Ca^{2+} into the lumen of the sarcoplasmic reticulum [1, 2]. A decline in SERCA function is associated with muscular dysfunction, and mice that are heterozygous for a mutant version of *Serca2* exhibit deficits of muscle relaxation as a consequence of impaired sarcoplasmic Ca^{2+} uptake [3]. We observed an approximately 10-fold down-regulation of *sca-1* with age. Given that *C. elegans* express *sca-1* in all major muscle types, the observed down-regulation is likely indicative of a body-wide impairment of muscle function.

The *C. elegans* protein NRA-2 (ortholog of human nicalin) also showed an approximately 10-fold down-regulation with age. *nra-2* encodes a transmembrane endoplasmic reticulum protein that acts as a molecular chaperone [4], and it contains an EF-hand motif indicating that the activity of the protein is possibly regulated by changes in Ca^{2+} levels. Significantly, RNAi knockdown of *nra-2* expression has been shown to sensitize *C. elegans* touch receptor neurons to Ca^{2+}-mediated necrotic cell death [5]. The expression of *nra-2* in neurons, body wall muscle, and pharyngeal muscle suggests that these cell types may be sensitized to necrotic cell death in older nematodes.

The *C. elegans* gene *mlp-1* encodes a LIM domain-containing cysteine-rich protein (CRP) expressed fairly ubiquitously in both larva and adults [6, 7], and MLP-1 levels were observed to decline in older *C. elegans*. Members of the homologous CSRP (cysteine and glycine-rich protein) human family of proteins are expressed in cardiac and skeletal muscle [8-10], and abnormal expression of CSRP has been associated with both cardiomyopathy and heart failure [11]. Furthermore, mice with deficient CSRP function experience pathological changes in their heart muscle structure as well as defects in sarcoplasmic reticulum Ca^{2+} storage [8, 12, 13].

The gene *cal-4* is one member of the *C. elegans* CAL gene family (8 genes total), which are homologous to human calmodulin. Proteins of the calmodulin family bind directly to Ca^{2+} and act as intermediaries in numerous Ca^{2+}-mediated signaling processes within cells. In addition to this role, calmodulin is necessary for Ca^{2+} to permit myosin binding to actin in smooth muscle. We observed an up-regulation of CAL-4 expression with age, possibly as a response to extra-sarcoplasmic Ca^{2+} within dysfunctional *C. elegans* muscle cells. Overall, the increase in CAL-4 expression, together with the decrease in expression of MLP-1, NRA-2, and SCA-1 indicate a large age-dependent change in Ca^{2+} homeostasis that likely contributes to muscular dysfunction.

As part of the proof-of-principle application of our developed methods (Chapter 3), we uncovered several genes that appear to contribute to the toxicity in *C. elegans* of high Ca^{2+} levels (100 mM) in the liquid media. These genes were identified through a series of screens using RNAi of 191 genes encoding EF-hand domains, which express proteins that are likely to bind to Ca^{2+}. Populations of green fluorescent protein (GFP)-expressing *C. elegans* were fed individual clones from the 191 genes, and assayed for live nematode volume (as determined by GFP fluorescence) and rate of death (as determined by anthranilate fluorescence). RNAi knockdowns that resulted in an average increase of live worm volume above 2 standard deviations, or a decrease in the rate of death below 2 standard deviations, were scored as mediating the toxic effects of high Ca^{2+} in culture.

Seven genes were identified using this criteria; T04F8.6, ZK673.7 (*tnc-2*), C09H5.7, C04B4.2, C47A4.3, F53F4.14, and K04F1.10 (*irld-40*). Of these genes, three are uncharacterized and lack strong human homologs (T04F8.6, C04B4.2, and F53F4.14). Of the remaining four genes, ZK673.7 (*tnc-2*), encodes a pharyngeal-specific form of troponin C, and it

is feasible that the associated increase in live nematode volume seen under the condition of high Ca^{2+} toxicity may be due to reduced pharyngeal pump contractibility caused by a decreased expression of troponin C. A reduced ability of the pharyngeal pump to contract could limit the intake of Ca^{2+}, resulting in a higher rate of survival for the effected *C. elegans*. The gene K04F1.10 (*irld-40* or Insulin/EGF-Receptor L Domain protein) contains an EGF receptor domain, and EGF receptor signaling has been shown to affect *C. elegans* lifespan through Ca2+/IP_3 receptor and phospholipase C-3 (PLC-3) dependent mechanisms [14]. The final two identified genes, (C47A4.3 and C09H5.7) encode catalytic subunits of serine/threonine-protein phosphatases homologous to human protein phosphatase 1 (PP1-β and PP1-γ respectively). These protein complexes are associated with numerous activities, including mitosis, muscle contraction, glycogen metabolism, protein synthesis, and the progression of apoptosis [15, 16]. However, 41 out of the 191 of the genes targeted in the EF-hand RNAi library (~21%) are predicted to be protein phosphatases or subunits of these complexes, meaning that the presence of two protein phosphatase subunits within the hits is not necessarily meaningful in a broader sense as ~2 such subunits should be expected to appear among a list of seven randomly selected genes from our starting library strictly by chance.

5.2.2 Genes Related to ATP and O_2 Decline with Age

We designed and performed three screens of metabolic parameters that decline with age in *C. elegans* – ATP content, oxygen consumption, and cellular reductive capacity (Chapter 4). For each screen, each gene of the *C. elegans* X chromosome was knocked-down in triplicate by RNAi. Hits were identified as 6-day-old *C. elegans* that expressed significantly less of a decline in these parameters, as determined by the mean robust z-score, and by unpaired two-tailed *t*-tests

using a theoretical mean robust z-score of zero as comparison. Using these methods, a total of 55 genes were identified among the three screens, with two genes present in more than one screen (*unc-2* was identified in the ATP and reductive capacity screens, and C18B12.1 was identified in the oxygen consumption and reductive capacity screens). An analysis of gene ontology (GO) was performed using the STRING (Search Tool for the Retrieval of Interacting Genes/Proteins) online database, as well as an analysis of associations to *C. elegans* lifespan using the Human Aging Genomic Resources (HAGR) GenAge database. The results of these analyses revealed that the majority of GO categories significantly enriched among the hits are negative regulators of cellular processes. Furthermore, 16.36% of the hits are either anti-longevity genes (*lin-2*, *lin-1*4, F42G10.1, and *daf-6*), or members of gene classes enriched with anti-longevity genes (*unc-2*, *hpl-1*, *sid-5*, *nac-1*, and *set-12*). We interpreted these results as suggesting that a large portion of the hits might be negative repressors of cellular processes that limit lifespan. This interpretation would explain why RNAi knockdown resulted in the measured age-dependent parameters (ATP content, oxygen consumption, and cellular reductive capacity) being maintained at levels more similar to those of younger *C. elegans*. Given that a large portion of the lifespan effects reported through GenAge are themselves the results of high-throughput screens, be believe that a more thorough investigation of the lifespan associated effects of these genes is warranted.

5.3 Identified Proteomic Factors

5.3.1 Histone Modifications and DNA Repair

C. elegans lack methylated cytosine nucleobases in their DNA, meaning that methylation primarily regulates gene expression through histone modification [17], with the caveat that there

is recent evidence for adenine methylation of the DNA [18]. Our proteomics investigation (Chapter 2) revealed that S-adenosyl methionine synthetase (SAMS-1) is significantly down regulated in older *C. elegans*. The enzyme SAMS-1 is responsible for generating S-adenosyl methionine (SAM) from ATP and L-methionine. Since SAM is the primary intracellular methyl donor, decreased in SAMS-1 levels likely restrict the occurrence of methylation events, including those on histones. Additionally, PRMT-3 (protein arginine methyltransferase 3) was observed to be dramatically decreased with age. PRMT-3 is one member of a family of six related *C. elegans* methyltransferase enzymes capable of transferring a methyl group from SAM onto arginine residues within histones [19], and the nearly 200-fold decrease in PRMT-3 levels found in older *C. elegans* is further evidence supporting an age-related change to histone methylation.

We also identified indirect evidence for decreased expression of *C. elegans* histone deacetylase-1 (HDA-1), which functions to remove acetyl groups from lysine residues within core histones. HDA-1 has been demonstrated to be a strong repressor of expression of the cysteine protease inhibitor CPI-1 [20]. We observed a ~6.4-fold age-related increase in CPI-1 levels, as well as an increase the levels of several proteins known to have a high confidence of co-expression with CPI-1 (C53B7.2, Y62H9A.6, CPG-1, and TTR-51), all of which support the hypothesis that HDA-1 is down-regulated with age in *C. elegans*.

The *C. elegans* poly(ADP-ribose) polymerase PME-1 also exhibited an approximately 6-fold decrease with age. This enzyme is orthologous to human PARP1, which functions to detect DNA single-strand breaks and signals to proteins responsible for single-strand break repair [21, 22]. Decreased levels of PME-1 could indicate a reduced capacity for DNA repair, which sensitized cells to apoptosis and senescence. Overall, these observations provide direct and

indirect evidence for age-dependent alterations to histone methylation and acetylation, as well as a reduced capacity for the identification and correction of DNA single-strand breaks.

5.3.2 RNA Metabolism and Translation

In total, we observed a significant decrease in the levels 8 proteins involved in transcription and translation (XRN-2, RSP-6, ZK512.2, PAB-2, RPL-11.2, RPS-26, DPH-2, and PUS-1). XRN-2 (5'-3' exoribonuclease 2 homolog) is an exonuclease involved in transcription termination, where it dislodges RNA polymerase II from DNA. RSP-6 (splicing factor, arginine/serine-rich protein 6) contributes to nuclear pre-mRNA processing [13, 23, 24], and ZK512.2 is largely uncharacterized but may play a role in pre-mRNA splicing or the initiation of translation as an ATP-dependent RNA helicase. PAB-2 (poly(A) binding protein 2) regulates translation by interacting with the 5'-cap eukaryotic initiation factor complex eIF4F and by recruiting the 60S and 40S ribosomal subunits [11], and RPL-11.2 and RPS-26 are components of the 60S and 40S ribosomal subunits respectively. DPH-2 (diphthamide biosynthesis protein 2) transfers three methyl groups from SAM molecules to form diphthamide, which is a non-standard amino acid found exclusively in translation elongation factor 2 (eEF2) [12], and PUS-1 (pseudouridine synthase 1) is essential for a post-transcriptional modification of tRNA essential for translation. Ultimately, the decreased levels of these 8 proteins could hinder multiple aspects of the progression from transcription, to splicing, to translation.

5.3.3 Fatty Acid Metabolism

Two important enzymes for fatty acid metabolism were observed to decrease in abundance in older *C. elegans*, IDH-1 (isocitrate dehydrogenase-1) and ACDH-13 (acyl CoA

dehydrogenase 13). Aconitase is a cytosolic and mitochondrial enzyme that serves a key role in both the TCA cycle and fatty acid synthesis. In the cytosol, aconitase functions to concert citrate into isocitrate thus diverting citrate away from entry into the metabolic pathway for fatty acid synthesis. IDH-1 then continues the process by converting cytosolic isocitrate into α-ketoglutarate. Decreased levels of IDH-1 could potentially serve as a bottleneck in the removal of cytosolic citrate, allowing more citrate to enter into fatty acid synthesis.

Likewise, the enzyme ACDH-13 is one member of a family of long-chain-acyl-CoA dehydrogenase enzymes that function in mitochondrial fatty acid breakdown through β-oxidation. ACDH-13 was also observed to decrease with age, reflecting a possible decline in free fatty acid breakdown. Of note, ACDH-13 is also an ortholog of human acyl-CoA dehydrogenase 9, which has been shown to play a role in the proper assembly of ETC complex I [25]. Two other proteins were found to have decreased with age, C23H4.3 and RME-2 (receptor mediated endocytosis 2). C23H4.3 is a homolog of human carboxylesterase-2 (CES-2), which contributes to the hydrolysis of long-chain fatty acid esters and thioesters, and RME-2 is a yolk receptor that regulated the uptake of yolk (vitellogenin lipoprotein particles) into *C. elegans* oocytes [26]. A decrease in RME-2 specifically could contribute to the ectopic accumulation of vitellogenin known to occur in older *C. elegans*.

5.4 Identified Metabolomic Factors

5.4.1 Free Amino Acids

By using GC/MS for metabolite identification (Chapter 2), we were able to identify a total of 186 metabolites present in both our young and older *C. elegans* populations. Of these metabolites, the levels of 9 free amino acids were observed to be significantly altered with age.

A trend toward the increase of hydrophilic amino acids, and the decrease of hydrophobic amino acids was observed, based on a glycine normalized scale of hydrophobicity [27]. This trend mirrors previously reported observations that attribute the changes to the altered surface-to-volume ratio of expanding *C. elegans* cells [28, 29]. Once cell division stops in *C. elegans*, growth continues by cell volume expansion, during which time cytoplasmic volume expands at a faster rate than membrane area, due to the geometry of the cells. This disequilibrium in rate then requires the greater synthesis of hydrophilic cytosolic proteins as compared to hydrophobic membrane bound proteins, and the change in demand is reflected in the free amino acid pool.

5.4.2 Purine and Pyrimidine Metabolism

Purine metabolism was found to be the pathway with the largest total decrease (and overall change) among the identified metabolites, due to a large age-dependent decrease in the levels of adenine, guanine, adenosine, adenosine monophosphate, ribose, ribose 5-phosphate, hypoxanthine, and inosine. We further validated the decline in hypoxanthine in older nematodes by performing an independent colorimetric assay. Pyrimidine metabolism was also largely decrease with age, with a large decline in uridine and uracil. Cytosine was also the sixth most decreased metabolite overall, but was not initially associated with the *C. elegans* pyrimidine metabolism pathway in our analysis since *C. elegans* lack a cytidine phosphorylase enzyme to salvage cytosine bases. Thymine also appeared to decrease with age, although the comparison of thymine levels in young and old *C. elegans* fell short of statistical significance (p-value = 0.076).

The overall decline in free nucleobases is surprising, and it may represent several possible overlapping cellular conditions. First, a decline in free nucleobases may be a consequence of a prolonged adjustment to a post-mitotic state. The somatic cells of an adult *C.*

elegans do not divide, and the cells may gradually limit their free nucleobase pools to reflect the decreased demand for DNA synthesis. Conversely, the decline could equally be attributed to a dysregulated increase in DNA synthesis. Older *C. elegans* cells often exhibit a heterogeneity of cellular genome copy number [30], and they often experience an age-dependent aggregation of transcriptionally active DNA masses within their uterus, both of which could deplete the free nucleobase pool if the appropriate metabolic pathways weren't up-regulated to meet the demand. Additionally, since a decline in nucleobase levels could potentially slow or impair mRNA transcription by reducing the availability of RNA bases, this finding could be viewed as either a cause or a consequence of the altered RNA metabolism discussed above. Either a decrease in available RNA bases contributes to a down-regulation of the cellular components of transcription, or one aspect of a cellular down-regulation of transcription is a restriction of the free nucleobase pools. Interestingly, we found that supplementing *C. elegans* media with cytidine or hypoxanthine extends lifespan, suggesting that the decline purine and pyrimidine metabolism may limit nematode lifespan.

5.4.3 The SAM Cycle

Three metabolites directly associated with the SAM cycle (the pathway responsible for the enzymatic production of S-adenosylmethionine) were found to decrease with age in *C. elegans*; L-methionine and L-homocysteine, and the downstream product 5-methylthioadenosine. Combined with the age-dependent down-regulation of SAMS-1 discussed above, SAM and the cellular methylation capability are expected to decline with age. This decline could then impact the various anabolic and epigenetic processes that rely on methylation. Other than the methylation of histones and the synthesis of diphthamide mentioned above, SAM is necessary

for the synthesis of phosphatidylcholine (PC), which is a common cellular membrane phospholipid and accounts for a large portion of the phospholipid content of lipid droplets membranes and mitochondrial inner membranes. For lipid droplets at least, a decrease in SAM content has been linked to a corresponding drop in lipid droplet PC content, which promotes the coalescence of smaller droplets into larger one [31, 32]. Decreased PC content through *sams-1* RNAi has also been associated with the activation of the endoplasmic reticulum (ER) stress response [33], which can lead to decreased protein synthesis if prolonged. SAM is also an important component in the synthesis of ubiquinone, and notably dietary restriction, which also decreases SAM levels, has been linked to both larger lipid droplets and decreased ubiquinone in *C. elegans* [31, 32, 34].

5.4.4 Free Fatty Acids

We observed an age-related increase in free fatty acids in *C. elegans*, as well as a decrease in monoacylglycerols. These two observations suggest the possibility for an age-dependent increase in free fatty acid formation from monoacylglycerol hydrolysis, and possibly a decrease in fatty acid β-oxidation. Interestingly, we also observed an increase in glycerol, which is a byproduct of acylglycerol (glyceride) hydrolysis, and a large increase in β-hydroxybutyrate, which is a ketone body produced from excess acetyl-CoA under conditions of either fatty acid β-oxidation or fatty acid synthesis. Citrate was also observed to increase in older *C. elegans*. As discussed above, cytosolic citrate is required to initiate fatty acid synthesis, and increased cytosolic citrate can be indicative of either a metabolic shift towards fatty acid synthesis, or the inactivation of mitochondrial aconitase by reactive oxygen species (ROS). Taken together, these metabolic changes suggest that *C. elegans* aging is characterized by the hydrolysis of cellular

glycerides, as well as alterations to fatty acid synthesis and/or β-oxidation. Notably, excess free fatty acids can also lead to (ER) stress [35].

5.4.5 Sorbitol

The sorbitol content of older *C. elegans* was found to be dramatically increased, which we further verified by an independent colorimetric assay. Sorbitol is produced by the activity of aldose reductase in response to elevated glucose levels [36-38], and it has been shown to be present at elevated concentrations in the tissues of diabetics [39-41]. Due to its hydrophilic nature and its inability to diffuse through cell membranes, sorbitol has even been theorized to contribute to the progression of diabetes by accumulating within cells to the point of causing osmotic stress [36]. Sorbitol can be further converted to fructose by the enzyme sorbitol dehydrogenase and the cofactor nicotinamide adenine dinucleotide (NAD^+). Therefore, the high concentrations of sorbitol detected in older *C. elegans* may be due to multiple factors, including a limited supply of NAD^+, or a defect of glycolysis such as through oxidative damage to glycolytic enzymes such as GAPDH [42]. Sorbitol has been identified as an osmolyte in some yeasts and fungi, as well as in mammalian kidney cells, where it adjusts the intracellular environment to compensate for osmotic stress [43-45]. The age-related increase in sorbitol may be employed by *C. elegans* as an osmolyte to counteract the tendency for water loss and to balance the dilution of cellular contents that would occur as *C. elegans* increase their volume during growth.

5.4.6 Redox

Several age-related changes in metabolite concentrations support the conclusion that the *C. elegans* intracellular environment transitions to a more oxidized state during aging. Ascorbic acid (vitamin C) can be oxidized under physiological conditions to form the compound dehydroascorbate (DHA), which can then be recycled back into ascorbic acid by the reductive capacity of glutathione. The ratio of DHA to ascorbic acid then represents both the available glutathione pool and the overall cellular redox state [46]. We observed an increase in the DHA/ascorbic acid ratio, suggesting a depletion of reduced glutathione and/or a shift toward a more oxidizing intracellular environment. Likewise, erythronic acid (EA) and N-acetylglucosamine (NAG) were both observed to be altered with age in *C. elegans*. NAG is a peptidoglycan monomer and a component of chitin and hyaluronic acid, and under physiological conditions NAG has been found to oxidatively degrade into EA [47]. We similarly detected an increase in the EA/NAG ratio, further indicating a more oxidizing cellular environment in older *C. elegans*. We did not to observe glutathione directly in our metabolomic analysis, nor did we observe NAD^+ or NADH. However, we were able to use the ratio of pyruvate to lactate as an estimator of relative NAD^+ and NADH concentrations, respectively, since these metabolites are held in equilibrium by the activity of the enzyme lactate dehydrogenase [48]. This estimation supports an age-dependent decrease in the NAD^+/NADH ratio, which is similar to what has been observed in both rats and humans [49-51]. Notably, the decreased NAD^+/NADH could restrict glycolysis, mitochondrial fatty acid β-oxidation, and the activity of the TCA cycle, since these cellular processes require a steady supply of NAD^+. The poly(ADP-ribose) polymerase PME-1 and sorbitol dehydrogenase both also rely on NAD^+ availability and may be affected by an age-dependent decrease in the ratio.

5.5 Significance of the Age-related Factors

Calcium plays many important biological roles, including the coordination of muscle contraction and the regulation of cell death through apoptosis or necrosis. Using our method for screening RNAi gene knockdowns in the presence of a toxic level of Ca^{2+}, we were able to identify calcium-binding genes that may play a role in mediating Ca^{2+}-induced cell death. Furthermore, our proteomic analysis of young and old *C. elegans* identified a down-regulation of muscle-specific genes involved in Ca^{2+} homeostasis, which supports previous observations of sarcopenia and impaired locomotion in older nematodes. The combination of our proteomic and metabolomic investigations further revealed evidence of age-dependent changes multiple physiological aspects, including altered amino acid concentrations, which are consistent with previous reports linking the change to the expansion of *C. elegans* cell size; an increase in free fatty acids and a decrease in the activity of the SAM cycle, both of which have been linked to ER stress; altered or impaired protein synthesis, which may limit lifespan and may also be indicative of ER stress; epigenetic changes and evidence of a change in DNA repair; a shift toward a more oxidizing cellular environment and an increase in NAD^+ relative to NADH; and an increase in sorbitol.

Yolk lipoproteins accumulate ectopically with age in *C. elegans*, and may contribute to some of these age-related changes, including an increase in free fatty acids. Also, sarcopenia of the pharyngeal pump progresses to an extreme level in older *C. elegans*, which likely results in late-life dietary restriction. Decreased SAM synthesis is one downstream effect of dietary restriction, and the relationship between these factors may explain our observations of an age-related decrease in SAM cycle activity.

Our RNAi gene knockdown screens for genetic contributors to the age-related declines in ATP content, oxygen consumption, and reductive capacity identified a diverse set of genes. Common attributes among the set appear to be a negative regulation of cellular processes and anti-longevity activity in *C. elegans*. It may be that the screens identified genetic factors limiting *C. elegans* lifespan, explaining their connection to age-related changes in the nematode.

5.6 Novel Methods

The methods that we developed to help perform our screens can be divided into three categories: (1) long-term maintenance of *C. elegans* liquid cultures, (2) assaying live *C. elegans* volume in culture, and (3) high-throughput assaying of *C. elegans* metabolic parameters while using bacteria-based RNAi gene knockdown. All three categories were valuable in obtaining the results discussed in the previous sections, although each has its own unique caveats.

5.6.1 Long-term Maintenance of *C. elegans* Liquid Cultures

Growing *C. elegans* for extended periods of time in microplate liquid cultures is challenging. Largely, the effort that goes into maintaining the culture involves finding a balance between assuring proper aeration and preventing excess evaporation. We began by investigating several commercially available microplate sealers (Chapter 3), as well as 12.7 micron fluorinated ethylene–propylene (FEP) Teflon® film, in an effort to find a suitable method for preventing liquid culture evaporation. FEP Teflon® film has been previously used to successfully seal and maintain neuronal cell cultures for periods in excess of 9 months [52], and under our conditions we found FEP Teflon® film to almost completely restrict media evaporation, even when tested in an arid environment. In addition to preventing fluid loss, FEP Teflon® film is an effective

barrier against microbes, and it is transparent enough to avoid interfering with optical measurements, meaning that microplates can remain sealed with the film during optically-based assays. We additionally discovered that the gas-permeable film allowed enough aeration to permit us to grow 96-well microplate liquid cultures without shaking, and with up to 300 nematodes per well, as long as the volume of media in each well was kept relatively low (~100 μL). Based on this finding, we developed and constructed a series of gasket-attached FEP Teflon® film 96-well plate lids, which we then used exclusively for all of our microplate-based liquid cultures.

5.6.2 Assaying Live *C. elegans* Volume in Culture

Both manual and automated methods for scoring living *C. elegans* currently require microscopy. In an effort to simplify the process and to possibly make lifespan analysis more available for high-throughput, we investigated the use of fluorescence markers that might correspond to the quantity of living or dead *C. elegans* in a culture at a variety of ages (Chapter 3). To test whether ubiquitously-expressed GFP could be used as an appropriate marker, we selected the bright *C. elegans* strain BC12907 *dpy-5(e907)*, with GFP expression driven by the promoter for T09B4.8 (a homolog for human mitochondrial AGXT-2 alanine-glyoxylate aminotransferase-2 gene) [6, 53]. By examining BC12907 *C. elegans* cultures through microplate reader-based fluorescence, as well as fluorescence microscopy and manual image analysis, we found that the total green-range fluorescence measured per microplate well exhibits a linear correspondence to the total volume of live *C. elegans* per well. We also found that dead BC12907 *C. elegans* exhibit a non-negligible, but greatly reduced fluorescence that should only marginally contribute to the total fluorescence per well.

This finding applied across most of the *C. elegans* 21-day maximum lifespan at 20 °C, and could be used to estimate the number or volume of live nematodes in each separate culture, and to normalize additional assay measurement to a per-nematode quantity. The restrictions that we discovered for this method however, limit its application in certain circumstances. First, the correspondence between GFP fluorescence and the number or volume of live nematodes per culture does not hold before the first or second day of *C. elegans* adulthood (approximately the fifth day of culture at 20 °C). Prior to that point, the relationship between GFP and nematode content is nonlinear and likely complicated by the small but rapidly-changing size of the organism. Second, *E. coli* possess autofluorescence in the green range that often increases with time, and change in ways that are difficult to predict. In early liquid cultures, *E. coli* present as a food source can account for nearly all of the fluorescence detected when assaying GFP. At later points the concentration of *E. coli* is usually lower, but increases in bacterial autofluorescence can still potentially interfere with measurements. When conducting the RNAi screen for Ca^{2+}-binding genes mediating high Ca^{2+} toxicity, our solution was to perform GFP fluorescence measurements on adult *C. elegans* at later time points when the nematodes were likely to have consumed the majority of the *E. coli* in culture.

Since endogenous anthranilate increases in *C. elegans* over an ~8 hour period surrounding the death of an individual nematode, we attempted to use anthranilate blue-range autofluorescence in a similar manner as a marker for the rate of death in a culture. The results were promising given that there was a strong inverse linear relationship between the total blue-range fluorescence and the number of live *C. elegans* in a culture. Furthermore, we were able to differentiate between high Ca^{2+}-treated and non-treated cultures based on the higher blue-range fluorescence (and presumable a higher rate of death) in the Ca^{2+}-treated sample. *E. coli* also

possess autofluorescence in the blue range that can increase over time, so it can be assumed that the same limitations for assaying GFP also apply to assaying anthranilate under our culture conditions. It should be noted however that there was only a weak correspondence between our GFP-based results and our blue-range fluorescence-based results when evaluating the RNAi screen of Ca^{2+}-binding genes. In hindsight, we suspect that this lack of correspondence was due to the confounding effects of Ca^{2+} in our screen. The increase in anthranilate autofluorescence at the time of *C. elegans* death is itself mediated by the intracellular release of Ca^{2+}. Given that we were investigating the knockdown of Ca^{2+}-binding genes under conditions of high Ca^{2+}, it is reasonable to assume that the role of Ca^{2+} in both the treatment and the measurement likely introduced variation in the measurement of anthranilate.

5.6.3 High-throughput Assaying of *C. elegans* Metabolic Parameters While Using Bacteria-based RNAi Gene Knockdown

One of the strengths of *C. elegans* as a model organism is its susceptibility to RNAi. Currently, the most common methods of gene knockdown in *C. elegans* is to simply feed the nematodes bacteria expressing dsRNA targeted to the gene of interest, and the simplicity of this method has led to the development of commercially available bacterial clone RNAi libraries. The presence of live bacteria in the *C. elegans* media presents challenges when assaying nematode metabolic parameters however, especially under high-throughput conditions when removing the bacteria prior to assaying is difficult or impossible. Methods have been developed to kill *E. coli* while preserving dsRNA for gene knockdown, using treatment with ultraviolet light or γ-irradiation, but these methods require expensive or dedicated equipment, likely damage the dsRNA, and are difficult to scale to the quantities necessary for high-throughput screening.

To address these limitations, we decided to screen for simple and scalable treatments and conditions capable of killing *E. coli* while preserving dsRNA content (Chapter 4). We discovered that treating *E. coli* with acetone prior to starting a *C. elegans* liquid culture meets these requirements and maintains RNAi knockdown. In the process, we also discovered that *C. elegans* fed acetone-killed *E. coli* have slowed growth and fail to develop past the larval stage. To overcome this growth restriction, we found that supplementing the acetone-killed *E. coli* with 10% live *E. coli* is enough to maintain proper larval development. Under our standard culture conditions, 10% live *E. coli* is also a low enough concentration to be easily killed by ciprofloxacin treatment. Once in *C. elegans* liquid culture media, *E. coli* enter a stationary phase of growth that makes them resistant to many forms of antibiotic eradication. Ciprofloxacin is an antibiotic capable of killing stationary phase bacteria, and treatment of 10% live, stationary phase *E. coli* with ciprofloxacin results in a dramatic decrease in bacterial ATP after 48 hours, and the complete eradication of bacterial reductive capacity after 6 days. We also discovered that treatment with ciprofloxacin immediately upon starting a culture with acetone-killed *E. coli*, 10% live *E. coli*, and L1 larval stage *C. elegans* is still sufficient to allow proper larval development. This finding suggest that a nutrient vital for nematode development may be lost in the acetone-treatment process, which can then be supplemented back into the culture with live bacteria.

We were able to use these methods to perform RNAi knockdown screens of *C. elegans* X chromosome genes, in an effort to detect genes that mediate the age-related decline in ATP content, oxygen consumption, and reductive capacity. Our investigations revealed that live HT115(DE3) *E. coli* does not significantly respire in long-term *C. elegans* liquid cultures, suggesting that acetone and ciprofloxacin treatment of bacteria may not be necessary for high-

throughput measurements of *C. elegans* oxygen consumption. The acetone and ciprofloxacin system appears helpful for ATP content measurements, however, and it seems absolutely vital for meaningful measurements of *C. elegans* reductive capacity using resazurin, which is especially sensitive to the presence of live bacteria.

Initially when constructing our screens, we planned to use the GFP fluorescence of BC12907 *C. elegans* to normalize our ATP, oxygen, and reductive capacity measurements to the amount of living nematodes in each separate culture. Acetone- and ciprofloxacin-treated bacteria still possesses autofluorescence in the green range, however, which confounded the measurements enough that we abandoned the strategy. Instead, we decided that the use of non-normalized measurements was adequate based on three assumptions. Specifically, (1) the initial number of *C. elegans* added to a 96-well plate would not vary significantly among the wells; (2) since we were interested in knockdowns that increased specific metabolic parameters, the death of *C. elegans* from toxic knockdowns would not affect our selection of hits; and (3) the calculation of robust z-scores for knockdowns on a per-plate basis should compensate for any variation in the initial number of *C. elegans* among individual 96-well plates.

One restriction resulting from these assumptions is that the decrease of a metabolic parameter could not be used as a criterion for hit selection since measured decreases in that parameter could not differentiate between a legitimate down-regulation of the parameter and the loss of *C. elegans* due to toxic gene knockdowns. For example, before we fully settled on this approach, we performed a full RNAi screen of X chromosome genes, in triplicate, measuring BC12907 *C. elegans* β-galactosidase activity, which increases with age due to the accumulation of senescent cells. Our original strategy was to use a decrease in β-galactosidase as a criterion for determining hits, and to use BC12907 GFP fluorescence to disregard gene knockdowns that

appeared lethal. The unavailability of GFP fluorescence as a normalizing factor limits the hit criteria for that screen to RNAi knockdowns that increase β-galactosidase – the results of which will appear in future work.

5.7 Significance of Novel Methods

The methods we developed make the long-term liquid culturing of *C. elegans* easier and more amenable to high-throughput applications. Specifically, we developed a way to grow liquid cultures in microplates for the full duration of an average *C. elegans* lifespan without suffering significant fluid loss due to evaporation, and without the need to shake or unseal the plates for aeration. We also developed a method for measuring the total volume of live *C. elegans* in microplate cultures using only a fluorescence microplate reader, and we have a similar method at least partially established for estimating the rate of *C. elegans* death. Finally we developed a novel method for performing RNAi using dead bacteria, for the purpose of assaying metabolic parameters without bacterial interference.

5.8 References

1. Shaye DD, Greenwald I. Ortholist: A compendium of c. Elegans genes with human orthologs. PloS one. 2011;6(5):e20085.

2. Prasad V, Okunade GW, Miller ML, Shull GE. Phenotypes of serca and pmca knockout mice. Biochemical and biophysical research communications. 2004;322(4):1192-203.

3. Periasamy M, Reed TD, Liu LH, Ji Y, Loukianov E, Paul RJ, et al. Impaired cardiac performance in heterozygous mice with a null mutation in the sarco (endo) plasmic reticulum ca2+-atpase isoform 2 (serca2) gene. Journal of Biological Chemistry. 1999;274(4):2556-62.

4. Almedom RB, Liewald JF, Hernando G, Schultheis C, Rayes D, Pan J, et al. An er-resident membrane protein complex regulates nicotinic acetylcholine receptor subunit composition at the synapse. The EMBO journal. 2009;28(17):2636-49. doi: 10.1038/emboj.2009.204.

5. Kamat S, Yeola S, Zhang W, Bianchi L, Driscoll M. Nra-2, a nicalin homolog, regulates neuronal death by controlling surface localization of toxic caenorhabditis elegans deg/enac channels. J Biol Chem. 2014;289(17):11916-26. doi: 10.1074/jbc.M113.533695. PubMed PMID: 24567339; PubMed Central PMCID: PMC4002099.

6. McKay S, Johnsen R, Khattra J, Asano J, Baillie D, Chan S, et al., editors. Gene expression profiling of cells, tissues, and developmental stages of the nematode c. Elegans. Cold Spring Harbor symposia on quantitative biology; 2003: Cold Spring Harbor Laboratory Press.

7. Meissner B, Rogalski T, Viveiros R, Warner A, Plastino L, Lorch A, et al. Determining the sub-cellular localization of proteins within caenorhabditis elegans body wall muscle. PloS one. 2011;6(5):e19937. doi: 10.1371/journal.pone.0019937.

8. Arber S, Hunter JJ, Ross J, Jr., Hongo M, Sansig G, Borg J, et al. Mlp-deficient mice exhibit a disruption of cardiac cytoarchitectural organization, dilated cardiomyopathy, and heart failure. Cell. 1997;88(3):393-403. doi: 10.1016/S0092-8674(00)81878-4. PubMed PMID: 9039266.

9. Weiskirchen R, Gunther K. The crp/mlp/tlp family of lim domain proteins: Acting by connecting. Bioessays. 2003;25(2):152-62. doi: 10.1002/bies.10226. PubMed PMID: 12539241.

10. Henderson JR, Pomies P, Auffray C, Beckerle MC. Alp and mlp distribution during myofibrillogenesis in cultured cardiomyocytes. Cell Motil Cytoskeleton. 2003;54(3):254-65. doi: 10.1002/cm.10102. PubMed PMID: 12589684.

11. Kahvejian A, Svitkin YV, Sukarieh R, M'Boutchou M, Sonenberg N. Mammalian poly (a)-binding protein is a eukaryotic translation initiation factor, which acts via multiple mechanisms. Genes & development. 2005;19(1):104-13. doi: 10.1016/S0008-6215(99)00186-X. PubMed Central PMCID: PMCPMC540229.

12. Liu S, Milne GT, Kuremsky JG, Fink GR, Leppla SH. Identification of the proteins required for biosynthesis of diphthamide, the target of bacterial adp-ribosylating toxins on translation elongation factor 2. Mol Cell Biol. 2004;24(21):9487-97. doi: 10.1128/MCB.24.21.9487-9497.2004. PubMed PMID: 15485916; PubMed Central PMCID: PMC522255.

13. Longman D, Johnstone IL, Caceres JF. Functional characterization of sr and sr-related genes in caenorhabditis elegans. EMBO J. 2000;19(7):1625-37. doi: 10.1093/emboj/19.7.1625. PubMed PMID: 10747030; PubMed Central PMCID: PMC310231.

14. Iwasa H, Yu S, Xue J, Driscoll M. Novel egf pathway regulators modulate c. Elegans healthspan and lifespan via egf receptor, plc-gamma, and ip3r activation. Aging Cell. 2010;9(4):490-505. Epub 2010/05/26. doi: 10.1111/j.1474-9726.2010.00575.x. PubMed PMID: 20497132.

15. Tournebize R, Andersen SS, Verde F, Doree M, Karsenti E, Hyman AA. Distinct roles of pp1 and pp2a-like phosphatases in control of microtubule dynamics during mitosis. The EMBO journal. 1997;16(18):5537-49.

16. Fong NM, Jensen TC, Shah AS, Parekh NN, Saltiel AR, Brady MJ. Identification of binding sites on protein targeting to glycogen for enzymes of glycogen metabolism. Journal of Biological Chemistry. 2000;275(45):35034-9.

17. Simpson VJ, Johnson TE, Hammen RF. Caenorhabditis elegans DNA does not contain 5-methylcytosine at any time during development or aging. Nucleic acids research. 1986;14(16):6711-9. doi: 10.1093/nar/14.16.6711.

18. Greer EL, Blanco MA, Gu L, Sendinc E, Liu J, Aristizabal-Corrales D, et al. DNA methylation on n(6)-adenine in c. Elegans. Cell. 2015;161(4):868-78. Epub 2015/05/06. doi: 10.1016/j.cell.2015.04.005. PubMed PMID: 25936839; PubMed Central PMCID: PMCPMC4427530.

19. Takahashi Y, Daitoku H, Yokoyama A, Nakayama K, Kim JD, Fukamizu A. The c. Elegans prmt-3 possesses a type iii protein arginine methyltransferase activity. J Recept Signal Transduct Res. 2011;31(2):168-72. doi: 10.3109/10799893.2011.555768. PubMed PMID: 21385054.

20. Whetstine JR, Ceron J, Ladd B, Dufourcq P, Reinke V, Shi Y. Regulation of tissue-specific and extracellular matrix-related genes by a class i histone deacetylase. Mol Cell. 2005;18(4):483-90. doi: 10.1016/j.molcel.2005.04.006. PubMed PMID: 15893731.

21. Hegedűs C, Virág L. Inputs and outputs of poly (adp-ribosyl) ation: Relevance to oxidative stress. Redox biology. 2014;2:978-82. doi: 10.1016/j.redox.2014.08.003.

22. Dequen F, Gagnon SN, Desnoyers S. Ionizing radiations in caenorhabditis elegans induce poly(adp-ribosyl)ation, a conserved DNA-damage response essential for survival. DNA Repair (Amst). 2005;4(7):814-25. doi: 10.1016/j.dnarep.2005.04.015. PubMed PMID: 15923155.

23. Kawano T, Fujita M, Sakamoto H. Unique and redundant functions of sr proteins, a conserved family of splicing factors, in caenorhabditiselegans development. Mechanisms of development. 2000;95(1):67-76. doi: 10.1016/S0925-4773(00)00339-7.

24. Cui M, Allen MA, Larsen A, Macmorris M, Han M, Blumenthal T. Genes involved in pre-mrna 3'-end formation and transcription termination revealed by a lin-15 operon muv suppressor screen. Proc Natl Acad Sci U S A. 2008;105(43):16665-70. doi: 10.1073/pnas.0807104105. PubMed PMID: 18946043; PubMed Central PMCID: PMC2571909.

25. Nouws J, Nijtmans L, Houten SM, van den Brand M, Huynen M, Venselaar H, et al. Acyl-coa dehydrogenase 9 is required for the biogenesis of oxidative phosphorylation complex i. Cell metabolism. 2010;12(3):283-94. doi: 10.1016/j.cmet.2010.08.002.

26. Kimble J, Sharrock WJ. Tissue-specific synthesis of yolk proteins in caenorhabditis elegans. Dev Biol. 1983;96(1):189-96. Epub 1983/03/01. doi: 0012-1606(83)90322-6 [pii]. PubMed PMID: 6825952.

27. Monera OD, Sereda TJ, Zhou NE, Kay CM, Hodges RS. Relationship of sidechain hydrophobicity and alpha-helical propensity on the stability of the single-stranded amphipathic alpha-helix. J Pept Sci. 1995;1(5):319-29. doi: 10.1002/psc.310010507. PubMed PMID: 9223011.

28. Swire J, Fuchs S, Bundy JG, Leroi AM. The cellular geometry of growth drives the amino acid economy of caenorhabditis elegans. Proc Biol Sci. 2009;276(1668):2747-54. doi: 10.1098/rspb.2009.0354. PubMed PMID: 19439436; PubMed Central PMCID: PMC2839950.

29. Jiang M, Ryu J, Kiraly M, Duke K, Reinke V, Kim SK. Genome-wide analysis of developmental and sex-regulated gene expression profiles in caenorhabditis elegans. Proc Natl Acad Sci U S A. 2001;98(1):218-23. doi: 10.1073/pnas.011520898. PubMed PMID: 11134517; PubMed Central PMCID: PMC14571.

30. Golden TR, Beckman KB, Lee AH, Dudek N, Hubbard A, Samper E, et al. Dramatic age-related changes in nuclear and genome copy number in the nematode caenorhabditis elegans. Aging Cell. 2007;6(2):179-88.

31. Li Y, Na K, Lee HJ, Lee EY, Paik YK. Contribution of sams-1 and pmt-1 to lipid homoeostasis in adult caenorhabditis elegans. J Biochem. 2011;149(5):529-38. doi: 10.1093/jb/mvr025. PubMed PMID: 21389045.

32. Ehmke M, Luthe K, Schnabel R, Doring F. S-adenosyl methionine synthetase 1 limits fat storage in caenorhabditis elegans. Genes Nutr. 2014;9(2):386. doi: 10.1007/s12263-014-0386-6. PubMed PMID: 24510589; PubMed Central PMCID: PMC3968293.

33. Hou NS, Gutschmidt A, Choi DY, Pather K, Shi X, Watts JL, et al. Activation of the endoplasmic reticulum unfolded protein response by lipid disequilibrium without disturbed proteostasis in vivo. Proc Natl Acad Sci U S A. 2014;111(22):E2271-80. Epub 2014/05/21. doi: 10.1073/pnas.1318262111. PubMed PMID: 24843123; PubMed Central PMCID: PMC4050548.

34. Fischer A, Klapper M, Onur S, Menke T, Niklowitz P, Doring F. Dietary restriction decreases coenzyme q and ubiquinol potentially via changes in gene expression in the model organism c. Elegans. Biofactors. 2015. Epub 2015/05/06. doi: 10.1002/biof.1210. PubMed PMID: 25939481.

35. Bosma M, Dapito DH, Drosatos-Tampakaki Z, Huiping-Son N, Huang LS, Kersten S, et al. Sequestration of fatty acids in triglycerides prevents endoplasmic reticulum stress in an in vitro model of cardiomyocyte lipotoxicity. Biochim Biophys Acta. 2014;1841(12):1648-55. doi: 10.1016/j.bbalip.2014.09.012. PubMed PMID: 25251292; PubMed Central PMCID: PMC4342292.

36. Gabbay KH. The sorbitol pathway and the complications of diabetes. N Engl J Med. 1973;288(16):831-6. doi: 10.1056/NEJM197304192881609. PubMed PMID: 4266466.

37. Oates PJ. Polyol pathway and diabetic peripheral neuropathy. Int Rev Neurobiol. 2002;50:325-92. doi: 10.1016/S0074-7742(02)50082-9. PubMed PMID: 12198816.

38. Lorenzi M. The polyol pathway as a mechanism for diabetic retinopathy: Attractive, elusive, and resilient. Journal of Diabetes Research. 2007;2007. doi: 10.1155/2007/61038.

39. Szwergold BS, Kappler F, Brown TR. Identification of fructose 3-phosphate in the lens of diabetic rats. Science. 1990;247(4941):451-4. doi: 10.1126/science.2300805. PubMed PMID: 2300805.

40. Dagher Z, Park YS, Asnaghi V, Hoehn T, Gerhardinger C, Lorenzi M. Studies of rat and human retinas predict a role for the polyol pathway in human diabetic retinopathy. Diabetes. 2004;53(9):2404-11. doi: 10.2337/diabetes.53.9.2404. PubMed PMID: 15331552.

41. Asnaghi V, Gerhardinger C, Hoehn T, Adeboje A, Lorenzi M. A role for the polyol pathway in the early neuroretinal apoptosis and glial changes induced by diabetes in the rat. Diabetes. 2003;52(2):506-11. doi: 10.2337/diabetes.52.2.506. PubMed PMID: 12540628.

42. Samson AL, Knaupp AS, Kass I, Kleifeld O, Marijanovic EM, Hughes VA, et al. Oxidation of an exposed methionine instigates the aggregation of glyceraldehyde-3-phosphate dehydrogenase. J Biol Chem. 2014;289(39):26922-36. Epub 2014/08/03. doi: 10.1074/jbc.M114.570275. PubMed PMID: 25086035; PubMed Central PMCID: PMC4175333.

43. Burg MB, Ferraris JD. Intracellular organic osmolytes: Function and regulation. J Biol Chem. 2008;283(12):7309-13. doi: 10.1074/jbc.R700042200. PubMed PMID: 18256030; PubMed Central PMCID: PMC2276334.

44. Kiewietdejonge A, Pitts M, Cabuhat L, Sherman C, Kladwang W, Miramontes G, et al. Hypersaline stress induces the turnover of phosphatidylcholine and results in the synthesis of the renal osmoprotectant glycerophosphocholine in saccharomyces cerevisiae. FEMS Yeast Res. 2006;6(2):205-17. doi: 10.1111/j.1567-1364.2006.00030.x. PubMed PMID: 16487344.

45. Garcia-Perez A, Burg MB. Renal medullary organic osmolytes. Physiol Rev. 1991;71(4):1081-115. PubMed PMID: 1924548.

46. Meister A. Glutathione-ascorbic acid antioxidant system in animals. J Biol Chem. 1994;269(13):9397-400. PubMed PMID: 8144521.

47. Jahn M, Baynes JW, Spiteller G. The reaction of hyaluronic acid and its monomers, glucuronic acid and n-acetylglucosamine, with reactive oxygen species. Carbohydr Res. 1999;321(3-4):228-34. doi: 10.1016/S0008-6215(99)00186-X. PubMed PMID: 10614067.

48. Williamson DH, Lund P, Krebs HA. The redox state of free nicotinamide-adenine dinucleotide in the cytoplasm and mitochondria of rat liver. Biochem J. 1967;103(2):514-27. PubMed PMID: 4291787; PubMed Central PMCID: PMC1270436.

49. Braidy N, Guillemin GJ, Mansour H, Chan-Ling T, Poljak A, Grant R. Age related changes in nad+ metabolism oxidative stress and sirt1 activity in wistar rats. PLoS One. 2011;6(4):e19194. doi: 10.1371/journal.pone.0019194. PubMed PMID: 21541336; PubMed Central PMCID: PMC3082551.

50. Zhu X-H, Lu M, Lee B-Y, Ugurbil K, Chen W. In vivo nad assay reveals the intracellular nad contents and redox state in healthy human brain and their age dependences. Proceedings of the National Academy of Sciences. 2015;112(9):2876-81.

51. Makrantonaki E, Bekou V, Zouboulis CC. Genetics and skin aging. Dermato-endocrinology. 2012;4(3):280-4.

52. Potter SM, DeMarse TB. A new approach to neural cell culture for long-term studies. Journal of neuroscience methods. 2001;110(1):17-24.

53. Hunt-Newbury R, Viveiros R, Johnsen R, Mah A, Anastas D, Fang L, et al. High-throughput in vivo analysis of gene expression in caenorhabditis elegans. PLoS biology. 2007;5(9):e237.